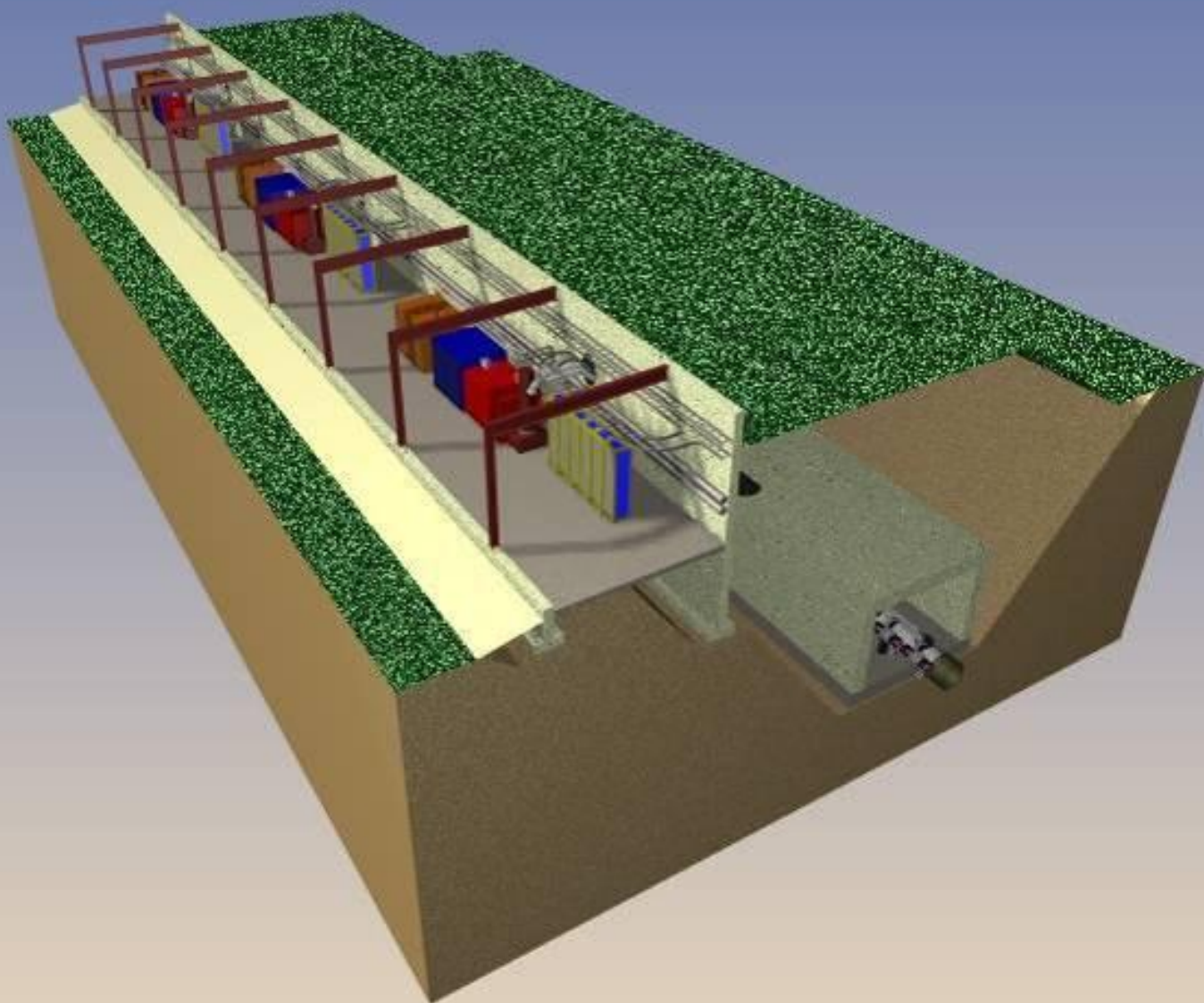


# ***An 8 GeV Superconducting Linac Proton Driver***



<b>1</b>	<b>INTRODUCTION.....</b>	<b>7</b>
1.1	The Technology Base for the Proton Driver Linac .....	8
1.2	The Proton Driver “CD-0” Design Study.....	9
1.3	Scope of this Design Study .....	9
1.4	Initial and Ultimate Linac Power Configurations .....	10
1.5	Related documents .....	11
<b>2</b>	<b>THE 8 GeV PROTON DRIVER LINAC.....</b>	<b>12</b>
2.1	Multi-Mission Linac .....	12
2.2	Main Injector Operations with the 8 GeV Linac .....	13
2.3	Relevance to Future Accelerator Projects .....	15
2.4	Superconducting RF Technology .....	16
<b>3</b>	<b>DESIGN OVERVIEW.....</b>	<b>18</b>
3.1	325 MHz Front-End Linac Overview .....	19
3.2	SCRF Spoke Resonator Linac Overview .....	23
3.3	1300 MHz Elliptical Cavity SCRF Linac Overview .....	23
3.4	RF Power Systems - Overview .....	25
3.5	Civil Construction Overview.....	26
3.6	Site Selection.....	28
3.7	One-Tunnel vs. Two-Tunnel Machine Layout.....	30
3.8	Above-ground Klystron Gallery.....	30
3.9	Tunnel Depth and Shielding.....	31
3.10	Main Injector Upgrades.....	32
<b>4</b>	<b>CHOICE OF PRIMARY PARAMETERS .....</b>	<b>33</b>
4.1	Beam Energy .....	33
4.2	Beam Charge per Pulse .....	33
4.3	Beam Current and Pulse Width: Initial and Ultimate Scenarios .....	33
4.4	Linac Pulse Repetition Rate (Average Beam Power) .....	35
4.5	Different Particle Types in the 8 GeV Linac.....	35
<b>5</b>	<b>ACCELERATOR PHYSICS.....</b>	<b>37</b>
5.1	End-to-End Simulation of the Baseline Lattice and Cavity Layout.....	39
5.2	Proton Driver Beam Loss Requirements vs. SNS.....	40
5.3	Linac Apertures .....	40
5.4	H- Ion Source .....	41
5.5	Radiofrequency Quadrupole (RFQ) .....	41
5.6	Medium Energy Beam Transport (MEBT). .....	42
5.7	Solenoidal Transverse Focusing for $E < 100$ MeV .....	43
5.8	Room-Temperature Triple-Spoke Resonator (RT-TSR).....	44
5.9	Superconducting Spoke Resonators .....	44
5.10	Quadrupole Transverse Focusing for $E > 110$ MeV .....	44
5.11	Longitudinal Focusing and Frequency Jumps.....	46
5.12	Linac Energy Stability Requirement .....	47
5.13	Strategies for Limiting Linac Energy Jitter.....	47
5.14	Debuncher .....	49
5.15	Longitudinal Phase Space Painting .....	50
5.16	Short Linac Bunches in the Broadband Impedance of the Main Injector .....	50

5.17	H Beam Transport .....	52
<b>6</b>	<b>FRONT-END LINAC DETAILED DESIGN.....</b>	<b>58</b>
6.1	H- Ion Source .....	58
6.2	Low Energy Beam Transport (LEBT).....	60
6.3	Radio Frequency Quadrupole (RFQ) .....	61
6.4	Medium Energy Beam Transport (MEBT) .....	62
6.5	Fast Beam Chopper in MEBT .....	63
6.6	Room-Temperature Spoke Resonators (RT-TSRs).....	64
6.7	Alternative of a Warm Copper DTL for the Front-End Linac .....	65
<b>7</b>	<b>325 MHz SPOKE RESONATOR SCRF LINAC.....</b>	<b>66</b>
7.1	SRF Spoke Resonators .....	66
7.2	Triple Spoke Resonators from 110-400 MeV (Baseline Design) .....	68
<b>8</b>	<b>1300 MHz ELLIPTICAL-CELL CAVITY SCRF LINAC.....</b>	<b>69</b>
8.1	TESLA Cavities in the $\beta=1$ Main Linac.....	70
8.2	$\beta < 1$ Cavity Designs .....	71
8.3	Assumptions for SCRF Elliptical-Cell Cavity Gradients.....	73
8.4	Cavity Tuners .....	74
<b>9</b>	<b>RF POWER COUPLERS .....</b>	<b>77</b>
9.1	1300 MHz RF Power Couplers .....	77
9.2	325 MHz RF Power Couplers .....	79
9.3	HOM Couplers .....	79
<b>10</b>	<b>KLYSTRONS.....</b>	<b>80</b>
10.1	325 MHz Klystrons (Toshiba E3740F).....	80
10.2	1300 MHz Multi-Beam Klystrons.....	82
10.3	Klystron test program for 4.5 msec pulse length.....	82
<b>11</b>	<b>MODULATORS .....</b>	<b>83</b>
11.1	Baseline (FNAL/TTF) “Bouncer” Modulator Design.....	83
11.2	Modulator Design Alternatives. ....	87
11.3	Reconfigurable Modulator for Initial to Final RF Upgrade .....	88
11.4	Modulator Location and Gallery Layout.....	89
<b>12</b>	<b>RF DISTRIBUTION SYSTEMS.....</b>	<b>90</b>
12.1	The TESLA-Style RF Fan-out for Multiple Cavities per Klystron.....	92
12.2	Microwave Conduits between Tunnel and Gallery.....	94
12.3	Waveguide Cooling.....	94
12.4	RF Power Margins in the Main Linac .....	95
12.5	325 MHz RF Distribution System for the Warm Front-End Linac.....	96
<b>13</b>	<b>CAVITY RESONANCE CONTROL AND ENERGY STABILITY.....</b>	<b>97</b>
13.1	Cavity Resonance Control in Proton vs. Electron Linacs .....	98
13.2	Lorentz Detuning and Piezoelectric Fast Tuners .....	98
13.3	Cavity Microphonics .....	99
13.4	Vector Sum Regulation in Electron and Proton Linacs .....	100
13.5	Weighted Vector Sum Regulation for Proton Linacs.....	101
13.6	Beam-Based Phase and Energy Feedback.....	103
13.7	Linac Energy Stability Simulations.....	103
13.8	Specifications for the Ferrite Vector Modulators.....	105

<b>14 FERRITE VECTOR MODULATOR TECHNOLOGY DEVELOPMENT .....</b>	<b>109</b>
14.1 FVM Operating Principles .....	109
14.2 Fast Ferrite Phase Shifters .....	113
14.3 Coaxial Phase Shifter Development .....	115
14.4 Waveguide Phase Shifter Development .....	118
14.5 Stripline Phase Shifter Development .....	122
14.6 Integrated 325 MHz FVM Module .....	123
14.7 Ferrite Bias Drive Amplifier Development .....	125
<b>15 DEBUNCHER .....</b>	<b>127</b>
15.1 Debuncher RF System .....	127
15.2 Warm Copper Debuncher Cavities .....	128
15.3 Debuncher RF Phase Jitter .....	128
15.4 Active Feedback Option for Debuncher .....	129
<b>16 CRYOMODULES .....</b>	<b>130</b>
16.1 1300 MHz Cryomodules .....	130
16.2 325 MHz Cryomodules .....	133
16.3 Cryomodule Design Choices for the Baseline Design .....	134
<b>17 SUPERCONDUCTING MAGNETS .....</b>	<b>136</b>
17.1 Superconducting Quadrupoles .....	136
17.2 Superconducting Solenoids .....	138
<b>18 CRYOGENIC SYSTEM .....</b>	<b>140</b>
18.1 Cryogenic System Layout .....	140
18.2 Cool Down and Module Replacement Time .....	142
18.3 Cryogenic Heat Loads .....	142
18.4 Cryogenic Plant .....	143
18.5 Possible use of Fermilab's Central Helium Liquefier for Linac Commissioning .....	143
<b>19 BEAM TRANSPORT AND COLLIMATON LINE .....</b>	<b>144</b>
19.1 Transport Line Optics and Cell Layout .....	144
19.2 Dipoles .....	146
19.3 Quadrupoles .....	147
19.4 Correctors .....	147
19.5 Beam Loss in the 8 GeV H- Transport Line .....	147
19.6 H <sup>+</sup> Stripping from Magnetic Fields .....	148
19.7 Vacuum for the Transport Line .....	149
19.8 Collimation of Betatron Beam Halo .....	150
19.9 Momentum Collimation .....	150
19.10 Linac Beam Absorber .....	151
<b>20 H<sup>+</sup> INJECTION .....</b>	<b>154</b>
20.1 Example Injection Layout .....	154
20.2 Phase Space Painting .....	155
20.3 Optimum Painting Waveforms .....	156
20.4 Stripping Foil Heating and Lifetime .....	157
20.5 Main Injector Beam Loss Calculation from Foil Scattering and Interactions .....	157
20.6 H <sup>0</sup> Excited States and Delayed Stripping .....	158
<b>21 MAGNET POWER SUPPLIES .....</b>	<b>159</b>
<b>22 INSTRUMENTATION IN THE SCRF LINAC .....</b>	<b>160</b>

22.1	Main Linac Instrumentation .....	160
22.2	Transfer Line Instrumentation.....	161
<b>23</b>	<b>COOLING WATER (ICW and LCW SYSTEMS) .....</b>	<b>163</b>
23.1	LCW Load Variability.....	163
23.2	Differences from the TESLA Cooling Design .....	163
<b>24</b>	<b>WALL POWER SUMMARY FOR PROTON DRIVER LINAC.....</b>	<b>165</b>
<b>25</b>	<b>MAIN INJECTOR RF UPGRADE.....</b>	<b>166</b>
25.1	New Cavity Design for Main Injector RF Upgrade .....	166
25.2	Beam Loading and R/Q.....	167
25.3	Electromagnetic Design of the RF Cavity.....	168
25.4	YIG Tuner Development.....	168
25.5	Power Amplifier .....	169
25.6	Civil Construction for the RF upgrade .....	169
<b>26</b>	<b>COST ESTIMATE.....</b>	<b>171</b>
26.1	Scope of the Cost Estimate.....	172
26.2	Methodology .....	172
26.3	Major Cost Elements .....	173
<b>Appendix 1</b>	<b>– MULTIPLE MISSIONS FOR THE PROTON DRIVER LINAC .....</b>	<b>177</b>
	Running Electrons and Protons in the same Linac.....	177
	Cavity phase shifts between $e^{\pm}$ and p with many cavities per klystron.....	178
	Sharing Transverse Focusing between Electrons and Protons.....	179
<b>Appendix 2</b>	<b>- CIVIL CONSTRUCTION DETAILED FACILITIES DESCRIPTIONS</b>	<b>180</b>
<b>Appendix 3</b>	<b>- CIVIL CONSTRUCTION FIGURES .....</b>	<b>184</b>
<b>Appendix 4</b>	<b>- FAQ's ON STAGING AND ULTIMATE PERFORMANCE .....</b>	<b>204</b>
<b>Appendix 5</b>	<b>- CHOICE OF LINAC OPERATING FREQUENCIES .....</b>	<b>206</b>

*The references and table of contents are hyperlinked, when reading this document as a Word file*

# An 8 GeV SCRF Linac Proton Driver

Edited by G. W. Foster for the

## SCRF Linac Proton Driver Study Group

Russ Alber  
Terry Anderson  
Mike Andrews  
Chuck Ankenbrandt  
Giorgio Apollinari  
Maurice Ball  
Pierre Bauer  
Leo Bellantoni  
Tim Berenc  
Chandra Bhat  
Shreyas Bhat (U. Chicago)  
Dixon Bogert  
Court Bohn (NIU)  
Jeff Brandt  
Bruce C. Brown  
Chuck Brown  
Howard Bryant (UNM)  
John Carson  
Harry Carter  
Fritz Caspers (CERN)  
Brian Chase  
Alex Chen  
Weiren Chou  
Brad Claypool  
Zach Conway (UIUC)  
Don Cossairt  
Jim Crisp  
Ed Crumpley  
Paul Czarapata  
Joe DiMarco  
Sasha Drozhdin  
Vadim Dudnikov  
Helen Edwards (FNAL/DESY)  
Chuck Federowicz  
Matt Ferguson  
Dave Finley  
Mike Foley  
Joel Fuerst (ANL)  
G. William Foster  
Fernanda Garcia  
Al Garren (UCLA)  
Norman Gelfand  
Michael Geynisman  
Henry Glass  
Ivan Gonin  
Bob Goodwin

Jim Griffin  
Nancy Grossman  
Dave Harding  
Debbie Harris  
Steve Hays  
Chris Hill  
Jeff Holmes (ORNL)  
Markus Huening  
Chez Jach  
Gerry Jackson (HBar Tech.)  
Chris Jensen  
Carol Johnstone  
Dave Johnson  
Vladimir Kashikhin  
Bob Kephart  
Arkadiy Klebaner  
Jim Kerby  
Paul Kesich  
Timergali Khabibouline  
Kiyomi Koba  
Mikhail Kostin  
Ioanis Kourbanis  
Bob Kustom (ANL)  
Jim Lackey  
Tom Lackowski  
Peter Limon  
Peter Lucas  
Jim MacLachlan  
Robyn Madrak  
Sasha Makarov  
Ernie Malamud  
Phil Martin  
Alberto Marchionni  
Mike May  
Elaine McCluskey  
Elliott McCrory  
Leo Michelotti  
Don Mitchell  
Shekhar Mishra  
Douglas Moehs  
Nikolai Mokhov  
Al Moretti  
Bill Ng  
Tom Nicol  
Francois Ostiguy  
Petr Ostroumov (ANL)

Carlo Pagani (INFN Milan)  
Ralph Pasquinelli  
Tom Pawlak  
Tom Peterson  
Howie Pfeffer  
Philippe Piot (NIU)  
Duane Plant  
Milorad Popovic  
Eric Prebys  
Peter Prieto  
Chris Prior (RAL)  
Zubao Qian  
Roger Rabehl  
Gina Rameika  
Grahame Rees (RAL)  
John Reid  
Gennady Romanov  
Allan Rowe  
Phil Schlabach  
Alexei Semenov  
Mike Shea  
Ken Shepard (ANL)  
Jeff Sims  
Nikolay Solyak  
Bill Soyars  
Rich Stanek  
Ding Sun  
Zhijing Tang  
Ed Temple  
Iouri Terechkine  
Jay Theilacker  
Ray Tomlin  
Kamran Vaziri  
Rod Walton  
Bob Webber  
Dave Wildman  
Dan Wolff  
Xi Yang  
Victor Yarba  
Bob Wagner  
Vincent Wu  
Phil Yoon  
Don Young  
Al Zeller (MSU/NSCL)

## 1 INTRODUCTION

Recent discoveries of nonzero neutrino mass and neutrino oscillations have led to a worldwide resurgence of interest in neutrino physics. Neutrino physics studies by the APS[ ] and a companion study of physics at the FNAL Proton Driver[ ] have concluded that a multi-megawatt Proton Driver is an essential element in the study of neutrino oscillations in any foreseeable scenario. The focus on Fermilab's future neutrino and fixed-target program has intensified with the announcement of a cessation of all collider physics in the U.S. by ~2009 [HEPAP 2005].

Simultaneously the International Linear Collider (ILC) has been making strides as the leading candidate for the next multi-regional collaborative endeavor in high-energy physics. The recent selection of the “cold” Superconducting RF (SCRF) technology for the ILC has allowed the design effort to proceed to the next steps of forming a Global Design Effort (GDE) with the goal of obtaining a fully vetted budget, project schedule, and CDR by 2006. In the United States HEP program, the substantial resources that will become available for following the cessation of the B-factory and Tevatron operations circa 2008 will be redirected to an aggressive pre-project R&D and industrialization program for the ILC [Staffin talk]. At the same time, the uncertainties in the time scale and location of the ILC mandate the need for near-term U.S. HEP program that can be accommodated in a realistic near-term budget [Staffin talk] that will provide a bridge program to the start of ILC physics.

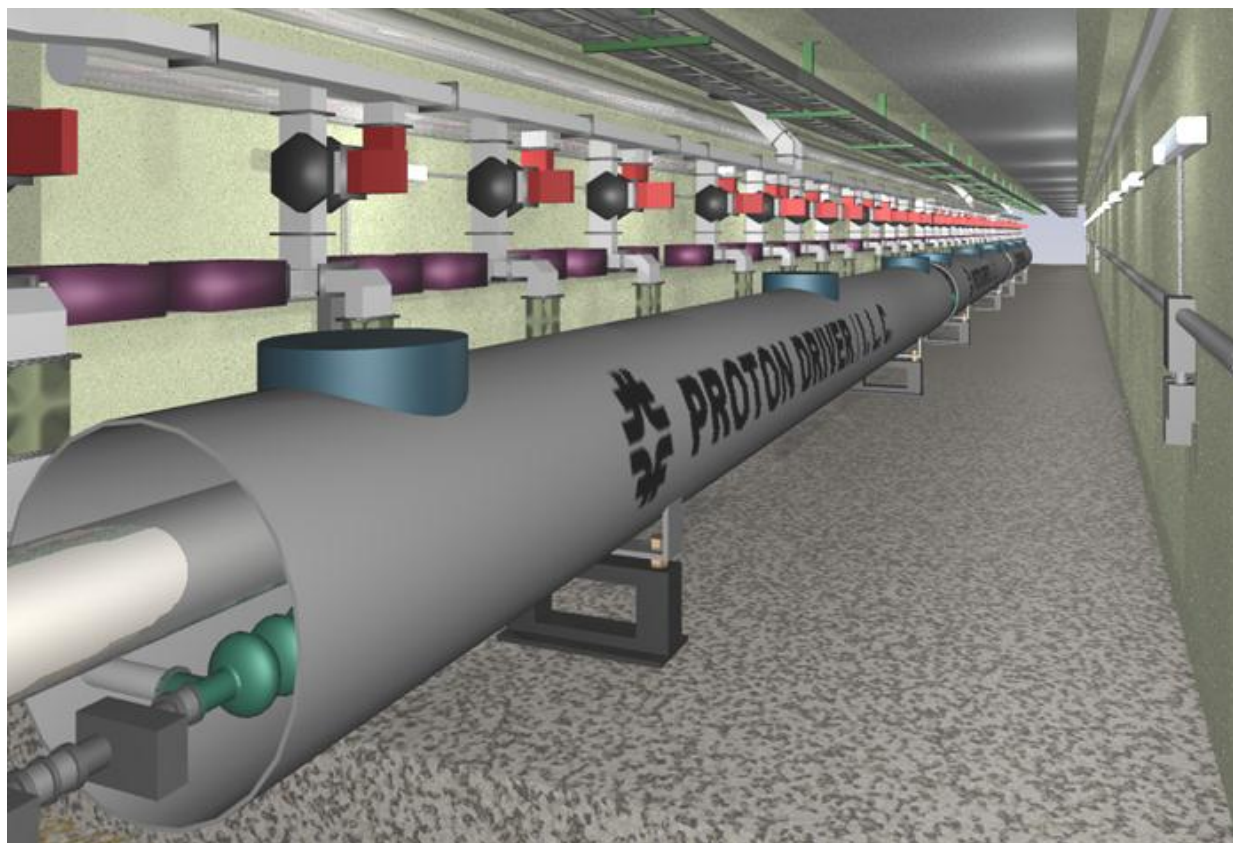


Figure 1 - The Proton Driver Main Linac from 1-8 GeV uses the same cavities, cryomodules, Klystrons and RF distribution system as the TESLA design for the ILC.

The concept of the SCRF Proton Driver Linac [ ] is to meld these two apparently competing priorities into a single synergistic program. An 8 GeV superconducting (proton) linac essentially

identical to the ILC design will serve as a 1.5% ILC demonstration project and a seed for SCRF industrialization in the U.S. As a Proton Driver, it will provide the intense clean beams necessary for operating the Fermilab Main Injector at 2-4 MW as well as providing independent, intense beams for a possible 8 GeV neutrino and fixed target program. Neutrino physicists will support the rapid U.S. industrialization of ILC technology because of the near-term benefits to the neutrino program. The US-ILC will support an extensive program of neutrino detectors and Main Injector upgrades that generate the “guaranteed U.S. physics payoff” for an extensive investment in ILC technology in the U.S. The financial credibility of the U.S. as a partner in HEP projects will be (re-)established by successful completion of a ~\$0.5B multi-laboratory superconducting RF project in the time frame 2008-2012, segueing into the construction start of a several-\$B US Linear Collider in the time frame of ~2012.

### 1.1 The Technology Base for the Proton Driver Linac

The Proton Driver Linac merges design concepts and technology from the ILC, the Spallation Neutron Source (SNS), the Rare Isotope Accelerator (RIA), JPARC, and other SCRF projects. See Figure 2. In many cases designs are taken over and copied directly; in other cases collaborators are helping Fermilab obtain “frequency scaled” adaptations of their design to the Proton Driver Linac. It thus fully embodies the technological synergies (“spin-offs”) that were a driving factor in the cold technology selection for the ILC [ITRP final report].

SNS commissioning<sup>1</sup>

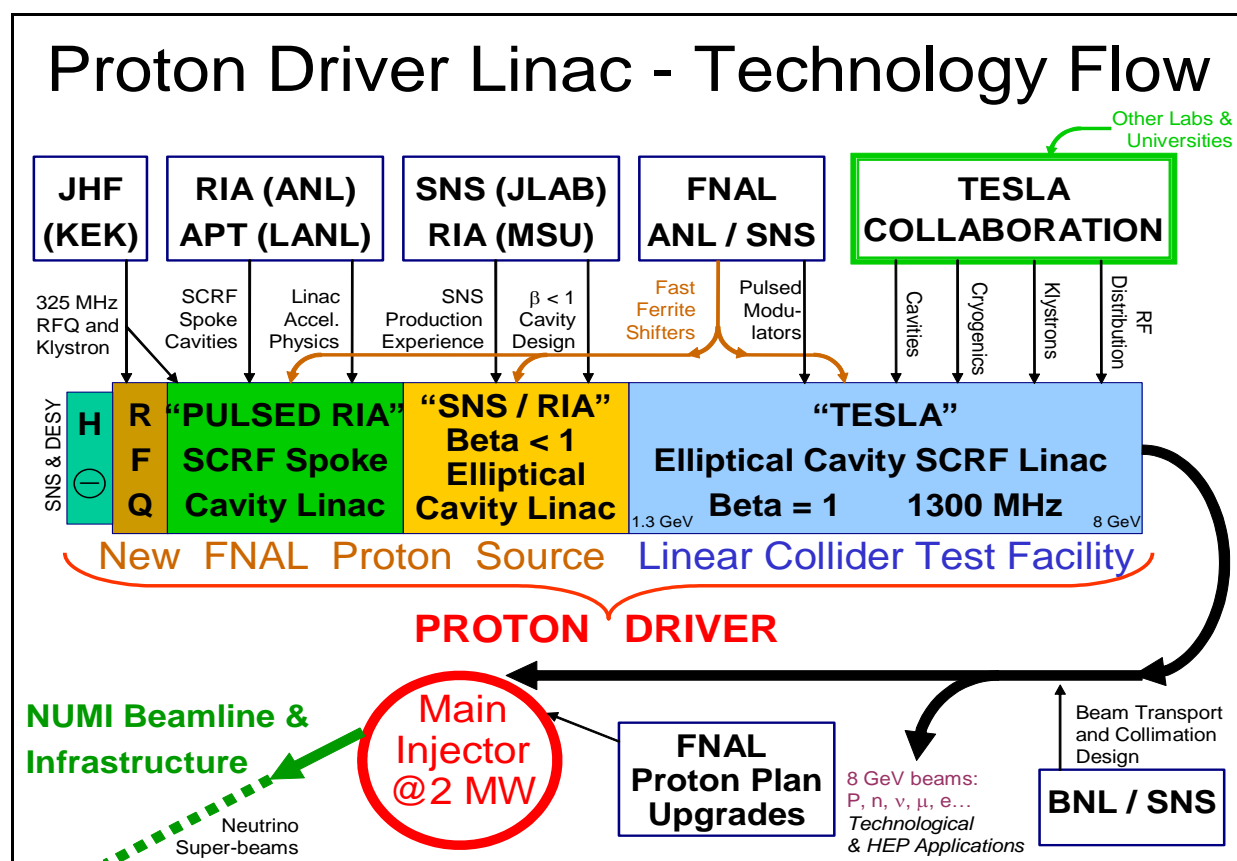


Figure 2 – The technology base for the Proton Driver is derived from many SCRF projects.

The design of the Proton Driver linac has evolved substantially in response to the ILC technology selection. ILC-compatible operating frequencies (1300 MHz and 325 MHz) have been selected. This means that the Proton Driver main linac (from ~1.3 - 8 GeV) is now an *exact* copy of the TESLA design, with identical cavities, cryomodels, Klystrons, assembly tooling fixtures, and so on. (The previous design study standardized on SNS-compatible frequencies, which meant that SNS cavities and Klystrons could be used for the front-end linac, but that not-quite-ILC-compatible 1207.5 MHz components had to be developed for the Main Linac.) This frequency change has had very positive implications for the R&D program for the Main Linacs of the ILC and Proton Driver, which are now well unified and nearly indistinguishable efforts at Fermilab. It has also been recognized that some of the technology developed for the Proton Driver (for example the fast ferrite vector modulators) could have benefits for the capital and operating costs of the ILC<sup>2</sup>. The synergy is real.

## **1.2 The Proton Driver “CD-0” Design Study**

This is the second iteration of a Design Study<sup>3</sup> of an 8 GeV Superconducting Linac<sup>4</sup> to be used as a replacement for Fermilab’s Booster and Linac. It is intended to provide backup documentation to support a CD-0 decision by DOE Office of Science to allow further project planning on the Proton Driver to proceed. The design goal is a five-fold increase in the beam power available through Fermilab’s Main Injector, an approximately ten-fold increase in the beam power available at 8 GeV. Substantial technical overhead is present in the design to allow for further increases in Main Injector beam power. Previous studies have also examined the technology and cost of an 8 GeV Synchrotron<sup>5</sup> and 12-16 GeV synchrotron as Booster replacement<sup>6</sup>.

The parameters for this Machine study and the associated Physics Study<sup>7</sup> were specified in the charge letter<sup>8</sup> from FNAL’s Director.

## **1.3 Scope of this Design Study**

The superconducting linac documented in this study serves only as an H- injector to enable 2 MW “Super-Beams” in the Fermilab Main Injector.

Hardware associated with beam lines, targets, and detector upgrades to exploit the 2 MW beam power of the Main Injector are not included in this design study. Beamline and detector costs for a possible 8 GeV physics program running directly from the linac are likewise excluded. It is presumed that these will either be included in individual experimental cost estimates on a case-by-case basis, be included in a (much larger) proposal containing both detector and accelerator initiatives at the Proton Driver, or compartmentalized into smaller (AIP-scale) projects outside the Proton Driver project.

Upgrades to the Main Injector ring to support 2 MW beam power are also not included in this design study. This follows the model of the Main Injector project, which contained the scope and costs of a new accelerator but not the detector (or downstream machine) upgrades needed to exploit its new capabilities.

The most important of the MI ring upgrades for 2 MW beam power is the Radio Frequency (RF) system upgrade. A new accelerator RF cavity and drive amplifier will be needed. An aggressive prototype program for this is being funded by the Proton Driver R&D program.

A number of technical options and upgrade paths are discussed in this document. These are included to motivate the choices made for baseline design, which is completely documented

and consistently cost-estimated. The reader is urged not to mistake these discussions for technical uncertainty.

Various hooks have been left in the technical design of the linac to allow it to accelerate electrons, positrons, protons and muons. This opens a number of alternative future missions for the linac, but is not in the baseline mission. These alternate missions, and their implications for linac hardware, are discussed in Appendix 1.

#### **1.4 Initial and Ultimate Linac Power Configurations**

Two design variants with different “stand-alone” linac beam power at 8 GeV are documented:

- An **Initial** configuration with 0.5 MW linac beam power at 8 GeV.
- An **Ultimate** configuration {denoted by braces} with 2.0 MW linac beam power.

Both configurations support 2 MW beam power at 30-120 GeV from the Fermilab Main Injector. The 0.5 MW Initial configuration was used for the cost baseline for comparison with an 8 GeV synchrotron of equal 0.5 MW beam power. The upgrade from the 0.5 MW to the 2 MW configuration is almost entirely an RF upgrade, with additional Klystrons, modulators, and ancillary equipment. The decision as to whether to proceed directly to the Ultimate configuration will depend on funding, and the physics interest in the high power 8 GeV program.

Table 1 - 8 GeV Proton Driver Linac - Primary Parameter List

PRIMARY PARAMETERS	8 GeV Initial 0.5 MW {Ultimate 2MW in Brackets}	
Linac beam kinetic energy	8 GeV	
Linac Particle Types	H - ions Protons Electrons	Baseline Mission via foil stripping in transfer line Possible w/upgrade of Phase Shifters & Injector
Linac Stand-Alone Beam power	0.5 {2.0} MW	8 GeV beam power available directly from linac
Linac Pulse repetition rate	2.5 {10} Hz	
Linac macropulse width	3.0 {1.0} ms	
Linac current (avg. in macropulse)	8.7 {26} mA	
Linac current (peak in macropulse)	9.3 {28} mA	
Linac Beam Chopping factor in macropulse	94 %	For adiabatic capture with 700ns abort gap.
Linac Particles per macropulse	1.56E+14	
Linac Charge per macropulse	26 uC	
Linac Energy per macropulse	208 kJ	
Linac average beam current	0.07 {0.26} mA	
Linac beam macropulse duty factor	0.75 {1.0} %	
Linac RF duty factor	1.00 {1.3} %	
Linac Active Length including Front End	614 m	Excludes possible expansion length
Linac Beam-floor distance	0.69 m =27 in.	same as Fermilab Main Injector
Linac Depth Below Grade	9 m	same as Fermilab Main Injector
Transfer Line Length to Ring	972 m	for MI-10 Injection point
Transfer Line Total Bend	40 deg	two 20-degree collimation arcs
Ring circumference	3319.4 m	Fermilab Main Injector
Ring Beam Energy	8-120 GeV	MI cycle time varies with energy
Ring Beam Power on Target	2 MW	~ independent of MI Beam Energy
Ring Circulating Current	2.3 A	
Ring cycle time	0.2-1.5 sec	depends on MI beam energy & flat-top
Ring Protons per Pulse on Target	1.50E+14 protons	
Ring Charge per pulse on target	25 uC	
Ring Energy per pulse on target	200-3000 kJ	at 8-120 GeV
Ring Proton pulse length on target	10 us	1 turn, or longer with resonant extraction
Linac Wall Power	5.5 {12.5} MW	approx 3 MW Standby + 1MW / Hz

## 1.5 Related documents

Proton Driver Physics Study Document<sup>7</sup>  
 Director's External Technical Review of the Proton Driver<sup>9</sup> (March 2005)  
 8 GeV Linac Parameter book<sup>10</sup>  
 Cost Estimate Spreadsheet<sup>11</sup> and various cost backup documents<sup>12</sup>  
 Linac 2000 paper<sup>4</sup> describing initial concept  
 Accelerator Physics Lattice Design Files<sup>13</sup>  
 Civil Construction Drawings<sup>14</sup>  
 PowerPoint presentations<sup>15</sup>  
 Online collection of papers on SCRF technology relevant to the Proton Driver linac<sup>16</sup>

These are available on the web at: <http://protondriver.fnal.gov>

## 2 THE 8 GeV PROTON DRIVER LINAC

A single stage injector linac<sup>4</sup> that replaces both the Booster and its injection linac is an old concept<sup>17</sup>. There are few questions about its accelerator physics or technical feasibility. By main force, it overcomes the bottleneck for accelerating protons at Fermilab, namely the space-charge tune spread at Booster injection. The beam optics are straightforward, especially above 1 GeV when the protons become relativistic. The simplicity of the design and control system should make it simpler to tune and operate than a Booster/Linac combination. The limited opportunities for emittance growth in a linac mean that it can deliver the high brightness, clean beams needed for running the Main Injector at high intensity. The rapid (1-3 msec) filling time from the linac means the Main Injector can maintain its 1.5-second minimum cycle time without extra delays to load multiple Booster batches. More rapid cycle times, and correspondingly higher beam power from the Main Injector, are feasible.

The major question for the 8 GeV linac is cost. In a linac, the expensive radio frequency (RF) systems must transfer their energy to the beam in a single pass, whereas in a synchrotron the RF costs are amortized over many thousands of beam passages through the accelerating cavities. As a result, synchrotrons are preferable for attaining the highest beam energies<sup>18</sup>. On the other hand a Linac is preferable at low energies due to its simplicity and its relative immunity to space charge self-forces of the beam. A linac is in fact the only technical option if bright proton beams are desired at energies below a few hundred MeV.

Traditionally, the economic crossover energy at which a synchrotron becomes more cost-effective than a linac has been in the range 0.1 ~ 0.5 GeV. Since over the last 30 years there has been little technological improvement in the cost-per-GeV of either warm iron synchrotrons or conventional warm copper linacs, the concept of an 8 GeV linac based on copper technology is indeed a non-starter. However recent indications of a dramatically reduced cost-per-GeV of superconducting linacs<sup>19</sup>, if verified in the case of a proton linac in the few GeV energy range, have the potential of changing that crossover point.

The approach taken in this design study is to start by copying existing systems to develop a baseline design that is solid from both the technological and accelerator physics points of view. Engineers familiar with the production experience for that design then produced a cost estimate. The selection among technical options was therefore biased in favor of those for which complete cost estimates were conveniently available (examples of these were the quotes obtained from vendors experienced in the production of DESY/TESLA cavity & cryomodule assemblies, and the choice of the FNAL/TTF “bouncer” klystron modulator). This single point design can serve as a basis for further technical optimization and, if a positive CD-0 decision is taken, for initial project planning.

### 2.1 Multi-Mission Linac

An additional motivation for the Proton Driver linac comes from the realization that an 8 GeV superconducting linac can be a multi-mission device. Its primary mission will be to operate as an H<sup>-</sup> injector linac to prepare high power “Super Beams”<sup>20</sup> in the Main Injector. This will support neutrino experiments, antiproton production, Tevatron collider operation, and conventional fixed-target experiments. However, the relativistic  $\beta = 1$  section of the linac (the final 7 GeV) can also efficiently accelerate electrons, protons, positrons, or relativistic muons. With technical components described in this Design Study, these different beam types can be selectable on a pulse-by-pulse basis.

At the specified 2.5 Hz {10 Hz Ultimate} repetition rate, only 1/4 {1/15} of the Linac beam pulses are required for Main Injector 120 GeV “Super Beam” operations. The remainder of the beam is available for other uses.

The total beam power available directly from the linac at 8 GeV is 0.5 MW {2 MW}. This, for example, gives it the potential of directly driving a high-statistics 8 GeV neutrino program, a free-electron laser, or the world’s most powerful long-pulse spallation neutron source.

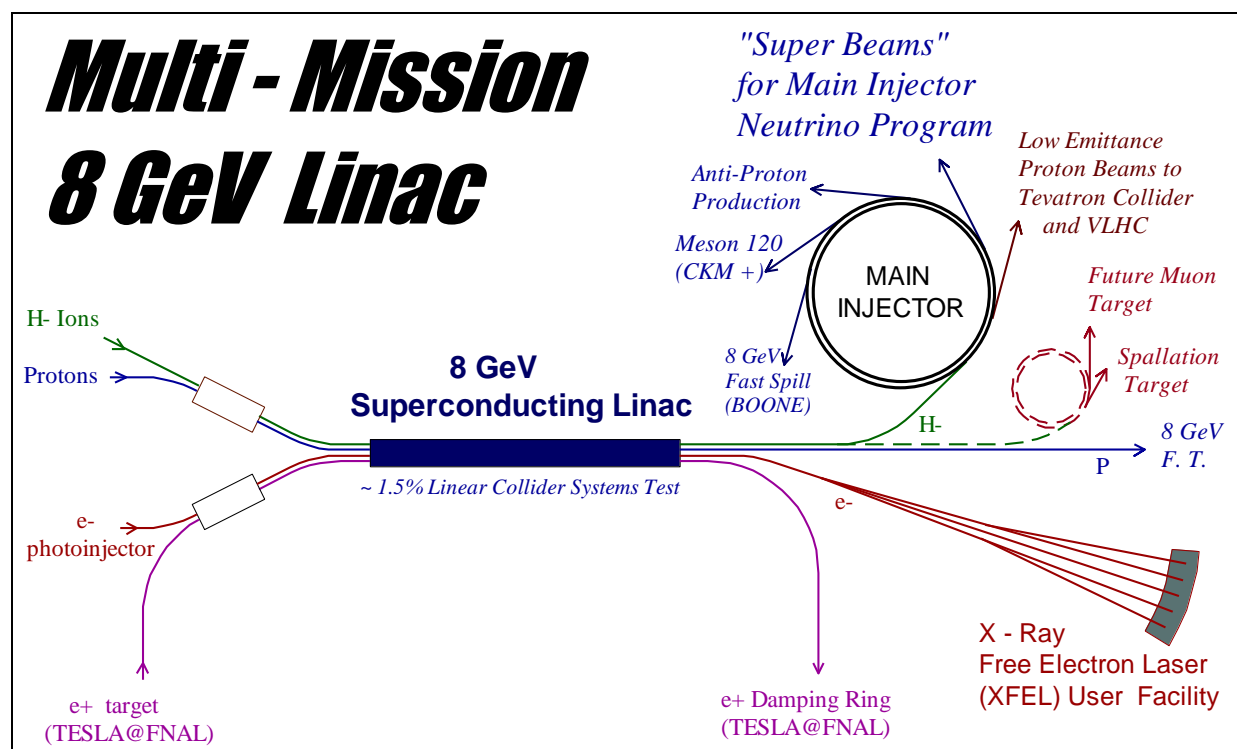


Figure 3 - The 8 GeV Multi-Mission Injector Linac simultaneously servicing “Super-Beams” in the Fermilab Main Injector for precision neutrino experiments, an X-ray Free Electron Laser (XFEL) for biomedicine, a Pulsed Neutron Source for material science applications, continuously extracted 8 GeV proton beams for precision Kaon experiments using the Recycler as a stretcher ring, an experimental storage ring for a future muon collider, an antiproton decelerator facility (not shown), and an ultra-low emittance injector to an energy frontier future hadron collider. The Proton Driver linac serves as a ~1.5% scale system test of the Linear Collider, and could eventually serve as the positron pre-accelerator for the damping rings for TESLA at FNAL, with circular damping rings stacked in the Tevatron tunnel.

## 2.2 Main Injector Operations with the 8 GeV Linac

The Proton Driver linac adds considerable operational flexibility to the Main Injector. Each pulse of the linac contains  $1.5 \times 10^{14}$  protons (25  $\mu\text{C}$ ), as much charge as 35 present-day Booster batches. The MI filling time is 3 msec {1 msec}, and can be repeated as often as 2.5 Hz {10 Hz}. This yields a variety of possible Main Injector operating modes:

For **High Beam Power Mode** (Figure 4) the Main Injector can be fully loaded (minus an abort gap) and cycled to 120 GeV at its minimum 1.5 second cycle time. This yields the maximum 2 MW beam power from the Main Injector for neutrino or other fast-spill fixed target physics. In parallel with this, another 1.87 MW (14/15th of the Linac beam power) is available directly from the linac as any desired mixture of  $\text{H}^-$  or electrons.

A **High Rep-Rate Mode** is possible in which the MI cycles at a higher repetition rate to a lower peak energy (Figure 4). Due to the small filling time from the Linac, the cycle time can be decreased proportionally to the beam energy so that the total beam power remains constant. (In contrast, the average beam power of the MI with a synchrotron-based injector would drop as the MI energy is lowered, due to the increasing fraction of time needed for multi-batch injection. This represents a major difference between the Synchrotron and Linac options for the Proton Driver.)

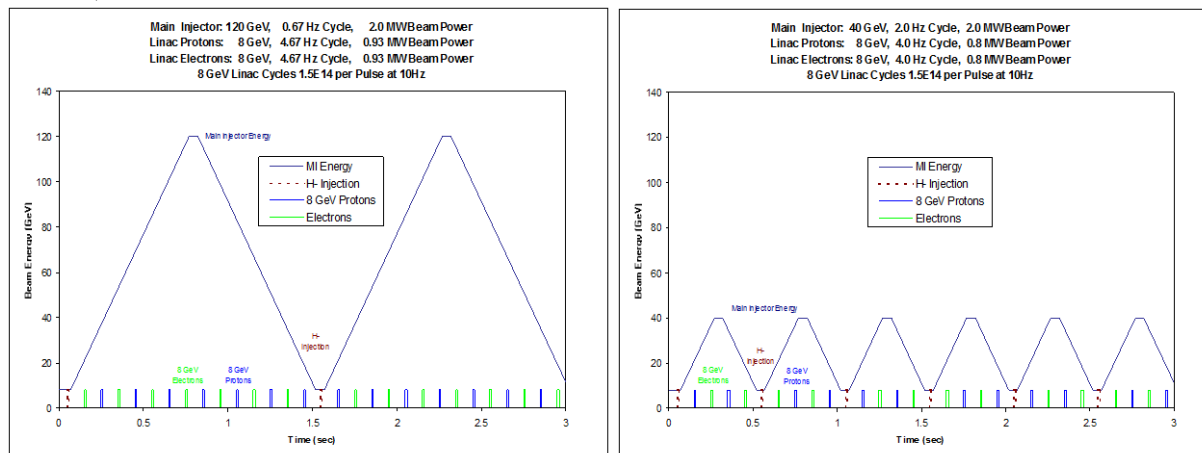


Figure 4 - Main Injector with 8 GeV linac injection. Left: (standard operation): The Main Injector cycles to 120 GeV every 1.5 seconds. With the design load of  $1.5 \times 10^{14}$  protons, this corresponds to 2 MW beam power at 120 GeV. During Main Injector ramping, the 8 GeV Linac operating at 2.5 Hz {10 Hz} can provide 0.35 MW {1.8 MW} of stand-alone beam power at 8 GeV, potentially in any combination of electrons, H<sup>+</sup>, or Protons. Bottom: Main Injector operating at a rapid cycle time at reduced beam energy (in this case 40 GeV). The same 2 MW beam power is delivered at this lower energy due to the small filling time from the linac.

Table 2 – Representative Main Injector Cycles Supported by the SCRF Linac Proton Driver

	Typical User	Cycle Time	Spill Time (typ)	Beam Power in Main Injector	8 GeV Linac Beam power
<b>120 GeV Standard Main Injector Cycle</b>	NOVA / FT	1.5	0.01-100ms	2 MW	0.37 {1.87} MW
<b>60 GeV Rapid Cycle</b>	60 GeV nu	0.8 sec	10us - 50ms	2 MW	0.25 {1.75} MW
<b>30 GeV Rapid Cycle</b>	30 GeV nu	0.4 sec	10us - 50ms	2 MW	0 {1.5} MW
<b>8 GeV Long Pulse Directly From Linac</b>	e+/- or n	0.4 {0.1} sec	3 {1} msec	negotiable	0.5 {2.0} MW
<b>8 GeV Accumulation (MI or Recycler)</b>	BooNe	0.4 {0.1} sec	10 usec	negotiable	0.5 {2.0} MW
<b>8 GeV Continuous Spill (MI or Recycler)</b>	8 GeV FT	0.1-100 sec	0.1-100 sec	negotiable	0.5 {2.0} MW
<b>150 GeV Tevatron Injection</b>	1 Tev FT	1.8	10 usec	2 MW	> 1.95 MW
<b>150 GeV Collider Injection</b>	BTeV/VLHC	1.5	10 usec	40kW	> 1.95 MW

An **8 GeV Stretcher Ring Mode** is possible in which the Main Injector is rapidly filled by the Linac, and then the beams are slowly extracted to 8 GeV fixed-target experiments at a duty cycle approaching 100%. The MI tunnel also contains an 8 GeV storage ring (the Recycler) which can be also be used for this even while the MI is ramping to accelerate beam for other purposes. Since the Recycler has demonstrated a beam lifetime of >500 Hours and a dynamic aperture of  $60\pi \times 40\pi$  (HxV), it is equal to the Main Injector in this application. An interesting variant of this is progressive bunch-by-bunch extraction from the Recycler, using a fast pulsed kicker instead of resonant extraction, to provide a series of intense single bunches for muon experiments<sup>21</sup>.

A **Low Emittance Mode** is also possible. For normal high-current operations, the Main Injector will be filled via “phase space painting” (sect 20.2) during which the injected beam is deliberately mis-steered in orbit and energy to spread out the beam space charge and thereby obtain maximum possible circulating current. Alternatively, a smaller amount of beam can be injected on-orbit (and on-Energy) to obtain emittances more than an order of magnitude smaller than presently available in the Main Injector.

In either mode, a unique advantage of the H<sup>-</sup> linac is that the beam can be very cleanly collimated to remove halo immediately prior to MI injection. This makes use of a clever technique developed for the SNS at BNL<sup>22</sup> which passes the H<sup>-</sup> beam through a stripping foil with a hole in the middle of it as it passes through the transfer line from the Linac to the storage ring. Beam in the central  $\sim 3\sigma$  pass through the hole in the foil, and “halo” particles outside this hit the foil and are stripped, magnetically separated, and steered cleanly to the beam absorber.

### 2.3 Relevance to Future Accelerator Projects

The **International Linear Collider** (ILC) has recently chosen “cold” superconducting RF option which uses identical technology and components as the Proton Driver linac. A US-based ILC will likely require a percent-scale demonstration facility to convince federal agencies (and ourselves) that it will run reliably and that we know its cost per US accounting procedures. The construction of a 1.5%-scale LC demonstration facility would by itself cost several hundred million dollars, but would provide no High Energy Physics (HEP) user facilities at a time when they are greatly needed. On the other hand, the 8 GeV Proton Driver Linac represents a  $\sim 1.5\%$  scale test of the main linacs (the major cost component) of the Linear Collider, while simultaneously offering a compelling near-term HEP physics program. Thus it offers an affordable, near-term project with a prospect of the widest possible base of support inside High-Energy Physics. It also serves as a potential project around which to nucleate a US collaboration capable of building a Linear Collider.

The **Neutrino Factory and Muon Programs** will be given a major boost by the construction of the Proton Driver linac. With the addition of an accumulator ring, the Proton Driver linac can provide fast-extracted beams to drive muon storage rings, “Neutrino Factories”, and perhaps eventually muon colliders. In muon facilities, the same 8 GeV linac used for the proton driver could be used to accelerate the cooled muons, using multiple passes to reach 24-32 GeV. Finally, it provides the cost basis for the recirculating linac, one of the dominant cost items in proposed muon-based facilities. Other relevant scenarios have been considered<sup>23</sup>.

For the **Very Large Hadron Collider** (VLHC)<sup>18</sup>, the Proton Driver linac will produce extremely small emittances and high brightness proton beams. This allows high luminosities to be achieved at reduced beam current. The lower beam currents reduce the stored energy in the beams, one of the significant technical concerns with the VLHC. In a two-stage VLHC scenario<sup>24</sup>, in the first stage the small beam currents permit a smaller aperture magnet to operate with fewer concerns about beam instabilities. In the second stage (high-field) VLHC where synchrotron damping of protons becomes effective<sup>25</sup>, the Proton Driver linac allows injection of the beams at their final (synchrotron-damped) emittances, rather than waiting for the proton emittances to damp.

**Collaborations with Materials Science and Life Sciences Programs** might occur in two possible ways. Firstly, the 8 GeV Linac could be used to directly drive a Free-Electron Laser

(FEL), Neutron Source, or related facility on site at Fermilab. This would imply a large expansion of the FNAL user base into the non-HEP community. This represents a major change in focus for FNAL, but is compatible with Universities Research Association's mandate for operating Fermilab. Such an expansion of Fermilab's mission would have to be carefully negotiated inside the Office of Science.

Alternatively, the Proton Driver linac could provide a common technology base and standardized components for "little sister machines" at dedicated facilities at scattered sites. Laboratories interested in SCRF facilities, but lacking the technical and financial means to develop an entire SCRF linac, will be able to specialize in development and production of individual components for the collaboration, thereby reducing machine costs for all collaborators. This is the concept of the "ILC-compatible" beta < 1 linac design. By anchoring such a collaboration, Fermilab could obtain its own machine at reduced cost, while enabling forefront facilities to be developed for non-HEP applications at other laboratories.

In summary, the Proton Driver linac will serve simultaneously as a present-day particle physics tool and a useful base on which to build the US HEP program in a number of possible directions. It represents a useful facility whether the LC is built in the U.S or elsewhere; and thereby provides the guaranteed payoff for an aggressive SCRF development program targeting the International Linear Collider at Fermilab.

## **2.4 Superconducting RF Technology**

The advent of Superconducting Radio Frequency (SCRF) technology<sup>26</sup> has resulted in a significantly smaller cost-per-GeV for linacs<sup>28</sup>. The main reason for this is the reduction of the peak power demanded of the RF sources compared to normal-conducting copper linacs. For superconducting RF systems, the RF power to be delivered slowly to the RF cavities by an RF source of relatively modest peak power, and extracted slowly from the cavities with relatively modest beam currents. Although the efficiency for converting wall power to beam power with SCRF is still of order 30% (not much better than a heavily loaded warm copper linac), the installed cost of the RF power sources (which scales significantly with peak power) is greatly reduced. Furthermore, the lower level of peak power in the RF components associated with SCRF significantly eases their design and enhances reliability.

A decade ago CEBAF (now JLAB) demonstrated the basic reliability of SCRF in a large system environment, albeit with relatively low gradients and low DC beam currents.

Accelerating gradients also increased dramatically. A milestone was achieved in 1993 when a Cornell/Fermilab/DESY collaboration demonstrated that >20 MV/m could be obtained in a multi-cell superconducting cavity -- a result which cut the linac length by half compared to then-existing technology. Progress continues today, with experimental cavities at KEK, Cornell, and DESY using electropolishing techniques to approach 50 MV/m -- very near the theoretical limit of the materials. The Proton Driver design assumes an accelerating gradient of 26 MV/m in the main section of the linac -- slightly above the value assumed in the TESLA-500 design report. Like the ILC, the Proton Driver can benefit from (and will drive) the industrialization and development of higher-gradient SCRF cavities.

Recently two new projects have emerged which extended and document the SCRF technology: TESLA and the Spallation Neutron Source (SNS).

The successful international R&D for the TESLA collaboration has demonstrated reliable operation of significant numbers of high-gradient cavities, as well as important technical methods for distributing the RF and controlling cavity microphonics in a pulsed SC linac. The TESLA Technical Design Report<sup>19</sup> indicated that a new cost per GeV may be attainable with

these methods, which include high cavity gradients, cost-effective packaging of multicell cavities in low heat leak cryostats, and the RF fan out from one large klystron to up to 36 multicell cavities.

The importance of this last contribution to the feasibility of the Proton Driver linac cannot be overemphasized: since the 8 GeV linac requires 450 cavities at present day gradients, a traditional system with one klystron per cavity would require 450 klystrons and the proposal would be stillborn. The Proton Driver linac design described here requires only 11 klystrons for the main linac in the initial 0.5 MW configuration. There are technical issues in extending this technique to proton linacs, which are addressed in sections 5 and 11.

A major new contribution came from the Spallation Neutron Source<sup>27</sup> (SNS), which in 1999 adopted a superconducting 1 GeV  $H^-$  linac<sup>28</sup> as a less expensive alternative to a previously baselined warm copper linac. The beam physics issues associated with using SCRF in a proton linac were extensively investigated by the SNS prior to making the switch<sup>29</sup>. As a result of the SNS project, we will soon have an existence proof of the feasibility of the front end of a superconducting proton ( $H^-$ ) linac with beam parameters similar to the Ultimate configuration of the 8 GeV Injector linac.

In most design aspects, the Proton Driver linac can point to other SCRF projects with comparable or more challenging parameters. See Table 3.

Table 3- Comparison of the Proton Driver linac with other SCRF Pulsed Linacs

	<b>8 GeV Initial</b>	<b>8 GeV {Ultimate}</b>	<b>SNS (Spallation Neutron Source)</b>	<b>TESLA-500 (w/ FEL)</b>	<b>TESLA- 800</b>
Linac Energy	8 GeV	8 GeV	1 GeV	500 GeV	800 GeV
Particle Type	$H^-$ , $e^+$ , or $e^-$	$H^-$ , $e^+$ , or $e^-$	$H^-$	$e^+$ , $e^-$	$e^+$ , $e^-$
Beam Power	0.5 MW	2 MW	1.56 MW	22.6 MW	34 MW
AC Power (incl. warm FE)	5.5 MW	13 MW	~15 MW	97 MW	150 MW
Beam Pulse Width	3 msec	1 msec	1 msec	0.95 msec	0.86 msec
Beam Current(avg. in pulse)	8.6 mA	26 mA	26 mA	9.5 mA	12.7 mA
Pulse Rate	2.5 Hz	10 Hz	60 Hz	5(10) Hz	4 Hz
# Superconducting Cavities	384	384	81	21024	21852 / 2
# Cryomodules	48	48	23	1752	1821
# Klystrons	12	33	93	584	1240
# Cavities per Klystron(typ)	36	12	1	36	18
Cavity Surface Fields (max)	52 MV/m	52 MV/m	35 MV/m	46.8 MV/m	70 MV/m
Accelerating Gradient(max)	26 MV/m	26 MV/m	16 MV/m	23.4 MV/m	35 MV/m
Operating Frequency (MHz)	1300, 325	1300, 325	805, 402.5	1300	1300
Linac Active Length	614 m	614 m	258 m	22 km	22 km



Table 4 below lists the segment lengths, and output energies, and number of modules in each section of the linac.

Table 4 - Segment Lengths and Output Energies of the Proton Driver linac

LINAC SEGMENT LENGTHS		8 GeV Linac		
	Length	Eout	# Modules	
Ion Source (H- and P)	~0.1 m	0.065 MeV		
Low-Energy Beam Transport (LEBT)	~0.1 m	0.065 MeV		
Radio-Frequency Quad (RFQ)	~4.0 m	3.0 MeV	TBD	RFQ modules
Medium-Energy Beam Transport (MEBT)	3.6 m	3.0 MeV	4	Rebuncher Cavities
Room Temperature Front End (RT-TSR)	10.4 m	15.8 MeV	21	Room Temp 3-Spoke Resonators
SCRF Single-Spoke Resonator (SSR)	12.5 m	33 MeV	1	Cryomodules
SCRF Double-Spoke Resonator (DSR)	17.2 m	110 MeV	2	Cryomodules
SCRF Triple-Spoke Resonator(TSR Baseline)	64.0 m	400 MeV	6	Cryomodules
Beta=0.47 SCRF (Low Beta Elliptical option)	18.8 m	175 MeV	2	Cryomodules
Beta=0.61 SCRF (Medium Beta Elliptical Opt.)	38.5 m	400 MeV	4	Cryomodules
Beta=0.81 SCRF (High Beta Elliptical)	70.1 m	1203 MeV	6	Cryomodules
Beta=1 SCRF (1300 MHz "ILC" Main Linac)	438.3 m	8000 MeV	36	Cryomodules
<b>LINAC ACTIVE LENGTH *</b>	<b>613.6 m</b>	<b>8000 MeV</b>		
Transfer Line to Ring	972.5 m	8000 MeV	47	half-cells (quads)
Tunnel to Front End Equipment Drop	20.0 m			TBD
<b>TUNNEL TOTAL LENGTH *</b>	<b>1606.0 m</b>			

Either 3-Spoke  
or Elliptical for  
110-400 MeV

### 3.1 325 MHz Front-End Linac Overview

The front end linac consists of an H<sup>-</sup> ion source, Radio-Frequency Quadrupole (RFQ) with a 3 MeV output energy, a Medium-Energy Beam Transport (MEBT) section, followed by room-temperature and superconducting spoke resonators. The front end runs at 325 MHz (one quarter of the ILC's 1300 MHz frequency) so that while every RF bucket is occupied at 325 MHz, only every 4<sup>th</sup> RF bucket is occupied in the 1300 MHz main linac. The entire front end linac (up to 110 MeV) is driven by a single Klystron.

An aggressive R&D plan is being pursued for the Proton Driver front end tests at the SMTF / Meson Area<sup>30</sup>. The primary goals are to demonstrate the use of the TESLA RF split and Ferrite Vector Modulators in an SCRF proton Linac, to perform first beam tests of SCRF spoke resonators, to verify the expected beam emittances and halo reduction with solenoidal focusing.

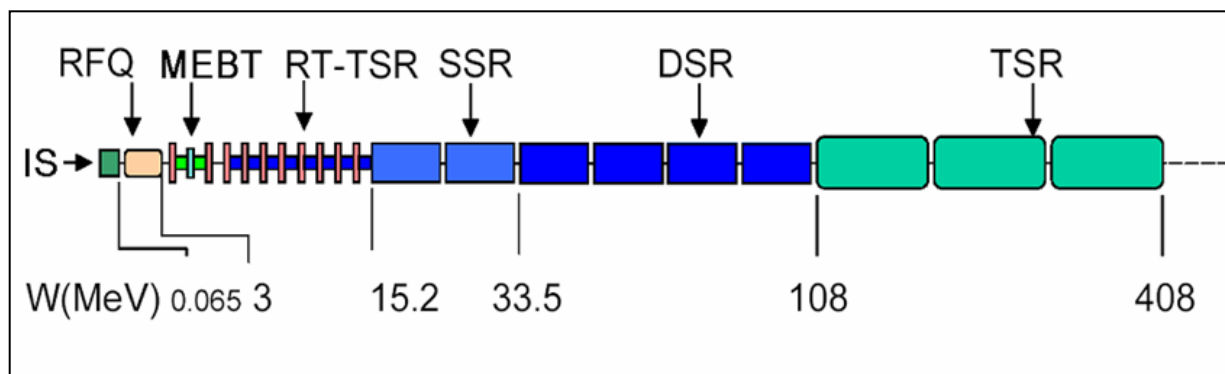


Figure 6 – Layout of the 325 MHz Front End Linac, which includes: the H- Ion Source (IS), Radiofrequency Quadrupole (RFQ), Medium-Energy Beam Transport (MEBT), Room-Temperature Triple-Spoke Resonators (RT-TSR), Superconducting Single-Spoke Resonators (SSR), Double-Spoke Resonators (DSR), Triple-Spoke Resonators (TSR).

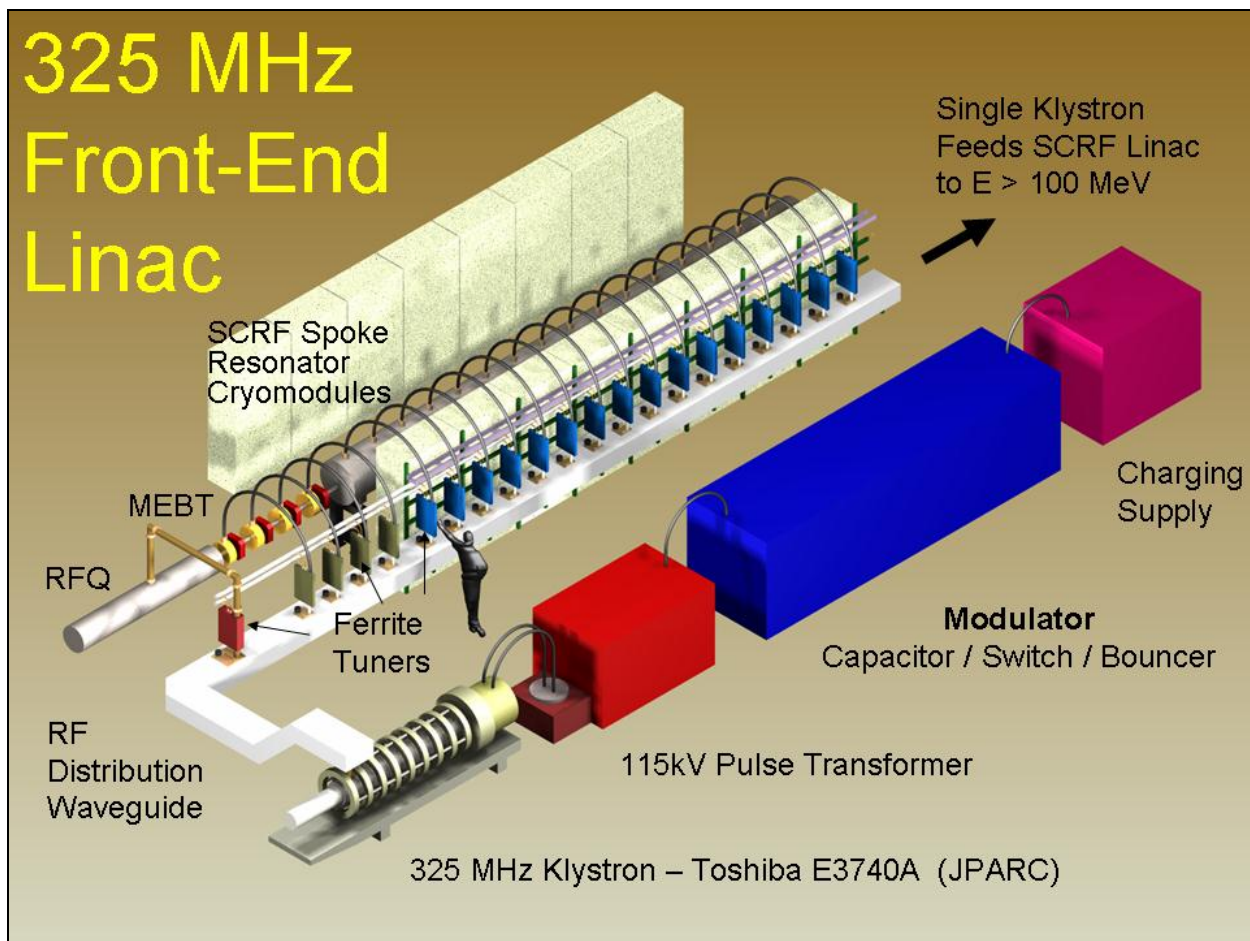


Figure 7- Schematic view of the 325 MHz front-end linac. A TESLA-style RF split drives many cavities, which allows a single 2.5 MW JPARC Klystron to drive the linac up to 110 MeV. Fast Ferrite Vector Modulators (FVM's) provide phase and amplitude control to individual cavities. The transition from warm copper to superconducting RF cavities occurs at 15 MeV.

## H- Ion Source

The H- Ion source (Figure 8) will be copied from the LBL/SNS, JPARC, or DESY designs. Specifications for the Ultimate configuration are 30 mA x 1 msec x 10 Hz, which is already exceeded by the LBL/SNS source which operates at 60 Hz. We have also collaborated with the SNS and to verify that their source operates well at the 10 mA x 3 msec pulse lengths needed for the baseline scenario. We plan similar long-pulse tests of the DESY H- source in the near future. Construction drawings for these devices are being obtained and we are in the process of choosing which H- source to clone for the SMTF/Meson proton driver front end test.

## Radio Frequency Quadrupole (RFQ)

The 325 MHz RFQ will be either a direct copy of the 324 MHz JPARC design, a frequency-scaled copy of the 402.5 MHz RFQ for the LBL/SNS front end, or a commercial procurement. We have obtained construction drawings for both the SNS and JPARC RFQs and are in the process of deciding which to replicate. Small changes in the details of the vane structure and overall length are planned (see sect 5.5).

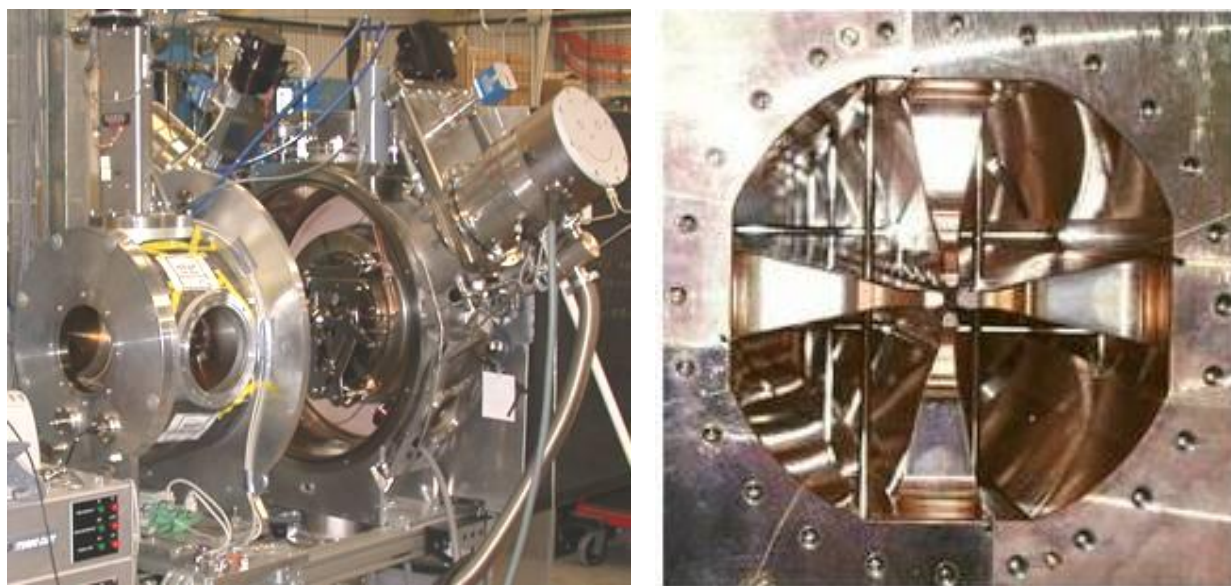


Figure 8 – H- Ion Source built by LBNL for the SNS, and the Radio Frequency Quadrupole (RFQ) built by KEK for the JPARC project. Both devices meet or exceed the specifications for the Proton Driver. We have obtained the construction drawings for these devices and plan to copy either these, or similar devices from DESY, for the Proton Driver front end tests at SMTF.

### **Medium-Energy Beam Transport (MEBT) Section**

This section performs matching and analysis of the 3 MeV output beam of the RFQ. Two bunching cavities (325 MHz warm copper spoke resonators) are used to maintain the longitudinal beam structure. The MEBT design also contains a beam chopper to generate the Main Injector beam extraction gap, and optionally also chops the beam to synchronously fill the 53 MHz RF buckets in the Main Injector.

Transverse focusing in the MEBT and following sections is provided by superconducting solenoids. It is expected that these will have significantly better properties with regard to emittance growth and beam halo formation than the quadrupole focusing normally used. The RFQ output section has been designed to produce an axisymmetric (round) beam at its output to match into this solenoidal focusing.

A flexible alignment rail system (Figure 9) is planned to allow module-by-module commissioning and convenient reconfiguration and replacement of beamline components and diagnostics. This modular system could allow experimental tests of the specific predictions of beam simulation codes about conditions under which emittance growth and beam halo formation occurs.

### **Room-Temperature Spoke Resonators (RT-TSR) Linac**

Room-temperature triple-spoke resonators (RT-TSRs) are used to accelerate the beam from 3 to 15 MeV. Each room temperature tank (Figure 10) is individually tailored to the proton velocity as the beam is accelerated. The room temperature cavities are interleaved with

superconducting warm-bore solenoids cooled via pool boiling from an overhead 2-phase helium distribution line. See Figure 9.

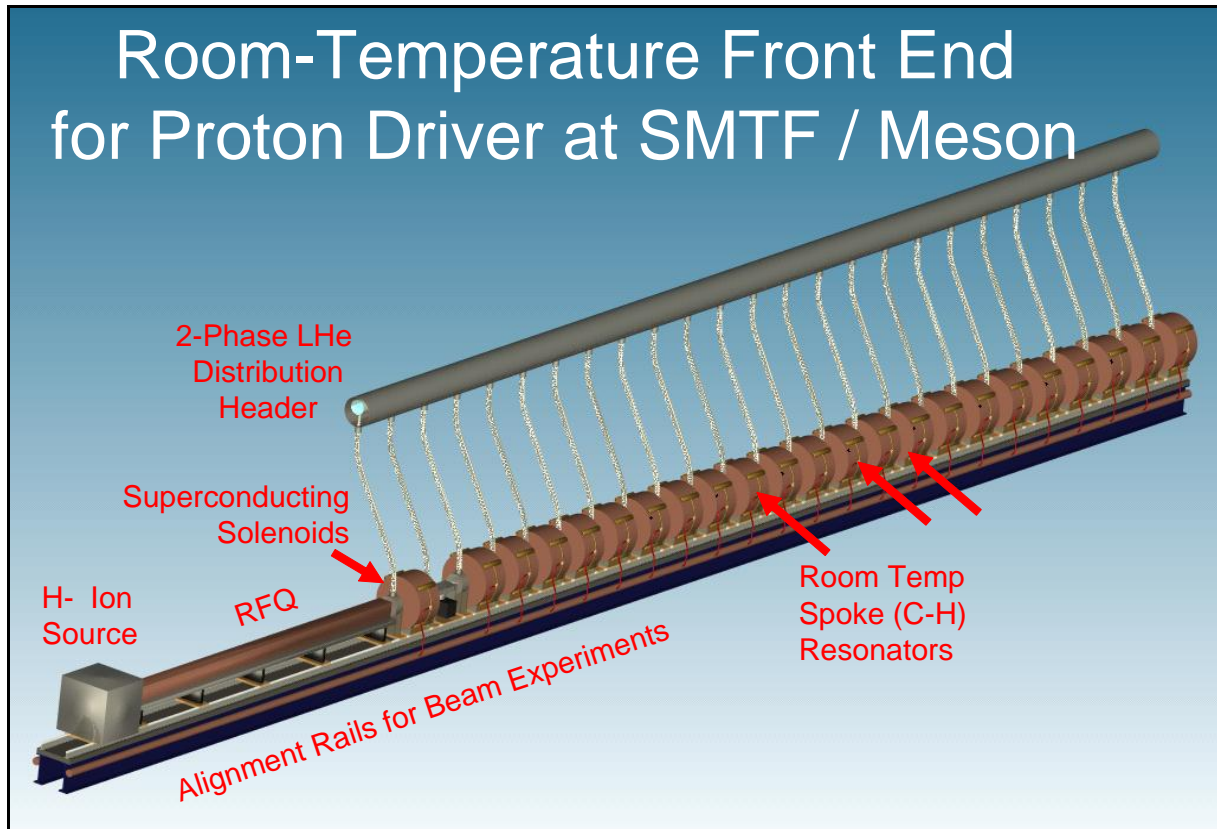


Figure 9 – Layout of the front end components of the Proton Driver linac.

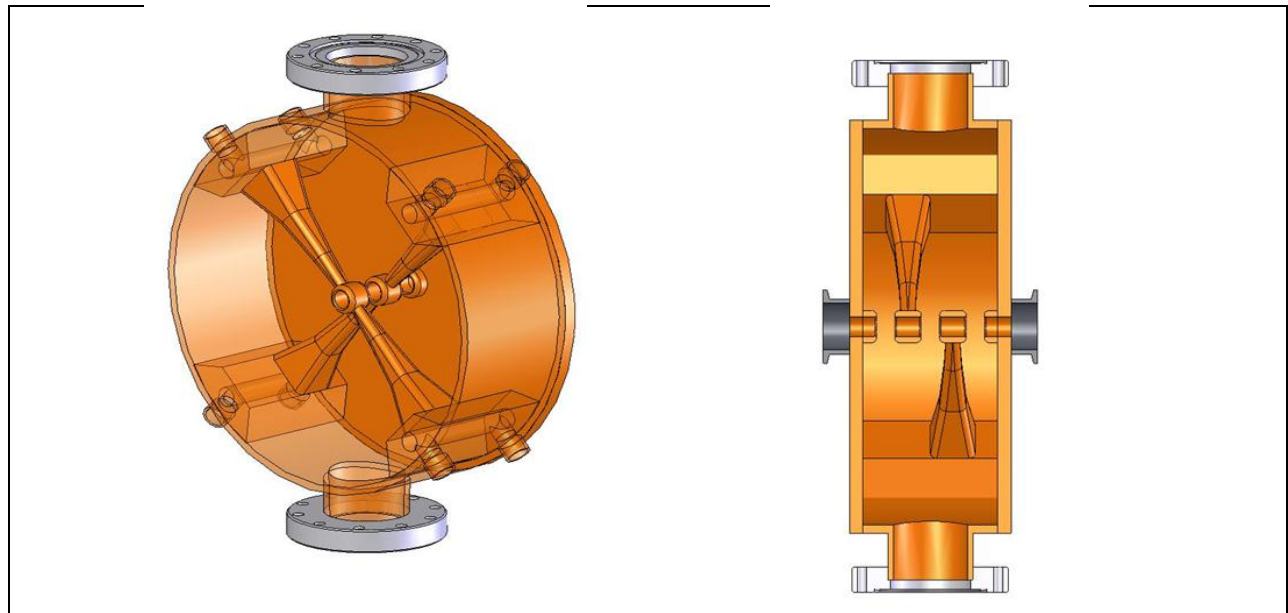


Figure 10 – Room-Temperature Triple-Spoke Resonators (RT-TSR) cavities designed for the Proton Driver Linac.

### 3.2 SCRF Spoke Resonator Linac Overview

Superconducting spoke resonators are used starting at 15 MeV. The resonators are similar to those developed for the RIA and APT projects (see Figure 11), but are operated in pulsed mode at 325 MHz. A single cryomodule containing 16 single-spoke resonators and 16 cold-bore superconducting solenoids accelerates the beam to 33 MeV. Two more RIA-style cryomodules containing 14 double-spoke resonators and solenoids accelerate the beam to 110 MeV. A pool boiling 4.5 K cryogenic distribution system is included in each cryomodule. A cold-to-warm transition and warm gate valve is included at the end of each cryomodule.

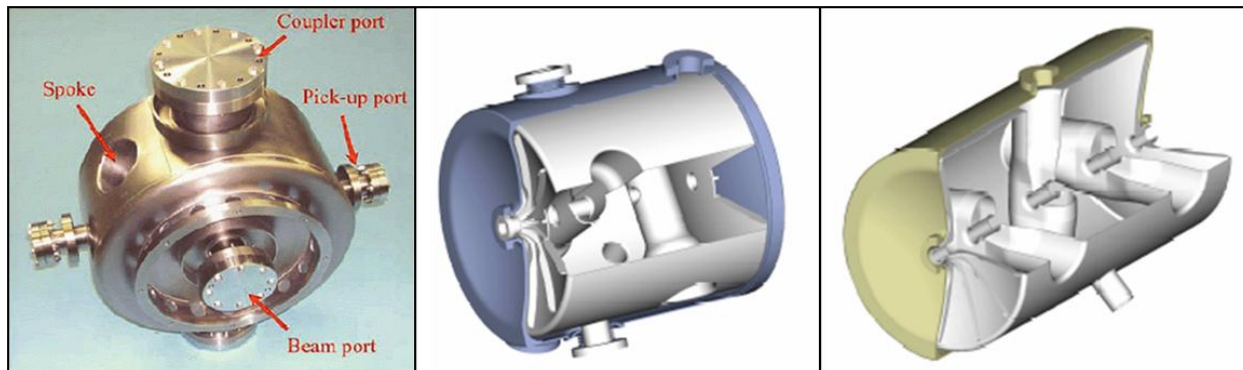


Figure 11 – One, Two and Three-Spoke SCRF Resonators for the APT and RIA Projects

### Spoke and Elliptical Options for the Medium- $\beta$ SRF Linac

In the energy range 110 - 400 MeV the baseline design uses 325 MHz superconducting triple-spoke resonators similar to the single and double spoke resonators of the front-end SCRF linac. A single modulator feeding 325 MHz klystrons drives six 10 m long cryomodules containing a total of 42 triple-spoke resonators. Focusing in this section is provided by superconducting quadrupoles spaced between every two cavities. This is the baseline design for both accelerator physics simulations and cost estimates. An alternative design for this energy range based on TESLA-style 1300 MHz elliptical cavities is discussed in the next section.

### 3.3 1300 MHz Elliptical Cavity SCRF Linac Overview

The elliptical cell SCRF linac uses 1300 MHz cavities, klystrons, RF couplers, and cryomodule cross sections copied from the TESLA (TTF3) design for the International Linear Collider. It is divided into four sections with different cavity and cryomodule designs.

**$\beta = 1.0$  Main Linac.** This section (~85% of the Proton Driver linac) is an exact copy of the TESLA (TTF3) design. It contains 8 copies of the TESLA RF unit (36 cavities driven by a single Klystron) and accelerates the beams from 1.2 GeV to 8 GeV. These 9-cell cavities are optimized for a geometric beta of 1.00 and are capable of accelerating both protons and electrons. An accelerating gradient of 26 MV/m (slightly higher than 24.5 MV/m of the TESLA-500 design, but lower than the 31-36 MV/m under discussion by the ILC<sup>31</sup>) is assumed.

**$\beta = 0.81$  Elliptical Cavity Linac.** Between 0.4 and 1.2 GeV the linac uses a single ILC Klystron to drive “squeezed TESLA” SCRF cavities optimized for protons with relativistic  $\beta = 0.81$ . A total of 48 eight-cell cavities are contained in six identical cryomodules.

**$\beta = 0.47$  and  $0.61$  Elliptical Option.** The energy range between 110 MeV and 400 MeV is covered by 325 MHz spoke resonators in the baseline design. An alternative design using 1300 MHz elliptical cavities with geometrical  $\beta = 0.47$  and  $0.61$  is also feasible and has been developed. This section contains a total of 48 Cavities in 6 cryomodules (see Figure 12). Both options use six cryomodules approximately 10 m long driven by a single modulator. At our present level of understanding the beam dynamics of either choice appear workable, and the final choice will be based on economic considerations.

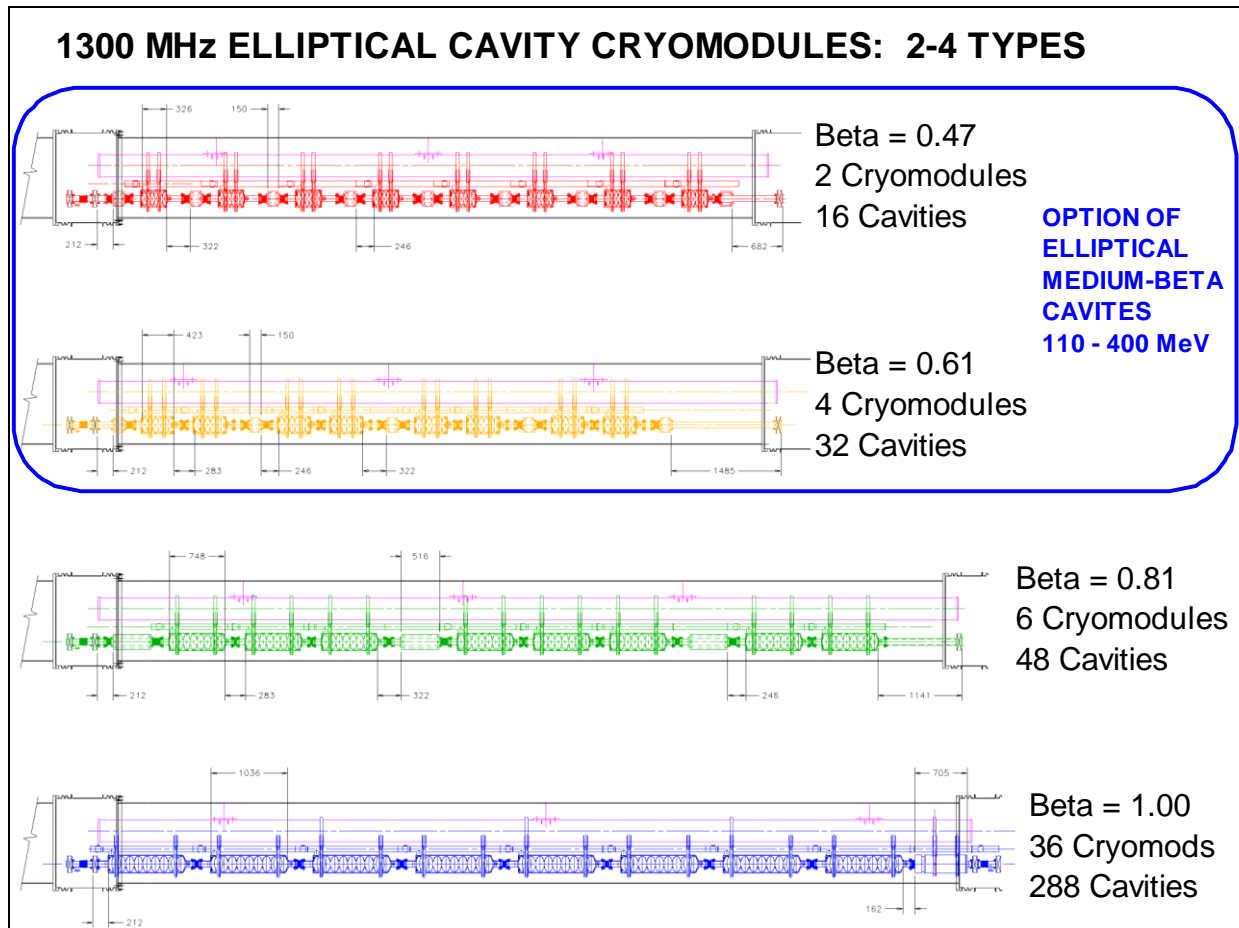


Figure 12 - 1300 MHz Elliptical Cavity Cryomodules for the Proton Driver. The Main Linac uses 36 standard TESLA (TTF3) cryomodules containing 288 standard  $\beta=1.00$  9-cell TESLA cavities. The “high beta” section contains six cryomodules with 8-cell cavities optimized for protons with  $\beta=0.81$ . The two lower  $\beta$  cryomodule types are a design alternative to the triple-spoke cavities of the baseline design.

As in the TESLA design, transverse focusing is provided by superconducting quadrupoles between the cavities. A quadrupole is located between every cavity in the  $\beta = 0.47$  cryomodules, and between every second, third, and 8<sup>th</sup> cavity in the  $\beta = 0.61$ ,  $\beta = 0.81$ , and  $\beta = 1.00$  sections.

### 3.4 RF Power Systems - Overview

The Proton Driver Linac has two RF systems (see Figure 5):

- 1) A 325 MHz front-end RF system drives the Radio Frequency Quadrupole (RFQ) and the Front End Linac. In the initial baseline configuration, a single modulator and a single 325 MHz, 2.5 MW klystron is used to power the entire front end linac up to an energy of 110 MeV. A second RF station (one modulator with 1-2 Klystrons) feeds the 3-spoke resonator in the energy range 110-400 MeV. The use of superconducting RF reduces the number of Klystrons needed to cover this energy range by about a factor of 3-5 compared to a warm-copper linac. The 325 MHz distribution system uses a TESLA-style RF power split and electronically controlled ferrite tuners to provide individual RF phase and amplitude control at each cavity.
- 2) A 1300 MHz Main Linac RF system is driven by 9 TESLA Multi-Beam klystrons (MBKs) (Thales TH-1801 or equivalent). The first two RF stations use “fast ferrite tuners” to independently control each cavity. The final 7 RF stations (above 1.8 GeV) use a passive RF power split and “vector sum regulation” (sect. 13.4) to control the beam energy. Additional “slow” ferrite phase shifters are required at each cavity if acceleration of both  $e^+$  and protons/ $H^-$  on alternate cycles is required. This option (not in the baseline) is described in Appendix 1.

A standard TESLA modulator (FNAL/TTF, 17 MW peak, 300 kW avg.) is used throughout. This standardization is a major strength of the 8 GeV Linac concept: there is a single type of pulsed power source for the entire linac. The modulators are built to be reconfigurable for either the Initial baseline (3 msec x 2.5 Hz) or Ultimate {1 msec x 10 Hz} beam pulse.

### RF Power Upgrade to Ultimate Configuration

The upgrade path to Ultimate 2 MW linac beam power is largely an RF power upgrade. This is accomplished by tripling the number of Klystrons and thereby tripling the peak RF power delivered to the beam. All RF components in the Initial configuration are therefore designed to handle the 3x higher RF power of the Ultimate configuration. The present versions of the ILC RF components, including the power coupler, can handle this.

### 3.5 Civil Construction Overview

Major components of the proposed civil construction<sup>32</sup> (Figure 13 and Appendix 3) for the Linac Proton Driver are as follows:

1. A **Beam Line Enclosure** ~ 5411 ft long houses the Linac and the Transport Line to the Main Injector. This is a concrete enclosure at Main Injector depth. The upstream 2200 ft Linac Enclosure is 11 ft high x 15 ft wide. The 3211 ft long Transport Line Enclosure is 8 ft high x 10 ft wide, and is comprised of an “S” of two reverse (848 ft each) arcs with 34 dipoles in each arc for momentum collimation. A straight section 848 ft m long is inserted between the two arcs to position the linac with respect to the Main Injector, and a matching straight is placed on each end of the “S”.
2. An above-grade **Klystron Gallery (L-1)** ~ 2200 ft long houses the klystrons, modulators and ancillary electronics. This building is on the surface parallel to the Linac Tunnel. Radiation shielding from the tunnel is sufficient to allow beam-on access to the klystrons and electronics.
3. An underground **Linac Beam Absorber Enclosure** comparable in size to the Main Injector absorber enclosure is provided at the end of the linac to allow test and commissioning of the linac independent of Main Injector operations.
4. An **Upstream Service Building (L-0)** comparable in function to the Main Injector MI-60 Service building is planned to provide access to the Linac Tunnel and for transport of large equipment. A limited amount of technician space and spare equipment storage is provided. It is connected to the Klystron Gallery.
5. A **Cryogenic Service Building (L-10)** is used to cool the superconducting linac and provide cooling water for the high-power RF electronics. This is comparable to the cryogenic plant of the Spallation Neutron Source (SNS). It is located across the access road at the midpoint of the Klystron Gallery, and access under the road for a cryogenic transfer line will be provided to the Linac Tunnel.
6. A **Pump Service Building (L-11)** also located at the midpoint of the Linac to house LCW pump equipment and heat exchangers. It will be integral to the Klystron Gallery, and will provide access to the enclosures below.
7. A **Center Service Building (L-25)** located north of the enclosures will provide personnel and equipment access via an enclosure that intersects the Transfer Line Enclosure near its upstream end. The building crane and hatch will be sized to handle cryomodules and magnets.
8. An **Arc Service Building (L-23)** located at the midpoint of the eastern “S” arc will house some of the arc corrector supplies. Access will be from Old Kautz Road.
9. A **Debuncher Service Building (L-42)** comparable to a Main Injector power supply building is located along the Transport Line to provide electrical services (klystron,

modulator) to the Debuncher cavities. The single arc dipole supply and the single arc quad supply will be located here, as well as some of the arc corrector supplies.

10. The **6.5 MW required operating power** for the facility will be supplied through 10.3 MVA of installed power fed from the Master Substation via a combination of existing and new duct banks. New duct banks will be sized to support the Ultimate upgrade to 14.8 MW wall power. Backup power for the conventional and machine power is accomplished via new duct banks from Kautz Road Substation (KRS). Backup power is already available via existing feeders for cryogenic power from KRS.
11. **Process Cooling for 2 MW** will be accomplished via existing cooling capacity at the Central Utility Building (CUB) with new piping to the facility. Cooling for the Cryogenic plant will be provided by local evaporative coolers.
12. Significant **Site Work and Infrastructure Improvements** are planned including new roads and parking lots, primary services, erosion control and wetland mitigation.
13. **Exit Stairs** provide egress at spacings similar to the Main Injector and SNS exit stairs. Exit stairs will discharge to the surface and in most cases also provide indoor direct access to a service building from the beamline enclosure.

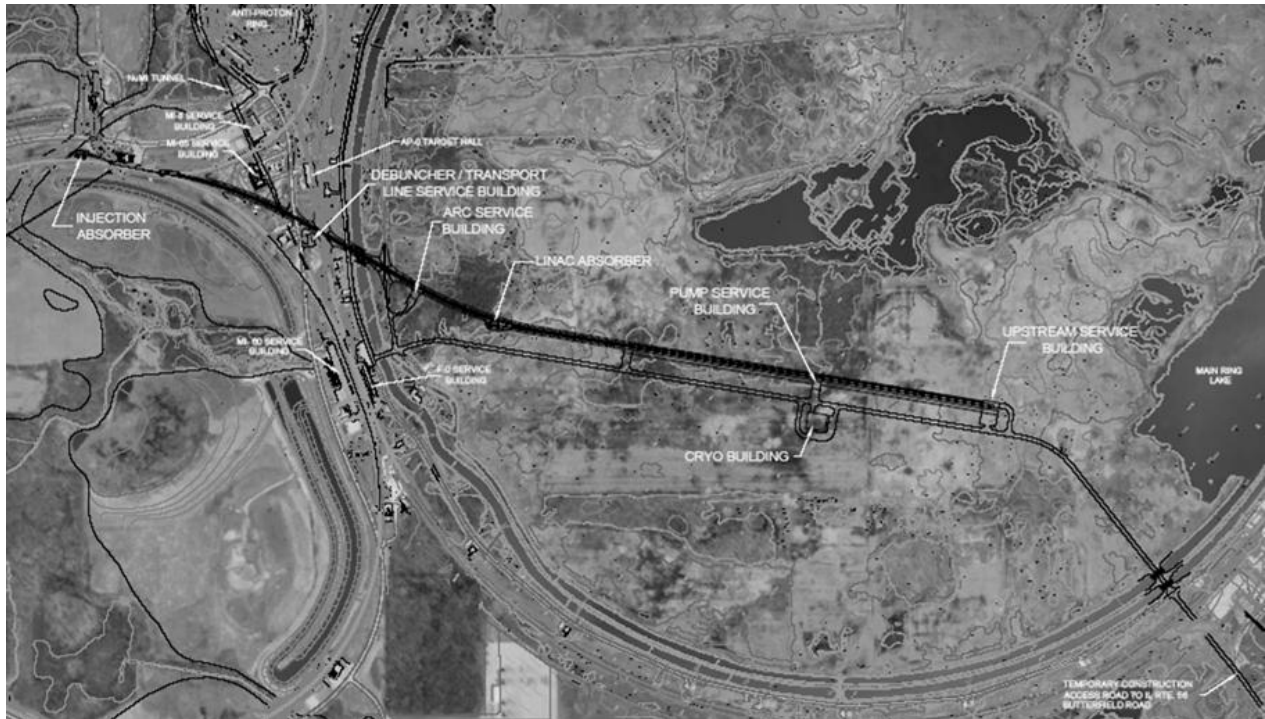


Figure 13 - The baseline site for the 8 GeV SCRF Proton Driver is inside the Main Ring and connects to the MI-10 straight section of the Main Injector. The cryogenics/LCW building is located near the midpoint of the linac. No new cooling ponds are needed for the baseline linac configuration. Appendix 3 contains a more detailed set of civil construction drawings.

The overall scale of the Proton Driver Civil construction is comparable to that of the Fermilab Main Injector (see Table 5).

Table 5 - Rough comparison of 8 GeV Linac and Main Injector Civil Construction

		Main Injector	8 GeV Linac	%
<b>Tunnel Length</b>	<b>meters</b>	4000	1600	40%
<b>Surface Buildings</b>	<b>sq. ft.</b>	60000	82000	137%
<b>Surface Area for Site Prep</b>	<b>acres</b>	50	30	60%
<b>Excavated Volume</b>	<b>cu. yd.</b>	475000	332000	70%
<b>Concrete Volume</b>	<b>cu. yd.</b>	40000	38000	95%
<b>AC Power &amp; Heat Rejection</b>	<b>MW</b>	22	6.5	30%

### 3.6 Site Selection

The baseline mission of the Proton Driver linac as an  $H^-$  injector requires a ~650 m straight linac section pointed approximately at one of the Main Injector straight sections. This length can be extended to 700 m if one allows for an additional RF station either for an energy upgrade or to provide performance margin on cavity gradients. The transfer line to the MI should be at least 300 m long for the debuncher drift (more is better), and must also contain a bend of 10-20 degrees for momentum collimation. (These last two are “soft” numbers, since the performance of the Debuncher and collimation improves continuously with increasing drift length and bend). A minimum 700 m radius of curvature must be maintained in the transfer line to avoid stripping the  $H^-$  beam (section 5.17) if one wishes to preserve the possibility of upgrading the Linac to 9-10 GeV. Auxiliary transfer lines, if any, for electrons and protons may contain sharper bends.

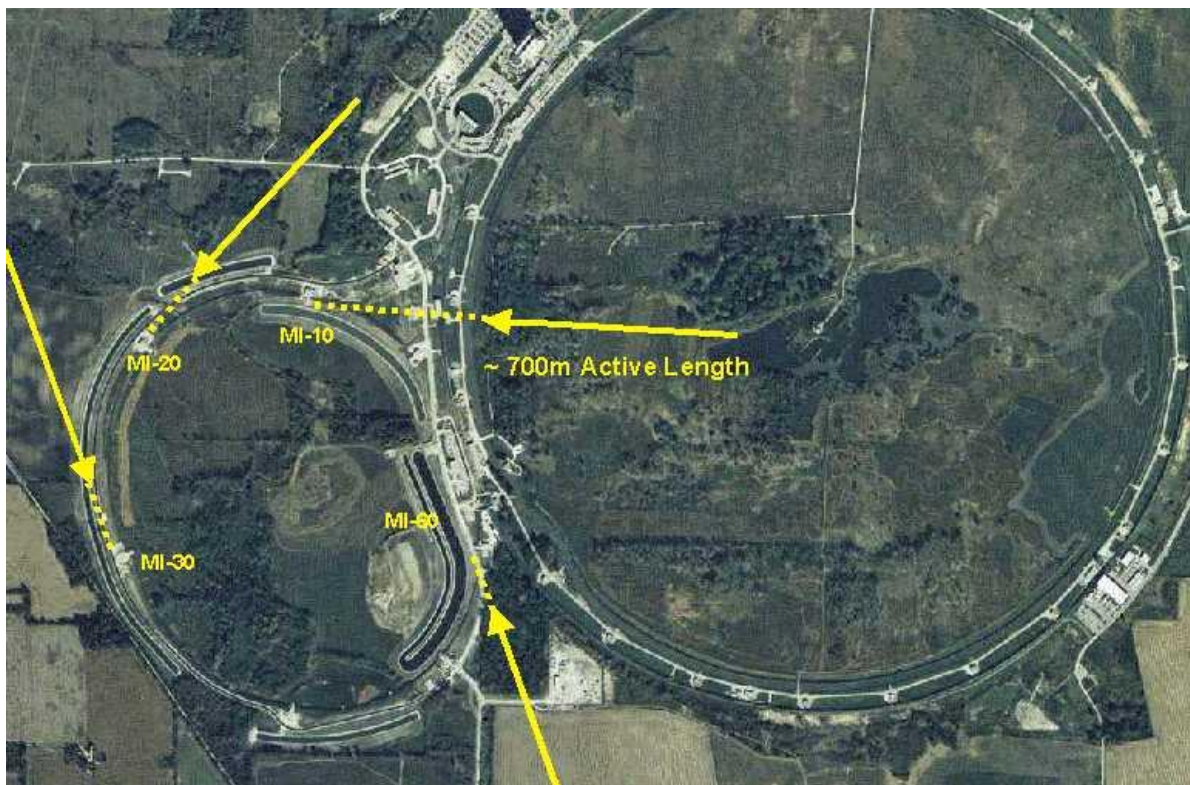


Figure 14 - Some possible 8 GeV Injector linac sitings tangent to Main Injector straight sections. The siting inside the Main Ring is chosen for this study. The initial linac site study<sup>3</sup> was based on the MI-30 injection point at left.

The initial (2001) Design Study<sup>3</sup> chose the MI-30 injection point because of the simplicity of civil construction in the undisturbed farmland. This site had no radiological issues with nearby beam lines, and a minimum of wetland mitigation. This makes the civil construction cost estimate straightforward. The major drawback of this site is that it lies near the Fermilab site boundary, which makes it difficult to develop beam lines supporting future missions for the linac.

This study chose the more flexible (and complicated) siting shown in Figure 15 below. This site could eventually support many of the secondary missions shown in Figure 3. The injection point near MI-10 would allow the beams to be either injected to the MI/ Recycler or sent directly to the BooNe 8 GeV neutrino beam line(s). The transfer line goes underneath the Main Ring tunnel and the AP2 line and over the NUMI tunnel. It is impossible to retain radiological separation of the Main Ring and Proton Driver transfer line tunnels, so the Main Ring F-sector will have to remain interlocked as it currently is during Main Injector operations.

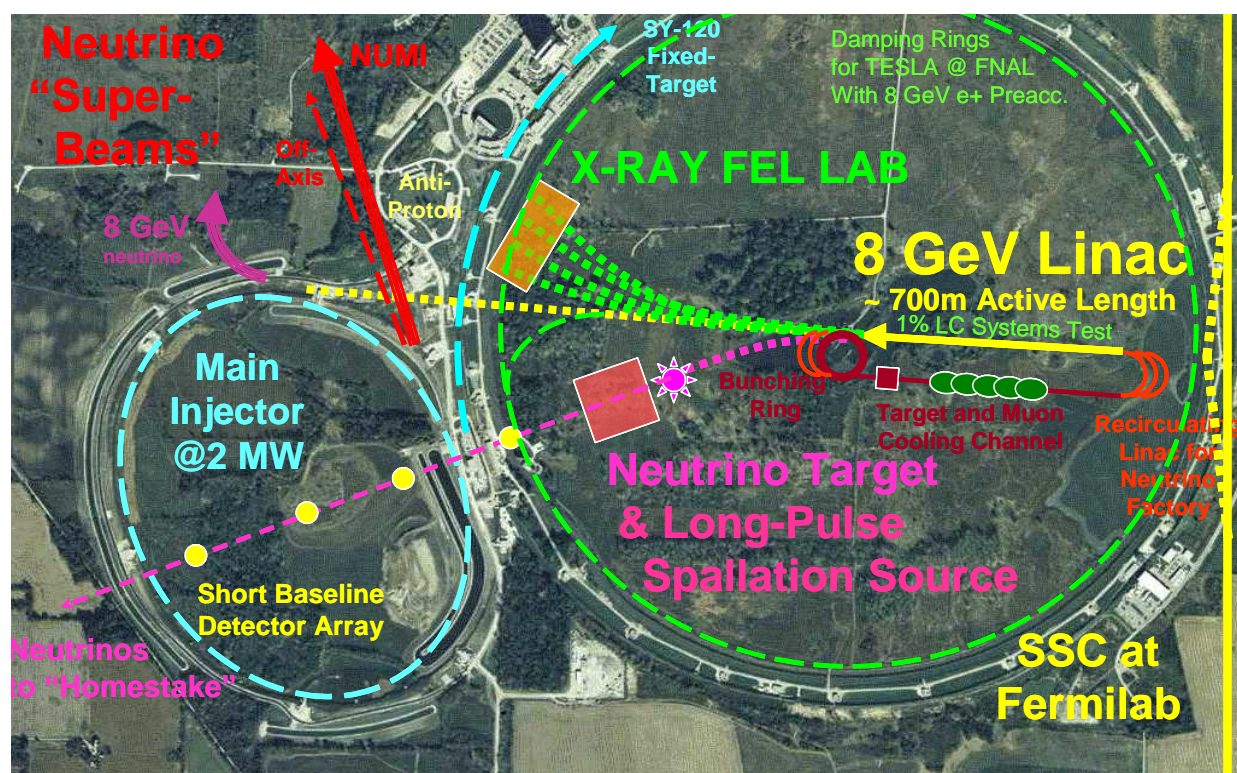


Figure 15 – The multi-purpose siting chosen for this 8 GeV injector linac design study. Alternative missions for the 8 GeV linac are discussed in Appendix 1.

By extending the transfer line and moving the linac eastwards and to the center of the Main Ring, a multi-species switchyard complex could separate the  $H^+$ , electron, and proton beams to target areas which could include FEL labs, 8 GeV neutrino and neutron facilities, future muon facilities, and so on (see Appendix 1). This siting is more expensive in initial implementation than the original MI-30 siting, but offers much greater flexibility for future site development.

One potential disadvantage of the MI-10 injection point is that the existing Booster-to-MI injection hardware must be removed for linac injection. However the Booster-to-Recycler connection<sup>33</sup> which will be used for high-intensity operations of the MI prior to Proton Driver construction can remain intact to permit simultaneous “parasitic” commissioning of the linac.

### 3.7 One-Tunnel vs. Two-Tunnel Machine Layout

The cost of the TESLA linac is significantly reduced by the single-tunnel layout<sup>34</sup>, which places the Klystrons, control electronics, RF distribution, power, and cooling in the same tunnel as the main linac. Cost savings accrue not only in the civil construction, but also in the technical interconnections (microwave chases, cable trays, etc.) between the tunnels. The penalty for this cost reduction is that none of this equipment is serviceable or diagnosable with the beam on, and rad-hard electronics must be used in the tunnel. This has implications for machine availability and operating costs.

Like the ILC baseline, the single tunnel layout was NOT adopted for this design study. Instead, additional costs are incurred for an independent Klystron Gallery, with microwave and cable chases between the tunnels, separate LCW and HVAC systems, etc.

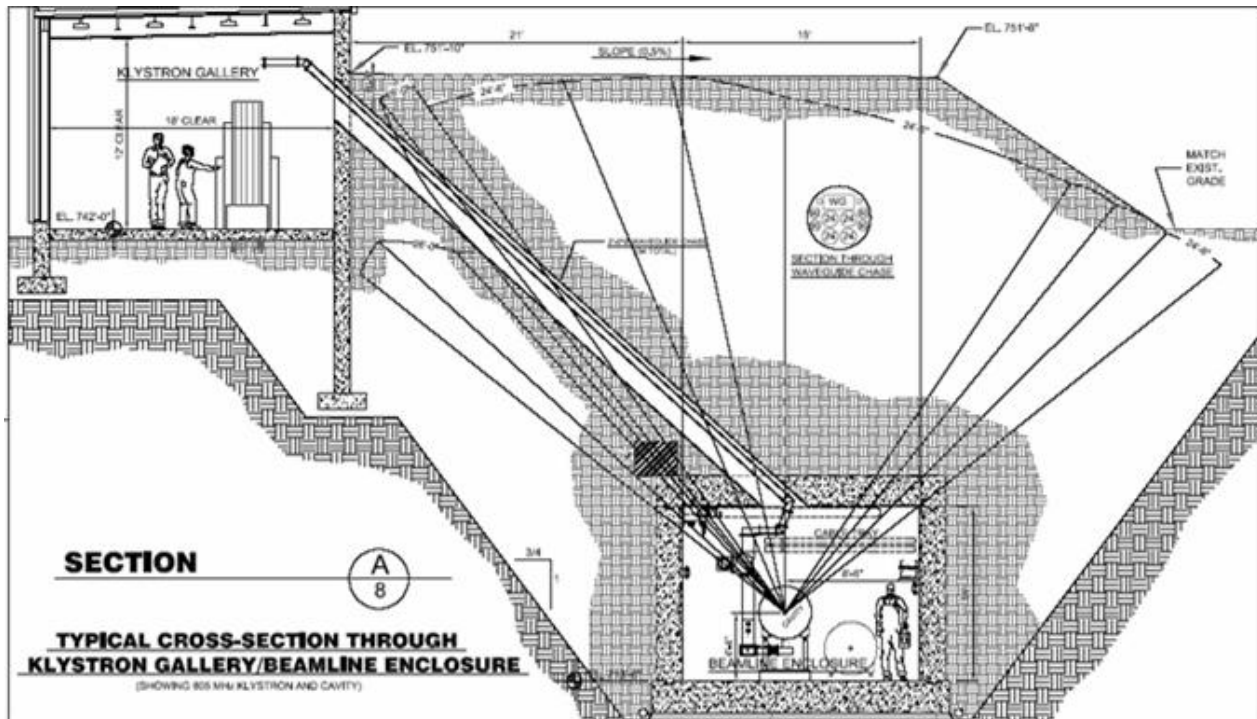


Figure 16 - Two-tunnel layout with above-ground Klystron Gallery. The Proton Driver linac beam line tunnel is Main Injector depth and constructed with the “cut and cover” technique. The klystrons are located in a separate gallery to permit beam-on access. Microwave chases and cable ducts connect the two tunnels every ~60 feet.

### 3.8 Above-ground Klystron Gallery

A Klystron Gallery on the surface was chosen to house the Klystrons, modulators, and control electronics, rather than the more expensive alternative of a second underground tunnel that was chosen for the first design study. One might revert to the two-underground-tunnel configuration to provide a more realistic mockup of the civil construction for the Linear Collider, which is so long that a surface gallery is probably not feasible. The gallery ceiling height was chosen to allow in-situ replacement of a vertical klystron without moving the oil tank/ transformer assembly. This ceiling height could be reduced if the ILC or TESLA Technology Collaboration succeeds in developing side-mounted versions of the multi-beam Klystron.

### 3.9 Tunnel Depth and Shielding

The entire length of the Proton Driver linac and H- transfer line is located at Main Injector depth. This shielding depth is adequate for 2 MW operation of the Main Injector<sup>35</sup>. This shielding requirement is probably excessive from two points of view. Firstly, the beam power available for accidents rises linearly along the length of the linac and is only 2 MW in the transfer line at the end of the linac. Tapering the shielding along the length of the Linac will be allowable.

Secondly, any beam losses approaching the MW level in the main linac would cause immediate heating, cryogenic disruption, and quenching that would rapidly trip off the main linac. Analysis and documentation of those beam loss scenarios which are physically possible would lead to reduced tunnel shielding requirements and the possibility of reduced excavation and construction costs. This argument does not apply in the room-temperature transfer line, where the full Main Injector depth will be necessary to preserve unlimited occupancy of the berm immediately above the beam line.

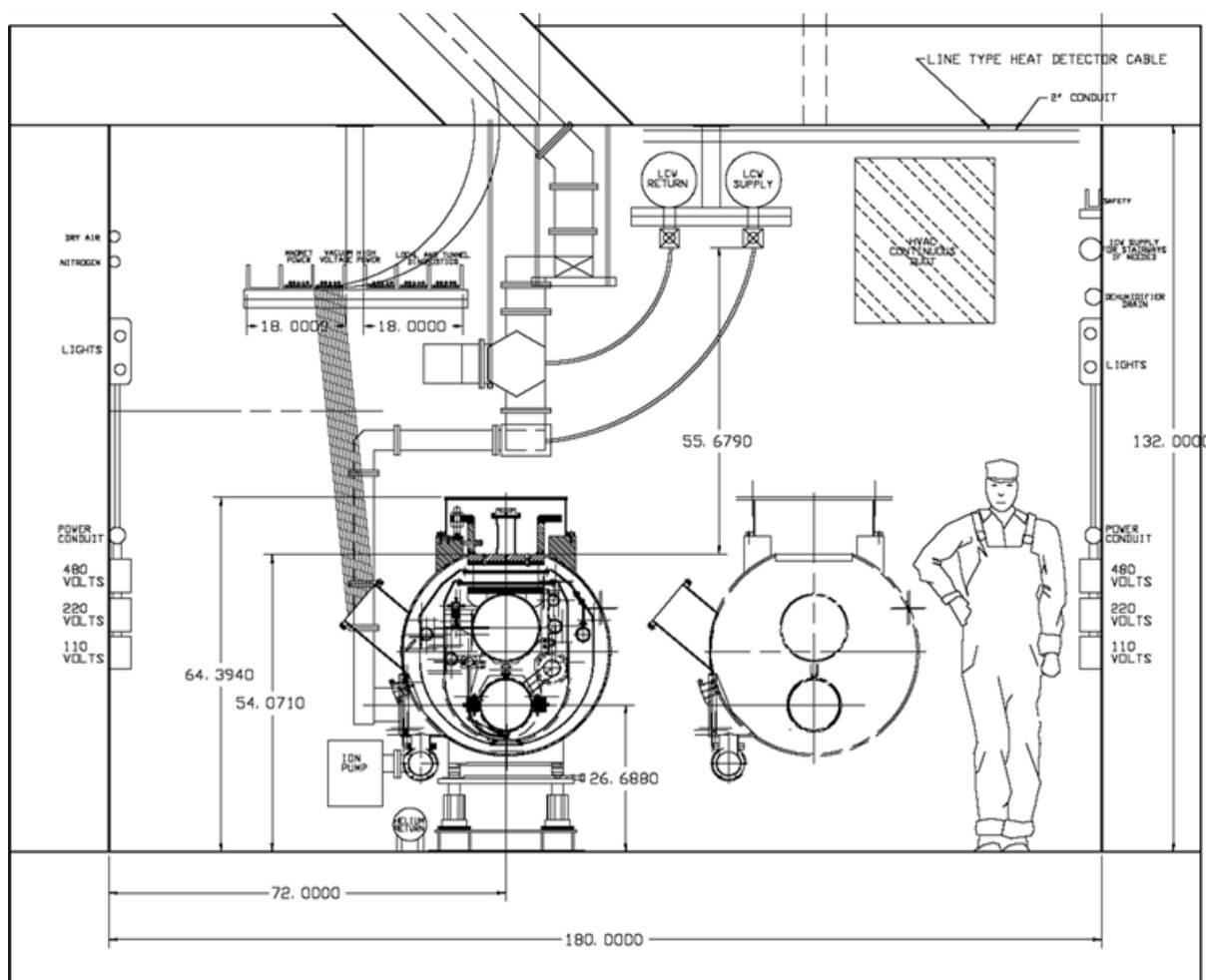


Figure 17 – Main Linac Tunnel w/equipment and personnel access. The 11' high x 15' wide tunnel is one foot higher and one foot wider than the SNS tunnel. Both the floor and the beam line are at Main Injector height. A main service aisle for both personnel and equipment transport is provided on one side of the cryomodules, and an equipment access area is provided on the other. Microwave guides and cable conduits penetrate through the ceiling to avoid obstructing non-aisle side access to beamline components (as is the case in the SNS tunnel).

### 3.10 Main Injector Upgrades

In addition to the 8 GeV Injector linac, operating the Main Injector at 2 MW requires:

- 1) An 8 GeV Transfer line to the Main Injector (section 19),
- 2) H- collimation systems to remove halo before MI injection (sections 19.8 - 19.9),
- 3) H- Foil Stripping Injection system at the MI-10 location (section 20),
- 4) New RF systems in the Main Injector (section 25) and PAC2005 paper<sup>36</sup>,
- 5) Betatron<sup>35</sup> and Momentum<sup>37</sup> Collimation systems for in the Main Injector.

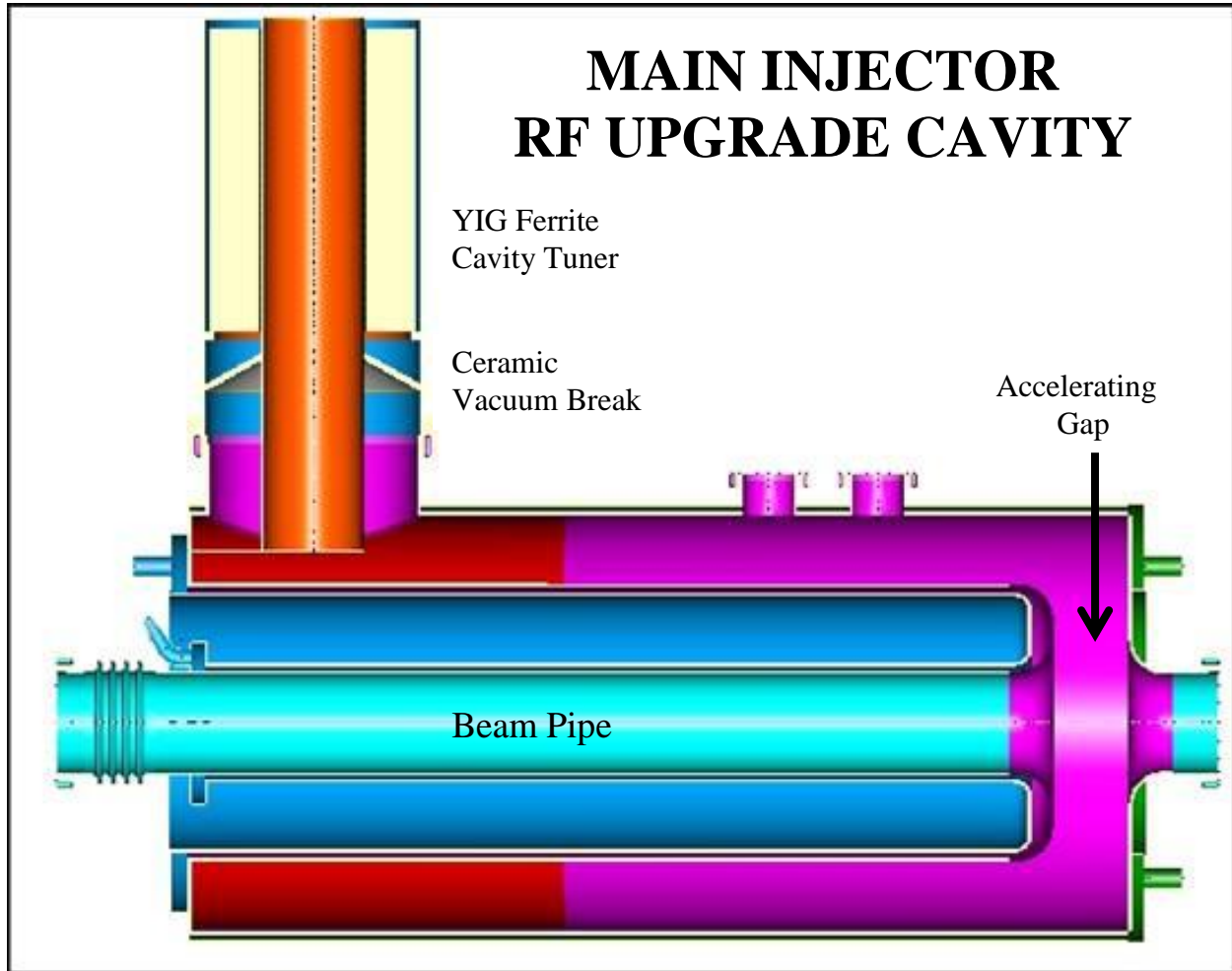


Figure 18 - Main Injector RF Upgrade Prototype Cavity to support > 2 MW beam power from the Main Injector (see section 25). This is a low R/Q design to minimize the effects of beam loading at high currents. The tuner for this cavity uses the same YIG Ferrite tuners as the coaxial phase shifters for the Ferrite Vector Modulators for the Proton Driver Linac. The Proton Driver R&D has been funding initial development of this cavity.

## 4 CHOICE OF PRIMARY PARAMETERS

### 4.1 Beam Energy

The Beam energy of 8 GeV was specified by the charge for the design study<sup>3</sup>, to provide a “drop-in” replacement for the existing Booster. This choice appears to be near optimal.

Lower linac energies might be considered in staging scenarios. Low-intensity beam has been decelerated below 6 GeV<sup>38</sup> in the Main Injector. The magnetic field quality remains good down to 5 GeV and perhaps below<sup>39</sup>. The space charge tune spread limit is not saturated at 8 GeV and 5x MI Design beam current. However, the RF cavities would need additional tuners to provide the frequency swing needed for beam energies below 8 GeV, and some accelerating voltage would be lost. Thus it is possible but not likely that initial low intensity commissioning could take place at lower energies. This is discussed further in Appendix 4.

Upgrading the H<sup>-</sup> injection energy above 10~12 GeV becomes very difficult due to H<sup>-</sup> stripping in magnetic fields (Sect. 5.17). The radius of curvature of the momentum collimation bend in the transport line sets a hard upper limit to the energy upgradeability of the facility as an H<sup>-</sup> injector. The baseline design uses 500 Gauss dipoles and can not be run with H<sup>-</sup> above ~10 GeV.

For protons the H<sup>-</sup> stripping limit does not apply. Thus for example if all cryomodules including the “Upgrade” RF station are filled with cavities meeting it the ILC R&D target gradients of 45 MV/m, the “8 GeV Neutrino Program”, or a multi-mission electron-based program, might be run with energies up to 15 GeV.

### 4.2 Beam Charge per Pulse

The charge for the design study specifies a total of  $1.5 \times 10^{14}$  protons (25  $\mu\text{C}$ ) per cycle in the Fermilab Main Injector (FMI). This is five times the original FMI design specification<sup>40</sup>. The energy per pulse is 200 kJ at 8 GeV, and 3 MJ per pulse at 120 GeV. At an already achievable MI cycle time of 1.5 seconds, this corresponds to 2 MW of average power.

The MI output power could be subsequently upgraded to 3 MW (or 4 MW) by reducing the MI cycle time to 1 second (or 0.75 seconds). This upgrade is feasible from the magnet and power supply point of view<sup>41</sup>, but would require substantial RF voltage upgrades (section 25). The linac will not be a limitation to this upgrade path due to the short filling time.

Another option to double the beam power of the Main Injector is to double-pulse the Linac. Two injections spaced by 0.1 seconds (possible for the ultimate scenario) would increase the MI cycle time from 1.5 to 1.6 seconds but double the protons per cycle. Again, a substantial RF power in the Main Injector would be required.

### 4.3 Beam Current and Pulse Width: Initial and Ultimate Scenarios

Once the charge-per-pulse has been set, choosing the pulse width and beam current in a superconducting linac is a multidimensional optimization involving RF costs, cryogenic power, component limitations, and beam physics considerations. See Table 6.

**Ultimate Beam Power Scenario:** The first Design Study adopted the single-pulse beam parameters of the Spallation Neutron Source (SNS) linac (25 mA \* 1 msec = 25  $\mu\text{C}$ ) as a convenient starting point. The SNS provided documented examples for the front-end systems, cavities, couplers, klystrons, modulators, beam loss handling, etc. which were specified to operate at this beam current and pulse width. The 25 mA beam current led to a fan-out of 12

cavities per Klystron, a repetition rate of 10 Hz (limited by the TESLA Klystron), and a stand-alone linac beam power of 2 MW. These parameters represent the so-called “Ultimate” scenario for the Proton Driver linac.

**Initial Baseline Beam Power Scenario:** At the end of the first design study it seemed likely that a longer beam pulse, with proportionally lower average current, would be cheaper. This has been adopted as the baseline. Roughly speaking, a 3x longer beam pulse (1 msec → 3 msec beam pulse) and a proportionally lower current (25mA → 8.7mA) cuts the number of SCRF klystrons and modulators by a factor of 3. (The total capacitor bank size and total modulator charging supply power are unchanged, since these are driven by the single-pulse beam energy and the average power, respectively). This leads to a RF fan out of 36 cavities per Klystron, which is identical to the TESLA design. Klystron pulse width limitations were investigated. After discussions with the TESLA and JPARC Klystron manufacturers, it was concluded that the 3 msec pulse width (and 4.5 msec RF pulse width) should not pose a problem as long as the repetition rate was limited to 2.5 Hz. This is being tested (see section 10.3).

Table 6 summarizes the pros and cons of long-pulse operation for an SCRF linac with fixed charge-per-pulse.

Table 6 - Trade-offs in Pulse Length vs. Current in an SRF Linac with Fixed Charge-per-pulse

CONSIDERATION	FAVORED PULSE LENGTH	REASONS
Klystron count	Long	Lower beam current allows fewer Klystrons with fan out to more cavities per klystron
Peak Power in RF distribution components	Long	Peak power proportional to beam current
Klystron Duty Cycle Limitations	Short	JPARC Klystron OK at up to ~5% Duty Factor; TESLA MBK needs changes above ~1.5% D.F.
H <sup>+</sup> Injection turns	Short	90 injection turns per msec of Linac pulse width
Cryogenic Dynamic Wall Power	Short	Cryogenic Losses Proportional to RF pulse length
Cryogenic Static Wall Power	Long	Lower power coupler designs have lower heat leak
Cavity Filling Losses in SCRF	-	Cavity filling energy is lost once per pulse
Modulator Capacitor Bank Size	-	Cap Bank Energy = Beam Energy + Filling Losses
Charging Supply (RF Wall power)	-	Only depends on average power
Resistive Power in Warm FE/RFQ	Short	Only ~ 2% of total RF power in baseline design
Sensitivity to Microphonics	Short	Easier with high beam current, lower loaded Q
Emittance Dilution for non-painted beams	Short	Reduce number of injection turns and foil scattering
RF Distribution Losses	-	(perhaps small effect in ferrite tuner)
Main Injector Cycle time	-	Pulse length is small contributor to cycle time
Linear Collider Application	~1 msec	Want to be close to TESLA linac parameters
8 GeV Neutrino	Short	Minimize cosmic ray backgrounds
8 GeV Proton Fixed Target	Long	Many experiments want high duty factor
8 GeV Electron Fixed target	?	Depends on experiment
XFEL	?	Depends on experiment

#### 4.4 Linac Pulse Repetition Rate (Average Beam Power)

A minimum pulse repetition rate of 0.67 Hz (133 kW average power) is required to support operation of the 1.5 sec minimum cycle time of the Main Injector. This is provided by either the Initial (2.5 Hz) or Ultimate {10 Hz} linac configurations. We have been advised<sup>42</sup> that commissioning a linac with a repetition rate this low may be challenging.

The total beam energy per Linac pulse is  $25 \mu\text{C} * 8 \text{ GeV} = 200 \text{ kJ}$ , so the stand-alone output power of the Linac is  $200 \text{ kW} * (\text{repetition rate in Hz})$ . The total operating wall power for the linac is roughly (3 MW standby) + (1 MW/Hz). The 2.5 Hz {10 Hz} repetition rate chosen for the Initial {Ultimate} configurations if this design study corresponds to 0.5 MW {2 MW} linac beam power, and 5.5 MW {13 MW} of wall power.

#### 4.5 Different Particle Types in the 8 GeV Linac

***H<sup>-</sup> Injector.*** The baseline design documented in this design study serves only as an H<sup>-</sup> injector to the Fermilab Main Injector. Other missions have been considered (Appendix 1) but not included in the baseline cost. The major concession to alternate missions is the flexible siting (sect. 3.6) chosen for the footprint of the baseline design.

***No Protons.*** The linac could accelerate protons using separate H<sup>-</sup>/proton sources and switchable RFQ front ends (like DESY). The higher currents available from proton sources are not useful since the maximum current that can be accelerated is limited by the RF power installed in the SCRF section. When running protons you lose the ability to do H<sup>-</sup> stripping injection in the MI or Recycler, you lose H<sup>-</sup> stripping collimation in the transfer line, and you lose the “Laser Wire” beam profile diagnostic<sup>43</sup>. Finally, if a proton beam is ever desired, it can be obtained from the H<sup>-</sup> beam with a stripping foil in the transfer line. For these reasons, no proton acceleration is specified in the baseline design. It remains a low-cost upgrade option.

***Electrons and Positrons.*** The main  $\beta = 1.00$  section of the linac (i.e. the last 7 GeV) has most of the hooks needed to accelerate both electrons and H<sup>-</sup>/protons, selectable on a pulse-by-pulse basis. This has implications for both the RF distribution system (section 11) and the quadrupole power supplies (sect 21). (The  $\beta < 1$  sections, including the 8-cell  $\beta = 0.81$  cavities, are nearly useless for accelerating electrons.) Running electrons will require a separate electron photoinjector with an output energy of 0.2-0.6 GeV (1-3 cryomodules), as well as appropriate beam merging optics<sup>203</sup>. This electron injector is not documented in this study, and not included in the cost estimate.

The accelerator issues raised by multi-species operation include operating the multi-cell superconducting cavities away from their design values of relativistic  $\beta$ , re-phasing individual cavities which are driven by a single large klystron, and adjusting or sharing the transverse focusing (quadrupole settings) on a pulse-by-pulse basis. Some details of the “slow” ferrite phase shifters (Appendix 1 and section 14) needed to accelerate electrons, muons, etc, in the last 7 GeV of the linac have been worked out but are not included in the baseline cost. These are discussed in Appendix 1. The “laser wire” H<sup>-</sup> beam profile measurement capability is also lost when running electrons, as is the ability to perform H<sup>-</sup> stripping-foil collimation in the 8 GeV transfer line (section 19.8).

The tighter resonance control requirements for ILC/XFEL applications means the Low-Level RF (LLRF) and clock distribution systems would have tighter specifications than required for the Proton Driver alone. Since we plan to use ILC LLRF components, this is not an issue.

***Cavity Spacings for an Energy Recovery FEL***

Another issue relevant to running electrons is whether to retain the option of running electrons simultaneously forwards and backwards through the linac. This could be useful for either “energy recovery” or “energy doubling” scenarios. This imposes the constraint of placing all cavities at half-wavelength spacings from each other. This compromises the cryomodule length and real estate gradient of the machine, which is felt to be undesirable for the ILC. The amount of linac length in play amounts to a few tens of meters for the Proton Driver. One disadvantage of placing cavities on half-wavelength intervals is that dark current can be accelerated backwards through the linac. At press time, this issue is being debated by the TESLA/XFEL/ILC collaboration, and we expect that we will go with whatever solution they adopt.

## 5 ACCELERATOR PHYSICS

Accelerator physics issues include linac design optimization, aperture and beam losses, H- beam transport and injection, and Main Injector RF capture and acceleration. The important issue of linac energy stability is discussed here, and the technological means to achieve the required energy stability is discussed in section 12 on RF distribution and Ferrite Vector Modulators.

### Comparison with SNS Accelerator Physics Parameters

The single pulse beam parameters of the Ultimate configuration are very similar to the Spallation Neutron Source (see Table 3). This makes the accelerator physics very similar. SNS accelerator physics issues have been exhaustively studied<sup>44</sup>, and to some extent we can simply refer to their results. The 8 GeV Linac parameter book<sup>10</sup> developed for this design study gives side-by-side comparisons of the SNS and Proton Driver linac for most major subsystems. The successful early commissioning results from the SNS add confidence to the Proton Driver linac design, and SNS operational experience will provide guidance as to appropriate design margins.

Table 7 - Accelerator Physics Differences Between the Proton Driver and SNS Linacs

	Proton Driver	Spallation Neutron Source
Output energy	8 GeV	1 GeV
Repetition rate	2.5 Hz{ 10 Hz }	60 Hz
Energy of Transition from Copper to SCRF sections	15 MeV	186 MeV
Focusing (E<100 MeV)	solenoidal	quadrupole
Focusing (E>100 MeV)	FODO	Doublet

The higher output energy (8 GeV vs. 1 GeV for SNS) creates no new problems for linac beam dynamics. This is because instabilities and emittance growth are most challenging at the front end of the linac, where beam space charge, emittance exchange, and other halo-generating effects are important. Longitudinally, the beam undergoes rapid synchrotron oscillations between 3 MeV and 1 GeV, but less than two phase oscillations between 1 GeV and 8 GeV as the beams become relativistic and the longitudinal motion is “frozen out” (see Figure 19).

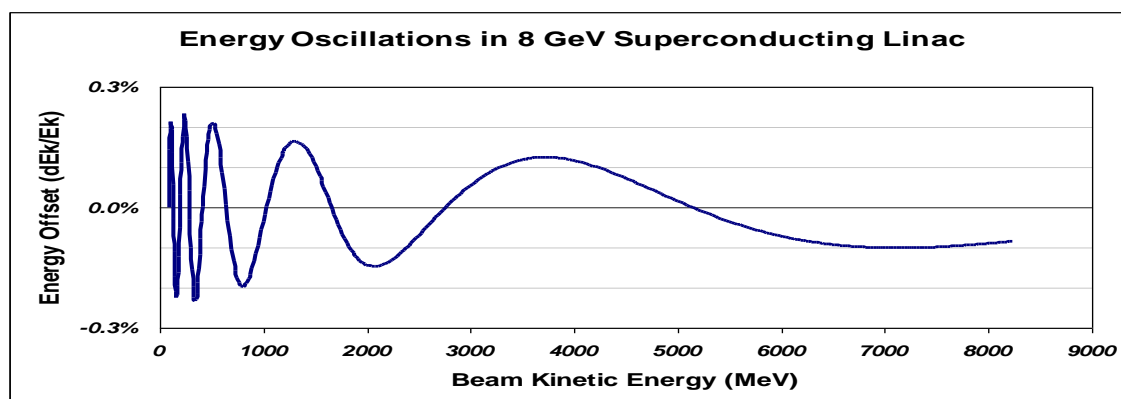


Figure 19 - Representative energy oscillations in the Proton Driver linac at zero beam current. The beam undergoes rapid synchrotron oscillations below 1 GeV, but less than 2 periods of synchrotron motion in the 1300 MHz ILC section between 1 and 8 GeV.

Table 8 – Linac Segment Details for the 8 GeV Proton Driver Linac

LINAC SEGMENT DETAILS									
				Open Technical Choice: 3-spoke or Elliptical					
	RFQ	Room Temp TSR	SRF 1-spoke	SRF 2-spoke	Spoke Option 3-spoke	Elliptical Option Low Medium		High	TESLA
Frequency, MHz	325	325	325	325	325	1300	1300	1300	1300
Energy Range, MeV	0.065-3	3-15	15-33	33-110	110-400	110-175	175-400	400-1200	1200-8000
Beta geometrical	-	0.08 to 0.18	0.21	0.4	0.61	0.47	0.61	0.81	1.00
Number of cavities or resonators	4	21	16	28	42	16	32	48	288
Number of accelerating gaps / cavity	-	4	2	3	4	6	6	8	9
Epeak, MV/m	32.1	TBD	32	32	32	52	52	52	52
Eacc, MV/m	-	2.3 to 3.7	10.67	10.67	10.67	15.2	19.2	23.7	26
Cavity effective length, cm	-	15 to 32	13	36.9	85.8	32.5	42.2	74.8	103.8
Synchronous phase, deg (typ.)	-	-40 to -30	-30	-30	-30 to -20	-30	-25	-20	-16
Length of Segment, m	~4	10.4	12.5	17.2	64	18.8	38.5	70.1	438.3
Number of Cryomodules	-	-	1	2	6	2	4	6	36
Cavities per Cryomodule	-	-	16	14	7	8	8	8	8
Magnetic Focusing Type	-	Solenoid	Solenoid	Solenoid	Quad	Quad	Quad	Quad	Quad
Coupler Power Initial {Ultimate}, kW	125	40 {54}	9 {26}	34 {102}	80 {238}	42 {125}	72 {214}	133 {398}	220 {660}
Cavities per Klystron Initial {Ultimate}			72 {36}		42 {14}	48 {24}		48 {24}	36 {12}
Number of Klystrons Initial {Ultimate}			1 {2}		1 {3}	1 {2}		1 {3}	8 {24}

Table 9 - Acronyms for Segments of the Linac

H- or IS	H- Ion Source
LEBT	Low-Energy Beam Transport (between H- and RFQ)
RFQ	Radio Frequency Quadrupole
MEBT	Medium Energy Beam Transport & Beam Chopping Section
RT-TSR	Room-Temperature Triple-Spoke Resonators
SSR	Single-Spoke Resonators (325 MHz superconducting)
DSR	Double-Spoke Resonators (325 MHz superconducting)
TSR	Triple-Spoke Resonators (325 MHz superconducting) (Baseline 110-400MeV)
Low-β	β = 0.47 elliptical 1300 MHz Superconducting Cavities (“Elliptical Option”)
Medium-β	β = 0.61 elliptical 1300 MHz Superconducting Cavities (“Elliptical Option”)
High-β, or	
S-ILC	β = 0.81 elliptical 1300 MHz “Squeezed-ILC” Cavities
ILC, or	
TESLA	β = 1.00 elliptical 1300 MHz cavities identical to those of the ILC.

## 5.1 End-to-End Simulation of the Baseline Lattice and Cavity Layout

The accelerator physics design and component layouts for this iteration of the design study took place in collaboration with ANL<sup>45</sup>. The design follows the “two frequency” proposal for using TESLA-compatible spoke resonators for the Proton Driver Linac<sup>46</sup>. Initial design work was performed using the TRACE-3D code<sup>47</sup> used for the SNS and other projects, and an end-to-end simulation and multiparticle tracking was performed using the TRACK code<sup>48</sup> used for RIA.

Linac accelerator physics limits are driven by the Ultimate (25 mA) current in the linac. Therefore the accelerator physics design was carried out at a current of 28 mA. By adopting the “current independent” design principles for longitudinal and transverse focusing that were used for the APT and SNS<sup>44</sup>, the same linac tune functions well at currents between zero and the maximum design current<sup>49</sup>.

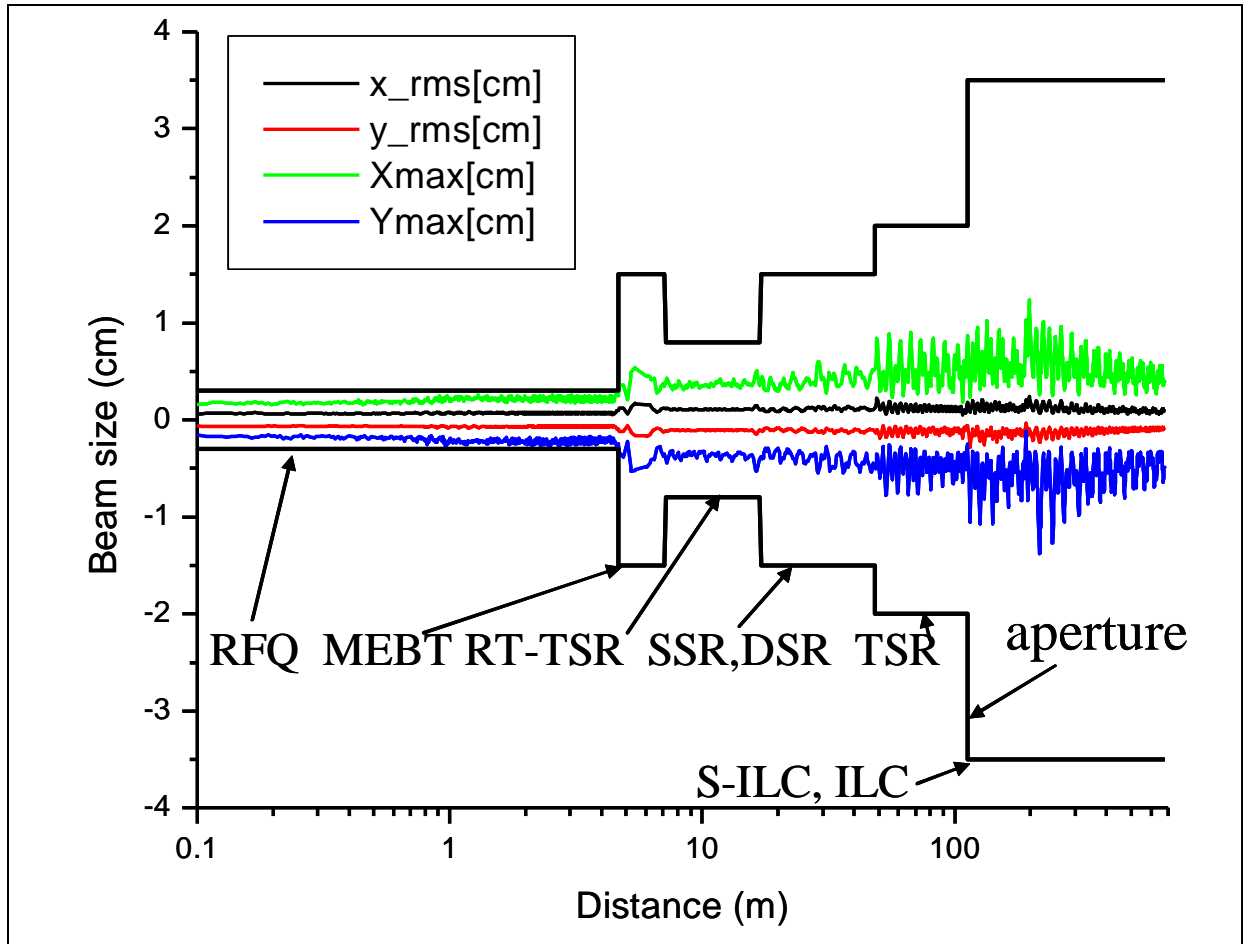


Figure 20 - Transverse beam envelopes for end-to-end simulation of the Proton Driver linac using the ANL TRACK code<sup>48</sup> (log scale). The code includes space charge and swims the particles through realistic 3-D electromagnetic fields calculated for the RFQ, cavities and focusing magnets. The RMS beam size stays ~1.5 mm throughout the linac, and the maximum amplitude (out of 20,000 particles tracked) stays well below the physical aperture once the particles enter the superconducting sections. Note the smooth and round beam envelopes from the solenoidal focusing in the MEBT, RT-TSR and DSR sections.

## 5.2 Proton Driver Beam Loss Requirements vs. SNS

Beam loss is an issue for irradiation of the warm front end linac and ultimately for quenching or damaging the SCRF linac. Depending on operating mode, average current in the Proton Driver linac will be between 6 and 100 times lower than the SNS due to the identical charge-per-pulse and lower repetition rate. This means that studies and early commissioning results projecting acceptable losses in the SNS Front-end linac<sup>50</sup> imply better-than-acceptable losses in the 8 GeV front-end linac. Operating experience with the SNS will be instructive. As discussed below, we anticipate the solenoidal focusing of the front end linac should provide cleaner beams with additional design margin against beam halo.

The comparison with SNS for the high energy end of the Proton Driver linac is less favorable. Because of the higher beam energy (and 2x higher average beam power in the Ultimate scenario), the Proton Driver linac can tolerate smaller fractional beam loss in the high energy end of the linac than the SNS. Fortunately in this region both linacs have a radial aperture (the elliptical superconducting cavity iris) more than 20x the RMS beam size.

SNS simulations predicted small halo losses in the CCL<sup>50</sup> and negligible losses once the beam enters the SCRF cavities<sup>51</sup>. To the extent that this has been confirmed by actual operation, predictions made with these tools can be extrapolated with confidence to the Proton Driver linac. Beam halo downstream of the linac output is not a major issue since halo is cleanly removed by the foil stripping collimation in the beam transfer line to the MI (section 19.8).

## 5.3 Linac Apertures

The transverse focusing in the Proton Driver Linac has been adjusted to maintain a RMS beam size of 1 mm - 1.5 mm throughout the linac. A series of gradually increasing radial apertures in the linac have been chosen as follows (see Figure 20):

Table 10 – Radial Apertures in the Proton Driver Linac

Linac Section	Aperture	Comments
RFQ	±3.7 mm	RFQ's operate with 10-20% beam loss and beam will extend out to physical aperture.
MEBT Transport	±15 mm	Option of MEBT collimation to reduce halo from RFQ. Lower average current makes collimation easier than SNS.
MEBT Chopper	±9 mm	Small aperture needed to kick individual bunches separated by ~75 mm, and to minimize chopper voltage
RT-TSR	±7.5 mm	Option for further collimation in the warm spokes.
SSR, DSR	±15 mm	Radius increase to protect superconducting structures from halo. Limited by iris diameter of spoke, not SC solenoids.
TSR (baseline) Elliptical (option)	±20 mm ±30 mm	Additional spoke aperture provided for increased beam size due to switch from solenoid to quad focusing.
Elliptical Cavities	±35mm typ.	Huge. Varies with $\beta$ and choice of low-loss cavity design.
Transport Line Betatron Collimation	±9 mm typ.	Six stations of adjustable foil stripping collimation strip halo outside this radius and send it to dump(s).
Transport Line Magnets (B2)	±40mm (H) ±20mm (V)	B2 Magnet aperture would be reduced by cryogenic beam screen (section 19.5).

## 5.4 H- Ion Source

The beam current and brightness of the JPARC, DESY, and SNS H- sources all meet or exceed our requirements. The decision as to which H- source to copy will be based on technological considerations such as reliability and pulse width properties. See section 6.1.

## 5.5 Radiofrequency Quadrupole (RFQ)

The 324 MHz, 30 mA RFQ design<sup>52</sup> for the JPARC project was used as the starting point for our 325 MHz, 28 mA design. Some changes were made to the vane geometry. The output section was modified to produce an axisymmetric beam to match into the solenoidal focusing of the MEBT and front-end linac. These changes<sup>49</sup> resulted in an increase in length of the RFQ from 3.1 m to 3.8 m.

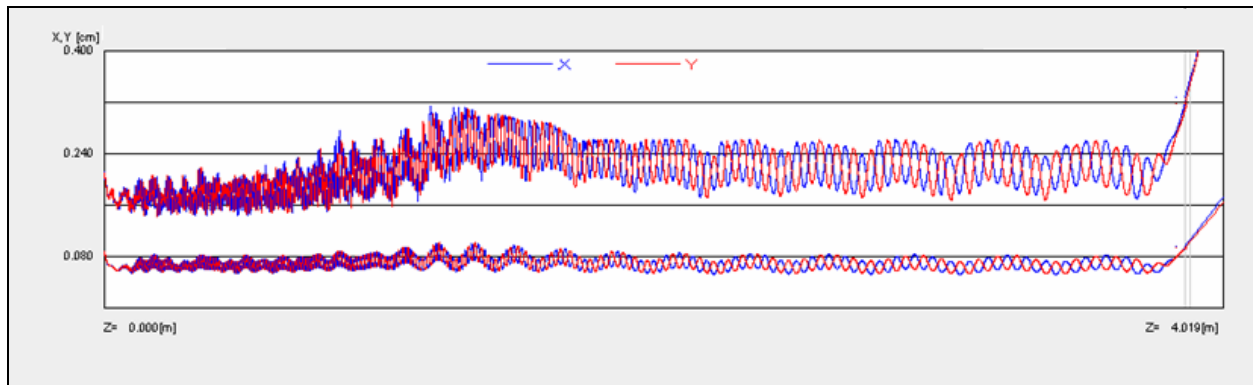


Figure 21 – Transverse Optics of the Radio Frequency Quadrupole (RFQ). Bottom traces: RMS X & Y beam sizes. Top traces: Maximum beam size. Note the X-Y symmetric (round) beam shape at the output of the RFQ. Round beams are required to match into the solenoidal focusing of the MEBT.

## 5.6 Medium Energy Beam Transport (MEBT).

This section performs beam analysis, beam chopping, and matching between the RFQ output and the first acceleration cavities. Two bunching cavities are included to maintain the longitudinal beam structure. See Figure 22.

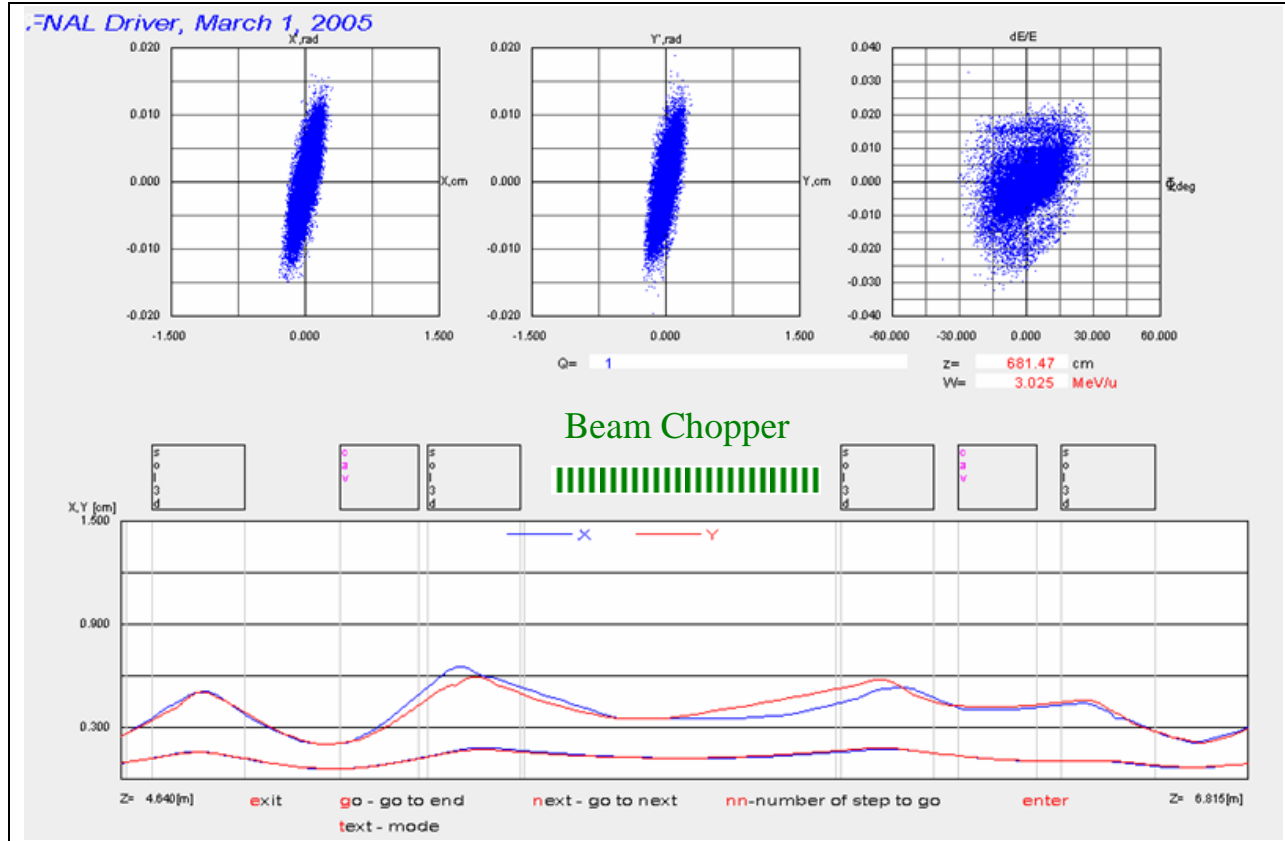


Figure 22 – Medium Energy Beam Transport (MEBT) includes two rebunching cavities and four superconducting solenoids for transverse focusing. Solenoidal focusing minimizes emittance growth and halo formation, and provides a long symmetric beam waist for the beam chopper.

**Beam Chopping in the MEBT vs. Adiabatic RF Capture in the Main Injector.** Like the SNS, JPARC, and the SPL, the 8 GeV Proton Driver MEBT contains a beam chopper. In the baseline design, a single chopper is used to generate only the abort gap in the ring (~800 ns minimum gap every 11  $\mu\text{sec}$  revolution of Main Injector). The 10 ns rise time of the SNS beam chopper and HV pulser supply is adequate for creating this gap.

This approach implies adiabatic RF capture at high intensities in the Main Injector. This has not been sufficiently studied to be certain that it will be problem-free. An informative reference point is that ISIS performs adiabatic RF capture of intense ( $>2.5E13$ ) beams with high ( $>95\%$ ) capture efficiency using a dual-harmonic RF system<sup>53</sup>. Each 1% of beam loss corresponds to 1500 Watts of beam power in the Main Injector momentum collimation system.

An alternative under consideration is to inject directly into pre-formed 53 MHz RF buckets in the Main Injector. This is the approach taken at the SNS and CERN SPL. This will require a bunch-by-bunch beam chopper with a rise and fall times of ~2 ns, i.e. fast enough to

turn on or off between 325 MHz bunches. This was the original specification for the SNS chopper<sup>54</sup> and is the design goal of the CERN SPL chopper<sup>55</sup>.

An additional mission of a bunch-by-bunch chopper is to provide fast digital control of the beam current in the linac. By controlling the fraction of pulses let through by the chopper, the LLRF control can effectively regulate the beam current (beam loading) in the linac. This could be used to provide a “soft start” to the leading edge of the beam pulse, or to effectively regulate the beam loading current to compensate for fluctuations in the ion source current.

**Anti-Chopper Option.** The baseline design contains only a single chopper, rather than a separate chopper and anti-chopper as at the SNS. The purpose of the anti-chopper is to cancel the effects of ringing or other chopper waveform imperfections on the non-chopped beam. This requires 180° betatron phase advance between chopper and anti-chopper, and good matching between the waveform imperfections of both devices. The solenoidal focusing between the chopper and anti-chopper would require that the anti-chopper be rotated with respect to the chopper. The beam dynamics of this have not been studied. The retrofit of an anti-chopper is mechanically allowed for by the alignment rails concept (Figure 9) for the front end linac.

## 5.7 Solenoidal Transverse Focusing for $E < 100$ MeV

Solenoidal focusing is used in the MEBT and spoke resonator linac below  $E < 110$  MeV, rather than the quadrupole focusing used by the SNS and most other machines. The main benefits of solenoidal focusing are round beams and the simultaneous focusing of both coordinates. A recent analysis of the SNS MEBT indicates that the highly elliptical beam shape from quad focusing is a significant contributor to emittance growth<sup>56</sup>.

The benefits of solenoidal focusing have long been recognized<sup>57,58</sup>. However, they have typically not been used because the required strength of the solenoids (4-8 Tesla) exceeds that easily obtained with normal conducting magnets. Since the Proton Driver linac uses cryogenics all the way up to the front of the linac, the cost of adding superconducting solenoids is not large. Verifying the high beam quality expected from solenoidal focusing is one of the main goals of the Proton Driver front-end tests at the Meson Lab SMTF area.

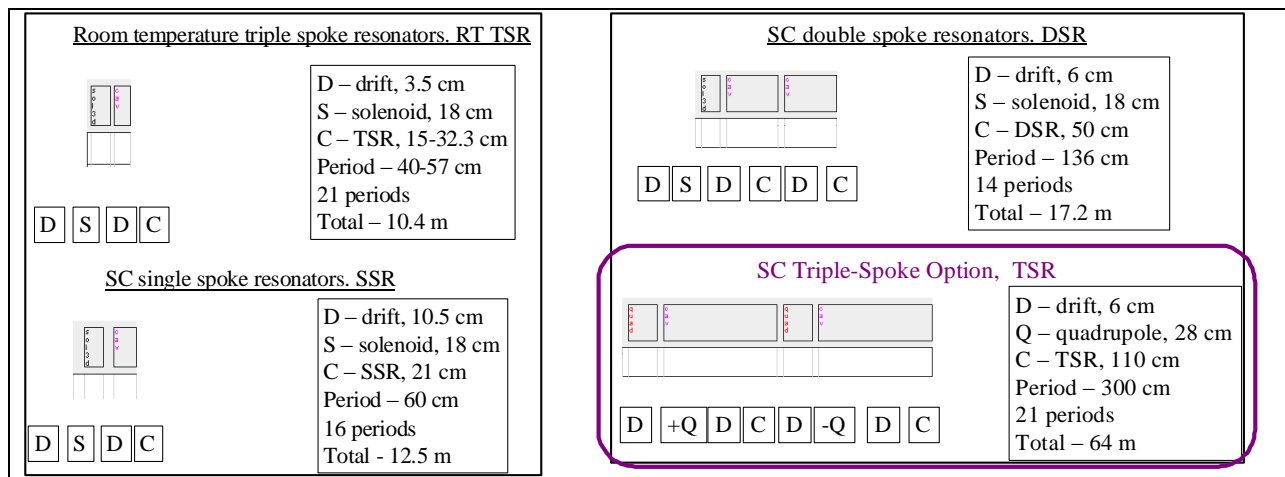


Figure 23- Focusing cell structures in the Proton Driver front end linac.

## 5.8 Room-Temperature Triple-Spoke Resonator (RT-TSR)

The Linac up to an energy of 15 MeV consists of room-temperature spoke loaded copper cavities interspersed with superconducting solenoids. The motivation for solenoidal focusing is the same as for the MEBT, namely to provide a smooth and round beam envelope to avoid emittance growth and halo formation. Since solenoids of the required strength cannot fit into the drift tubes of a conventional DTL, separate cavities and focusing magnets are required.

Separating the functions of RF acceleration and focusing has several benefits for a room temperature linac. Firstly, the drift tube & beam iris can be small, so the large capacitance at the accelerating gap of a DTL is avoided. This results in a high shunt impedance and low power dissipation. Secondly, one retains the option of commissioning the linac in sections smaller than an entire drift tube module (or cryomodule), so that unexpected sources of emittance growth can be individually identified and remedied. This approach also fits well with a TESLA-style RF system with many RF loads powered from a single Klystron.

Room-temperature cavities are chosen for a mixture of beam-physics and engineering reasons. Longitudinal beam dynamics are optimized with a gentle start to the acceleration. This limits the maximum accelerating gradient in the early cavities of the linac to a value below the technological limit of  $\sim 10$  MeV/m for superconducting resonators. At the low accelerating gradients preferred for beam dynamics, the structure power dissipation in the copper cavities (which scales as the square of the gradient) is small compared to the beam power (which scales linearly with gradient). At the 15 MeV crossover between room-temperature and superconducting cavities chosen for the baseline design, the copper structure power and beam power are roughly equal (see Figure 40).

The individual room temperature cavities are matched to each beta as the beam accelerates. This provides smooth acceleration and optimum longitudinal dynamics. While this is also possible in principle with SCRF cavities, the tooling charges for each individual SCRF cavity would be prohibitive.

## 5.9 Superconducting Spoke Resonators

The 325 MHz Superconducting Spoke Resonator sections start at 15 MeV immediately after the RT-TSR. Single-, Double-, and Triple-Spoke Resonators are used at successively higher energies. See Figure 23 and Figure 11. The number of spokes per cavity is increased to reflect the longer cell size and the decreasing fractional  $\beta$  spanned by each cavity design as the beam accelerates. The cell length for transverse focusing is gradually increased to maintain an approximately constant RMS beam size of  $\sim 1$  mm.

To date, no beam has ever been put through a SCRF spoke resonator. The accelerator physics of spoke resonator linacs has been extensively simulated for the RIA, APT and other projects. No problems are anticipated since the beam physics is determined by the EM fields near the iris, which are very similar to those of DTLs and other low-beta linacs. Verifying the expected performance of spoke resonators is a goal of the Meson / SMTF test effort.

## 5.10 Quadrupole Transverse Focusing for $E > 110$ MeV

The transition from solenoidal to quadrupole focusing takes place at 110 MeV for both the elliptical and spoke resonator options. See Figure 23. The driving considerations are the decreasing effectiveness of solenoidal focusing as energy increases, the reduced benefits of round beams as space charge forces decrease with energy, the potential H<sup>-</sup> stripping in the fringe

fields of the 6 T solenoids, and the real estate required for shielding nearby superconducting cavities from the fringe fields of the solenoids.

FODO quadrupole focusing is used in the baseline design. The economic incentive is to minimize the number of quadrupoles. Opposing constraints include keeping the transverse beam size small compared to the cavity iris, maintaining a stable lattice in the presence of space charge and RF defocusing, avoiding parametric resonances, and the desire to adopt standardized cryomodule designs (including quadrupole numbers and locations) within each section of the linac. The baseline quadrupole layouts are shown in Figure 23 and Figure 89.

Either FODO or doublet cell optics are workable. The SNS chose a warm copper doublet between each cryomodule, a choice that was largely forced by the use of CEBAF-style cryomodules with warm-to-cold beam pipe transitions at the end of each cryomodule. For the Proton Driver 1300 MHz main linac, the TESLA-style cryomodule gives considerable freedom to relocate the cold quadrupoles and cavities as desired. A FODO lattice requires weaker quadrupoles than a doublet lattice with the same maximum beam size and average quadrupole spacing. Quadrupole strengths are limited by magnetic stripping (sect 5.17) rather than magnet technology, so that a stronger quadrupole must be made longer which increases costs. For these reasons a FODO lattice was adopted as the baseline design.

RF (de-)focusing is a large effect, especially in the 1300 MHz sections of the linac. For the synchronous particle it is proportional to  $\sin(\phi_s)$ . For individual particles undergoing synchrotron oscillations, it is modulated over a range proportional to the synchrotron amplitude. If one adopts the conservative criteria that stable transverse focusing be obtained for all particles inside the longitudinal separatrix, an additional quadrupole (i.e. two per cryomodule) the first  $\sim 1$  GeV of the  $\beta=1.00$  section of the linac would be required<sup>49</sup>. (This is one of several minor inconsistencies between the present accelerator physics simulations and the engineering design, all with minor cost implications). This criteria is only an issue for particles more than  $\sim 7\sigma$  away from the synchronous particle, so that relaxing this requirement should have negligible impact for particles inside the phase/energy acceptance of the linac, transport line, and main injector. This has recently been verified by tracking studies, so it appears that unmodified ILC cryomodules are acceptable for the entire  $\beta = 1$  linac.

An additional constraint is that the rate of transverse phase advance be greater than twice that of the longitudinal phase advance, to avoid low-order “parametric resonances”<sup>59</sup>. These occur when the periodic modulation of the space charge force from the transverse focusing resonantly cross-talks to the longitudinal envelope oscillations. This requirement is adequately satisfied by the one-quadrupole-per-cavity lattice at 110 MeV section, and is easily satisfied in the higher energy sections as the longitudinal phase advance “freezes out”.

Like the SNS, the linac design adopts the principle of “Current Independent Focusing”, which means that the longitudinal and transverse phase advance per unit length is roughly constant across boundaries of linac operating frequency or transverse focusing. This creates a first order insensitivity to changes in linac current, since the effects of space charge will be the same on either side of a linac transition. Thus a design which is matched at full current will be matched at any current between zero and the full current. Operationally this has advantages since the linac can be tuned up at low currents and will not require large retuning of quads and synchronous phases in response to changes in operating current. With the exception of a bunch rotation performed as part of the frequency jump (which will require some retuning with changes in beam current) this design principle is respected throughout the baseline design. Current-independent focusing also improves the linac’s ability to transport a mixture of half-chopped bunches and full bunches if the MEBT beam chopper’s performance dictates this.

### 5.11 Longitudinal Focusing and Frequency Jumps

The Proton Driver linac contains a 325 MHz  $\rightarrow$  1300 MHz frequency jump. (Every bucket is occupied at 325 MHz and every 4<sup>th</sup> bucket at 1300 MHz). This frequency jump has been modeled using TRACK simulations including space charge. It can be handled without additional hardware by appropriate modifications of the synchronous phase and amplitudes of the RF drive to individual cavities in the transition region. Longitudinal beam envelopes are given in Figure 24.

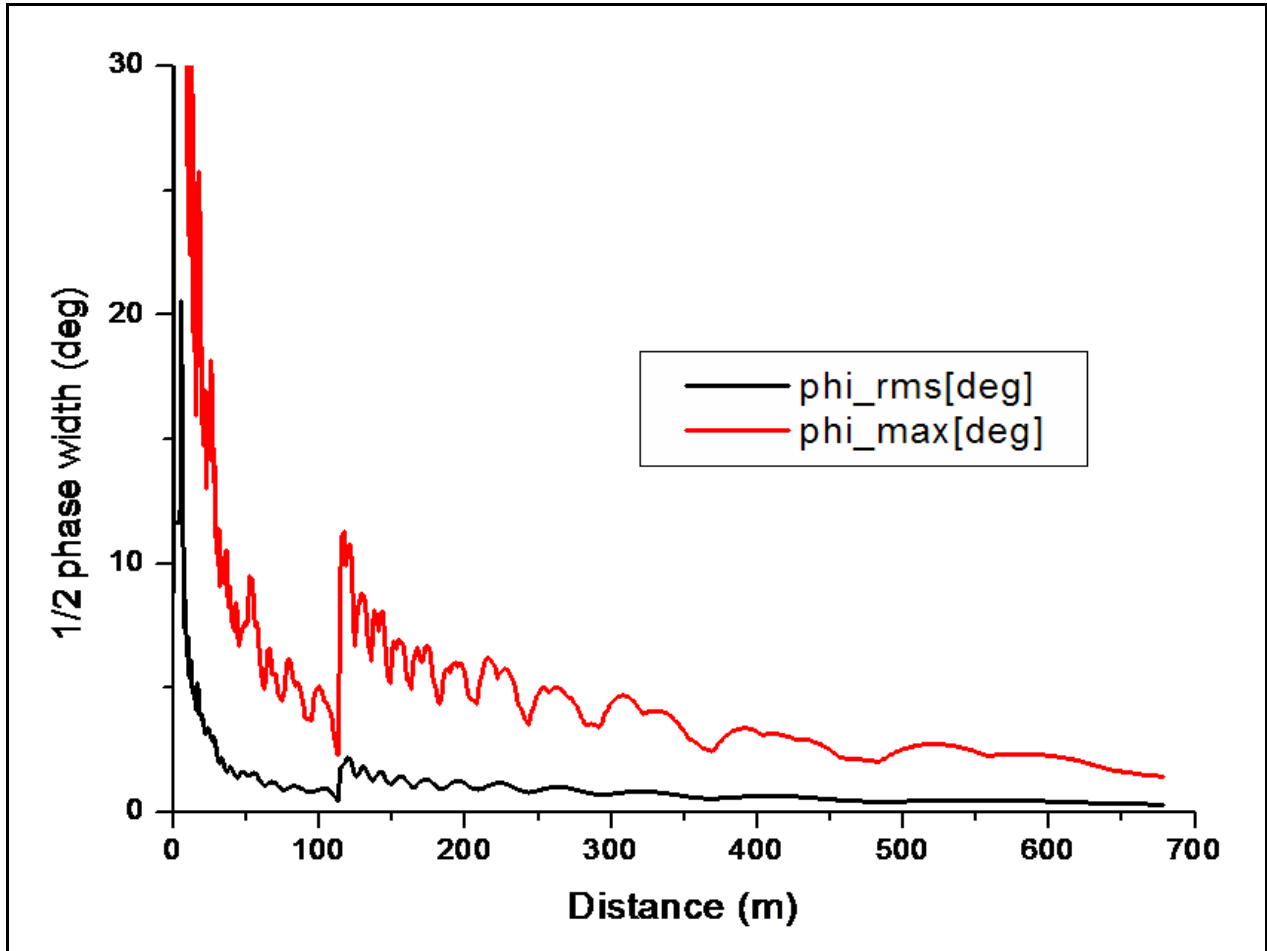


Figure 24 – Longitudinal Bunch Size (phase width) vs. Distance along Proton Driver Linac. The jump in phase width at 120 m is due to the redefinition of phase width at 325 MHz vs. 1300 MHz.

The RMS bunch length decreases gradually from 170 psec (20 degrees at 325 MHz) to ~2 psec (~1 degree at 1300 MHz) as the beam accelerates. This is accompanied by a corresponding increase in energy spread and jitter, and decrease in phase jitter. The situation is ideal from the point of view of the Debunching cavity (see sect. 5.14 below) which removes energy spread and jitter but works best with a small incoming phase jitter.

## 5.12 Linac Energy Stability Requirement

The energy jitter requirement of the Proton Driver linac has important implications for the RF system design (sects. 12 and 13) and the specification for the fast ferrite phase shifter tuners (sects. 13.8 and 14). The allowable energy spread of the beam to the Main Injector must satisfy two requirements:

- 1) It must fit inside the momentum aperture of the Main Injector at injection (approximately  $\pm 50$  MeV, or  $\pm 0.7\%$ )
- 2) The longitudinal emittance of the 53 MHz RF captured beam must be small enough to make it through transition in the Main Injector with small losses. A reasonable assumption is that loss-free transition crossing will be possible for intense bunches smaller than 0.5 eV-s. See Figure 25. Assuming perfect adiabatic capture, this corresponds to  $\pm 13$  MeV ( $\pm 0.16\%$ ). ***This sets the most stringent requirement for energy spread.*** If direct RF capture with linac beam chopping is selected, the allowable energy spread will be reduced to approximately  $\pm 10$  MeV.

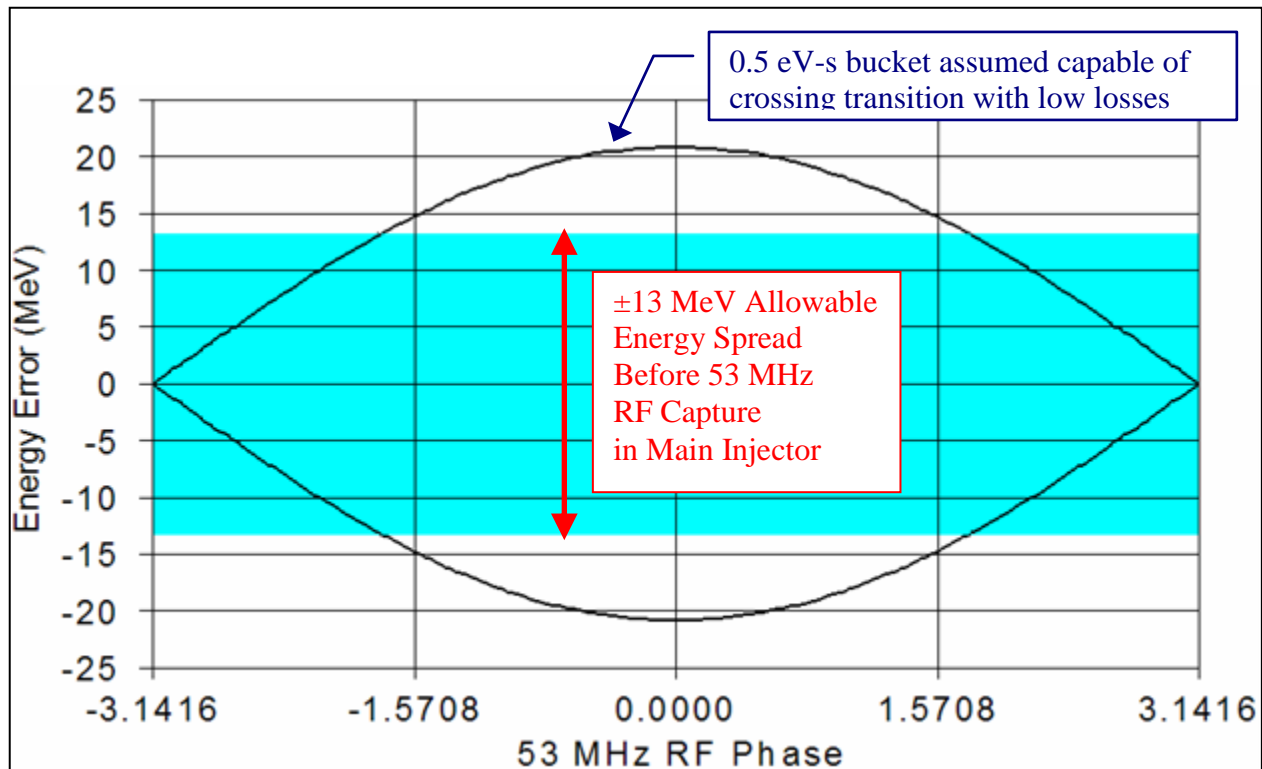


Figure 25 – Allowable linac energy spread for injection and transition crossing in the Fermilab Main Injector. Figure from ref. 60. Linac beam inside the colored  $\pm 13$  MeV band can be adiabatically captured inside a 0.5 eV-s bucket area which is assumed to be safely transportable through transition in the Main Injector. This might be doubled with a  $\gamma_T$  jump system in the MI.

## 5.13 Strategies for Limiting Linac Energy Jitter

The most important source of energy jitter is fluctuation in the resonant voltage of SCRF cavities due to microphonics, beam loading, and Lorentz detuning. The most straightforward way to correct these effects is to overpower them with a local feedback loop with one Klystron per cavity, and excess RF drive power at each Klystron. This is the approach taken at the SNS.

For economic reasons, the Proton Driver uses a single large Klystron to drive many cavities. This compromises the flexibility of the one-klystron-per-cavity approach. This flexibility is recovered to some extent by providing individual cavity phase and amplitude control via relatively sluggish (50  $\mu$ sec) Ferrite Vector Modulators (FVMs) for each cavity in the linac at energies below  $\sim 1.8$  GeV. The resonance control issues are discussed from a hardware point of view in sect. 13, and performance requirements for the FVMs are discussed in section 13.8.

Because of the importance of meeting the linac energy spread requirement, multiple assurances or good energy jitter are provided<sup>60</sup> in the baseline design:

1. The H- collimation system in the 8 GeV transfer line (section 19) ensures that no longitudinal beam halo or off-momentum pulses outside a defined momentum collimation window will be transported to the Main Injector. This collimation window can be set as tightly as  $\pm 4$  MeV at nominal betatron emittances. With this system, the result of a worse-than-expected energy jitter from the linac will be larger-than-expected controlled loss in the collimation dump, rather than an uncontrolled beam loss in the Main Injector.
2. A Debuncher Cavity (sect. 5.14 and sect. 15) is provided to reduce the momentum spread by about a factor of 6. The debuncher is effective at reducing both bunch-to-bunch jitter and energy spread inside each bunch. For nominal SNS emittances, the single-bunch energy spread after the debuncher will be below 1 MeV (see Figure 26).
3. Intra-pulse feedback during the 3 msec beam spill (sect. 13.6) can also be used to eliminate pulse-to-pulse energy jitter of the linac<sup>61</sup>. Measuring the linac output energy via the transverse position of the beam in the 6 m dispersion of the H- transport line, then feeding back the energy error to the warm-copper debuncher cavity, can provide sub-MeV energy regulation with an  $\sim 10$   $\mu$ sec response time. As a worst case, a fraction of the first 10  $\mu$ sec (0.3%) of an off-momentum beam spill would be sent to the collimation dump of the transfer line before the debuncher feedback either serves the beam energy into the collimation window, or gives up and aborts the linac pulse.
4. Global LLRF algorithms (section 13.5) can also be expected to significantly reduce the pulse-to-pulse energy jitter in the linac. Conventional feedback loops independently regulate the resonant voltages of a cavity or local group of cavities. Worst-case linac energy excursions occur when simultaneous fluctuations of the independent feedback loops accidentally add up to produce a large fluctuation in the linac output. With modern electronics the cavity resonance signals can be digitized with an accuracy an order of magnitude better than the resonance control requirements, and the effect of each cavity's resonance error on the linac output energy can be calculated in real time. This allows the circuitry to predict the linac energy fluctuation before the start of the beam spill, and to correct the fluctuation by applying a small correction to the klystron drives or Debuncher cavities prior to the start of the spill. (Following the start of the beam spill, the intra-pulse beam-based feedback described above will regulate the linac output energy).

### 5.14 Debuncher

The Proton Driver design includes a 60 MV Debuncher RF module 640 m downstream of the Linac output to reduce the momentum spread and jitter of the beam (see sect. 15). It is patterned on a similar design for the SNS. It is a “passive” debuncher that functions by letting the beam drift for a length sufficient for the high momentum particles to move ahead of the slower particles, then putting the beam through a group of RF cavities with the phase set to decelerate the early (high energy) particles and to accelerate the late (low energy) particles. This reduces the energy spread and jitter at the expense of increasing the bunch length and phase jitter of the bunches. (The bunch length and phase jitter are irrelevant after MI injection, since the 325 MHz bunch structure is effectively thrown away by the injection process).

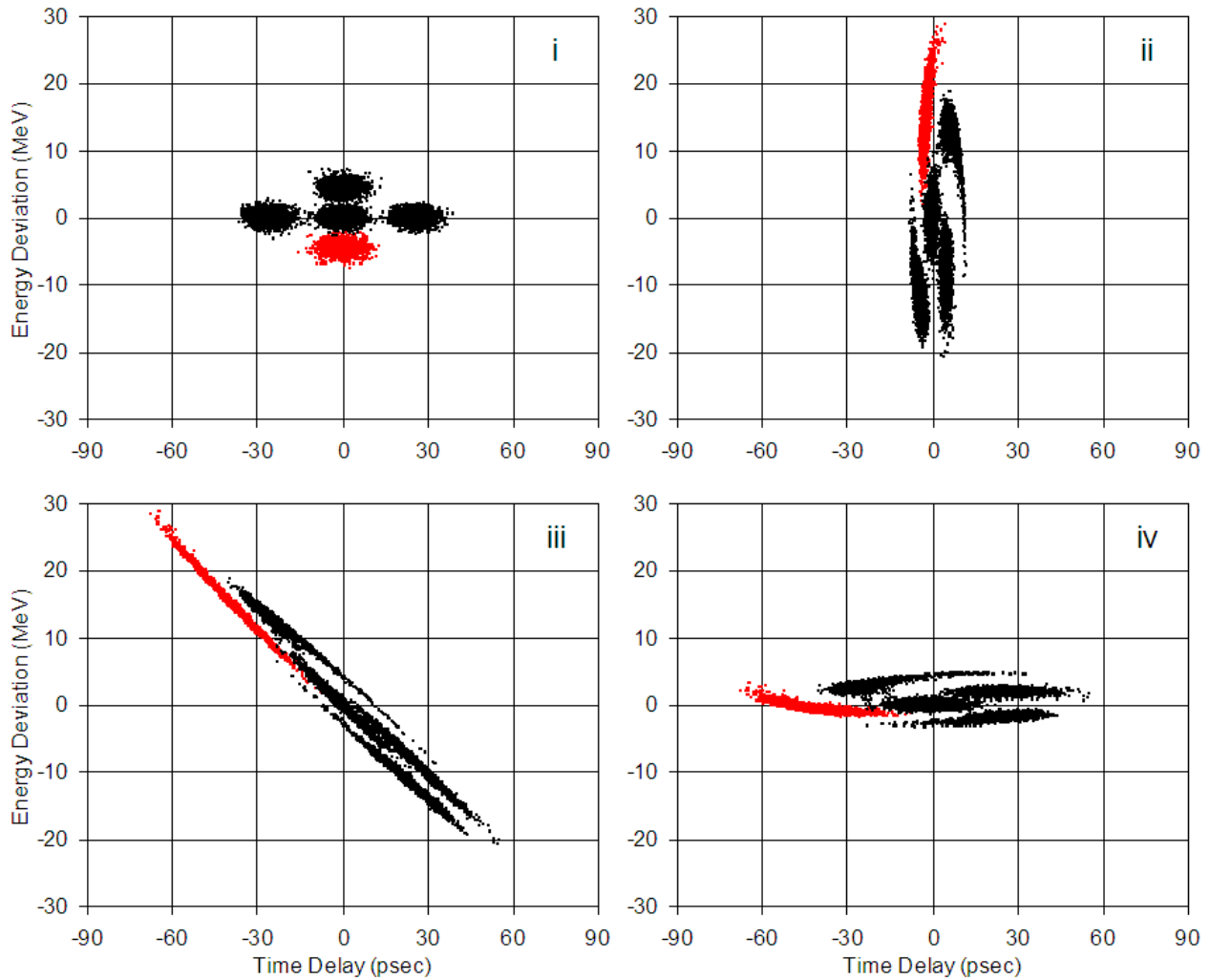


Figure 26 – Reduction of Energy Spread and Jitter via Passive Debuncher Cavity. i) - Five bunches at 1 GeV with nominal SNS longitudinal emittances and 3x nominal SNS bunch-to-bunch jitter in phase and energy. ii) - same bunches after acceleration to 8 GeV, with energy spread increased by a factor of  $\sim 4$  and phase width correspondingly decreased via adiabatic damping. iii) - Same bunches after 650m drift to debuncher cavity. iv) - Same bunches after “passive” Debuncher cavity removes energy correlation. The energy spread of the central bunch has been reduced to  $\sigma \sim 1$  MeV and the bunch-to-bunch jitter still leaves the entire beam well inside the  $\pm 13$  MeV window required for RF capture and transition crossing in the Main Injector.

The “passive” debuncher principle (see Figure 26) works well for both momentum spread within a bunch, and for bunch-to-bunch momentum jitter that occurs on a time scale too fast to be tracked by the superconducting cavities and LLRF system. It is also effective for pulse-to-pulse energy jitter or for slow energy drifts within a beam pulse; however these will be more effectively dealt with using active feedback of the linac output energy during the beam spill.

### **Active Feedback to the Debuncher Cavity**

Although it should not be necessary given the expected performance of the LLRF resonance control system using Ferrite Vector Modulators, an additional safety factor against “slow” beam energy errors can be obtained by feeding back and correcting the linac output energy at the Debuncher cavity<sup>61</sup>. One way to accomplish this feedback is to measure the transverse beam position in the 6 m dispersion of the transport line, and feed this forward to the Debuncher cavity. A beam position measurement with a resolution of 0.1 mm gives a resolution of 0.15 MeV, small compared to the  $\pm 13$  MeV window for energy output regulation (sect 5.12). The response time of such a feedback loop would be dominated by the 5-10  $\mu$ sec filling time of the warm copper debuncher cavities. This bandwidth easily could track microphonics or Lorentz detuning within the beam spill. A similar feedback loop, with a slower response time but more energy compliance, could be constructed by feeding back the transverse beam position (or debuncher phase) to the Klystron drives in the last few RF stations of the main linac.

### **5.15 Longitudinal Phase Space Painting**

The combined effect of the debunching and energy stabilization procedures above could in principle result in a beam energy width of order 1 MeV<sup>62</sup>. This is unnecessarily low and will possibly produce instabilities in the Main Injector. To avoid this difficulty, the LLRF & Debuncher feedback systems can be programmed for longitudinally phase-space-painting of the injected beam, i.e. deliberately spoiling the energy spread of the beam by rapidly slewing the beam energy by up to  $\pm 10$  MeV as the Main Injector is being filled. Since the response time of the warm-copper debuncher cavity is faster than the revolution time of the Main Injector, the beam energy can be arbitrarily programmed on a turn-by-turn basis in the MI. No additional hardware is required.

### **5.16 Short Linac Bunches in the Broadband Impedance of the Main Injector**

It has been noted<sup>62</sup> that the short linac bunches injected in the Main Injector will undergo an energy loss of order 10 MeV/msec due to the broadband impedance estimated for the ring. This appears as a sort of “frictional” energy loss of individual bunches, that gradually disappears as the bunches naturally lengthen and debunch due to their internal energy spread. These preliminary simulations also indicate that no bunch-to-bunch coherent microwave instabilities generated for Proton Driver injection parameters.

The zero-order effect of the broadband impedance is a gradual deceleration of the bunches in the Main Injector for the first few milliseconds after injection. This can be partially compensated for by tracking the beam deceleration by slewing the linac energy downward over the course of injection. Subsequent adiabatic RF capture will have to be performed factoring in that this beam deceleration has occurred, i.e. the debunched beam must be captured at a slightly lower energy than the energy at which it was injected.

The second effect of the broadband impedance is relevant only if the beam chopper is used to deposit the beam directly in 53 MHz buckets. The energy loss from the broadband

impedance will cause the 53 MHz capture bucket to appear as a “moving bucket” with a distorted shape and significantly smaller bucket. This will impair RF capture of the chopped beam. A solution to this (suggested from the audience of the HPSL05 workshop) is for the 53 MHz RF Frequency and the chopping frequency to ramp downward during the course of injection so that it appears as a “stationary bucket” to the decelerating circulating bunches. This would allow essentially ideal RF capture of the chopped beam. Following 53 MHz RF capture and disappearance of residual 325 MHz bunch structure, the main RF voltage would be raised and acceleration would begin.

## 5.17 H<sup>-</sup> Beam Transport

The Proton Driver linac produces H<sup>-</sup> ions with a kinetic energy an order of magnitude higher than the 800 MeV H<sup>-</sup> beams routinely handled at LANL, and a factor of six higher than the SNS 1.3 GeV upgrade. To verify that no problems are foreseen with H<sup>-</sup> transport and injection at these energies, a workshop<sup>63</sup> with experts in the field was held in December 2004. Issues addressed included H<sup>-</sup> stripping from magnetic fields, beam line vacuum, blackbody radiation, and other possible sources of beam loss. One new effect, the stripping of H<sup>-</sup> ions by room-temperature blackbody radiation, was identified. The conclusion<sup>64</sup> of the workshop was that the design parameters of the Proton Driver linac transport line were valid and the performance could be reliably extrapolated from current experience.

### H- Stripping from Magnetic Fields.

Magnetic stripping of H<sup>-</sup> is caused by the intense electric fields (Lorentz-transformed B-fields) seen by relativistic H<sup>-</sup> ions as they pass through bend and focusing magnets. The formulae for stripping probability are given in<sup>65</sup> and references therein, and are plotted as a function of bend field and beam energy in Figure 27 and Figure 104. The Proton Driver linac operates in a region of molecular physics (H<sup>-</sup> lifetime vs. rest-frame electric field) which has already been probed by both experiment<sup>66</sup> and operational experience at accelerators<sup>67</sup>. Since special relativity in the range  $\gamma \sim 10$  seems to have adequate experimental support, the basic equations for calculating H<sup>-</sup> magnetic stripping losses are not in question.

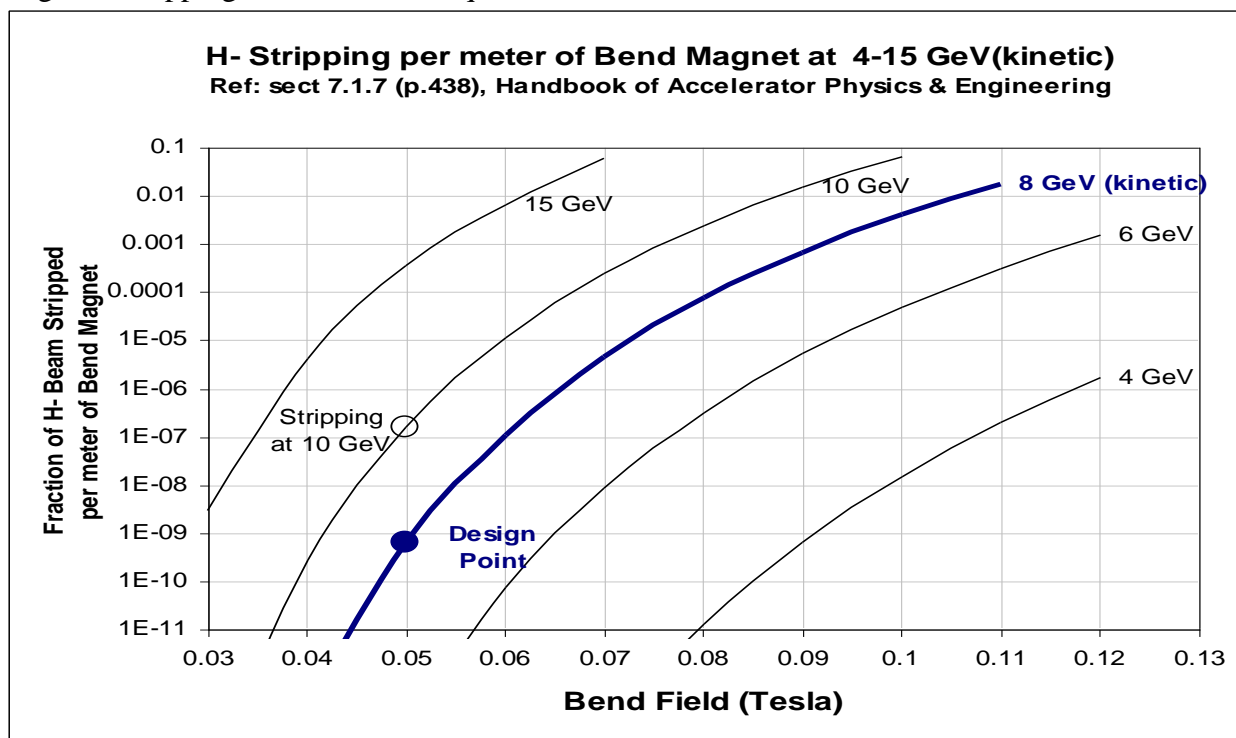


Figure 27 - Probability of stripping an H<sup>-</sup> ion per meter of bend magnet, as a function of the strength of the magnet, for H<sup>-</sup> kinetic energies between 4 GeV and 15 GeV. The chosen limit of 500 Gauss corresponds to an average 8 GeV beam loss power of 0.002 W/m when the Ultimate 2 MW of H<sup>-</sup> beam is transported through the line, or < 0.001 W/m when the line is used only to support 120 GeV Main Injector “Super-Beams”. These formulae plotted in Watts per meter as a function of beam energy in Figure 104.

To keep H- stripping to an acceptable level, magnetic fields are limited to 500 Gauss in both the dipoles and quadrupoles of the H- transport line. This bend strength limitation corresponds to a 700 m radius of curvature at 8 GeV. The design point (Figure 27) corresponds to a stripping probability of  $1\text{E-}9/\text{m}$  and  $0.002\text{ W/m}$  of beam loss.

The chosen radius of curvature of the transfer line places a hard upper limit on possible energy upgrades to the 8 GeV injector linac. The quasi-exponential dependence of H- stripping on the product of the beam momentum and bend field means the H- stripping turns on very rapidly as a beam line of fixed curvature is operated at higher energies. Assuming the canonical  $1\text{ W/m}$  allowable beam loss for “hands-on” maintenance, this limit to H- linac energy upgrades is roughly 9-10 GeV.

Magnetic stripping from quadrupoles in the superconducting linac is a potential concern. The magnetic field strength in a quadrupole increases linearly with radius, so the H- lifetime will be a strong function of the transverse displacement from the beam axis. This produces a soft “aperture” for magnetic stripping in the quads which can be compared to the physical aperture of the quads and iris if the cavities (see Figure 28). Beam halo surviving collimation in the room-temperature section of the linac will not be subject to H- stripping in quads, unless the beam is grotesquely mis-steered ( $>1\text{ cm}$ ) or there is anomalous halo growth in the SCRF linac sections.

Magnetic stripping of the H- by the radial component of 6 Tesla solenoidal end fields has been considered and does not appear to be a problem at beam energies below 110 MeV where the solenoids are used. This should be revisited when final field maps are available.

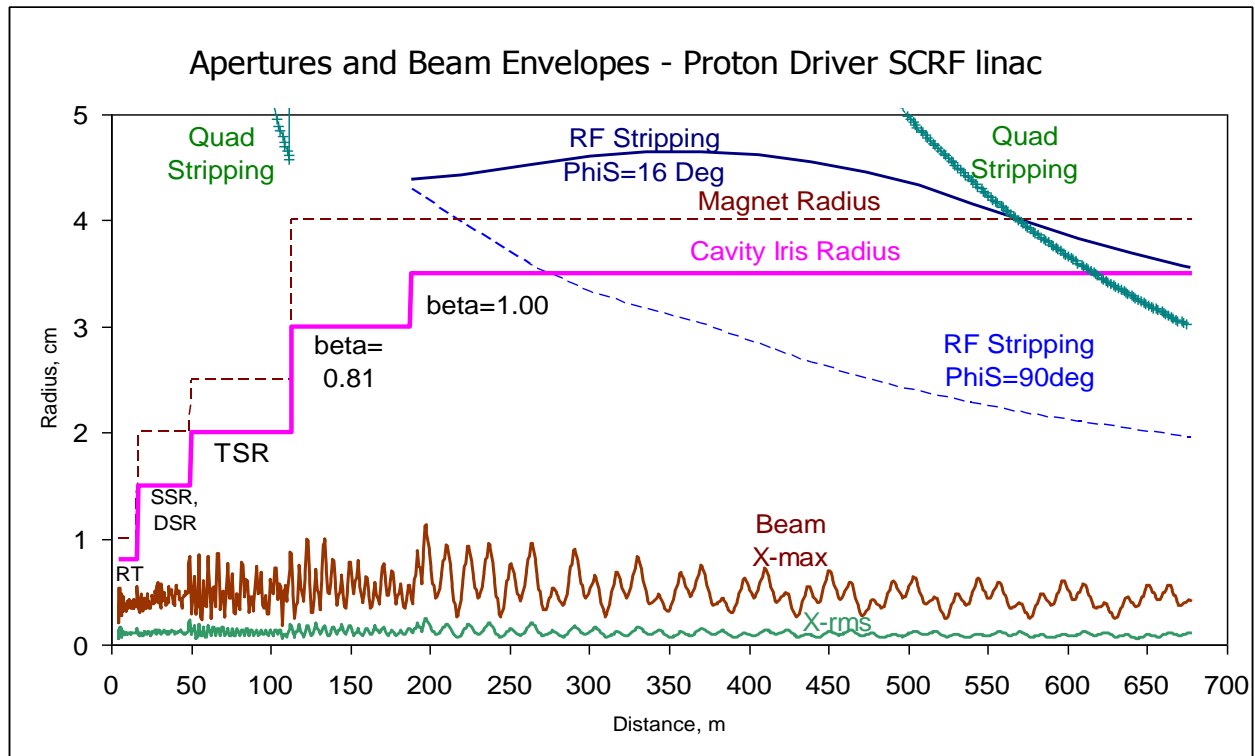


Figure 28 – Apertures and Beam Envelopes along the Proton Driver Linac. Beam envelopes are  $1\text{-}\sigma$  (RMS), and Maximum (out of 100k particles tracked). Also shown are SCRF cavity iris apertures, quadrupole radial bores, and H- magnetic stripping radius (probability  $.0001/\text{m}$ ) in quadrupole magnetic fields, and stripping apertures in the RF fields of the cavities at two different values of synchronous phase. Note the beam is collimated to  $R=3.7\text{ mm}$  in the RFQ and to  $R=7.5\text{ mm}$  in the Room-Temperature TSR section.

### H- Stripping from the Superconducting Cavity EM Fields

H- ions experience both electric and magnetic fields from the accelerating cavities. Both contribute to the H- rest frame electric field which determines the H- lifetime. The radial electric field is amplified by the gamma factor in the Lorentz boost from the cavity frame to the H- frame. As a result<sup>68</sup>, its magnitude can greatly exceed that of the lab-frame peak cavity electric field  $E_{PEAK}$ .

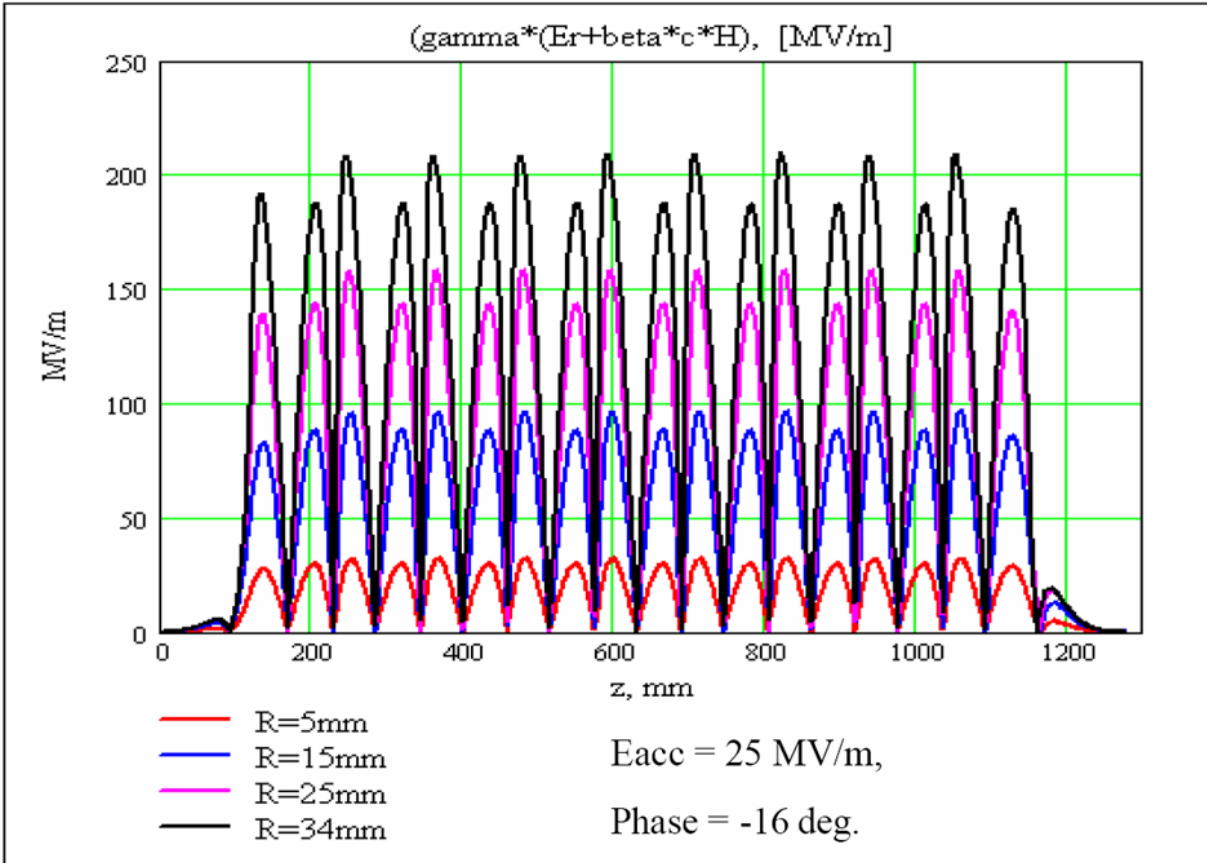


Figure 29 – Magnitude of H- rest-frame radial electric field seen by an 8 GeV H- traveling off-axis in the  $\beta=1$  superconducting cavities of the Proton Driver linac. The H- frame electric field can exceed the peak (lab frame) cavity electric field  $E_{PEAK}=52$  MV/m due to the gamma factor in the Lorentz boost. The peak field also depends on the synchronous phase, and is maximal for  $\phi_{SYNCH}=90^\circ$  when the particle passes near the cavity iris as the field goes through its maximum. A second maximum occurs when the particle passes off-center through the equator of the cavity, where the B-field maximum creates an electric field in the H- rest frame.

Like the quadrupole magnetic stripping, the cavity RF field stripping can be thought of as a “soft radial aperture” that varies along the length of the linac. This can be compared to both the physical apertures and the magnetic stripping apertures. See Figure 28.

RF stripping also depends on the accelerating field  $E_{ACC}$  and the synchronous phase. For beams passing through multi-cell cavities with  $\beta \neq \beta_{DESIGN}$ , the beam samples a variety of synchronous phases and the energy dependence of the stripping exhibits interesting behavior (see Figure 28).

### H- Stripping from Beam Line Vacuum.

H- losses from residual gas in the beam pipe are dominated by H- stripping by gas in the beam pipe rather than coulomb scattering or nuclear collisions. Cross sections for H- stripping decrease with increasing beam energy (see Figure 30).

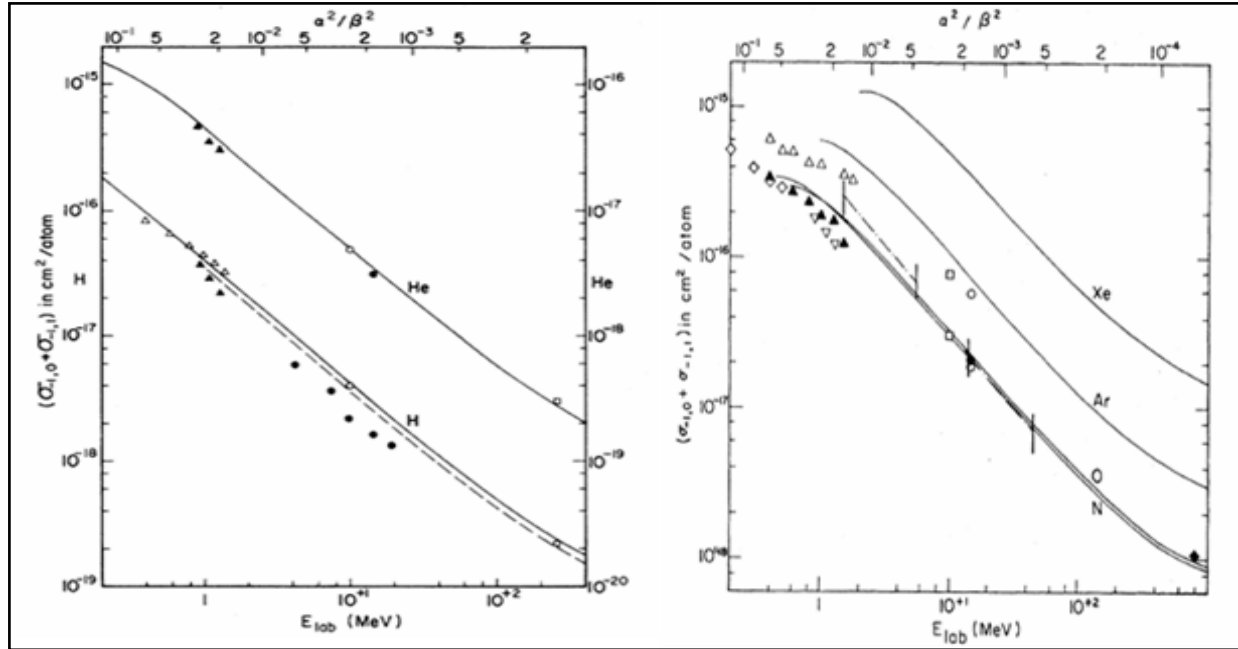


Figure 30 – Energy dependence of H- Stripping cross sections. Left: G.H. Gillespie, Phys. Rev. A 15, 563 (1977). Right: Gillespie, Phys. Rev. A 16, 943 (1977).

These cross sections have been combined with measurements of the residual gas in a beam line at Fermilab which is made with the same vacuum components proposed for the 8 GeV transport line. The calculated beam loss is  $10^{-7}/\text{m}$  corresponding to 13 mW/m of beam loss for the baseline design (see section 19.7 and Table 29). This is small compared to the losses from Blackbody radiation stripping (below).

### H- Stripping from Black Body Radiation.

A new and interesting source of H- stripping was uncovered in preparations for the Proton Driver H- transport workshop<sup>69</sup>. This is the stripping of high energy H- ions from room temperature black-body photons, which works as follows:

The room-temperature beam pipe of the beam transfer line is filled with a black body spectrum of thermal photons with typical energies of  $kT \sim 0.026$  eV. Since the binding energy of the spare electron in the H- ion is 0.75 eV, negligible numbers of blackbody photons are available to strip an H- at rest (see Figure 31). However if the H- is boosted to 8 GeV, thermal photons traveling towards the H- can be Doppler shifted by a factor of  $2\gamma \sim 20$ . This promotes a significant number of blackbody photons above the ionization threshold for H-.

The calculation of the absolute stripping rate has been independently performed by Howard Bryant of UNM and Chris Hill of Fermilab. The key inputs are the H- photoionization cross section (which has been calculated and measured in detail<sup>70</sup>), and the boosted blackbody spectrum (which is well known theoretically in the “GZK Cutoff” for ultra high energy cosmic rays to interact with boosted black body radiation from the Big Bang).

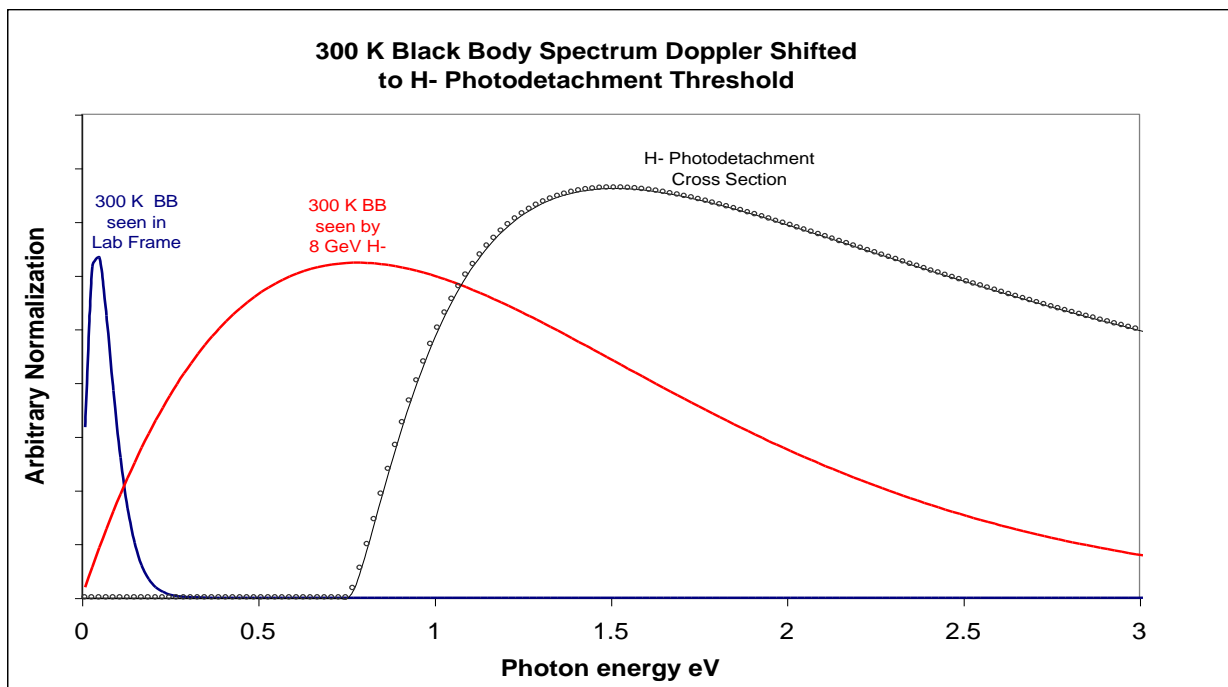


Figure 31 – Mechanism for 8 GeV H- Stripping from Black Body radiation<sup>69</sup>. The 300K black body photon spectrum (left curve) does not significantly overlap the H- photodetachment cross section (right curve) and thermal stripping of H- at rest is negligible. The Black Body spectrum seen by an 8 GeV H- ion (center curve; un-normalized) is Doppler shifted so that it significantly overlaps and the photodetachment cross section and the rate is non-negligible.

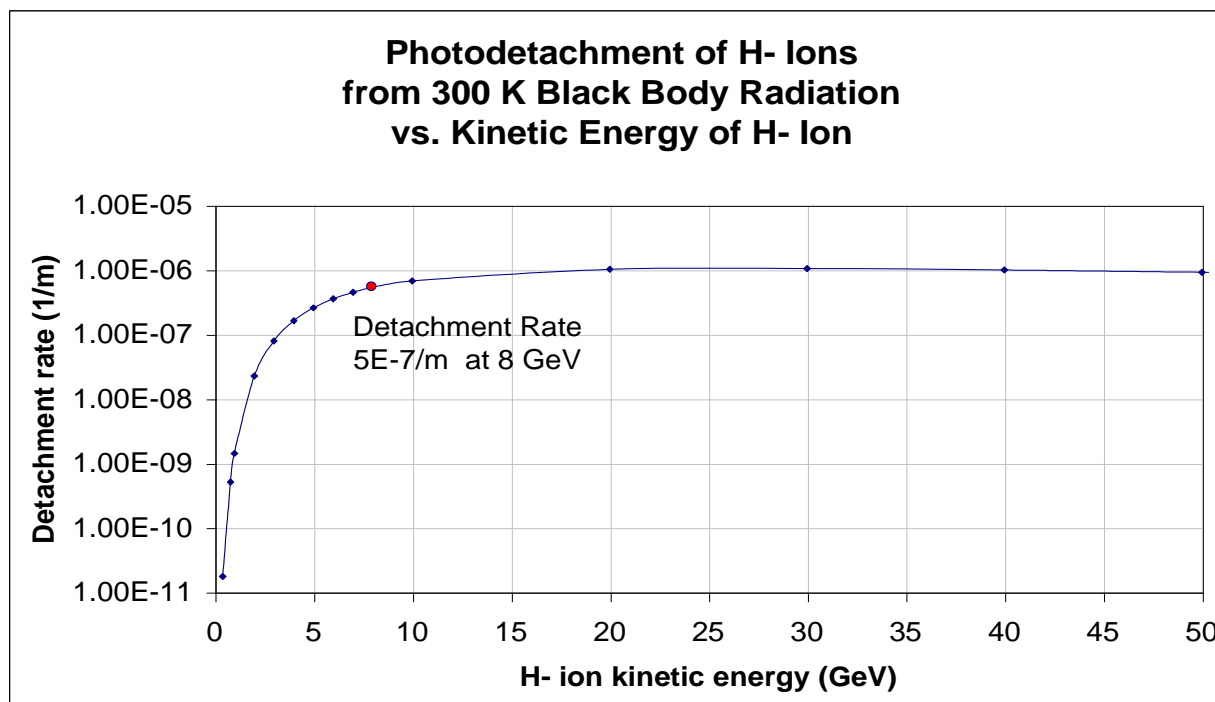


Figure 32 – Dependence of H<sup>-</sup> Photodetachment rate on kinetic energy.

Black body radiation causes an integrated beam loss of 0.048% in the 972 m long H- transfer line. For the baseline mission (120 GeV Main Injector operation), the average H- beam power is 166 kW and the loss rate is 80 Watts. While the average beam loss will be only 80 mW/m, there will be local hot spots such as the first bend downstream of a long straight section.

The Ultimate upgrade scenario might put as much as 2 MW average beam power through the H- transfer line, for example if the Recycler were used as a stretcher ring at 10 Hz. This would raise the H- loss from black body stripping to  $\sim 1$  W/m. Although this is right at the canonical 1 W/m limit for “hands on” maintenance, preliminary simulations indicate that activation of components at the magnet ends would make maintenance difficult. Inserting a simple collimation block which concentrates  $>99\%$  of the beam losses inside the body of the dipole magnets would greatly improve the situation for maintenance of the magnet ends<sup>164</sup>.

For the Ultimate scenario one might also consider a refrigerated beam screen inside the transfer line beam pipe. A beam screen running at 77 K (liquid nitrogen) would reduce the H- beam loss from black body radiation by a factor of  $\sim 4000$  (see Figure 33) and probably reduce the beam vacuum stripping losses as well.

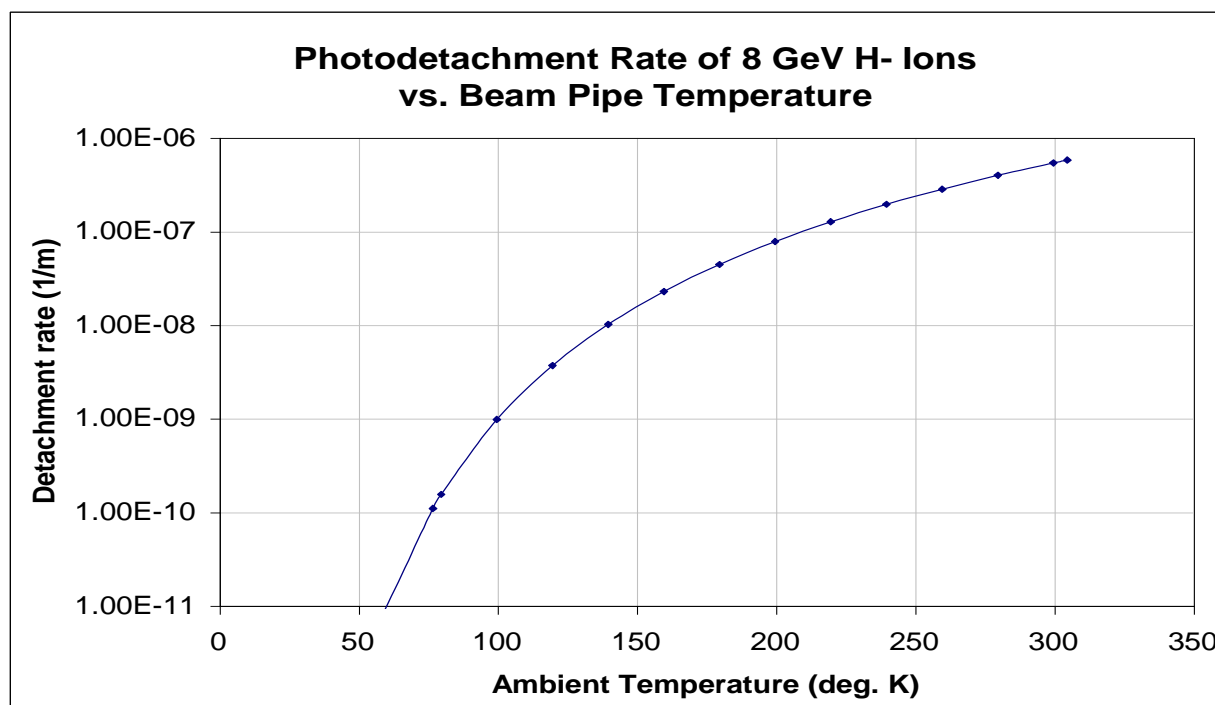


Figure 33 – Dependence of H- Photodetachment rate on Temperature of the Beam Pipe. A beam screen operating at 77°K drops the H- stripping rate by three orders of magnitude. A cooled beam screen is a backup option not required for the baseline design.

## 6 FRONT-END LINAC DETAILED DESIGN

An overview of the front-end linac<sup>71</sup> has been given in section 3.1. This section gives technical details, parameters, and justification for design choices made in the baseline design.

The baseline design of the Proton Driver Front-End Linac is based on the existing designs for the SNS, JPARC, and RIA. It operates at 325 MHz, one fourth of the ILC's 1300 MHz. Significant differences with respect to the SNS and JPARC include the use of solenoidal focusing below 110 MeV, a transition from warm copper to superconducting cavities at 15 MeV, and an RF system that extends the TESLA RF power split technique to the front-end linac with the use of Ferrite Vector Modulators. The parameters are given in Table 11 and the overall layout is shown in Figure 6.

Table 11 – Warm Front End Linac Main Parameters

WARM FRONT-END LINAC	8 GeV Linac	
Linac Type	Room-Temp. Triple Spoke Resonator (RT TSR) with Solenoidal Focusing	
Input energy	3 MeV	RFQ Output Energy
Output energy	15.8 MeV	Feeds SCRF Spoke Linac
Duty Cycle (beam)	1 %	
Length	10.4 m	
RF frequency	325 MHz	RF Split from main Klystron, with ferrite tuners
Average synchronous phase	-35 to -25 degrees	TBD
Number of tanks	21	Warm 3-spoke Resonators
Maximum field	TBD MV/m	
Bore radius	8 mm	
Focusing Magnet Type	Warm-Bore Superconducting Solenoid	
Focusing structure	Solenoids between each 3-spoke warm tank	
Number of focusing magnets	21 solenoids	
Focusing period	~6 beta-lambda (Independently phased resonators)	
Focusing Strength	4.0-6.0 T	
Number of steering dipoles	42	two per solenoid - # powered TBD
Average operating vacuum pressure	1.80E-07 Torr	TBD
Length of differential pumping section	TBD m	use cryopumping of SC Solenoids in RT-TSR?

### 6.1 H- Ion Source

The 30 mA peak current required for the Ultimate Scenario can be met with a conventional RF driven “volume” H- source similar to those at DESY, JPARC, or developed by LBNL for the SNS. Our strategy is to copy an existing design with minimal modifications, after first making certain that the chosen design operates well at both the Initial (3 msec x 10 mA x 2.5 Hz) and Ultimate {1 msec x 30 mA x 10 Hz) beam parameters.

A major design choice is whether the RF coil is located inside the plasma volume such as the SNS source, or outside of the ceramic tube containing the RF-driven plasma as in the DESY source. See Figure 34. A inside coil has performance advantages, and an outside coil has reliability and maintenance advantages.

In collaboration with ORNL we have verified<sup>71</sup> that the SNS/LBL source works well at the Initial (3 msec x 10 mA) pulse width as well as the Ultimate pulse width which is the standard (1 msec x 30 mA) operating point for the SNS source. We plan to conduct similar tests of the DESY source in the near future. The DESY source is normally operated at a lower duty factor than needed by the Proton Driver. If the DESY source performance is adequate, and if the cooling of the DESY source is can be made adequate at our higher duty factor we will probably adopt the DESY source due to the more maintenance-free external coil design.

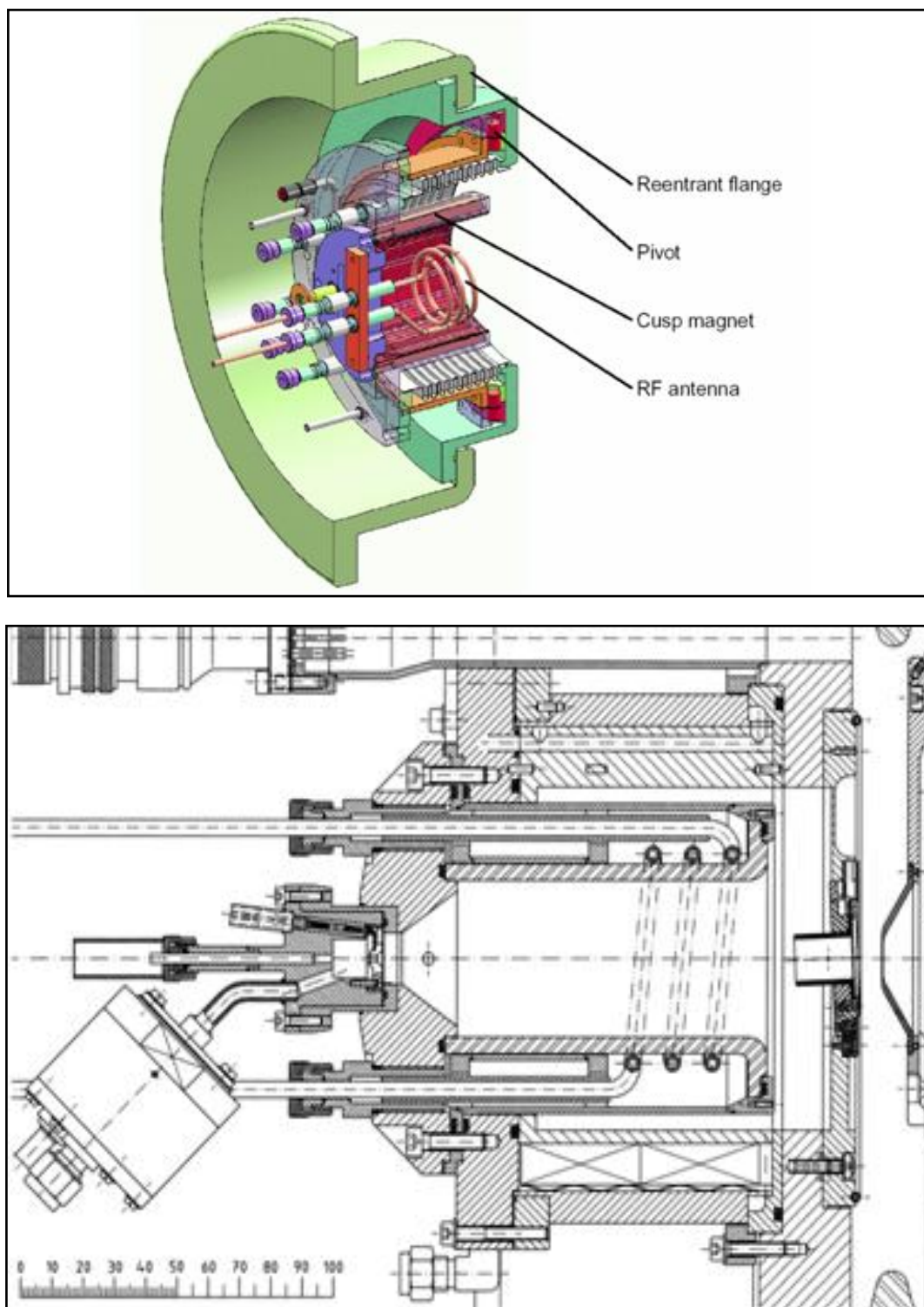


Figure 34 – Comparison of the SNS/LBNL H- source (top) and the DESY H- source (bottom). The H- in both sources is created in a plasma volume driven by RF coil excitation. The SNS source has the RF drive coil located inside the plasma volume, while for the DESY source the drive coil is located outside of a ceramic tube containing the plasma volume. The DESY source offers a potentially longer lifetime at the expense of requiring more RF power to drive the plasma, with an as-yet-untested performance at longer pulse lengths.

Table 12 – Parameters for the Proton Driver H- Source, LEBT, LEBT Chopper, and RFQ

FRONT END (H-)	8 GeV Initial {Ultimate}	
Ion type	H-minus	
Pulse Rate	2.5 {10} Hz	
Pulse Width	3.0 {1.0} ms	
Output energy	3 MeV	RFQ output
Length	6.47 m (TBD)	From Ion Source outlet flange first RTSR
Output peak current	9.3 {28} mA	
<b>ION SOURCE AND LEBT</b>		
Output energy	65 keV	
LEBT length	0.1 m	
Output peak current	12.7 {38} mA	Assuming 80% front end transmission
Ion source type	RF volume	Multicusp Cs-enhanced
Electron suppression	magnetic	Interception at low energy
LEBT focusing type	electrostatic	
Estimated output rms norm H & V emit.	0.2 pmm-mrad	
Ion source lifetime	72 weeks	?? Scale by pulse rate from SNS ??
Ion source replacement time	2 hours	With conditioned replacement ion source
<b>LEBT CHOPPER</b>		
Type	LBL/SNS	
Purpose	Establish 700ns abort kicker rise time gap in ring	
Deflection	transverse	uses split focusing electrodes in LEBT
Output peak current	9.3 {28} mA	
ON/OFF beam current ratio	5E+03	TBD
Rise, Fall Time	< 20 ns	1% - 99%
Operating energy	< 65 keV	
Operating Voltage	10 kV	TBD
<b>RFQ ACCELERATOR</b>		
Output energy	3 MeV	
Length	~4 m	
Output peak current	9.3 (28) mA	
RF frequency	325 MHz	RF Split from main Klystron, with ferrite tuner
Nominal aperture radius	3.7 mm	
Peak surface field during macropulse	1.85 Kilpatrick	
Macropulse structure power	630 kW	Assumes 67% of Cu Q
Expected output rms norm H & V emit.	0.21 pi mm-mrad	
Expected output rms L emittance	0.1 pi MeV-deg	At 325 MHz

## 6.2 Low Energy Beam Transport (LEBT)

The functions of the LEBT are to remove electrons from the H- beam, accelerate and focus the H- Ions to the input of the RFQ, and (optionally) to pre-chop the beam.

Either magnetic or electrostatic focusing is workable. The DESY and SNS LEBTs represent successful designs of each type. Integration of the LEBT chopper design may be the decisive factor in which to copy.

The function of the pre-chopper LEBT is in principle redundant with the fast chopper in the MEBT. The main function in the case of the SNS is to reduce the power dissipation on the MEBT chopper target by eliminating beam current during long chopper-active periods. The average current in the Proton Driver is ~6x lower than the SNS, so this function is less crucial, and a magnetic LEBT may be preferred.

### 6.3 Radio Frequency Quadrupole (RFQ)

The design of the 30 mA RFQ built for the JPARC project by KEK can be used directly for the Proton Driver. The JPARC operating frequency of 324 MHz is within tuning range of the 325 MHz required by the Proton Driver. Small changes in the vane profiles are described in section 5.5. Changes to the mechanical support and alignment scheme will be needed to incorporate the “alignment rails” for the front end linac beam line components (see Figure 36). Parameters of the RFQ are given in Table 12.

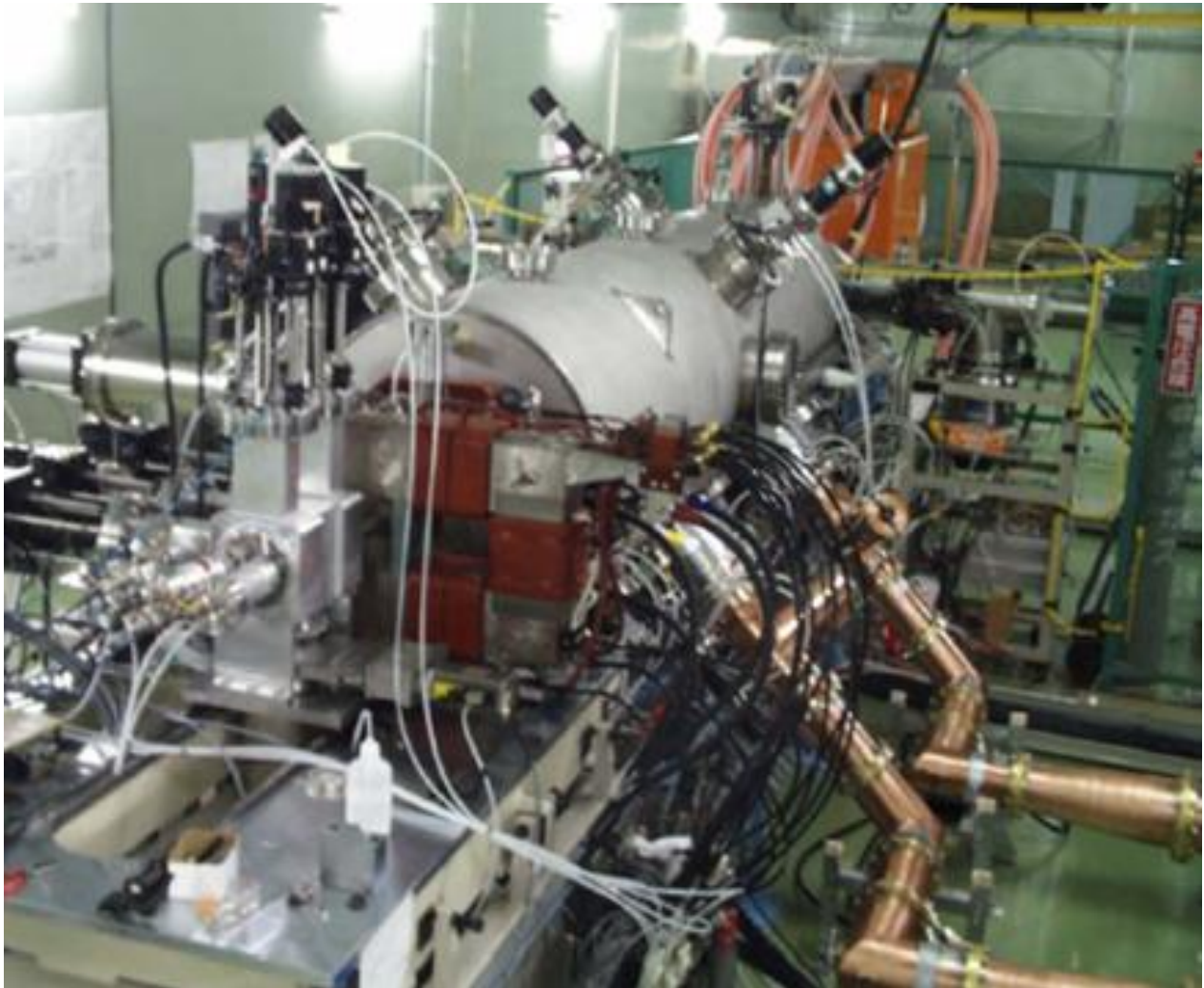


Figure 35 – The Radio Frequency Quadrupole (RFQ) built for the JPARC project by KEK.

The ~600 kW of RF power for the RFQ will be derived from a hybrid power split from the 2.5 MW Klystron used to power the rest of the linac. 1-2 channels of 325 MHz Ferrite Vector Modulator will be used. See section 12.5.

#### 6.4 Medium Energy Beam Transport (MEBT)

The function of the MEBT is described in Section 3.1 and the optics of the MEBT are described in Section 5.6. The concept of using alignment rails for beam line components is shown in Figure 36. Solenoids, cavities, choppers, and diagnostics will be fiducialized and electromagnetically centered with respect to the rails as they are calibrated. This will allow a flexible deployment of beam line components as the linac is commissioned. Similar rail alignment systems used at RAL and for magnet production tooling have accuracies of  $\sim 0.1$  mm over spans of a few meters, and reproducibility of component alignment better than this<sup>72</sup>.

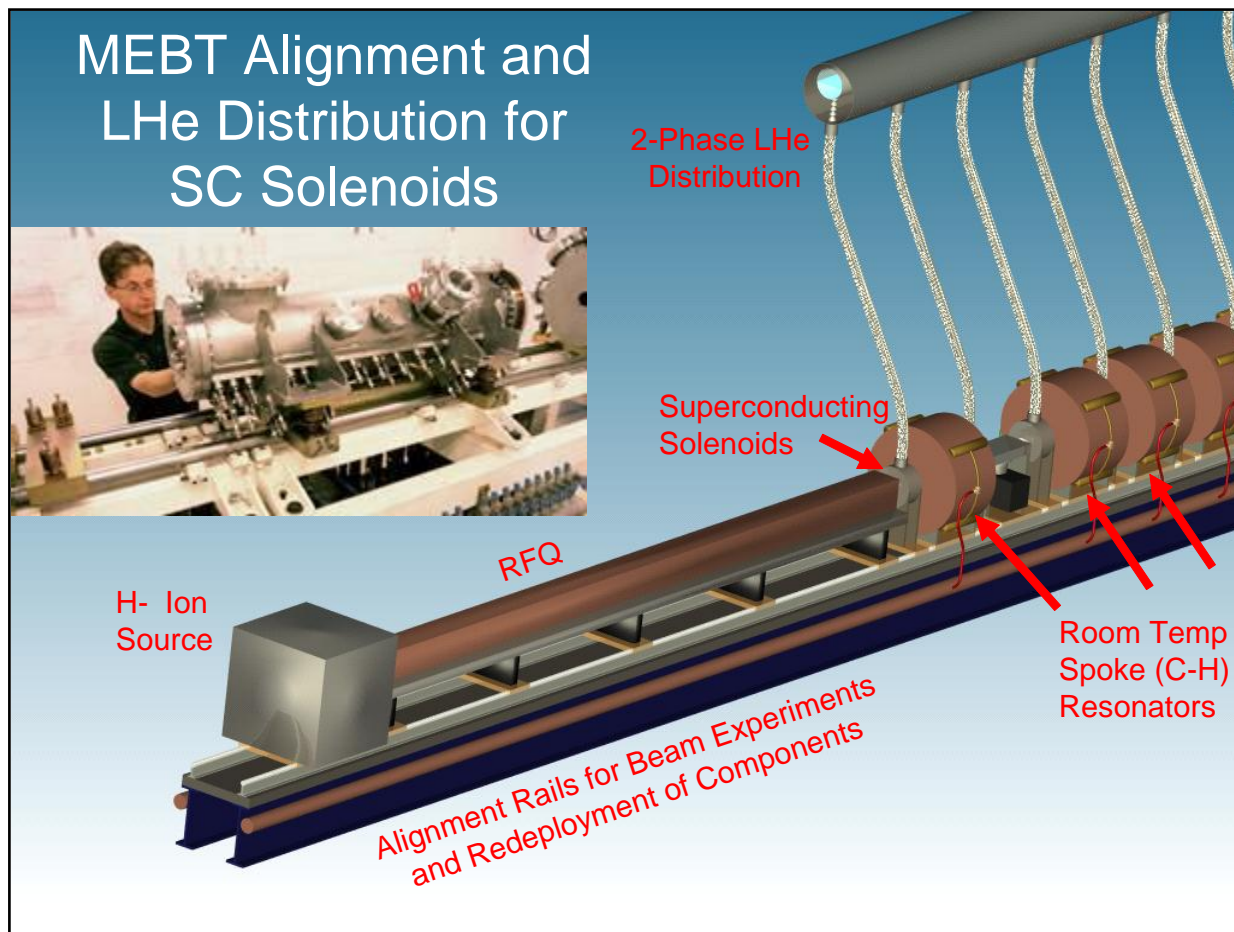


Figure 36 – Schematic of the front-end linac beam line component alignment rails and cryogenic distribution system. Insert: similar alignment system at Rutherford Applications Lab (RAL).

The two-phase helium distribution system to the 23 warm-bore superconducting solenoids in the MEBT and RT-TSR is also shown in Figure 36. It is a TESLA-like scheme in which a half-full pipe located above the beam line supplies liquid to, and returns vapor from, the flex hoses connected to each solenoid. The flexibility is necessary to permit redeployment of the solenoids to make room for diagnostics, beam optics experiments, etc. To expedite cool down, either the flex hoses will be slightly oversized for steady-state operation, or a distribution and filling manifold inside the helium space will be used to supply LHe to the individual loads during cool down.

The two bunching cavities used in the MEBT are identical to the RT-TSRs (section 6.6).

## 6.5 Fast Beam Chopper in MEBT

A bunch-by-bunch beam chopper is provided in the MEBT design. The goal is to provide digital bunch-by-bunch chopping control over the beam, with acceptably small transverse disturbance of the non-chopped beam (sections 3.1 and 5.6). (The chopper parameters given in Table 12 are for the “slow” chopper required to produce the beam abort gap in the Main Injector).

At 3 MeV the 325 MHz bunches are separated by 7.5cm and the bunches are ~3 cm long. Thus the electrostatic kick must be spatially localized within  $\pm 2$  cm and the electrical rise time must be faster than 2 nsec. So-called “meander-line” structures (Figure 38) with the required properties have been built for the SNS and the CERN SPL project<sup>55</sup>. At present the performance is limited by the electrical pulsers and true bunch-by-bunch chopping has not been achieved. This is the focus of an ongoing collaborative R&D at the Proton Driver front end test facility<sup>73</sup>.

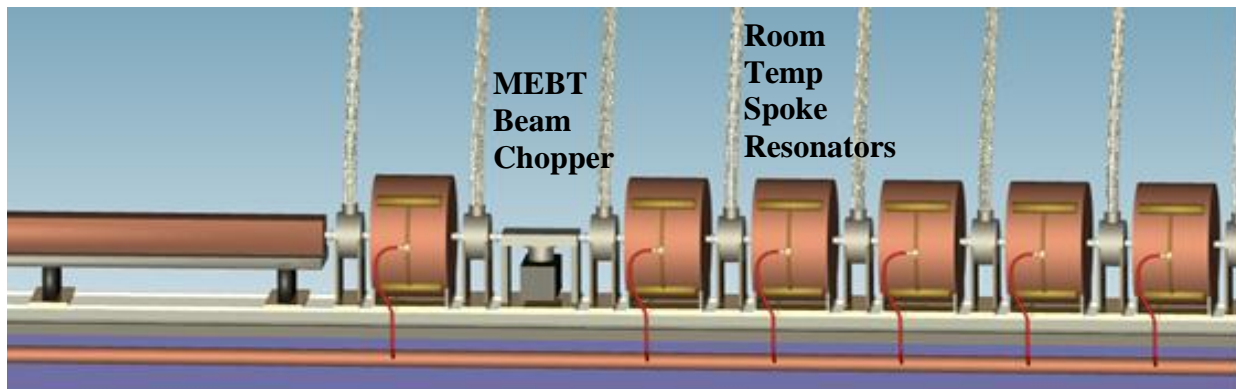


Figure 37 – MEBT Fast Chopper and the beginning of the RT-TSR section.

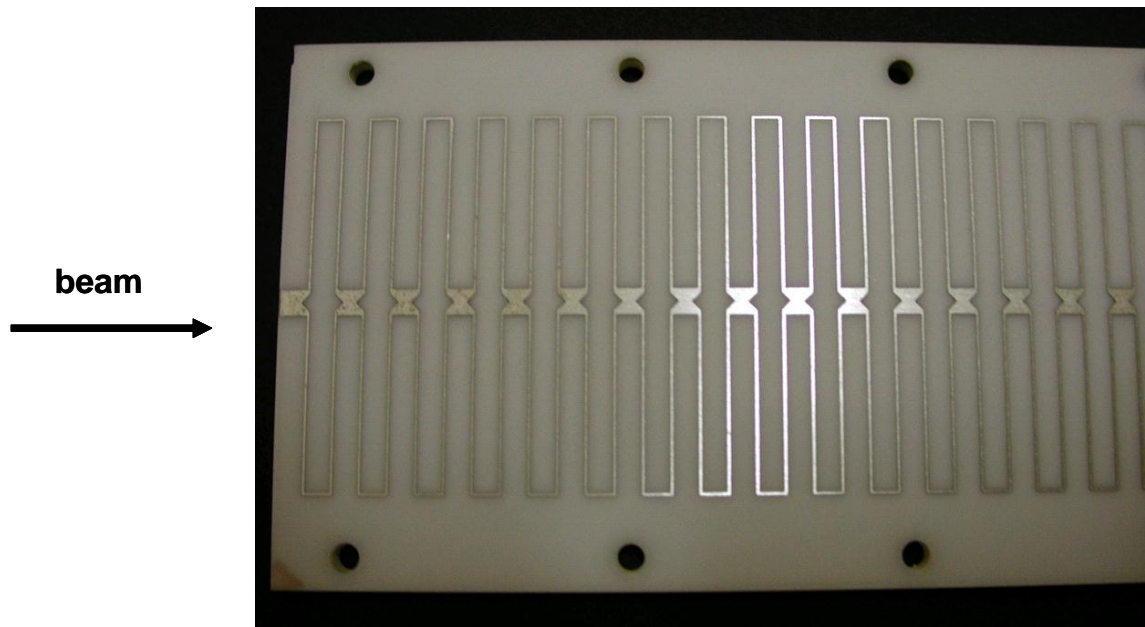


Figure 38 – Chopper electrode for the CERN SPL chopper<sup>55</sup>. The propagation of the pulse down the stripline matches the velocity  $\beta \sim 0.08$  of the beam. The beam is deflected by a pair of electrodes located above and below the beam.

## 6.6 Room-Temperature Spoke Resonators (RT-TSRs)

Water-cooled copper spoke resonators are used to accelerate the beam from the 3 MeV output of the RFQ to the 15 MeV input of the superconducting spoke resonators. The rationale for using spoke resonators in this energy range is discussed in section 5.8. Room temperature multi-spoke resonators (sometimes called C-H Resonators) have been developed for a number of applications<sup>74</sup> over the last 10 years. The baseline design uses 3-spoke resonators throughout, although this may be subject for further optimization. Baseline parameters for the spoke resonators are given in Table 13.

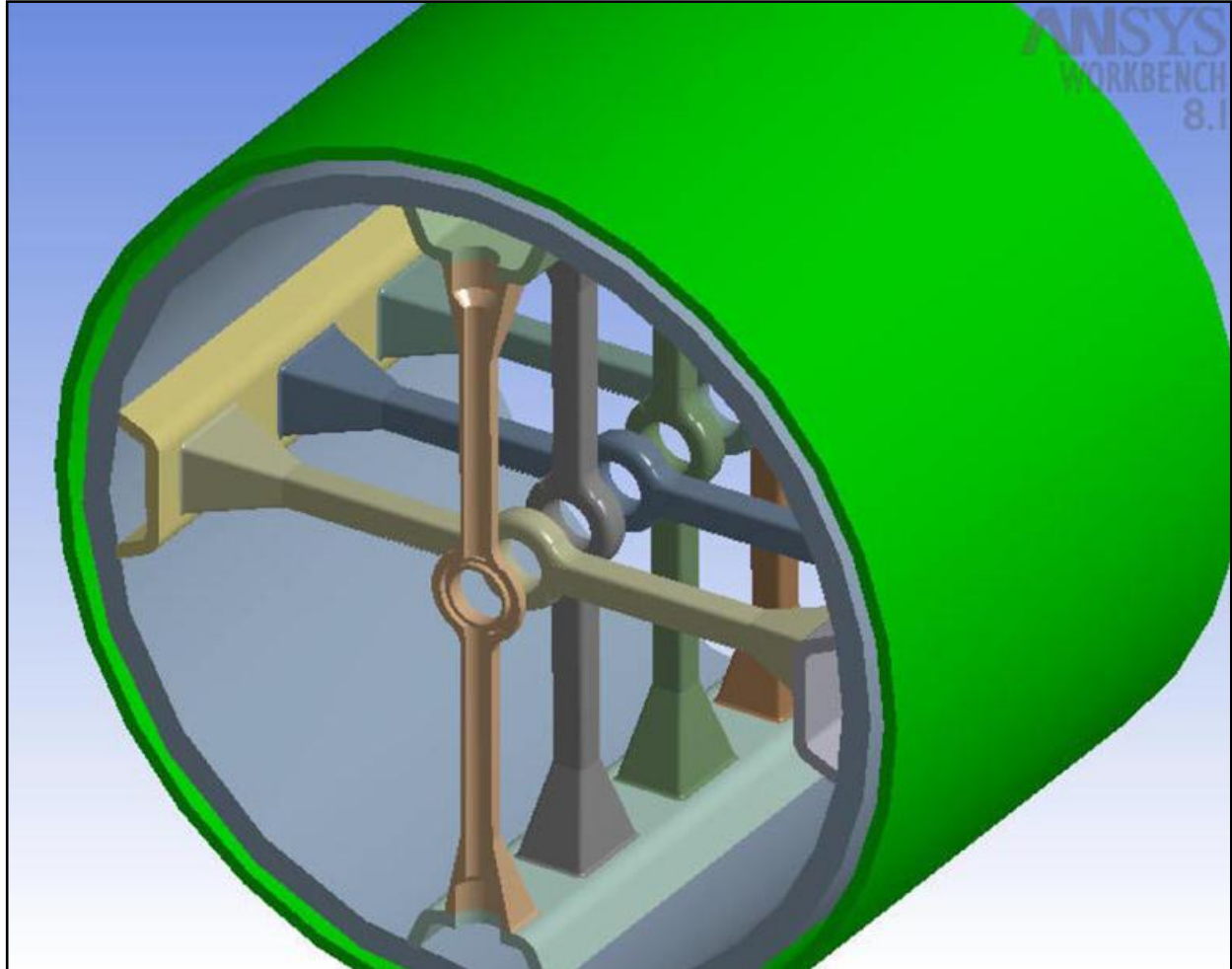


Figure 39 – Room Temperature Spoke Resonator (RT-TSR, sometimes known as C-H resonator) developed for the GSI Linac. The structure has a high shunt impedance due to the small gap capacitance that is possible due to the absence of focusing magnets of a DTL. Most of the power dissipation is in at the base of the water-cooled spokes. Mechanical designs of the first RT-TSRs for the PD linac are shown in Figure 10.

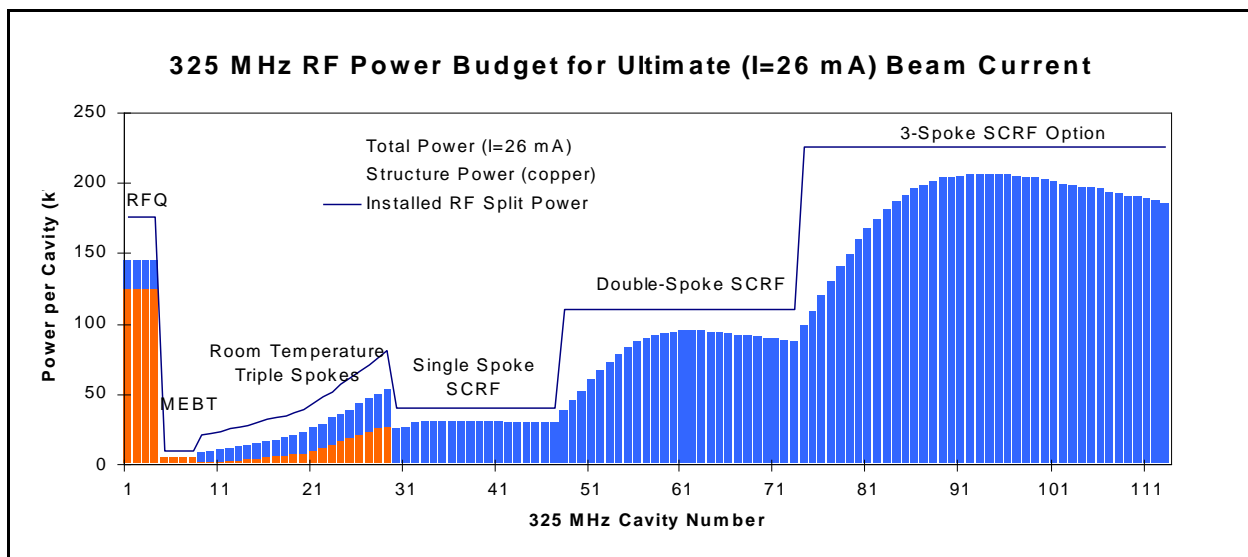


Figure 40 – Peak RF Power per channel for 325 MHz Linac for the Ultimate (26 mA) beam current. The copper structure power is indicated in orange bars, the total power in blue bars. The blue line is a first estimate of the installed RF power, i.e. the maximum output power from the Ferrite Vector Modulators (FVM's) on each RF channel. The RFQ is assumed to be driven by four channels of FVM operating at 175 kW. The transition from normal-conducting to superconducting spoke resonators occurs at 15 MeV where the copper power and beam power are roughly equal.

## 6.7 Alternative of a Warm Copper DTL for the Front-End Linac

The baseline option SCRF linac described here differs from the front end linac for the first design study<sup>75</sup>. This was based on purchasing a modified version of a commercially available warm-copper Radio Frequency Quadrupole / Drift Tube Linac (RFQ/DTL) assembly with an output energy of 86 MeV.

At 325 MHz, a similar approach could be taken by cloning the JPARC DTL and using the 2.5 MW JPARC Klystron. Although vendor pricing was not developed for this option, it also remains a technically feasible, but more expensive, alternative.

The main disadvantage of a warm copper DTL is the high RF power required. The shunt impedance of a DTL is limited by the capacitance of the large drift tubes required to house the focusing quadrupoles. Therefore 7-9 Klystrons, with modulators, would be required to reach an energy of 85-110 MeV. This results in a significantly more expensive overall system than the superconducting front end in the baseline design.

A warm copper DTL is also incompatible with solenoidal focusing, due to the large size of the focusing solenoids. These would greatly increase the drift tube gap capacitance and RF power requirements.

Another disadvantage is that the DTL is a rigidly defined structure with little opportunity to debug the beamline optics. As a result, there is a history of unexpected and uncorrectable emittance growth in the first DTL tanks of many projects. The modular construction and solenoidal focusing of the baseline design will hopefully avoid this difficulty.

## 7 325 MHz SPOKE RESONATOR SCRF LINAC

At 15 MeV the transition is made from normal-conducting to superconducting accelerating structures. The SCRF sections begin with spoke resonators (Figure 11 and Figure 41) similar to those developed for RIA<sup>76</sup>, APT, and other projects. Single, double, and triple spoke resonators are used to cover successive velocity ranges.

The major parameters of the Spoke Resonator SCRF linac are given in Table 13 below. A single cryomodule containing 16 single-spoke resonators accelerates the beam from 15 to 33 MeV. Two additional cryomodules each containing 14 Double-spoke resonators accelerate the beam to 110 MeV. Solenoidal transverse focusing is used in these cryomodules.

**Table 13 – Spoke Resonator SCRF Linac Parameters for the Proton Driver linac**

<b>Spoke Resonator SRF Linac</b>	<b>Med-Beta = Elliptical</b>	<b>Med-Beta = Spoke</b>		
Linac Option Chosen for Medium Beta:				
Input energy	15 MeV	15 MeV	from warm spokes	
Output energy for Spoke Cryomodules	110 MeV	400 MeV	start of 1300 MHz Elliptical Cavities	
Length of Spoke Section	40.1 m	104.1 m		
Number of Spoke Resonators	65	107	including warm resonators	
Number of Spoke Cryomodules	3	9		
Number of Spoke Cryomodule Designs	2	3		
Number of 325 MHz Klystrons (initial)	1	2		
Cryomodule Type (Beta)	<b>RT-TSR</b>	<b>1-Spoke</b>	<b>2-Spoke</b>	<b>3-Spoke Option</b>
Operating Temperature	WARM	4.5K	4.5K	4.5K
Geometrical Beta of Sections	<b>.008-.018</b>	<b>0.21</b>	<b>0.40</b>	<b>0.61</b>
RF frequency (MHz)	325 MHz	325 MHz	325 MHz	325 MHz
Input Energy of each section (MeV)	3 MeV	15 MeV	33 MeV	110 MeV
Epeak	TBD	32 MV/m	32 MV/m	32 MV/m
Eacc	3 MV/m	11 MV/m	11 MV/m	11 MV/m
Number of Cryomodules for each Beta	n/a	1	2	6
Length of Cryomodule slot for each Beta	n/a	12.5 m	8.6 m	10.67 m
Total Length for each Beta	10.4 m	12.5 m	17.2 m	64.0 m
Number of Spokes Per Resonator	3	1	2	3
Number of Resonators Per Cryomodule	n/a	16	14	7
Number of Magnets Per Cryomodule	n/a	16	7	7

### 7.1 SRF Spoke Resonators

An accelerating gradient  $E_{ACC}=11$  mV/m and a peak electric field of 32 MV/m is assumed for all spoke resonators in this study. Using modern cavity processing and high pressure rinsing techniques, gradients in this range have been attained in CW operation of prototype single, double, and triple-spoke cavities at ANL, LANL, and Orsay. See Figure 42.

Unlike previous projects which use the spokes for acceleration of continuous (CW) beams and RF power dissipations of 25-50 W/cavity, the Proton Driver linac operates these resonators in pulsed mode. The RF duty factor is 1.5% and the cryogenic power is < 1 Watt/cavity – smaller than the expected static heat leak. This reduces the incentive for 2 K operation, and in the baseline design the resonators are run with a 4.5 K (pool boiling) cryogenic system.

An optimized design for the 325 MHz spoke resonators is being prototyped by a FNAL/ANL collaboration. The design improvements lead to a ~25% increase in  $E_{ACC}/B_{PEAK}$  compared to existing designs. The detailed mechanical design<sup>77</sup> is nearly complete and fabrication should begin in late 2005. If successful, this could reduce the number of spoke resonators in the baseline design, or increase the design margin and tolerance for cavity failures.

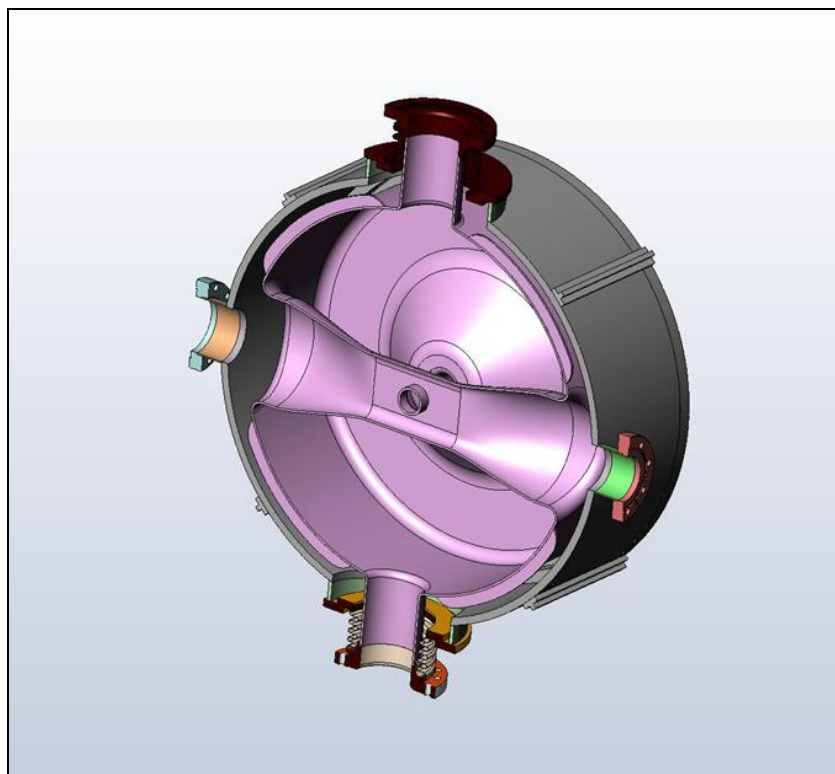


Figure 41 – FNAL/ANL prototype design for an optimized 325 MHz single spoke resonator is expected to lead to a ~20% increase in  $E_{ACC}/B_{PEAK}$  compared to existing designs.

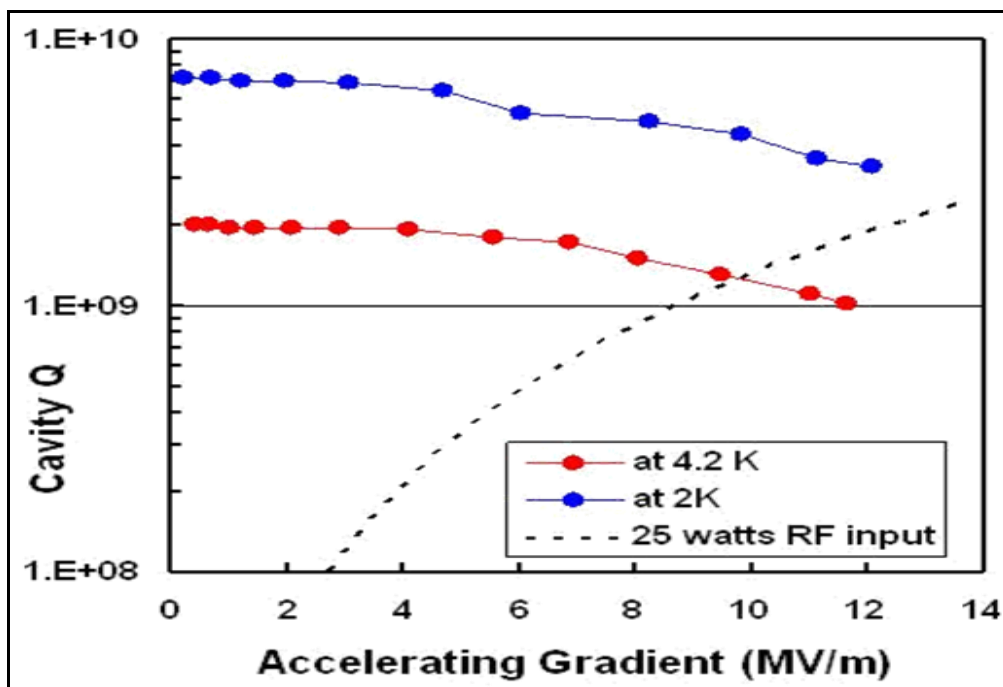


Figure 42 – Accelerating gradients obtained for ANL Double-Spoke cavity prototypes<sup>78</sup>.

## 7.2 Triple Spoke Resonators from 110-400 MeV (Baseline Design)

In the range from 110-400 MeV, both 325 MHz Triple-Spoke resonators and 1300 MHz elliptical-cell cavities are under consideration<sup>79</sup>. The 325 MHz Triple-Spoke resonators are the baseline for both cost and accelerator physics calculations. Six cryomodules approximately 10 m long will be used in either option. The parameters for the 325 MHz baseline option are given in Table 13, and parameters for the 1300 MHz elliptical option are given in Table 14. The energy gain per cavity is plotted for the baseline design in Figure 43, and for the elliptical option in Figure 46.

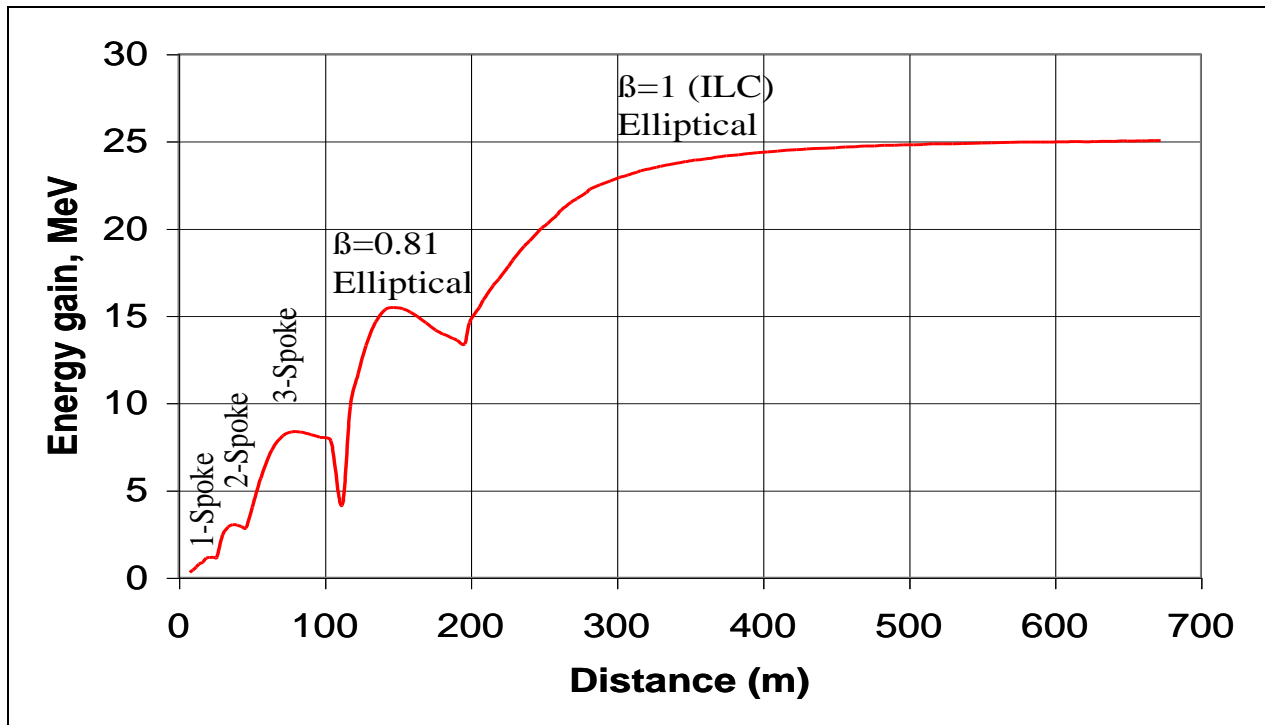


Figure 43 – Energy Gain per cavity vs. distance along the Proton Driver linac for the baseline (triple spoke cavity) option. The dip in the energy gain at the spoke-to-elliptical transition at 110 MeV is from the bunch rotation at the frequency jump, where the synchronous phase is adjusted to match the bunch shape across the frequency jump transition.

## 8 1300 MHz ELLIPTICAL-CELL CAVITY SCRF LINAC

The major parameters of the main 1300 MHz SCRF linac are given in Table 14 below. The first two columns (“low” and “medium” beta) correspond to the elliptical cavity option in the energy range 110-400 MeV. This energy range is covered by 3-spoke cavities in the baseline design. The 1300 MHz cryomodules are described in Section 16.

Table 14 – 1300 MHz SCRF Linac Parameters for the Proton Driver

Elliptical-Cell SRF LINAC	8 GeV Initial {Ultimate}			
Output energy	8000 MeV			
Input energy	110 MeV	(~400 MeV if triple-spoke resonators used)		
Length of Elliptical-Cell Linac Section	565.6 m	(~ 508 m if triple-spoke resonators used)		
Number of Elliptical Cryomodules	48	( 42 if triple-spoke resonators used)		
Cryomodule Style	TESLA (TTF3)	no warm spaces between cryomods		
Number of Cavities	384	( 336 if triple-spoke resonators used)		
RF frequency	1300 MHz			
Cavity Maximum Field Epeak	52 MV/m	TESLA(500)=47, TESLA(800)=70 MV/m		
Cavity Accelerating Field Eacc	13-23 MV/m	varies along length - see graph		
Cavity Voltage Profile	Constant Gradient			
Number of Beta Sections	4	( 2 if triple-spoke resonators used)		
	<u>Elliptical Cavity Option</u>			
	<u>LOW</u>	<u>MEDIUM</u>	<u>HIGH</u>	<u>"TESLA"</u>
Cryomodule Type (Beta)				
Geometrical Beta of Sections	0.47	0.61	0.81	1.00
Input Energy of each section (MeV)	110 MeV	175 MeV	400 MeV	1200 MeV
Number of Elliptical Cryomodules	2	4	6	36
Length of Cryomodule slot for each Beta	9.40 m	9.62 m	11.68 m	12.2 m
Total Cryomodule Length for each Beta	18.8 m	38.5 m	70.1 m	438.3 m
Number of Cells Per Cavity	6	6	8	9
Number of Cavities Per Cryomodule	8	8	8	8
Number of Cavities per Klystron	48 {16}	48 {16}	48 {16}	36 {12}
Number of Quads Per Cryomodule	9	5	3	1
Quad + BPM Assembly Lengths	0.42 m	0.42 m	0.86 m	0.86 m
Space between cryomodule valves	0.5 m	TBD - cold beam pipe with profile monitor		
Length for additional cryomodules	TBD m			
Number of Klystrons	11 {31}	+1 for optional Debuncher Cavity		
Klystron Total Peak Power	110 {310} MW			
Peak Beam Power	65 {200} MW			
Warm beam pipe vacuum	N/A Torr			

The Proton Driver main linac uses unmodified TESLA (TTF3) cavities operating at an accelerating gradient of 26 MV/m. This is slightly above the 23.4 MV/m assumed in the TESLA-500 design but well below both the 35 MV/m assumed in the TESLA-800 design. Recent state-of-the-art results for single cavities are above 45 MV/m.

Although the baseline does not depend on them, the higher gradients being pursued by the ILC are useful for the Proton Driver in that they will increase the linac output energy, the operating margin for cavity gradient, the fault tolerance for single-cavity failures, or a combination of all three.

The  $\beta=0.81$ ,  $\beta=0.61$  and  $\beta=0.47$  cavities are frequency scaled versions of the 805 MHz cavities successfully developed for SNS and RIA<sup>80,81</sup>. See Figure 44 and Figure 45. This allows the  $\beta<1$  linac to share klystrons, RF couplers, cavity end groups, and the cryomodule basic design and assembly infrastructure with the main linac of the ILC and Proton Driver. Cavity parameters are given in Table 15.

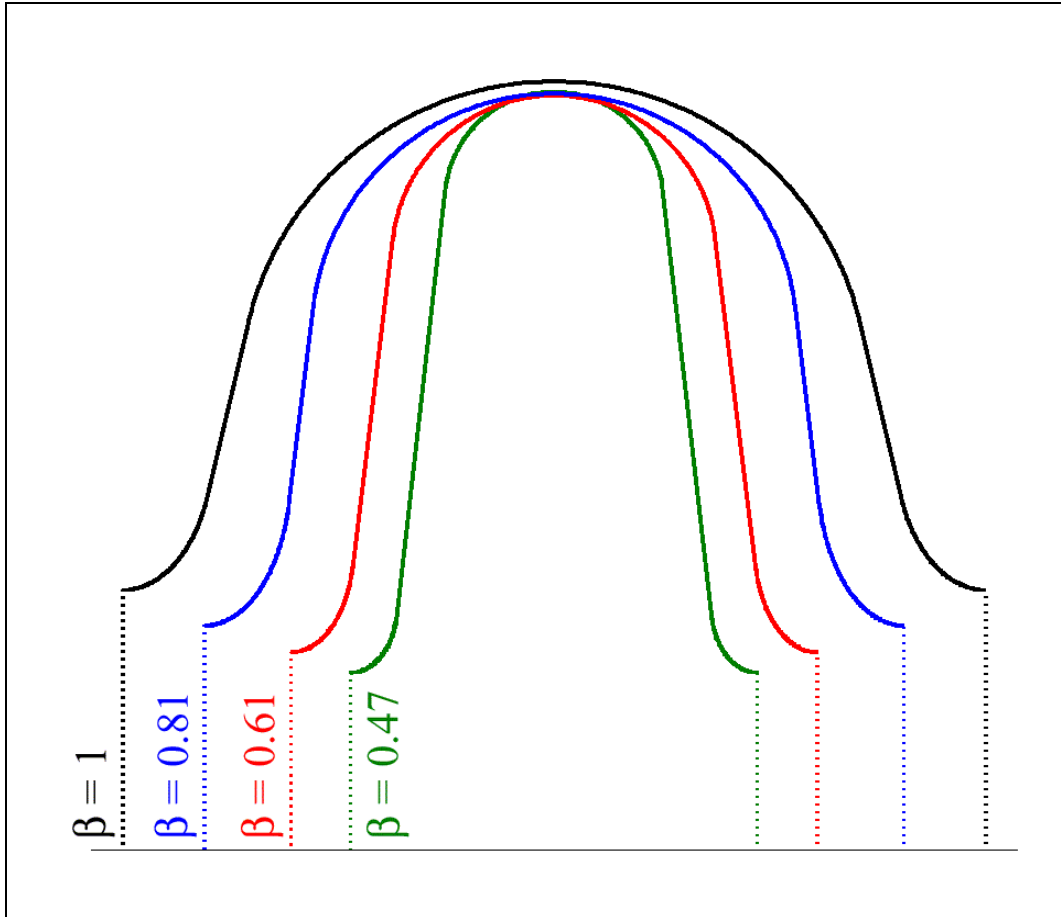


Figure 44 - Comparison of the frequency-scaled shapes of the  $\beta = 0.47$  cell (RIA) with a  $\beta = 0.61$  cell (SNS), a  $\beta = 0.81$  cell (SNS), and a  $\beta = 1$  cell (TESLA/TTF). Figure taken from ref. 82.

### 8.1 TESLA Cavities in the $\beta=1$ Main Linac

Above 1.3 GeV the baseline Proton Driver linac uses standard  $\beta = 1.00$  9-cell cavities identical to those of the TESLA main linac<sup>19</sup>. This section discusses possible cavity improvements in this energy range.

**Low-Loss Cavities:** Since the release of the TESLA TDR, continued SCRF development has pointed to “low-loss” cavities as a promising route to achieving a ~10% increase in accelerating gradient in a regime where cavity processing has improved to the point where  $B_{PEAK}$  (rather than  $E_{PEAK}$ ) limits the achievable gradient. We intend to follow the ILC R&D results and adopt whatever provides the highest gradient (or gradient margin) for the Proton Driver.

**$\beta \sim 0.98$  cavities in the main linac.** It has been noted<sup>83</sup> that the optimum geometrical beta for the 8 GeV main linac is  $\beta \sim 0.98$  rather than  $\beta=1$ . This would result in either a 1% reduction of the overall linac length or a 1% increase in the design margin on SCRF accelerating gradient. This would slightly reduce the efficiency for accelerating electrons, so the optimization will depend on the mixture of electrons and  $H^-$  that will ultimately be accelerated in the facility. There would be little cost reduction in the RF systems since these are driven by beam power instead of cavity gradient. True  $\beta=1$  cavities are used in the baseline design to maintain hardware commonality with the ILC.

**The TESLA “superstructure” concept<sup>19</sup>** is probably not useful for the Proton Driver Linac. Firstly, only a small range of  $\beta$  can be efficiently accelerated by the superstructures, which are effectively as long as a 20-cell cavity. Secondly, the 26 mA beam current in the Proton Driver linac is twice that of TESLA-800. This would require an RF coupler power of 1.2 MW at the TESLA-500 gradients and 1.9 MW at the TESLA-800 gradients. These exceed the present state of the art.

Table 15 – 1300 MHz Elliptical Cell Cavity Parameters for the Proton Driver linac

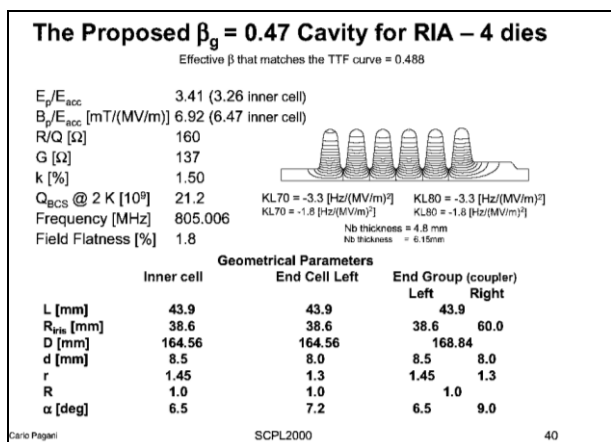
SRF ELLIPTICAL CAVITIES	8 GeV Linac				
Number of Cavities in Linac	392	including 8 in debuncher cryomodule			
Cavity type	elliptical				
Cavity operating mode	pi				
Cavity material	Niobium				
Cavity material thickness	4 mm	3.8 mm after processing			
Cavity final processing	electropolish				
Cavity stiffeners	yes				
Allowed frequency swing due to Lorentz force	470 Hz	(maybe more--depends on Beta)			
Frequency swing after Piezo Feed-Forward	TBD Hz				
Microphonic amplitude limit	+/- 60 Hz	Six sigma TBD			
Cavity operating temperature	~1.9 K				
Cryomodule Type (Beta)		LOW	MEDIUM	HIGH	TESLA
Geometrical Beta of Sections		0.47	0.61	0.81	1.00
RF frequency (MHz)		1300	1300	1300	1300
Cavity Type		Scaled RIA	Scaled SNS	FNAL	TESLA (TTF)
Number of Cells Per Cavity		6	6	8	9
Cell-to-Cell Coupling Constant		1.50%	1.61%	1.80%	1.87%
Unloaded Qo		>5E9	>5E9	>5E9	>1E10
External Q		7.5E+05	7.3E+05	7.0E+05	1.5E+06
External Q Variation		+/- 20%	+/- 20%	+/- 20%	+/- 20%
R/Qo (function of beam velocity)		160	220-440	170-570	1036
Typical band width FWHM=f0/(2Qex)		867 Hz	890 Hz	929 Hz	433 Hz
Cavity Active Length (geometrical)		0.325 m	0.422 m	0.747 m	1.038 m
Cavity Total Length incl. Couplers		0.545 m	0.642 m	0.967 m	1.258 m
Cavity Slot Length incl. avg. Bellows		0.610 m	0.707 m	1.032 m	1.323 m
Iris Diameter		47.8 mm	47.7	60.0	70 mm
Beam pipe Diameter		TBD	TBD	78 mm	78 mm
ID at Equator		203.8 mm	204 mm	199 mm	206 mm
Epeak (max)		52	52	58.6	52
Bpeak/Eacc		6.92	5.73	4.33	4.26
Bpeak		105.5	109.9	102.8	110.76
Epeak/Eacc		3.41	2.71	2.47	2.00
Eacc (max, on crest for Beta-design)		15.2	19.2	23.7	26.0
Synchronous Phase Phi (typ)		-30	-25	-20	-15
Eacc*cos(Phi)		13.2	17.4	22.3	25.1
Energy Gain Per Cavity (max)		4.3	7.3	16.7	26.1
Coupler Power (max) for 25mA Beam		107	183	417	652
Cold Mass of Dressed Cavity					

## 8.2 $\beta < 1$ Cavity Designs

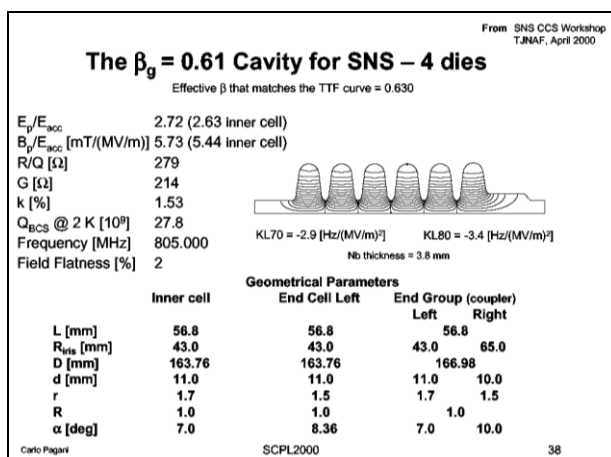
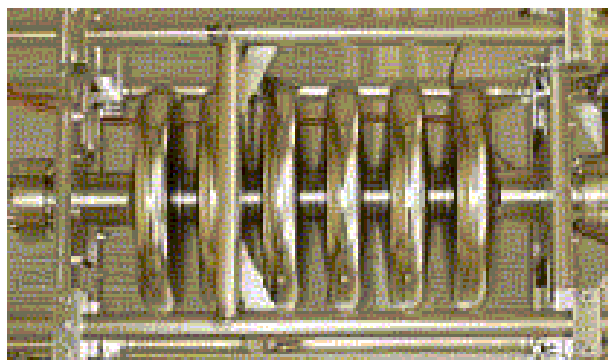
The cells of the baseline  $\beta < 1$  cavities are frequency-scaled copies of the SNS & RIA designs (Figure 44). The remaining free parameter is the number of cells in each cavity design. This is a tradeoff between the maximum accelerating gradient at optimum  $\beta$  (which favors a large number of cells) and the desire to span the necessary  $\beta$  range with a minimum number of cavity and cryomodule designs (which favors the broadly peaked velocity acceptance of a cavity with few cells).

A  $\beta = 0.81$  design and prototype collaboration with MSU and JLAB is underway. We are investigating the possible applications of low-loss cavity designs<sup>84</sup> and large-crystal niobium to  $\beta < 1$  cavities of the Proton Driver. These cavity designs reduce  $B_{PEAK}/E_{ACC}$ , which is an optimal design criteria assuming that cavity performance is limited by peak magnetic rather than electrical fields. Initial investigations indicate that the accelerating gradient of a  $\beta = 0.81$  cavity could be increased by ~10% by this optimization. This saves one cryomodule in the Proton Driver linac, or alternatively provides more performance margin.

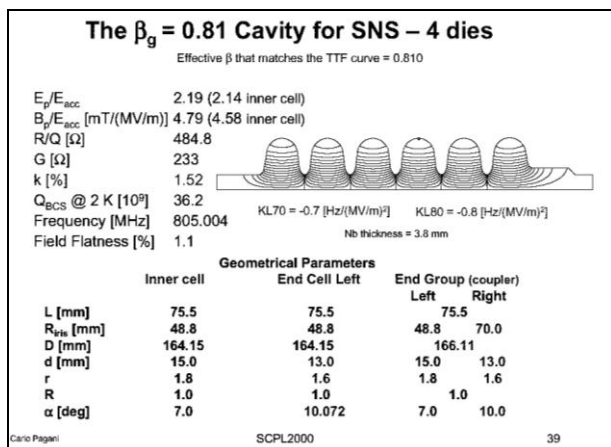
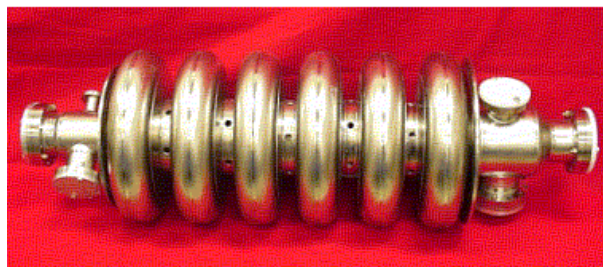
In addition to investigating the merits of low loss designs for  $\beta < 1$  cavities, this will provide microphonics and Lorentz detuning data necessary to finalize the design of the Low-Level RF systems and Ferrite Vector Modulators.



RIA  $\beta=0.47$



SNS  $\beta=0.61$



SNS  $\beta=0.81$

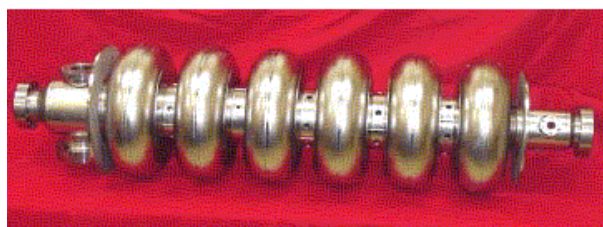


Figure 45 - Cavity Design Summaries<sup>85</sup> and actual cavities<sup>86</sup> for the 805 MHz ( $\beta < 1$ ) cavities for the SNS and RIA. The commercially produced SNS cavities underwent final chemistry and checkout at JLAB. The RIA ( $\beta = 0.47$ ) cavity produced by an MSU/JLAB/INFN collaboration was successfully tested. The Proton Driver  $\beta < 1$  elliptical cavities are versions of these scaled to 1300 MHz.

### 8.3 Assumptions for SCRF Elliptical-Cell Cavity Gradients

There is significant scope for either conservatism or aggressiveness on SCRF cavity gradients. These assumptions have a considerable effect on linac cost, since the number of cavities, cryomodules, tuners, and power couplers varies inversely with the assumed gradient.

If gradients are limited by cavity surface processing, then the degree of aggressiveness can be parameterized by the peak surface electric fields ( $E_{PEAK}$ ) present in the cavity designs. We have uniformly assumed peak surface electric fields of 52 MV/m (corresponding to  $E_{acc} \sim 26$  MV/m in the  $\beta=1$  main linac). These are slightly above those in the TESLA-500 design report<sup>87</sup> but consistent with what DESY has recently achieved on full cryomodules (Figure 47). If and when the TESLA-800 surface fields of 70 MV/m ( $E_{acc} \sim 35$  MV/m) become established as achievable production targets, the number of RF components (cavities, couplers, tuners, cryomodules) as well as the length of the Proton Driver linac could be decreased by  $\sim 30\%$ .

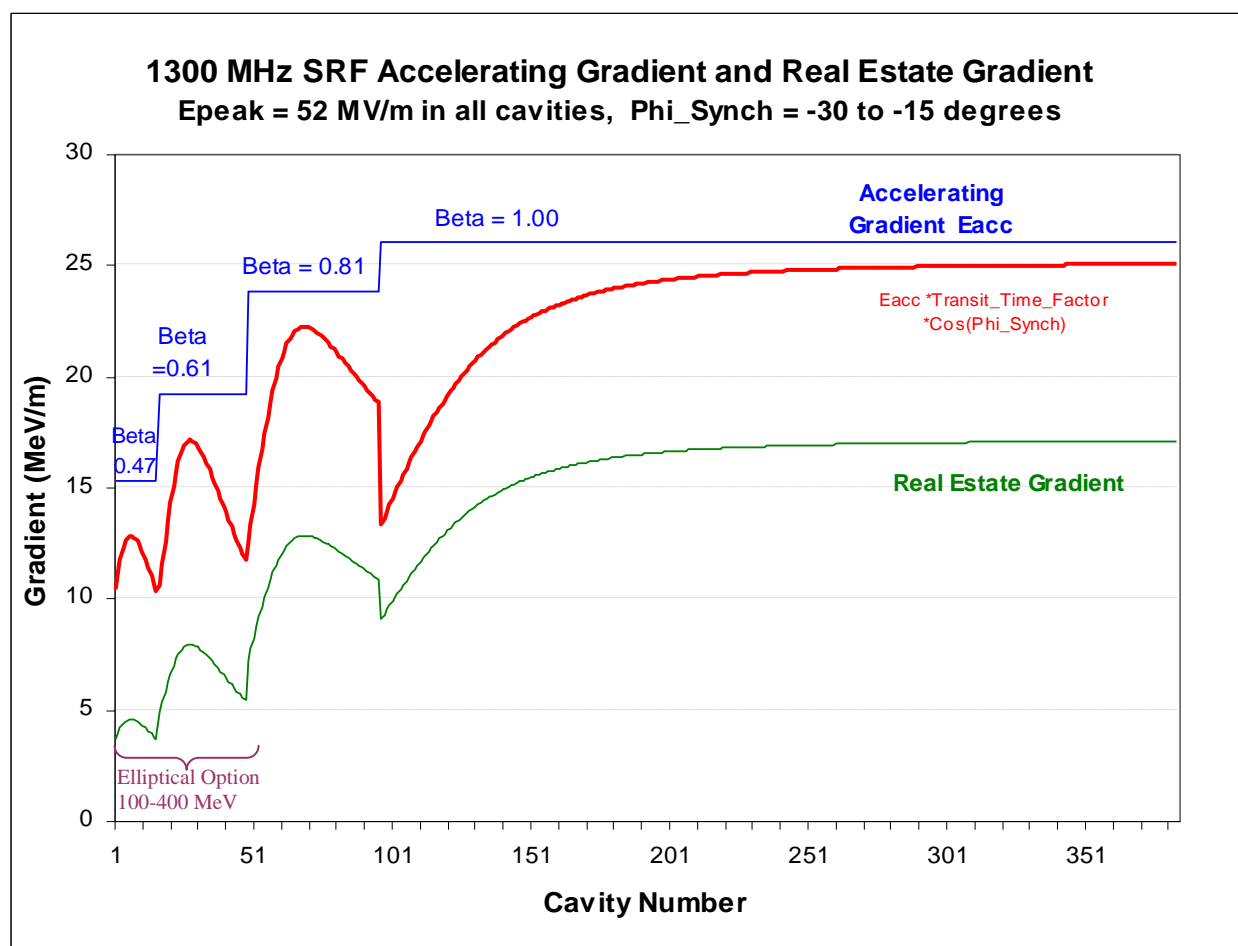


Figure 46 - Accelerating gradients vs. elliptical SCRF cavity number in the Proton Driver linac. The top curve is the accelerating gradient, the theoretical energy gain per meter for a particle with the optimal  $\beta$  for each cavity group that traverses the cavity on the crest of the accelerating field. The middle curve is the actual energy gain per meter of cavity, for particles with the actual  $\beta$  which traverse the cavity at the design synchronous phase which varies from  $-25^\circ$  to  $-16^\circ$  along the linac. The bottom curve is the “real-estate gradient”, or the average energy gain per meter of linac which reflects the additional length of beam line required for quadrupoles, instrumentation, bellows, cryogenic connections, etc.

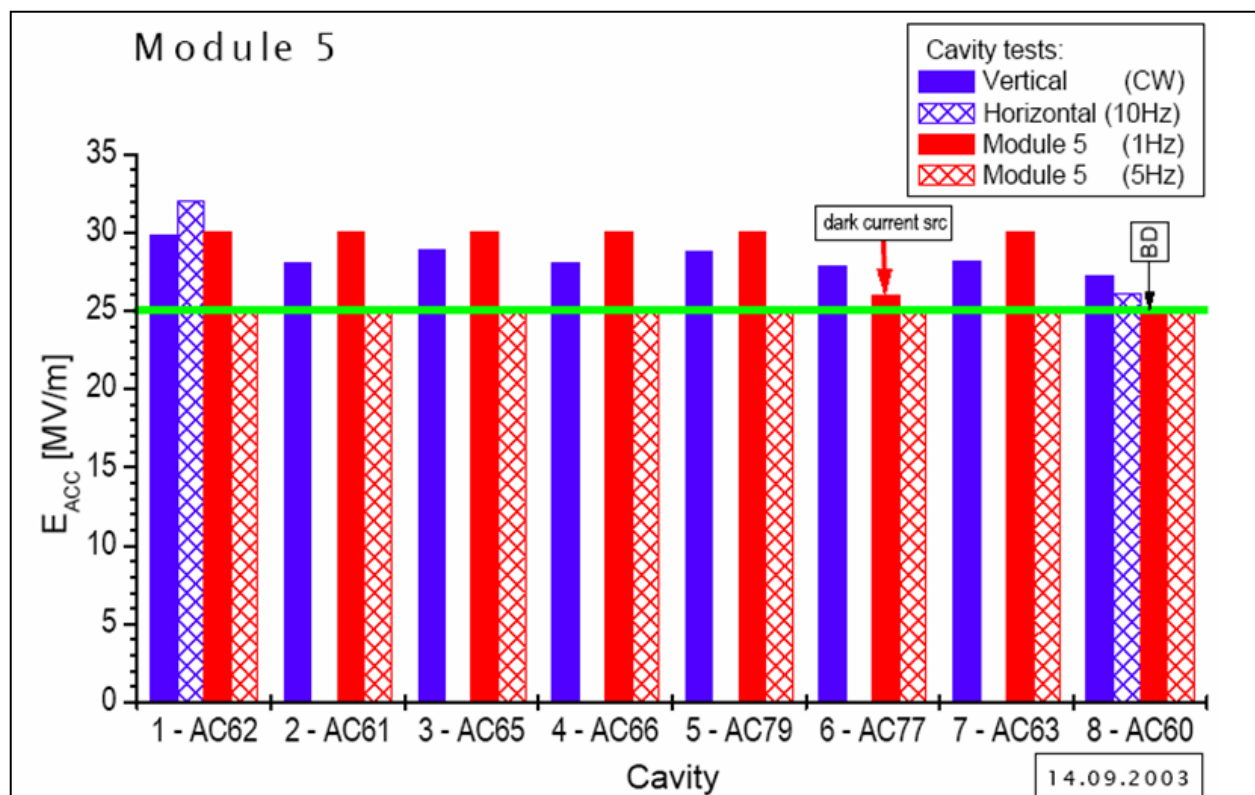


Figure 47 – Cavity Gradients achieved on a recent cryomodule (ACC5) at TTF.

## 8.4 Cavity Tuners

Mechanical and piezoelectric tuners identical to those of the Saclay design<sup>88</sup> for TESLA are provided on each 1300 MHz cavity. The SNS tuner<sup>89</sup> is similar.

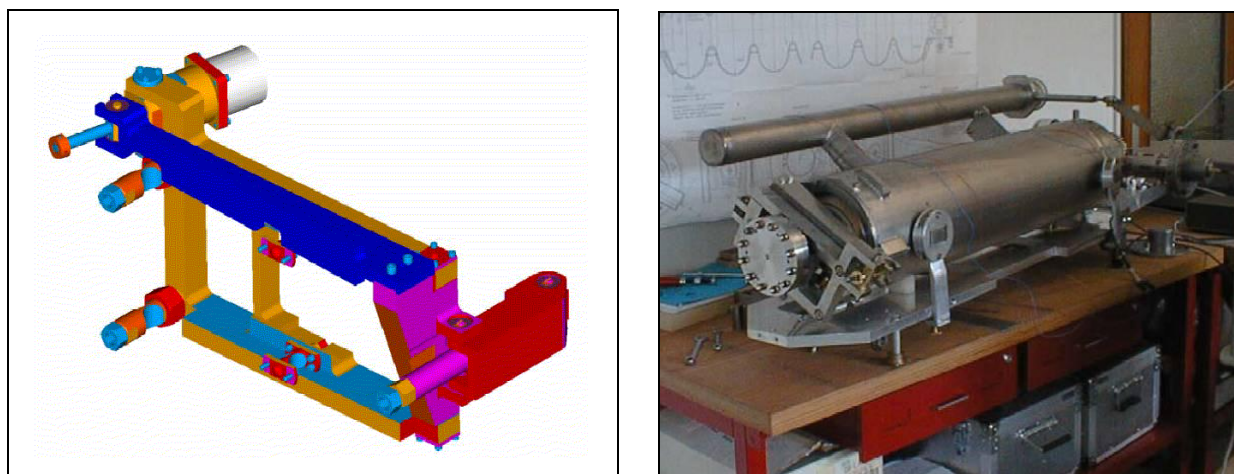


Figure 48 - SNS Cavity Tuner (left) and TESLA Cavity/Tank/Tuner assembly (right). The TESLA tuner incorporates both slow (stepping motor) mechanical tuners and fast (piezoelectric) tuners in a single assembly.

### Mechanical tuners

The mechanical tuner uses an in-vacuum stepping-motor and harmonic drive to axially compress the multi-cell cavities. This tuner is used for initial frequency tuning, to compensate for long-term drifts, and for detuning a failed cavity to bring it off-line.

Table 16 – 1300 MHz SCRF Cavity Tuners for the Proton Driver linac

CAVITY TUNERS	
Number of tuners	384
Mechanical Tuner Range	+/-100 kHz
Mechanical Tuner Slew Rate	3000 Hz/min
Mechanical Tuner Actuator	cold stepping motor in insulating vacuum
Cavity Spring Constant	~200 kgf/mm
Fast Piezo Fine Tuners Included	yes

### Piezoelectric Tuners

The piezoelectric tuner provides a rapid response to “Lorentz Detuning” of the cavity due to repetitive forces from the RF fields on the cavity. It has a limited range of adjustment, but a fast response time. The piezo tuners have been successfully in feed-forward mode at TTF.

The possibility of using the piezo tuners as feedback elements to control ambient microphonics (as opposed to just feed-forward elements to cancel Lorentz detuning) is being actively pursued at DESY<sup>90</sup>. If this program is successful, it would provide extra margin on the RF power budget and reduce or eliminate the requirements for Ferrite Vector Modulators on the cavities of the first  $\beta=1$  RF station (see section 13).

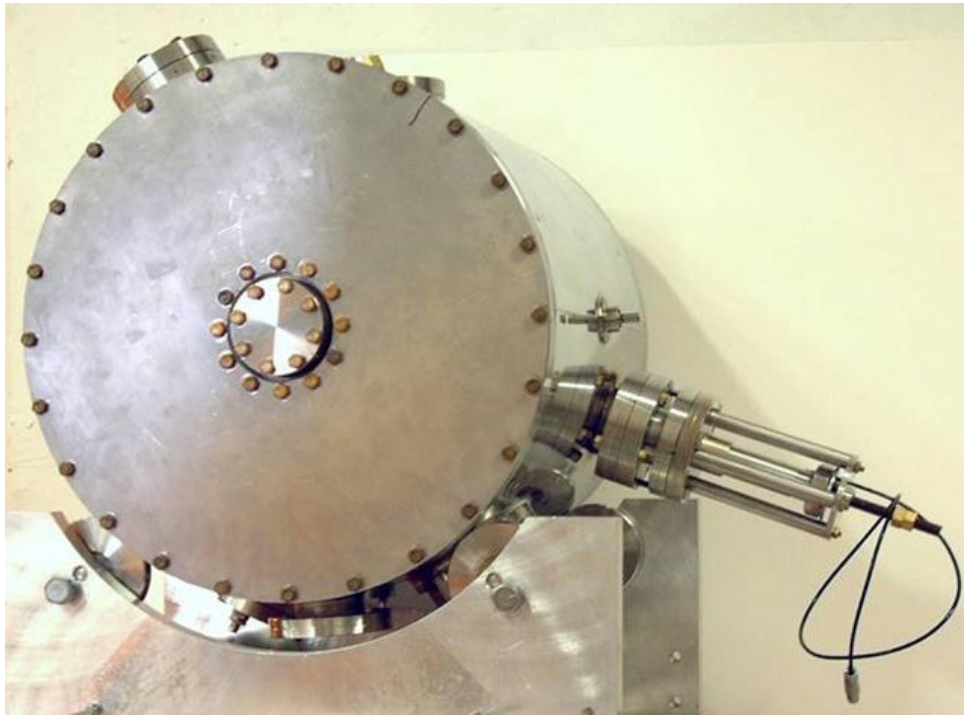


Figure 49 – Prototype Piezoelectric tuner mounted on a Double-Spoke cavity under development for RIA with potential application<sup>91</sup> for the Proton Driver.

### **Tuners in the 325 MHz Linac**

Slow mechanical tuners on the Spoke Resonators can follow the RIA designs. Development of piezoelectric fast tuners for spoke resonators has begun (Figure 49) but the performance requirements for pulsed operation have not been determined. The key experimental input is the behavior of spoke resonators under pulsed RF excitation. This requires a high power pulsed RF source and Fundamental Power Coupler than transmit the power required to rapidly fill the cavity. This is one of the key goals of the SMTF/Meson test facility.

### **Tuners in the 325 MHz Copper Front-End Linac**

Driving multiple copper cavities from the same RF source will require individual mechanical or ferrite tuners on each cavity. This is necessary to allow the cavities to be warmed up to their operating points. During initial warm-up, the Klystron frequency will be swept during one pulse and the resonance feedback signal will be monitored to identify the resonant frequency of each cavity. Mechanical tuners will then drive the cavities to the nominal resonant frequency. As the cavities warm up as the RF power is applied, the phase of the resonance signal will be monitored and the tuners continuously adjusted to keep the cavities in resonance.

## 9 RF POWER COUPLERS

The Proton Driver linac requires SCRF power couplers for both the 325 MHz and 1300 MHz cavities. All couplers are designed to handle the Ultimate beam current, and therefore operate with considerable margin in the Initial scenario. The main specification of the SCRF power couplers are given in Table 17.

Table 17 - RF Power Coupler and HOM Coupler Parameters for the 8 GeV Linac

SRF POWER COUPLERS		8 GeV Initial {Ultimate}		
Cavities per Power Coupler		1		
RF Frequency		325 MHz	1300 MHz	MHz
Power coupler design		RIA	TESLA	
Number of Couplers		69	384	depends on 3-spoke vs. elliptical medium-beta
Maximum power through coupler		79 {238}	217 {652}	kW
Tested power of coupler		TBD	TBD	kW
Coax Impedance		50	50	Ohm
Bias Voltage on Center Conductor		0 V	+/-2.5kV	Bias not needed at TTF after conditioning
Input Waveguide		Heliax	WR-650	
Separate Power coupler vacuum		none	YES	
Liq. Helium Consumption per Coupler		none	none	conductive cooling w/6K & 50K intercept
Static Heat Load at 2K		n/a	0.10 W	(these heat loads are for ultimate coupler power, with maximum beam loading)
Total Heat Load at 2K		n/a	0.11 W	
Static Heat Load at 6-8K		TBD	0.26 W	
Total Heat Load at 6-8K		TBD	0.41 W	
Static Heat Load at 50K		TBD	2.69 W	
Total Heat Load at 50K		TBD	10.11 W	
Power Coupler Water Cooling		No	No	not needed for 10Hz operation
<b>HOM COUPLERS</b>				
HOM couplers per cavity		TBD	2	
Number of HOM couplers		TBD	2 x 384	
HOM coupler design		TBD	TTF	preserve option of running e+/- in beta=1 linac
<b>HOM HEAT LOADS</b>		<b>2K</b>	<b>6K</b>	<b>50K</b>
	per coupler	0.34 W	0.87 W	4.69 W
	per cryomodule	2.7 W	6.9 W	37.5 W
	linac total	133 W	340 W	1838 W

### 9.1 1300 MHz RF Power Couplers

The baseline 1300 MHz coupler design is TTF-III coupler (Figure 50). This is the latest of three coupler types built and operating for TTF. A total of 40 have been used from 1997-2004 with a total of over 1/4 million coupler-hours. The 1300 MHz power coupler varies from 0.06 MW {0.2 MW} to 0.2 MW {0.6 MW} along the length of the Proton Driver linac (Figure 64). The TTF-III coupler has been cold-tested on a 35 MV/m cavity, at 600 kW and 10 Hz, for 2400 hours with no breakdown<sup>92</sup>.

Although the TTF-III coupler is satisfactory for the baseline design, the Proton Driver shares an interest with the ILC to develop a coupler which handles higher power and is simpler, faster to process, and cheaper. One design alternative is a coupler with fixed coupling to the cavity. This implies a performance compromise when operating over a range of beam currents, cavity gradients, and transit-time factors. An attractive option is to design a fixed coupler for maximum beam current, then at lower currents to use waveguide tuners to adjust the effective coupling constant to the cavity to the input waveguide. If ferrite tuners are used to adjust the cavity coupling “on the fly”, the cavities can be filled and emptied faster, resulting in a significant power savings for both the Proton Driver and the ILC (see ref. 2).

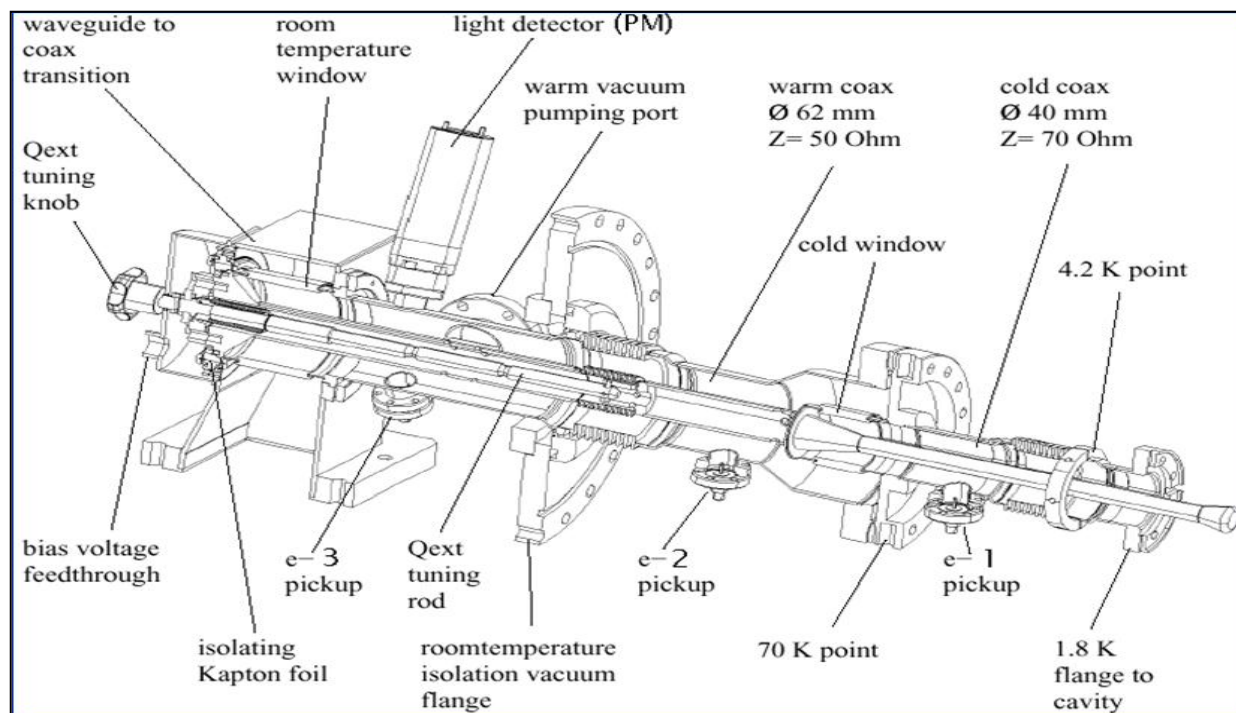


Figure 50 - The TESLA (TTF3) RF Power Coupler that is the baseline design for the 1300 MHz main linac of the Proton Driver. It is a flexible, adjustable, coax design with warm and cold ceramic windows and a separate coupler vacuum space between the windows.



Figure 51 - RF Power Couplers installed on TTF Cryomodule. RF power enters from below via a flex waveguide. The waveguide transitions to a horizontal coaxial structure inside the coupler. The stainless pipe is the header that distributes the coupler vacuum.

## 9.2 325 MHz RF Power Couplers

The 325 MHz power couplers are patterned on the designs for RIA and the APT. Couplers developed to date for these projects (see Figure 52) can handle the average power, but not the peak power, required for the Proton Driver linac. The triple-spoke option for the Ultimate scenario requires a maximum of 3.5 kW average power (240 kW peak), so a new coupler design will need to be developed. Most of the 325 MHz cavities require much less power (see Figure 40). In addition to in-house coupler development, an SBIR is approved<sup>93</sup> to develop a range of 325 MHz power couplers to cover the needs of the PD linac.

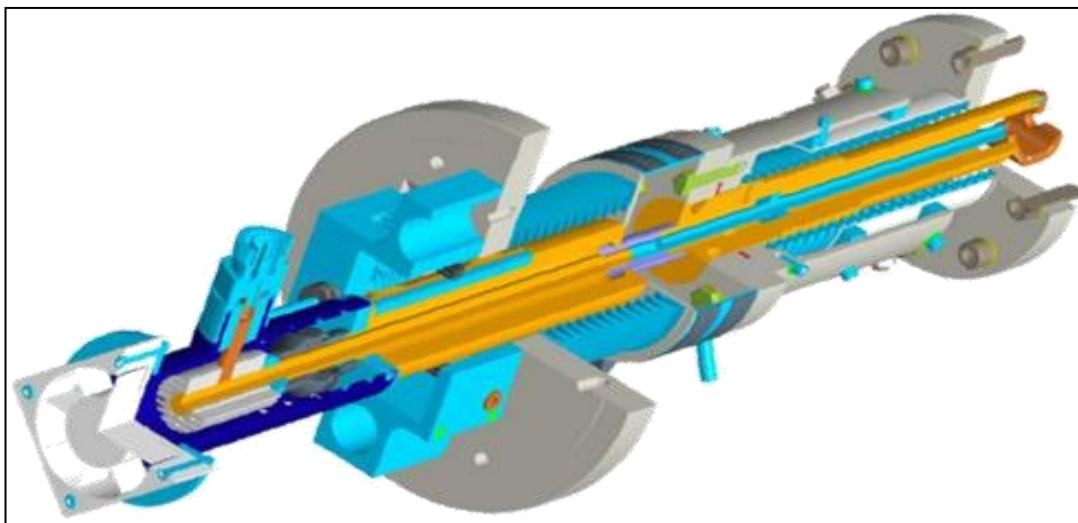


Figure 52 – 350 MHz magnetically-coupled SCRF Power Coupler rated for 10 kW CW operation. For the Proton Driver we are developing<sup>94</sup> a coaxial capacitively coupled power coupler capable of handling > 200kW peak power required for Ultimate operation of the 325 MHz triple-spoke resonators.

## 9.3 HOM Couplers

Intense single bunches are accelerated by the fundamental mode of the cavities, but as they pass through the cavities, the bunches re-radiate power into a number of potentially high-Q modes which could disturb subsequent bunches. The function of the HOM coupler is to extract this energy and damp these modes.

The 1300 MHz Higher-Order-Mode (HOM) coupler design is copied directly from the TESLA/TTF design<sup>95</sup>. The need for HOM couplers in a proton linac such as the SNS is not so clear<sup>96</sup> since the peak currents are much lower than a TESLA/TTF type machine. One aspect of the specification which remains to be investigated is whether the fast beam chopper can be inadvertently programmed to introduce pathologic beam loading patterns which could excite monopole modes in the cavities. The SNS chose to include TTF-style HOM couplers on all cavities. In our case, retaining the possibility of operating the Proton Driver as an 8 GeV “Multi-Mission” linac with a variety of beam conditions including intense electron bunches make the choice of the proven SNS/TTF design appropriate. The HOM coupler signals may also serve as a useful Beam-Position Monitor (BPM) and a check on cavity alignment.

The need for HOM couplers for the 325 MHz spoke resonators has not been analyzed. A similar analysis for the 100 mA beam current of the APT linac did not indicate any problems<sup>97</sup>.

## 10 KLYSTRONS

The Proton Driver linac requires a total of 12 {*Ultimate 33*} klystrons<sup>98</sup> for the Initial 0.5 MW {Ultimate 2 MW} beam power configurations. Two different designs, operating at 325 MHz and 1300 MHz, are required. Both are being produced for major projects (JPARC and the TESLA/Euro-XFEL project and the ILC) and thus have good assurance of long term vendor support.

Table 18 - Klystrons for the Proton Driver linac

KLYSTRONS	8 GeV Initial {Ultimate}	
Number of Klystrons	12 {33}	linac(11) {32} + debuncher(1)
Number of Klystron Types	2	325 MHz (JPARC) and 1300 MHz (TESLA)
Number of Modulators	12 {31}	linac(11) {31} + debuncher(1)
Location of Klystrons & Modulators	Linac Gallery	
<b>Klystron Individual Details</b>	<b>325 MHz</b>	<b>1300 MHz</b>
Number of Klystrons (main linac)	1 {2}	10 {30}
Number of Klystrons (debuncher)	0	1
Number of Klystrons (test stands)	1	1
Klystron System Loads	RFQ,MEBT, RT-TSR & Spokes	Elliptical SCRF Linac & Debuncher
Klystron Peak Power	2.5 MW	10 MW
Klystron Test Power	3.0 MW	10 MW
Klystron Type	JPARC	TESLA MBK
Klystron Reference Manufacturer	Toshiba	Thales*
Klystron Reference Model #	E3740A	TH-1801
Klystron RF Pulse Width [msec]	4.2 {1.4}	4.2 {1.4}
Klystron Repetition Rate [Hz]	2.5 {10}	2.5 {10}
Klystron RF Duty Cycle (%)	1.1 {1.4}	1.1 {1.4}
Klystron Average Power [kW]	26 {35}	105 {140}
Klystron Rated Average Power [kW]	93	150
Klystron Rated Efficiency	55%	65%
Klystron Assumed Efficiency	50%	60%
Klystron Beam Voltage	110 kV	117 kV
Klystron Beam Current	45 A	142 A
Klystron Number of Beams	1	7
Klystron Perveance (Amps per V <sup>3/2</sup> )	1.2E-06	3.6E-06
Klystron Gain	50 dB	40 dB
Klystron Bandwidth (1dB)	~0.7 MHz?	3 MHz
Klystron Number of Internal Cavities	5	6
Klystron Filament Voltage	15 V	9 V
Klystron Filament Current	26 A	50 A
Klystron Solenoid Power	9.8 kW	5 kW
Klystron Mounting Orientation	horizontal	vertical
Klystron HV Connection	SNS Cable	Oil Socket
Klystron Length	15 ft	8.2 ft

### 10.1 325 MHz Klystrons (Toshiba E3740F)

Two 2.5 MW 325 MHz Klystrons are used in the front end linac. We plan to use the 3 MW Klystron which was developed for the main linac of the JPARC<sup>99</sup> facility. Toshiba is producing a slightly modified version of this tube (designated E3740F) that will also meet the slightly

different specifications for the front end of the Proton Driver linac. An order has being placed for the first tube, with delivery expected in February 2006 for use in the Meson area test facility.

The tube operating parameters for the Proton Driver linac will differ from the JPARC application as follows:

- a) Our operating frequency will be 325 MHz rather than the 324.2 MHz that the E3740A is normally tuned to. Although this frequency marginally inside the bandwidth of the standard Klystron, Toshiba will retune the tube for our operating frequency. The main implication of this change is that under emergency conditions, JPARC and the Proton Driver linac will not be able to exchange spare Klystrons without sending them back to the factory for retuning.
- b) The tube is normally operated with a modulating anode. To maintain electrical compatibility with the ILC modulators used elsewhere in the linac, we plan to ground the anode and operate the tube as a diode. This has been successfully done with other modulating-anode Klystrons<sup>100</sup>. Simulations at Toshiba indicate that our required 2.5 MW output power (with >50% efficiency) can be obtained operating the tube in this mode.
- c) For JPARC this tube is normally operated at 50 Hz at a pulse width of 0.62 msec (3.1% Duty Factor). The Proton Driver linac requires longer pulse widths of (4.5 msec x 2.5 Hz = 1.1% D.F.) and (1.5 msec x 10 Hz = 1.5% D.F.) for the Ultimate configuration.
- d) The pulsed 110 kV swing on the gun when the tube is operated as a diode exceeds the voltage that can reliably be handled by the cables and connectors used in the JPARC linac. We plan to use SNS cables and connectors rated at 160 kV.

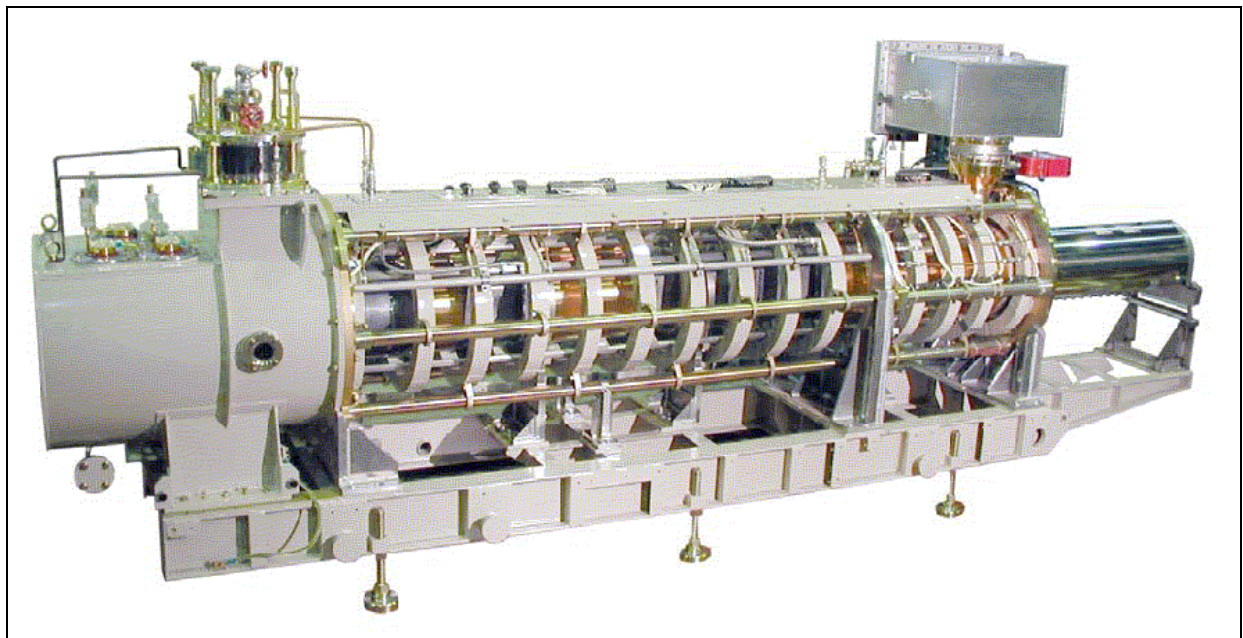


Figure 53 – The 325 MHz (Toshiba E3740F) Klystron used by the front end linac. High voltage connections are made via cables to the socket in the oil-filled tank at left. The RF leaves the tube via a WR-2300 rectangular waveguide at right. The tube is shipped on a horizontal frame that includes the focusing solenoids. The tube with socket is approximately 5m long.

## 10.2 1300 MHz Multi-Beam Klystrons

The main linac uses 1300 MHz multi-beam klystrons<sup>101</sup> (MBKs) developed for TESLA/XFEL and the ILC. Eleven of these klystrons are required to power the elliptical-cell SCRF linac, the Debuncher cavities, plus a test stand. The TESLA/XFEL project has developed three vendors (Thales, CPI, and Toshiba) for these devices.

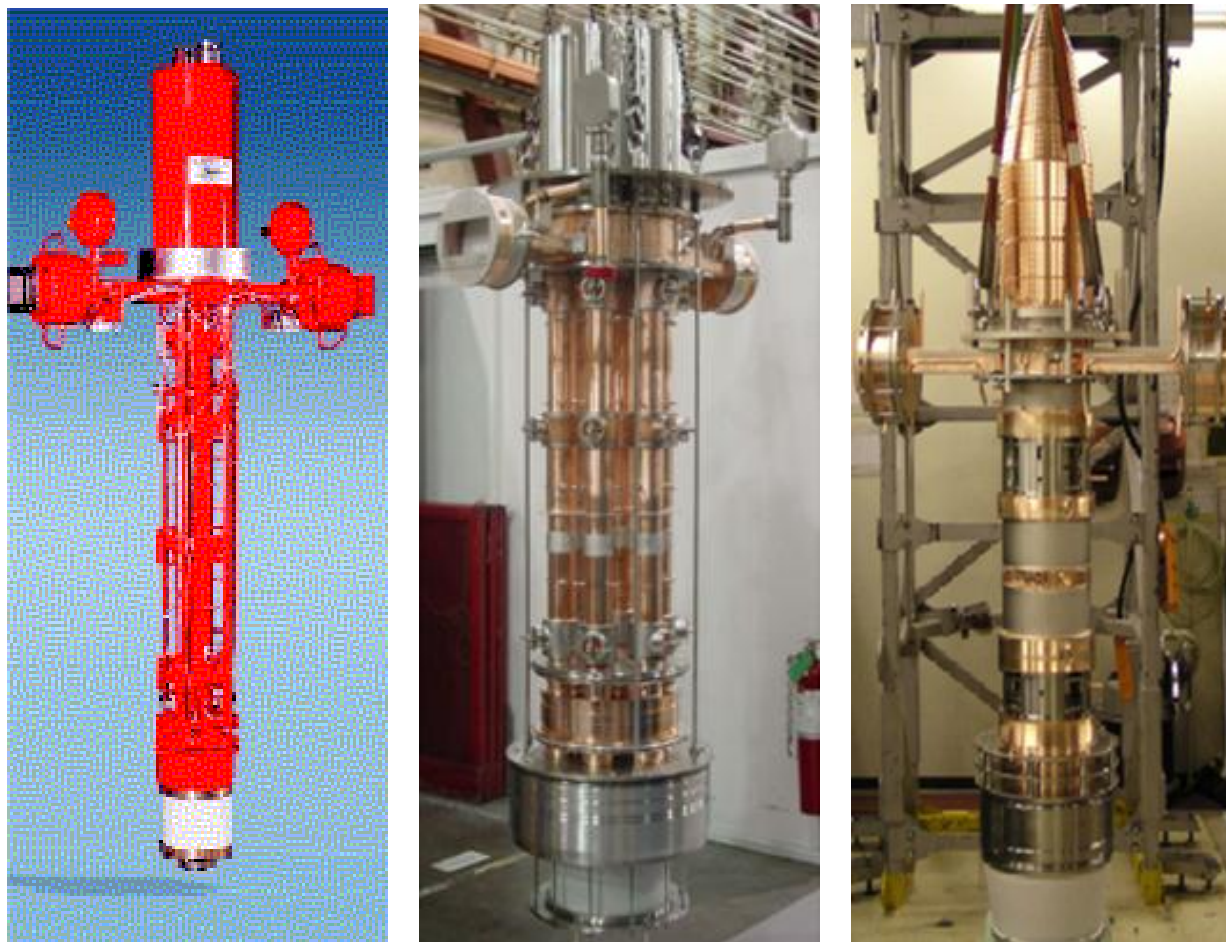


Figure 54 – The 1300 MHz 10 MW Klystrons for the Proton Driver linac are identical to those developed for the ILC (TESLA/XFEL). Left: Thales TH-1801. Middle: CPI #VKL-8301. Right: Toshiba E3736.

The status of the Klystron development program has been reviewed elsewhere<sup>102</sup>. At present it appears that all three the three vendors are providing acceptable products. An interesting development being pursued at DESY is the development of a side-mounted version of the MBKs. This would simplify service procedures and reduce the required ceiling height of the Klystron Gallery.

## 10.3 Klystron test program for 4.5 msec pulse length

The initial configuration of the Proton Driver linac requires a 4.5 msec RF pulse length. The Klystron manufacturers have indicated they will deliver a tube specified for this pulse length, but none of the manufacturers own a long-pulse modulator capable of testing this. Therefore we are building (section 11) a modulator which can provide both the 4.5 msec x 2.5 Hz pulse for the initial configuration, and the 1.5 msec x 10 Hz pulses required for the ultimate configuration. It is planned to have this modulator ready by Feb. 2006 when the Toshiba Klystron (E3740) arrives for testing.

## 11 MODULATORS

Klystron modulators<sup>103</sup> are the most expensive single component of the RF systems of the Linac. Modulators convert 480V 3-phase AC power into the 117 kV pulsed power for the klystron. A capacitor bank is slowly charged via a “Charging Power Supply”, and then rapidly discharged into a step-up pulse transformer to energize the klystrons during the 4.5 msec x 2.5Hz {1.5 msec x 10 Hz} RF pulse in the linac. The RF pulse width must be roughly 1.5 x longer than the beam pulse is necessary to provide the “filling time” needed to establish the resonant voltage in the cavities.

Technical challenges for the modulator include maintaining a sufficiently stable and accurate flat-top on the voltage pulse to the klystron as the capacitor bank is discharged, maintaining an acceptably smooth AC line load and power factor over a range of linac pulse repetition rates, and reliable operation including protection of the klystron under fault conditions.

The Proton Driver linac adopts a single, standard modulator design serving all linac components: the 325 MHz Front-end linac, the main SCRF Linac, and Debuncher cryomodule. This module provides a 10 kV x 1.5 msec pulse to a step-up transformer located in an oil-filled tank. In the case of the 1300 MHz 10 MW Klystrons of the main linac (Figure 3), a single Klystron is mounted vertically in an oil-filled socket integral to the pulse transformer. For the 325 MHz Klystrons, two 3 MW Klystrons are powered from a single transformer via 110 kV cables. The modulators are otherwise identical. Having a single, standard component as the only high-powered supply in the Proton Driver linac represents a substantial simplification with respect to the synchrotron option.

### 11.1 Baseline (FNAL/TTF) “Bouncer” Modulator Design

The FNAL modulators<sup>108</sup> for the TESLA Test Facility (TTF) are the baseline design for the Proton Driver Linac. This modulator meets all specifications, has an acceptable and well-understood cost, and proven reliability<sup>104</sup> since 1994. The modulator provides a 10 kV x 1.7 kA = 17 MW square-wave pulse 4.5 msec {1.5 msec} long to the 12:1 step-up pulse transformer to the klystron. Modulator parameters for the Proton Driver linac are shown in Table 19.

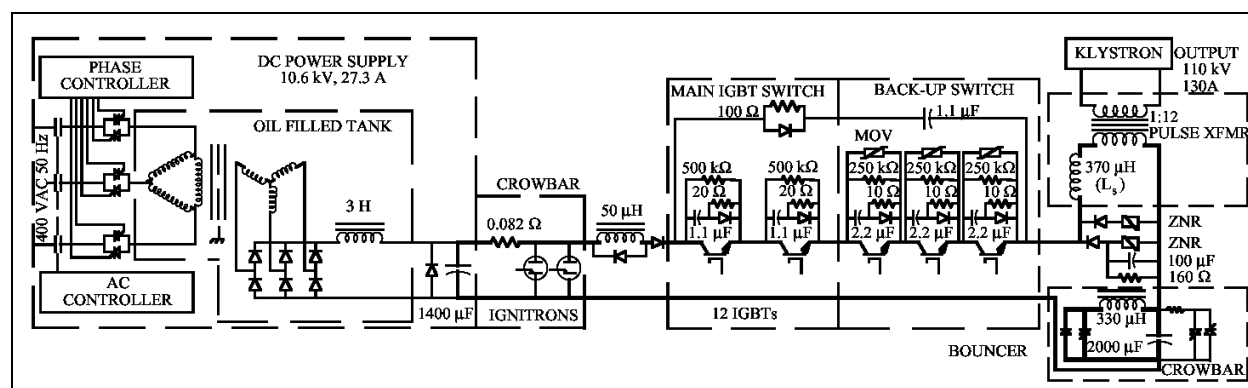


Figure 55 - Simplified Schematic of the FNAL/TTF “Bouncer” Modulator, from ref 108.



Figure 56 - The FNAL “Bouncer” style modulator for TTF. This is the baseline design for the Proton Driver linac. In the background the large red box contains the capacitor bank, charging supply and IGBT modulator switches. In the foreground (partly obscured by water manifolding) is the oil tank for the pulse transformer and klystron socket. The tall aluminum and lead box on the right hand side contains the klystron. The klystron beam shoots upwards into the collector and the microwaves exit at the top right (not shown). The Klystron Gallery of the Proton Driver linac contains 12 {33} of these units, spaced every 60 m {21 m} along its length.

Table 19 - Modulator Parameters for the Proton Driver linac

MODULATORS	8 GeV Initial {Ultimate}		
Number of Modulators Initial {Ultimate}	12 {33} total	linac + debuncher	
Modulator Types	1 type	drives both 1300MHz and 325MHz Klystrons	
Modulator Peak Power Required	17-20 MW	depending on location in linac	
Modulator Maximum Average Power	275 kW	typ.	
Modulator Specified Max Pulse Width	4.5 {1.5} msec	must hold flat top tolerance within this time	
Modulator Expected Max Pulse Width	4.2 {1.3} msec	expected RF pulse width	
Modulator Output Voltage	10 kV	before step-up from pulse transformer	
Modulator Rep Rate	2.5 {10} Hz		
Modulator type	IGBT bouncer		
Modulator Flat Top Accuracy	+/- 0.5 %	maybe negotiable	
Modulator RMS Pulse-to-Pulse variation	+/- 0.2 % RMS	maybe negotiable	
Modulator Spark Protection for Klystron	Redundant IGBT switch		
Modulator Max Fault Energy into Klystron(s)	20 J	including capacitance for 2 ganged klystrons	
Modulator Supply Voltage	480 VAC, 60 Hz, 3 Phase		
Modulator Charging Supply Type	SCR phase control with output filter and Power Factor Correction		
Modulator Power Factor Correction	meeting FNAL standards for large installations		
Modulator Size (W x D x H)	28 x 6 x 8 ft	{14 x 6 x 8 ft}	
<b>Modulator Individual Details</b>	<b>325 MHz</b>	<b>1300 MHz</b>	
Number of Modulators	1 {2}	11 {31}	including Debuncher
Number of klystrons per modulator	1 {2}	1	
Modulator Voltage	110	117	kV
Modulator Current	45	142	A
Modulator Peak Power	5 {10}	17	MW
Modulator Average Output Power [kW]	58 {120}	192	kW
Modulator HV Pulse Width (flat top) [ms]	4.5 {1.5}	4.5 {1.5}	msec
Modulator Switch Conduction Time [ms]	4.6 {1.6}	4.6 {1.6}	msec
Modulator Switch Duty Cycle [%]	1.2 {1.6}	1.2 {1.6}	%
Modulator Efficiency incl. Charging Supply	85%	85%	
Modulator Wall Power (max)	68 {140}	225	kW varies along linac
Modulator Cooling Water (LCW) Flow	2.6	8.5	GPM 15 degC temperature rise
Total Modulator Wall Power	0.07 {0.17}	2.48 {6.97}	MW tot. installed
<b>Modulator Pulse Transformers</b>	<b>Initial</b>	<b>Ultimate</b>	
Pulse Width at Flat Top	4.5	1.5	msec
Number Required	11	11+20	initial transformers reused in ultimate config.
Tank Size (L x W x H)	8' x 6' x 5'	7' x 5' x 5'	new transformers for Ultimate are smaller
Transformer Ratio	1:12	1:12	
Tank Weight including Transformer(s)	TBD	TBD	
Tank Oil Inventory (approx)	4 k-liters	3 k-liters	
Tank Avg Power Dissipation	3	3	kW from TESLA TDR fig 8.5.3
Transformer Cooling Water (LCW) Flow	0.8	0.8	GPM 15 degC temperature rise
<b>Modulator-to-Klystron Interface</b>	<b>325 MHz</b>	<b>1300 MHz</b>	
Number of Tubes per Transformer	1 {2}	1	
Filament Transformers per tank	1 {2}	1	Separate Filament Transformers
Height needed to remove Klystron	N/A (horiz.)	12 ft	Vertical liftout of Solenoid & MBK as unit
Tank Moved for Klystron Replacement	NO	MAYBE	
Oil Purification Method	Travelling cart		

**Capacitor Bank.** Recent improvements in capacitor technology for the traction industry have reduced the cost and size of capacitor banks required for each modulator. These include hazy polypropylene dielectric film, self-fusing foil metallization, and low viscosity rapeseed oil impregnation<sup>105</sup>. Operational experience with these new capacitors will be gained in the klystron modulators of the SNS<sup>106</sup>. This type of capacitor has been purchased for the capacitor modulators under construction for SMTF.

**Safety crowbar.** A critical feature of the modulator is that it limits the energy delivered to the klystron under fault conditions. In particular, one must avoid dumping the entire stored energy of the capacitor bank into the klystron when it sparks. The original FNAL/TTF bouncer limited the energy to  $< 20$  J with an ignitron crowbar and a backup switch (see Figure 55) that must be actively triggered when a spark is detected. In the current design the Ignitron is being eliminated in favor of a redundant IGBT output switch.

**Output Switch.** A redundant Insulated-Gate Bipolar Transistor (IGBT) switch is being built at SLAC for both the ILC & Proton Driver modulators. The IGBTs are de-rated below the manufacturer's nominal specifications to limit the pulse-to-pulse temperature swing in the silicon to a value that operational experience has determined is compatible with reliable long-term ( $>10$  year) operation of large power semiconductors<sup>107</sup>.

**Bouncer Circuit.** Minimizing the size of the capacitor bank is an economic and safety advantage. The tradeoff is that a smaller capacitor will droop more than a larger one as the pulse energy is extracted. The bouncer circuit (Figure 55) is a clever trick of Quentin Kearns<sup>108</sup> that uses a small resonant circuit to compensate for the voltage droop due to capacitor discharge and pulse transformer effects. This allows a relatively large fractional discharge ( $\sim 20\%$  of voltage, 36% of energy) of a modestly sized capacitor bank while maintaining a good flat-top (Figure 57).

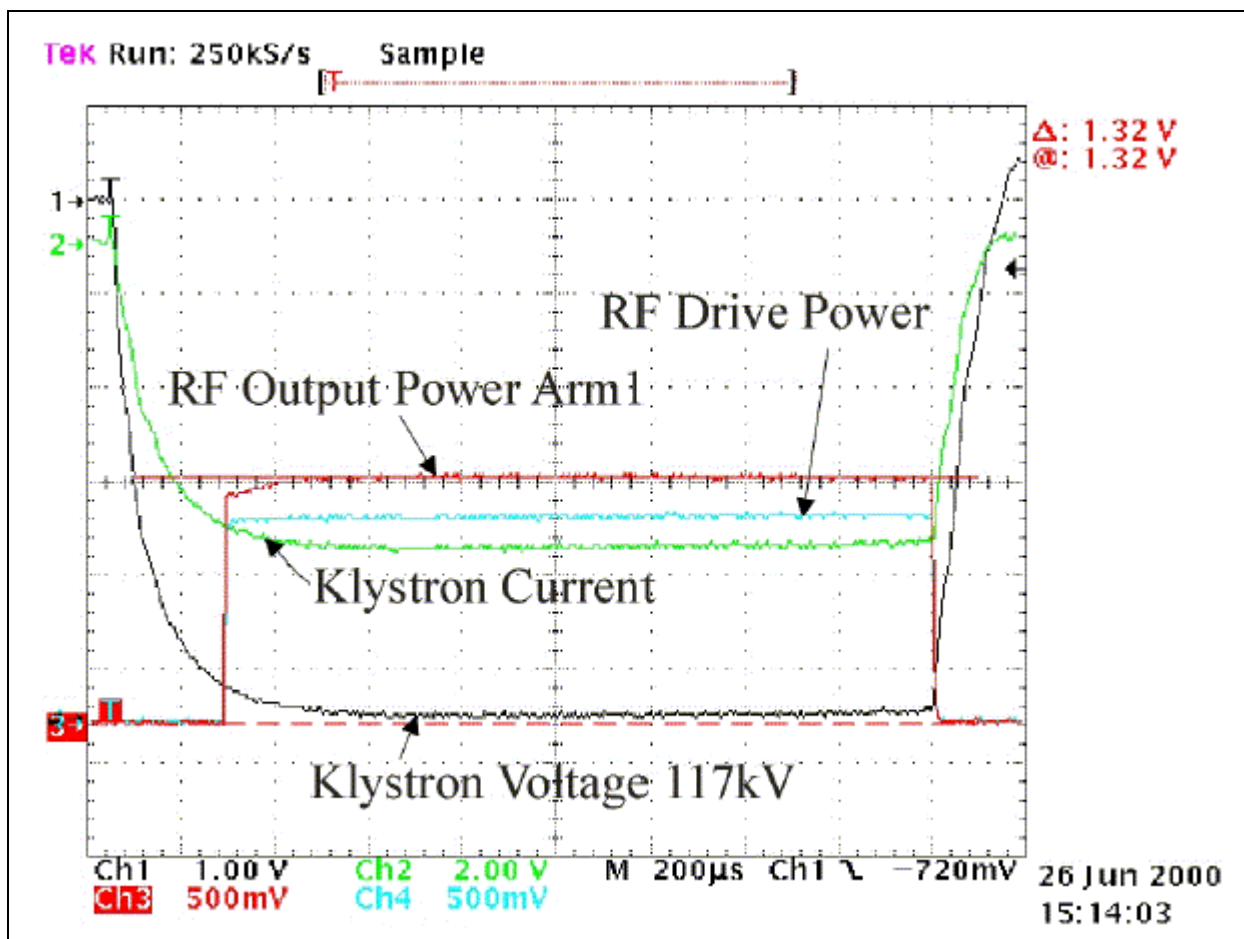


Figure 57 - Fermilab Bouncer Modulator output waveforms driving a Multi-Beam Klystron (MBK) at TESLA Test Facility. The flatness of the klystron voltage waveform is  $\pm 0.5\%$  over the 1 msec beam pulse. The waveform flatness is not critical during the first 450  $\mu\text{sec}$  (the filling time of the cavity).

**Pulse Transformer Tanks.** The 10 kV modulator pulse feeds output pulse transformers with step-up ratios of 12:1. The transformer and klystron sockets are in an oil-filled tank to prevent breakdown. Unlike the TESLA/XFEL design, 8 GeV klystrons are in the standard vertical orientation (Figure 56). If DESY or the ILC successfully develops side-mounted versions of the multi-beam Klystrons, these will likely be used by the Proton Driver because of the simplification to the civil construction and service procedures in the Klystron Gallery.

The 4.5 msec pulse width for the initial modulators requires in a somewhat larger pulse transformer. The recent procurement of two 4.5 msec pulse transformers for the Meson Area modulators indicates that there is little or no cost penalty for the longer pulse length.

**Charging Supply.** The baseline is a conventional phase controlled thyristor with output filtering. This is the most cost-effective approach known. It was used in the FNAL/TTF modulators, and is being used for the new modulators under construction.

## 11.2 Modulator Design Alternatives.

Several alternative modulator designs in various stages of development are available for use in the Proton Driver linac. The baseline design is the FNAL/TTF “bouncer” modulator<sup>108</sup>. This design has almost a decade of reliable operation at the TESLA Test Facility (TTF) and the A0 photoinjector. This choice was also expedient for this design study since FNAL has in-house production and detailed cost experience based on production of three units of this type<sup>109</sup>. If an alternative design proves less expensive than the FNAL/TTF modulator, it can be substituted to reduce the cost of the Proton Driver linac.

The *SNS Polyphase Switch-Mode Modulator*<sup>110</sup> was also considered. Its advantages include more compact magnetic components, a potentially simpler (passive) method of protecting the klystron, and possibly lower overall costs. The compactness of the design is a big plus in the rather crowded SNS linac gallery<sup>111</sup>, but is less important in the less crowded Proton Driver linac gallery (Figure 59). Being a new design, there is neither the operational experience nor the final cost data for this design. It remains a potentially attractive option.

The *TESLA modulator* concept<sup>112</sup> attempts to save costs in the context of a single-tunnel Linac design. The charging supplies, capacitor banks, and pulse modulators are located in a central building, and pulsed power is delivered via long HV coaxial cables to step-up transformers located at each klystron in the main tunnel. This approach has the advantage of minimizing the amount of active electronics in the tunnel in a single-tunnel design. However in the design adopted here, the klystrons and all active electronics are located in a service gallery and this advantage disappears. One also expects that, as a general principle, it should be easier and less expensive to distribute power continuously over the 100 msec second charging time between linac pulses using commercial AC power components, than to distribute the same power in a 1 msec HV pulse using specialized cables and components.

A *Mismatched Pulse-Forming Network*<sup>113</sup> is a potentially simpler alternative that might provide a good flat-top without an active bouncer circuit. This has never been prototyped. A disadvantage that it shares with all PFN modulators is that the pulse energy is provided by sequentially discharging all capacitors of the PFN, resulting in higher instantaneous stress on capacitors and therefore a more expensive capacitor for a given level of reliability.

A *Marx Generator Long-Pulse Modulator* concept being developed at SLAC for the ILC. This has the advantages of eliminating the pulse transformer and its large oil inventory, as well as a potential degree in fault tolerance if single Marx generator stage can fail without bringing the whole modulator down.

**Charging Supply Design Alternatives.** A number of alternative 10 kV capacitor charging supplies are possible. Charging supplies can be made with stacked switching power supplies (TESLA), phase controlled thyristors with output filtering (chosen here), or hybrid designs. TESLA's choice of switching supplies had largely to do with conforming to unique German regulations on AC line filtering. At Fermilab the 13.8 kV circuit is on site (not shared with the general public) and filter requirements are less severe.

The charging supplies can be located in a central building as in TESLA, or in the same cabinet as the capacitor bank as in the baseline FNAL/TTF design. A remote charging supply does not need a high current pulsed power cable like TESLA since it delivers the charging power to the capacitor bank over the 0.1 seconds between pulses. An advantage of a central location is that a "hot spare" charging supply can be swapped in by moving a cable. A disadvantage is that safety lockout procedures are difficult due to the separate locations of the power source and load.

### 11.3 Reconfigurable Modulator for Initial to Final RF Upgrade

Two modulators are being built by a FNAL/SLAC collaboration that can be reconfigured to provide the combinations of pulse width needed for the Initial, Ultimate, or an intermediate scenario. See Figure 58.

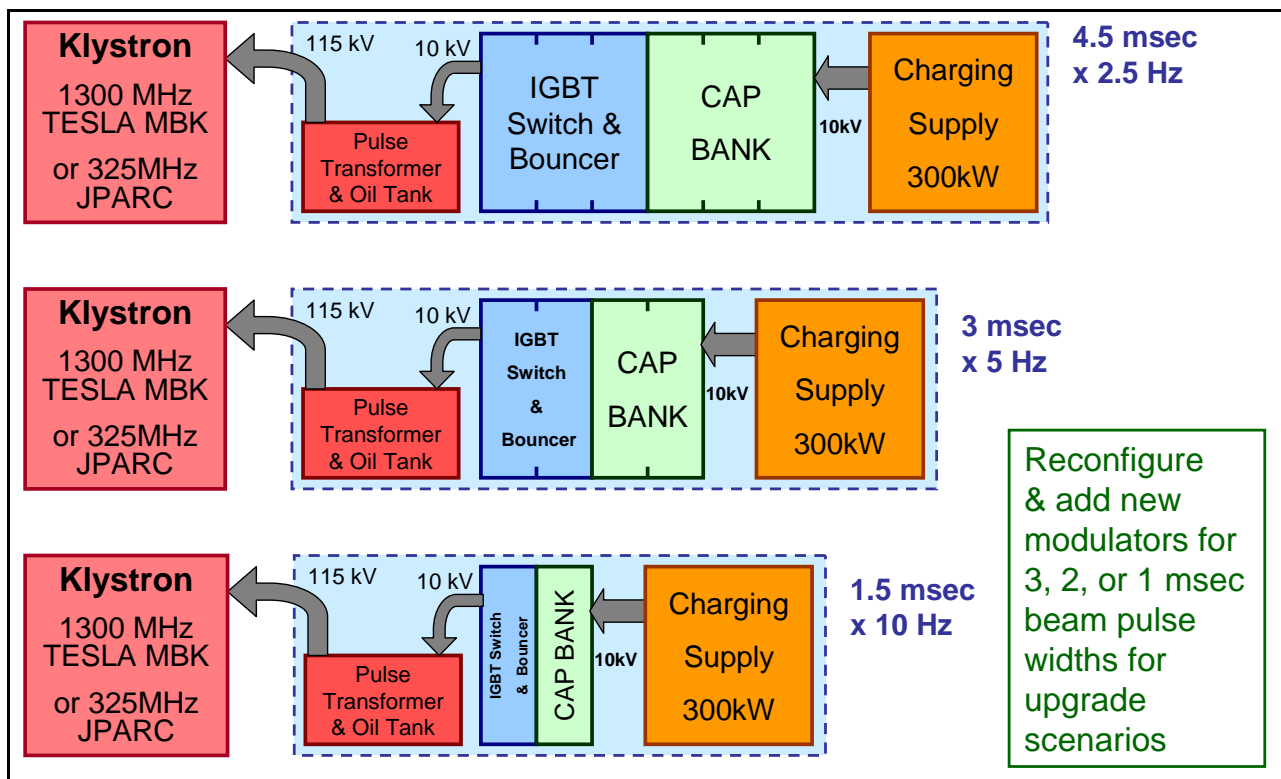


Figure 58 - Reconfigurable Klystron Modulator being built to support the Initial, Ultimate, or an intermediate RF power and pulse width scenario. This will be used at the Meson test area to verify proper Klystron and system operation at all design points.

The key design feature is that by appropriate series and parallel reconfigurations of the main capacitor bank and bouncer inductors and capacitors, the same components can be re-used in all three configurations. No changes to the charging supply or IGBT switch are required,

since the average power (duty factor) of the Klystron is approximately constant in all three scenarios. For the RF upgrade in the final machine, no new capacitor or bounce components are required since the 4.5 msec cap/bouncer unit can be split into three modular 1.5 msec units.

#### 11.4 Modulator Location and Gallery Layout

A simple straight-line layout of the equipment in the klystron gallery is possible (Figure 59) due to the 180 ft. {60 ft} spacing between klystrons in the main linac. The low density of equipment in the Klystron Gallery is a significant advantage of the many-cavities-per-klystron approach. The 12 ft. aisle width in the gallery is sufficient to allow a klystron, oil tank, or modulator to comfortably pass by for maintenance. A 4-foot maintenance aisle is provided on the back side of the modulator and klystron, and a 6-foot back side aisle is provided behind the control racks.

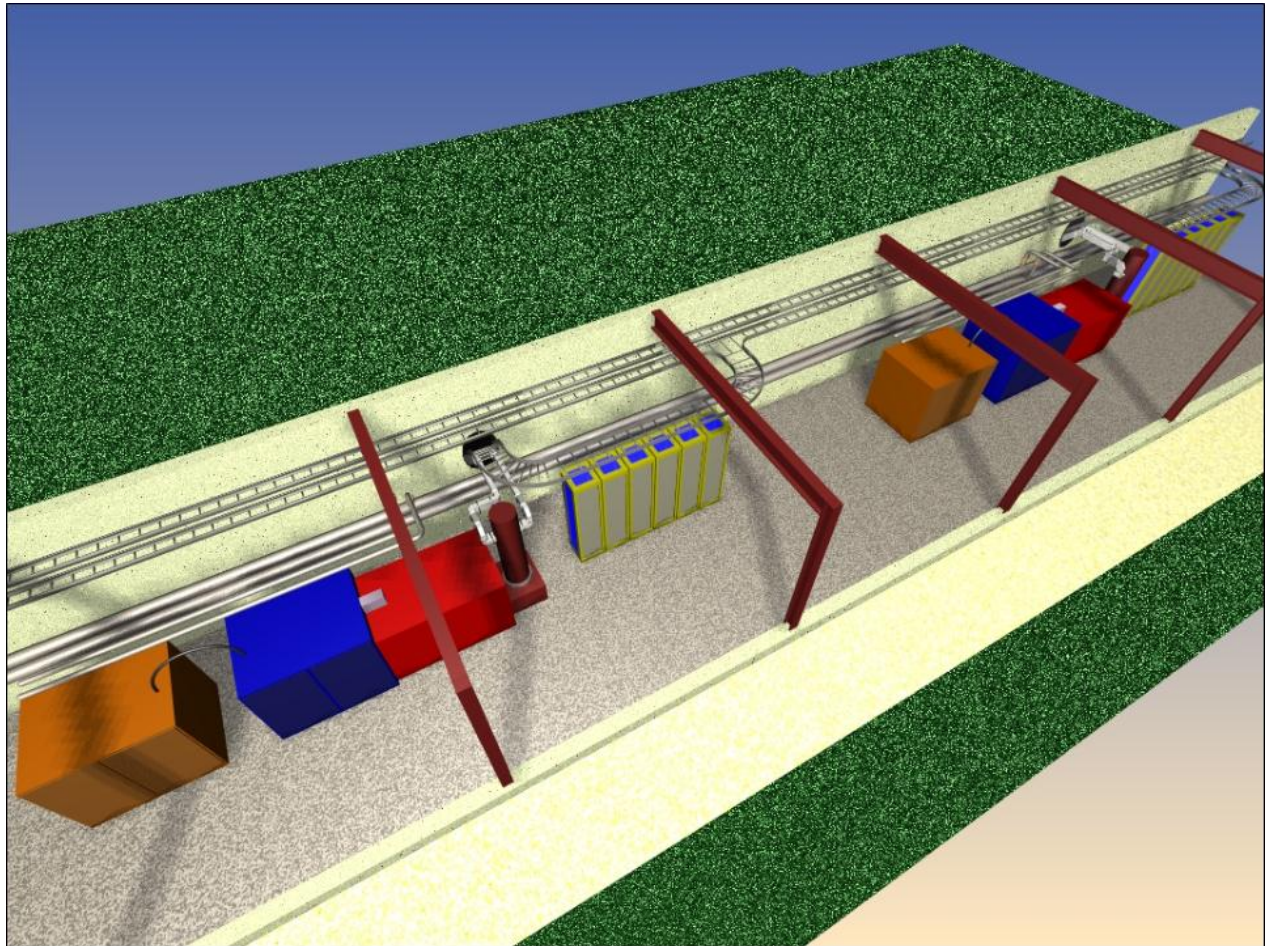


Figure 59 - Layouts of the Klystron Gallery for the Ultimate scenario in which all Klystrons are installed at 60-foot intervals. In the initial scenario, 1/3 of the RF Stations are present and the Klystron spacing is 180 feet. Each RF station consists of (from left to right): the 300 kW Charging Supply, the Capacitor Bank / Bouncer / Switch module, the Pulse Transformer, the Klystron and waveguide feed to tunnel, and the associated racks of electronics. The present allocation is two racks of electronics for each Klystron / Modulator, plus four racks of electronics for the 12 cavities associated with each cable duct interconnect to the tunnel.

## 12 RF DISTRIBUTION SYSTEMS

The Proton Driver linac has two RF Distribution systems: a 1300 MHz distribution system for the main linac and a 325 MHz RF system for the front-end linac. Both systems follow the cost-effective TESLA approach of fanning out the RF power from a small number large klystrons to many cavities. The block diagram for the Initial and Ultimate RF systems of the Proton Driver linac is shown in Figure 60. A block diagram of one of the Main Linac RF stations is shown in Figure 62.

The RF distribution is identical to TESLA for beam energies above ~2 GeV (the second  $\beta=1$  RF station). Above this energy, the protons are sufficiently relativistic that the TESLA passive RF power split with “vector sum regulation” (sect. 13.4) is effective. Below this energy, extending the TESLA RF split technique to proton linacs required the development of fast high power “Ferrite Vector Modulators” (FVM’s). These provide independent phase and amplitude control on individual cavities driven from a common Klystron. These have been the subject of intense and successful R&D which is described in sections 13 and 14.

Table 20 - RF Distribution systems for the Proton Driver Linac

RF Distribution	8 GeV Linac		
RF Distribution System	325 MHz	1300 MHz	
Peak Power from Klystron	2.5 MW	10.0 MW	
Cavities per Klystron (typ)	72 (24)	36 (12)	
RF Distribution Efficiency (see below)	79%	83%	including Ferrite Phase shifter losses
Max Power Required at SRF Cavity Coupler	70 (210)	220 (660)	kW
Excess RF Power Available after losses (typ)	25%	15%	TESLA ~6% (see curves per system)
Waveguide	325 MHz	1300 MHz	
Waveguide Type (in long chase & fanout)	WR-2300	WR-650	
Number of Output Waveguides per Klystron	1	2	
Rated Waveguide Power @freq.	600 MW	85 MW	No SF6
Max Power in Waveguide (at Klystron)	2.5 MW	5 MW	
Average Power in Waveguide (at Klystron)	2875 kW	5750 kW	
Waveguide Temperature Rise Above Ambient	TBD	TBD	
RF Distribution Losses	325 MHz	1300 MHz	
Average Waveguide Length	100 ft	95 ft {65 ft}	50ft from Klystron to nearest Cavity
Nominal Attenuation dB/100ft @freq.	0.05 db/cft	0.25 db/cft	
Waveguide Attenuation Losses	0.05 db	0.24 db	
Power Splitter Directivity Losses	0.10 db	0.05 db	
Circulator Losses	0.20 db	0.10 db	0.08 meas. at TTF
Ferrite Tuner Internal Losses	0.20 db	0.20 db	prototype measurements & spec from AFT
Ferrite Tuner Setpoint Losses	0.50 db	0.20 db	estimate from preliminary simulation
Overall Losses (avg)	1.05 db	0.79 db	
percent power losses	21%	17% *	* 9% for cavities without tuners (> 1.7 GeV)

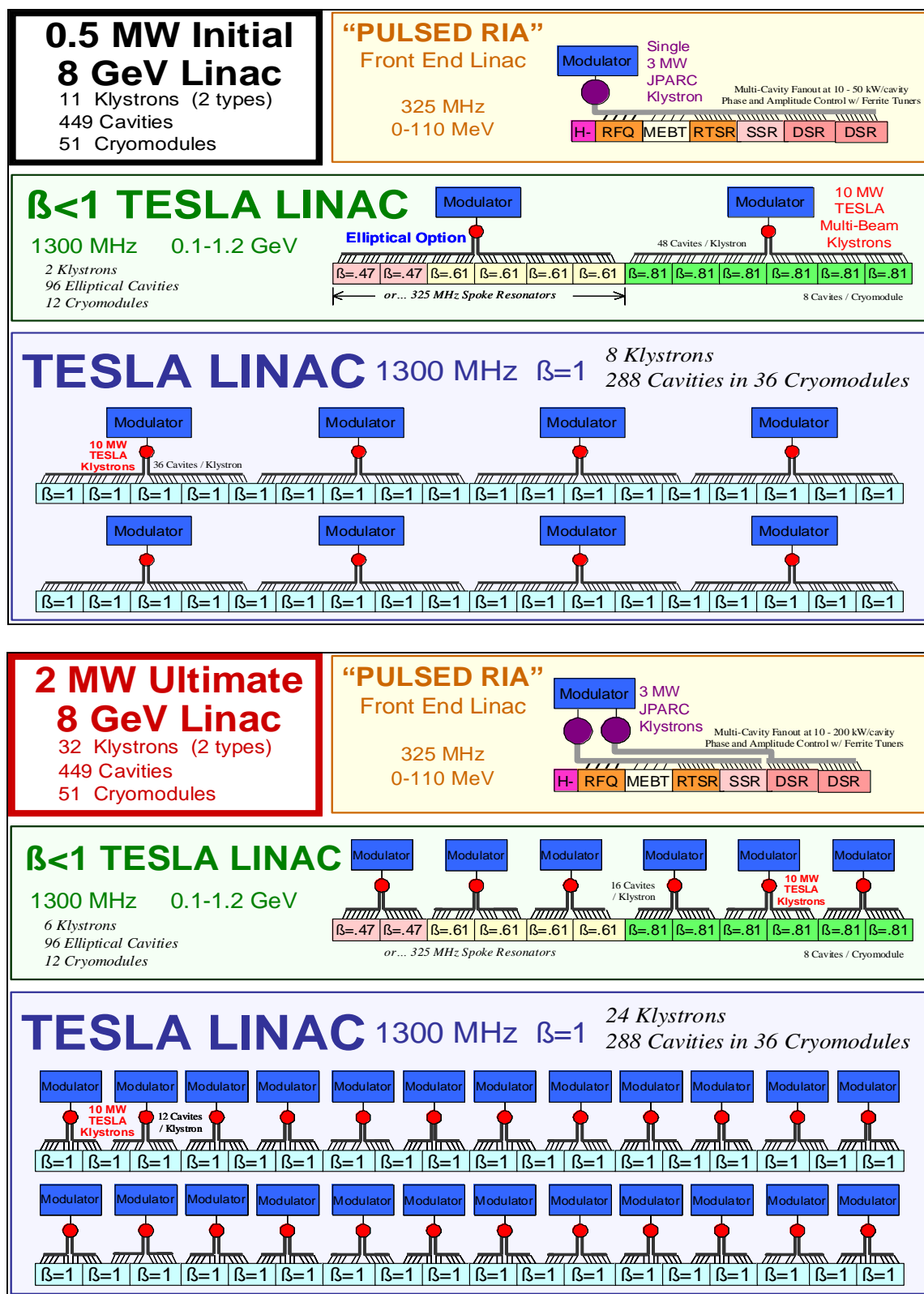


Figure 60 - RF Power Upgrade from the “Initial” (0.5 MW linac beam power) to “Ultimate” (2.0 MW beam power) configurations of the Proton Driver linac. The upgrade takes place by tripling the number of Klystrons and modulators to support a 3x higher beam current. The 1300 MHz elliptical cavity option is shown here. The Baseline configuration is shown in Figure 5.

### 12.1 The TESLA-Style RF Fan-out for Multiple Cavities per Klystron.

One of the major cost breakthroughs of the TESLA design<sup>114</sup> involves the ability to drive many SCRF cavities with a single, large klystron. In both the TESLA-500 design and the Proton Driver baseline design, 36 cavities are driven from a single 10 MW multi-beam klystron<sup>115</sup>. This is a reflection of the similar peak beam currents in each machine.

The TESLA RF fan out works as follows (see figs. Figure 61 and Figure 62). A fraction of the power from the klystron is split off to each cavity as the microwaves pass through a series of RF waveguide couplers. The power to each cavity then passes through a “circulator” which allows RF power to pass forward towards the cavity, while diverting power reflected from the cavity to a water-cooled load. In the TESLA design, a motorized mechanical three-stub tuner allows a limited range of phase and amplitude adjustment to the cavity drive. This also provides a limited ability to adjust the coupling (loaded Q) of the cavities<sup>116</sup>. In the front end of the Proton Driver linac (below ~2 GeV) these are replaced by Ferrite Vector Modulators (sect. 14) that provide phase and amplitude control which is electronically adjustable during the beam pulse.

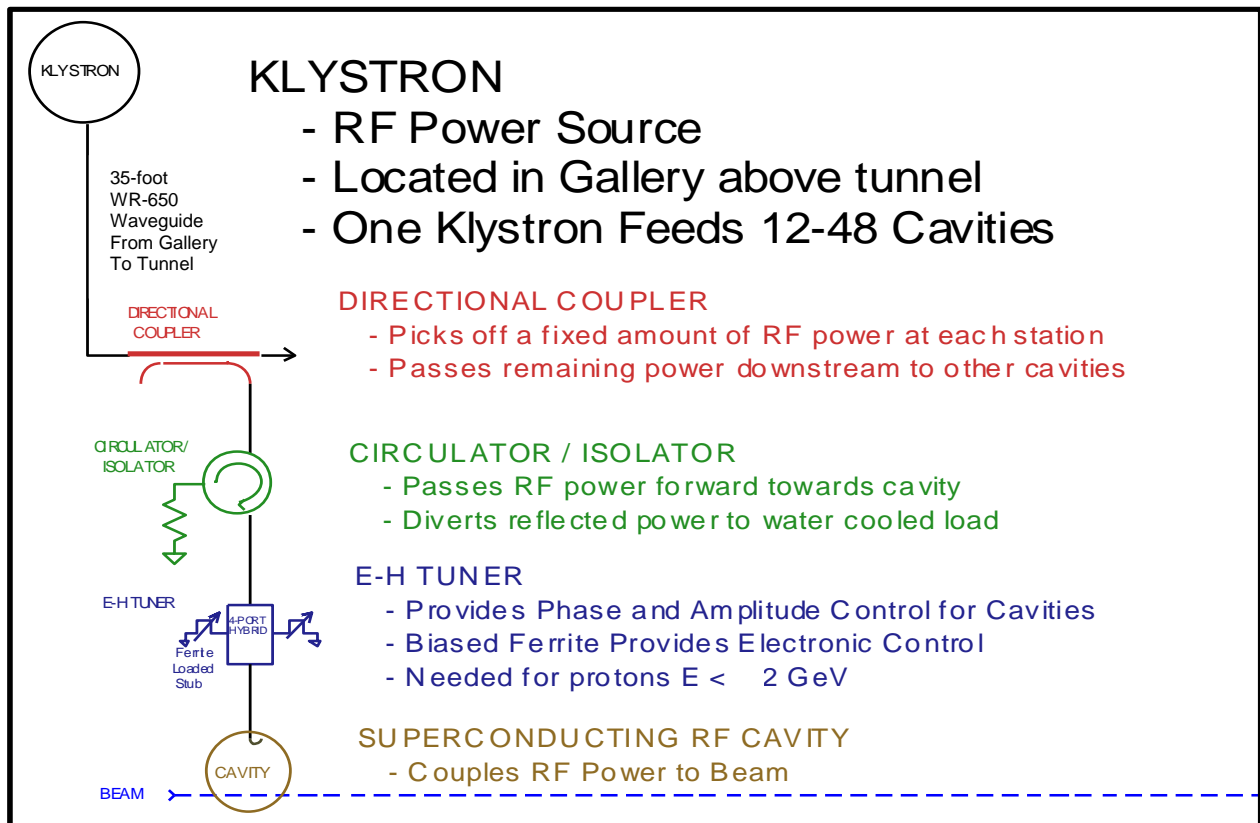


Figure 61 - Functions in one leg of the RF Distribution fan out in the Proton Driver Linac. Above 2 GeV, the E-H tuner (or Ferrite Vector Modulator) is replaced by the motorized 3-stub tuner of the TESLA design.

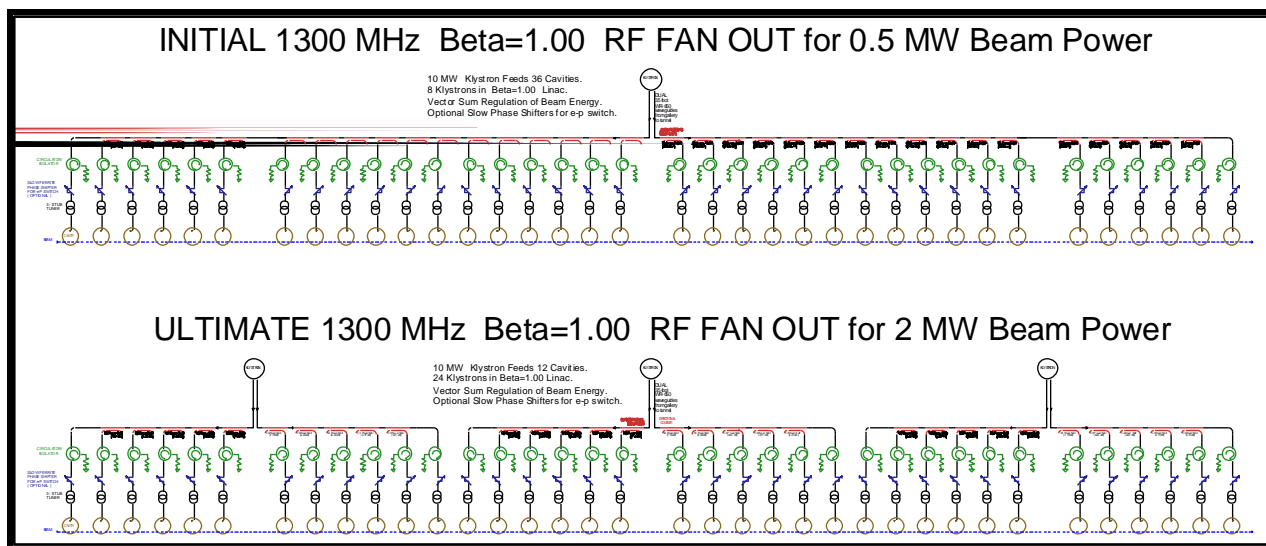


Figure 62 - Initial and Ultimate RF station in the Proton Driver Linac main linac. The upgrade from the Initial to Ultimate configuration adds two more Klystrons to each group of 36 cavities, thereby increasing the RF power available to each cavity to support higher beam currents. The main linac has eight RF stations, plus a similar station for the  $\beta=0.81$  cavities.



Figure 63 - TESLA RF Fan-out components installed on a cryomodule at TTF.

## **12.2 Microwave Conduits between Tunnel and Gallery.**

In the RF system for the TESLA TDR, the klystrons and modulator transformers are located in the same tunnel as the beam line components. For the Proton Driver linac, the klystrons and ancillary equipment are located in a parallel “Klystron Gallery” (sect. 3.7 - 3.8). The major benefit of this design is that “beam-on” access to the Klystron and associated electronics are allowed. The RF is transported to the beam line tunnel via waveguides housed in “microwave chases” or conduits between the enclosures. The RF power split is performed in the beam line tunnel, so that there is one conduit per klystron rather than one conduit per cavity.

The baseline (Initial) configuration uses a 36:1 RF power split identical to TESLA, with an upgrade to 12:1 RF fan-out as shown in. Figure 62. The Initial configuration requires microwave conduits every 180 feet, while the Ultimate configuration requires conduits every 60 feet. The civil construction for the baseline design includes all conduits needed for the Ultimate configuration. The readout cabling and electronic racks are also spaced at 60 feet.

An alternative RF power staging scenario under consideration is to initially install all microwave components needed for the Ultimate configuration in the tunnel and microwave chases. The 36:1 fan-out needed for the Initial configuration would be accomplished via a 6:1 power split in the tunnel, a 3:1 power split in the Klystron gallery, and a 2:1 split from the two output waveguides of the Klystron. The 3:1 RF power split in the gallery would be removed when the number of Klystrons is tripled. This scheme has the advantages that the 6:1 power split for the Ultimate RF upgrade is installed from the start, so the upgrade does not require any work in the beam line tunnel. This approach also means that a smaller variety of waveguide hybrids are required for the RF power split in the tunnel.

## **12.3 Waveguide Cooling**

The ~30 ft waveguide length in the microwave chases needed for the two-tunnel design results in ~2% additional RF losses in the waveguide compared to a single-tunnel layout. The power dissipation is 1.5 kW maximum in each of the 1300 MHz main waveguides. This will probably require some form of cooling inside the microwave chases. The 10x lower losses in the larger waveguide of the 325 MHz system will not require cooling. After the RF power split, individual components (circulators, loads, FVMs) will be water cooled but the waveguide itself will not.

## 12.4 RF Power Margins in the Main Linac

Excess RF drive power is required for compensating low-gradient or failed cavities, as an allowance for Klystron aging, and for overpowering cavity resonance errors due to microphonics and dynamic Lorentz detuning. RF Power loss budgets for the Proton Driver linac are summarized in Table 20. The excess power margin for the linac as a whole, after allowing for distribution losses and copper structure power, is 34%. This is comparable to, but somewhat less than, the excess RF power requirements for the SNS which are discussed in ref. 117.

The distribution of excess RF power along the linac is also important. The RF power levels, distribution losses, and RF power margin are plotted as a function of SCRF cavity number in Figure 64 for the 1300 MHz main linac. The excess power margin in the 1300 MHz  $\beta < 1$  linac is typically a factor of two, and decreases to a few percent at the back end of the linac as the protons become relativistic and tolerant of single-cavity resonance voltage errors.

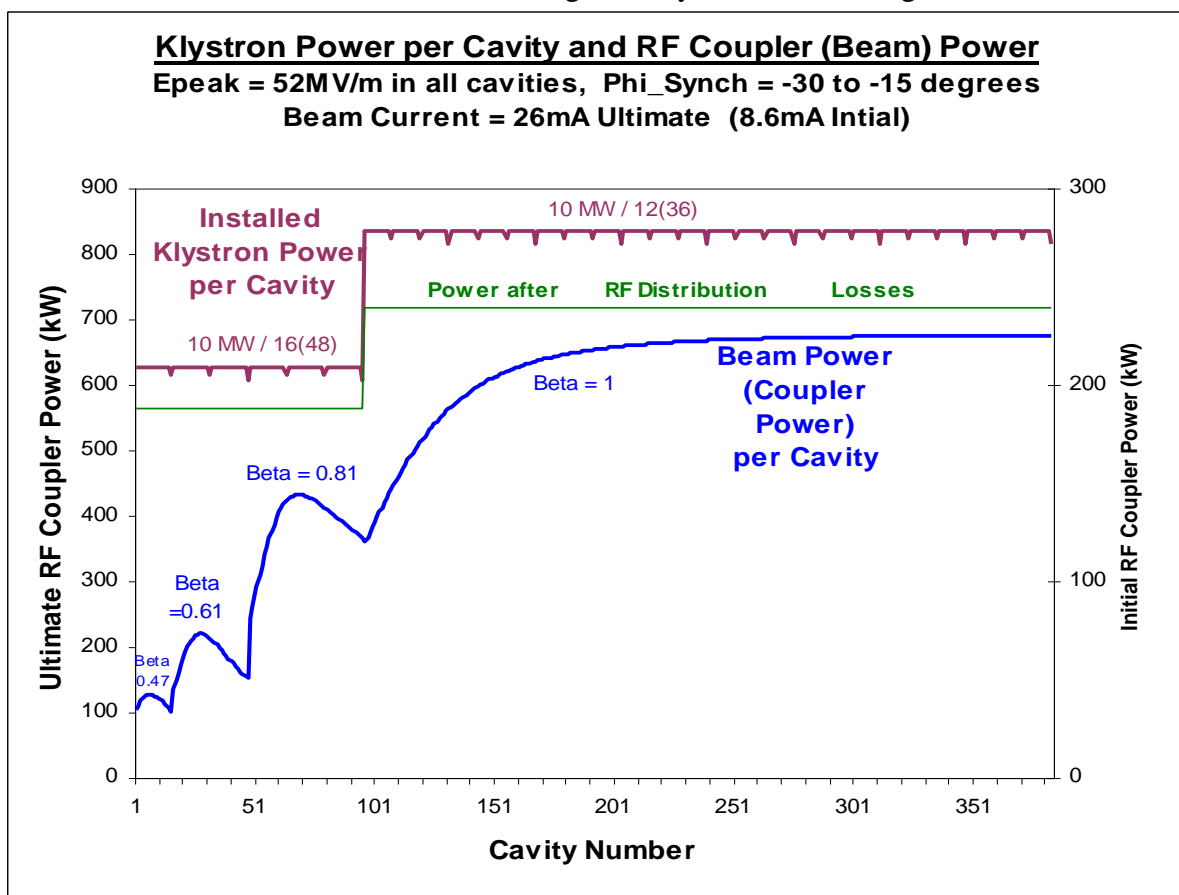


Figure 64 - RF distribution power in different stages of the 1300 MHz SCRF linac. The left axis scale reflects the power per cavity for the Ultimate configuration, and the axis at right reflects the RF power required for the 3x smaller beam current of the Initial baseline configuration. Top curve: klystron power per cavity before any losses or operating margins are taken into account. This is equal to the klystron power divided by the number of RF cavities fed by the klystron. Middle curve: Power per cavity after losses in the RF waveguide, circulator, and fast-ferrite tuner are included. A detailed breakdown of expected RF losses is in Table 20. Bottom curve: Beam Power (= RF Coupler Power) per cavity along the linac. This determines the nominal coupler power required at each station. The difference between the middle and bottom curves represents the surplus power margin available for cavity voltage regulation and feedback.

## 12.5 325 MHz RF Distribution System for the Warm Front-End Linac

The 325 MHz RF system is electrically similar to but mechanically very different from the 1300 MHz RF distribution. The entire front end linac up to 110 MeV is powered by a single Klystron. A single large WR-2300 waveguide, driven by the Klystron, travels alongside the beam line. At each cavity location, RF power is split off via directional (strip line or loop) couplers into coax lines. The split RF power passes through FVM boxes to each RF load. These FVM boxes (section 14.6) contain all components to provide cavity phase and amplitude control, isolation, etc. The various RF loads include 1, 2, and 3-spoke SCRF resonators, warm copper C-H Resonators, rebunching cavities in the MEBT, and the Radio Frequency Quadrupole (RFQ).

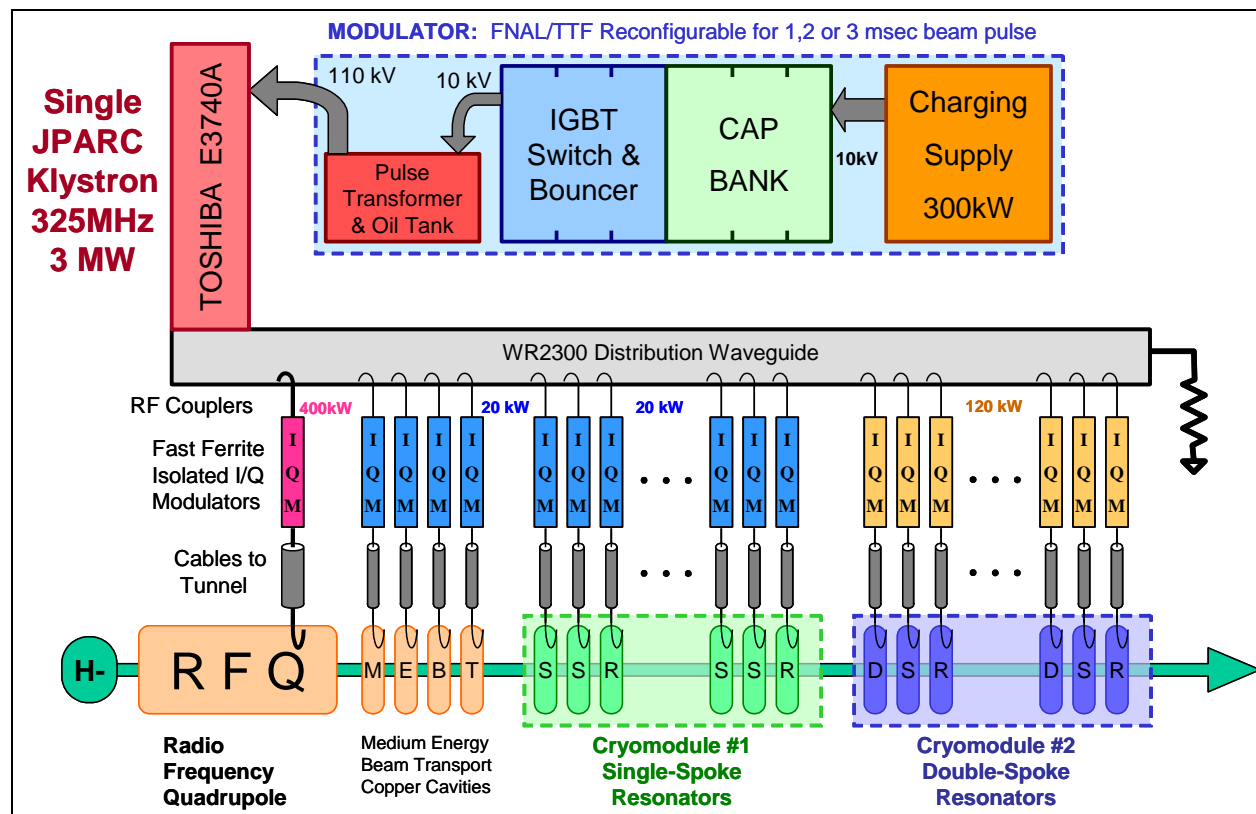


Figure 65 - 325 MHz RF Distribution for the front end linac (E<110 MeV).

### 325 MHz RF Power Margins

The RF power per channel and approximate RF power margins for the 325 MHz front end linac are shown in Figure 40. The required margins are difficult to estimate since the RF loads are a mixture of copper and superconducting cavities, with a range of filling times, filling energies, structure power dissipation, and beam loading power. The required power margins will be determined by operational experience at the SMTF/Meson front end test facility.

The RF system will be set up to anticipate the upgrade to the Ultimate configuration, so it will be possible to add a second Klystron. One possibility is to have separate Klystrons, driven by a common modulator, driving the copper and SC sections<sup>118</sup>. This may simplify the resonance control algorithms.

### 13 CAVITY RESONANCE CONTROL AND ENERGY STABILITY

Linac energy stability sets stringent requirements for phase and amplitude errors in the cavities' RF voltage. The specification for linac output energy fluctuations is  $\pm 15$  MeV maximum as explained in sect. 5.12. This requirement applies after the output of the Debuncher cavity, which significantly eases jitter requirements at the linac output (see sect. 5.14).

“Momentum halo” from occasional off-momentum pulses downstream of the linac output should not be a major concern since they will be cleanly removed with  $H^-$  stripping foil collimation in the transfer line (sect 19.8). Badly off-momentum pulses should result in large beam loss signals in the momentum collimation dump and a prompt abort of the beam spill ( $< 10$   $\mu$ sec out of a 3 msec beam spill). The SNS operating experience will be useful in confirming this strategy for loss minimization.

The main culprits in the energy stability of SCRF linacs are “Lorentz detuning” and “Cavity microphonics”. These are systematic and stochastic mechanical deformations of the cavities that alter their resonant frequency. If the frequency shift is significant compared to the resonant bandwidths of the cavities, the phase and amplitude of the cavity resonance will shift. This results in an error in both the energy and (to a lesser extent) the longitudinal focusing of the beam. Typical tolerances for proton linacs are 1% in amplitude and 1 degree in phase for uncorrelated errors.

The extent to which microphonics and Lorentz detuning are a problem depends on their magnitude of the frequency shift with respect to the cavity loaded bandwidth. Additional RF power must be expended to overcome the frequency shift and “push the cavity” back to the nominal phase and amplitude. For frequency shifts small compared to the resonant bandwidth, the dominant effect is a phase error which can be compensated by a change in phase and a small increase in amplitude of the RF drive. Larger frequency shifts require additional RF power. For example, a frequency shift equal to one (FWHM) cavity bandwidth requires approximately doubling of the power of the RF drive, depending on beam loading conditions. Since it is obviously very expensive to design for this extra RF power, it is important to understand and limit the cavity detuning from all sources.

The SNS RF system was designed for microphonic frequency shifts of 100 Hz out of a  $\pm 250$  Hz bandwidth<sup>119</sup>. However, recent measurements for SNS cavities (see Figure 66) give full spread less than 20 Hz and an RMS of 1-5 Hz. For the Proton Driver linac simulations (sect. 13.7) we have assumed microphonic shifts of 10 Hz RMS. We also assume that the Lorentz detuning will be compensated via fast piezoelectric tuners with an accuracy equal to that attained at TTF<sup>19</sup>. This is discussed in the following sections.

The use of the TESLA-style RF power split for a proton linac introduces many unique features to the beam energy control problem. The Proton Driver addresses these with TESLA-style piezo tuners to compensate Lorentz detuning, “Vector Sum Regulation” in the  $\beta=1$  sections of the main linac, and Ferrite Vector Modulators (FVM's) to provide phase and amplitude control on the individual cavities in the front end linac.

The detailed specifications for the FVMs (sect. 13.8) are important to the system performance. Key specifications include the phase and amplitude compliance, speed of response, and the fraction of cavities which contain the FVM's. Section 13.7 describes results of preliminary simulations which validate the performance requirements for the FVM's, and the technological R&D results are covered in sect.14. More details are given in the references<sup>120</sup>.

### 13.1 Cavity Resonance Control in Proton vs. Electron Linacs

The TESLA collaboration has had great success at demonstrating beam energy stability in a many-cavities-per-klystron configuration for an electron linac. The VUV-FEL has achieved energy stability of a few parts in  $10^{-4}$ , far better than needed for the Proton Driver. However, cavity resonance control and beam energy regulation is more complicated for non-relativistic protons than for electrons, for the following reasons:

1. Cavity voltage errors cause protons to undergo downstream phase/energy oscillations, whereas for relativistic electrons only an energy error is produced. For electrons, the energy error is the sum of the voltage errors of all cavities the beam passes through. For protons, the beam energy error associated with a cavity voltage error will be positive, negative or zero depending on the synchrotron phase advance between the cavity error and the downstream location.
2. The phase oscillations of protons affect the beam loading of the downstream cavities. This introduces a coupling between upstream voltage errors and downstream beam loading which is not present in electron linacs. This is especially important for SCRF linacs where beam loading is the dominant consumer of RF power.
3. The transit time factor for protons will vary across a group of identical cavities as the protons accelerate. This will produce a range of beam loading power in a group of otherwise identical cavities operating at identical gradients. Thus there will be a cavity-to-cavity variation in the ratio of cavity filling power to beam loading power, an important consideration for driving multiple cavities with a single Klystron.
4. The synchronous phases for cavities in proton linacs are larger and more varied than in an electron linac. This is significant since the RF drive must provide a phase and amplitude shift between cavity filling (which occurs in-phase with the RF waveform) and flat top beam loading replenishment (which happens at the synchronous phase angle). Normally this phase shift is accomplished by a phase jump of the Klystron associated with each cavity -- however this is impossible when one klystron drives many cavities with different synchronous phases. A more complicated filling strategy is required.
5. The mixture of warm copper & SCRF cavities present in the front end linac will have very different resonant properties and response times to both beam loading and RF drive.

Because of these complexities, previous SCRF proton linacs have taken the approach of one klystron-per-cavity. The individual klystron drive provides a fast and high gain feedback path to regulate the resonant voltage of each cavity. This is unaffordably expensive for the Proton Driver due to the cost of each Klystron and its associated infrastructure and control electronics.

### 13.2 Lorentz Detuning and Piezoelectric Fast Tuners

The first problem to be dealt with in resonance control is the “Lorentz detuning” which arises from mechanical deformations of cavities from the pressure of EM fields. These deformations cause shifts in the cavity frequency which are comparable to (or, for high gradient elliptical cell cavities, larger than) the loaded bandwidth of the cavity. Without compensation, Lorentz detuning would require substantial RF power to drive the cavities back to their nominal resonant amplitudes. Fortunately, Lorentz detuning is repetitive and predictable from pulse to pulse, and thus is relatively straightforward to control.

The TESLA collaboration has shown that piezoelectric tuners can be used to provide fast mechanical pulses to precompensate for the Lorentz detuning of the cavities<sup>121</sup>. The effectiveness of piezoelectric tuners has recently been confirmed for the SNS cavity/tuner assemblies<sup>122</sup>. These are included in our baseline design and cost estimate, and we assume that our results from piezoelectric compensation will be equally good.

The Lorentz detuning scales as the square of the gradient. Since our baseline design assumes 26 MV/m compared to 35 MV/m for the ILC, the Lorentz detuning should be a smaller issue for the Proton Driver main linac. If larger accelerating gradients are obtained at the time of Proton Driver cavity production, taking advantage of these higher gradients will require piezoelectric compensation comparable to that of the ILC (and larger than that of the Euro-XFEL).

The front end linac contains a variety of SRF resonator designs, each of which will also require an analysis of Lorentz detuning. The situation is most severe for the elliptical-cavity option for 100-400 MeV, where the heavily convoluted cell structures are expected to have large Lorentz coefficients. The Lorentz coefficients measured for spoke resonators<sup>123</sup> are substantially smaller. A quantitative analysis of these are planned, and a program of measurements on  $\beta < 1$  cavity prototypes is a high priority for the R&D program. In the interim, we are allowing substantial excess RF power in the  $\beta < 1$  linac (Figure 64).

Our resonance control simulations<sup>133</sup> also include an approximation of the effects of Lorentz detuning and piezo tuners. At present a single-pole (low pass filter) model with a stochastic spread in the Lorentz detuning coefficients is used. This does not reflect the richness and variability of response to Lorentz forces present on actual cavities, especially for the 4.5 msec RF pulse widths of the baseline design<sup>124</sup>. We plan to add more realistic details to the simulation, based eventually on measurements of the  $\beta < 1$  cavities as well as TESLA/ILC prototypes.

### 13.3 Cavity Microphonics

The second challenge in cavity resonance control is that of “Cavity Microphonics” which arise from mechanical deformations of cavities due to ambient vibration. These deformations cause shifts in the cavity frequency. These vary both in time and from cavity to cavity (see Figure 66). For modern cavity and cryomodule designs, these are smaller than the bandwidth of cavities with loaded Q’s appropriate for pulsed operation. Unlike Lorentz detuning, microphonics are random from pulse to pulse, although they may exhibit systematic behavior from external vibration sources. This complicates considerably the control requirements.

Microphonics control for the front end linac will also differ from the main linac due to the variety of SRF resonator designs and the rapid synchrotron phase advance between cavities. The microphonics measured for spoke resonators<sup>125</sup> are substantially smaller than for elliptical cavities due their stiffer structure. A quantitative analysis of these is planned, ending with a demonstration of the required beam energy stability in real-world conditions in the front-end tests at the Meson Lab starting in 2006.

For several years the TESLA collaboration has been working on piezoelectric tuners can be used provide real time feedback for microphonic detuning of the cavities. The baseline design does not assume this works; but if it does, the requirements for surplus RF power will be reduced and the specifications of the FVM’s in the  $\beta < 1$  linac will be relaxed.

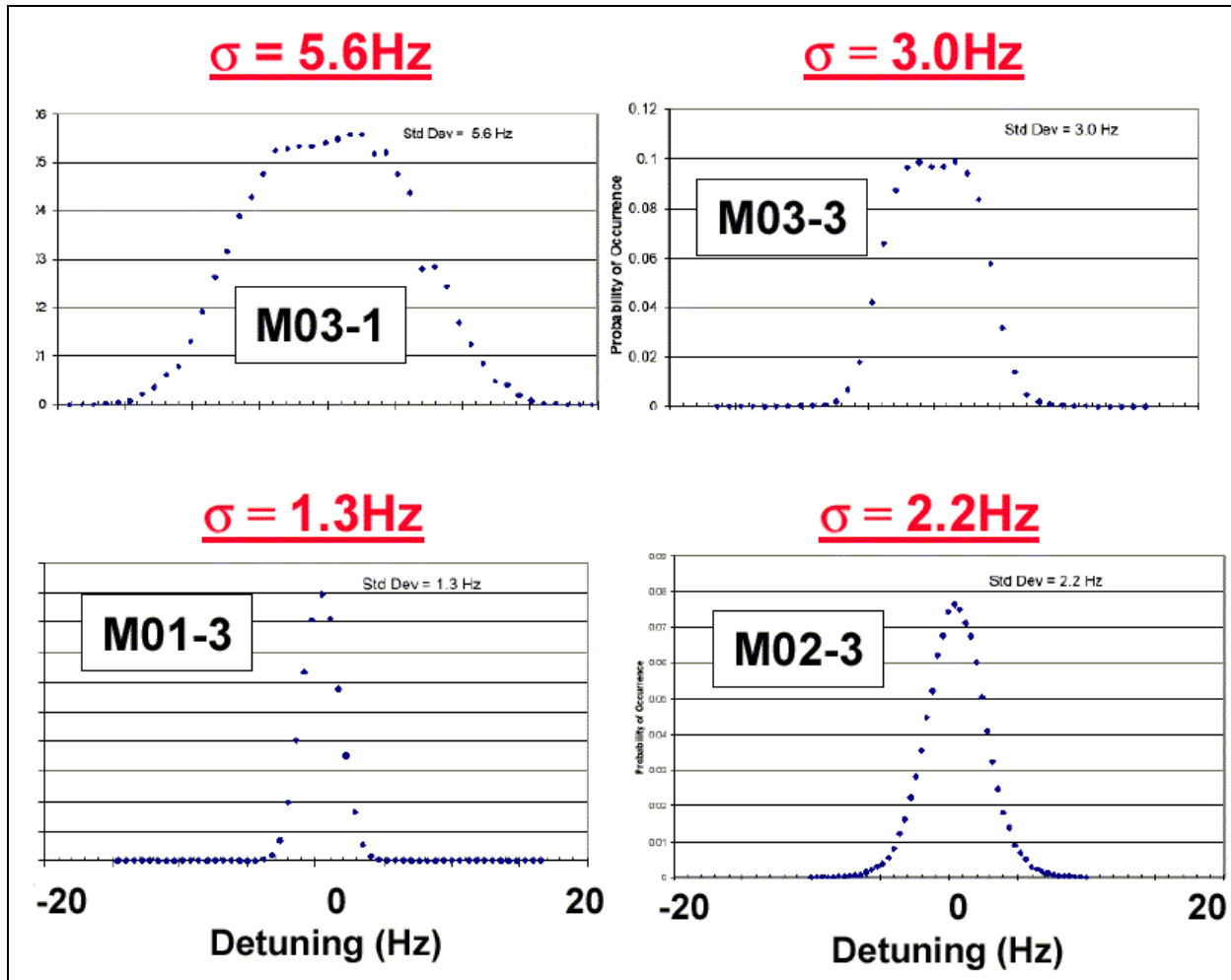


Figure 66 - Recent microphonics measurements<sup>81</sup> of several SNS  $\beta = 0.61$  cavities in their cryostats at JLAB. The full spread of the instantaneous cavity resonance frequency is less than  $\pm 20$  Hz, well below the  $\pm 100$  Hz specification for the SNS RF control system. Simulations for the Proton Driver linac assume microphonic shifts with  $\sigma = 10$  Hz, about 3x worse than the above measurements.

### 13.4 Vector Sum Regulation in Electron and Proton Linacs

The “Vector Sum Regulation” method<sup>126</sup> developed at TTF is the main tool used to accurately control the energy of an electron beam in the SCRF linac with multiple cavities per Klystron. In this technique the resonance signals from all cavities driven by a single klystron are electronically added together, and this “Vector Sum” signal is used as the feedback signal to the Klystron drive to regulate the *average* accelerating phase and amplitude of a group of cavities.

This avoids the need for FVMs to provide phase and amplitude control on the RF drive for each cavity. This procedure does an excellent job of regulating the beam energy for fully relativistic particles such as electrons, which travel at fixed velocity of  $c$  and therefore gain an energy increment equal to the total voltage from all cavities they pass through.

Vector sum regulation does not work as well for non-relativistic protons, since the synchrotron phase advance between cavities means that an upward voltage fluctuation in one

cavity in a group cannot necessarily be cancelled by a downward fluctuation in the other cavities. This means that the “vector sum” of the cavity resonance signals is not necessarily a good predictor of the output energy of a  $\beta < 1$  linac.

The vector sum method becomes progressively more accurate as  $\beta \rightarrow 1$ . A basic requirement is that the synchrotron phase advance across each group of cavities be “small” (less than  $\sim 45$  degrees). Thus the minimum proton energy for which Vector Sum Regulation will be effective will be a function of the number of cavities per klystron, the longitudinal phase advance per cavity, as well as the assumed magnitude of the cavity microphonics and uncompensated Lorentz detuning. Simulations of vector sum regulation<sup>134</sup> indicate that for proton energies above  $\sim 1$  GeV this method provides adequate energy regulation. See section 13.7.

The baseline design uses vector sum regulation above 1.3 GeV (the second  $\beta=1$  RF station). A more advanced version of the vector sum algorithm (section 13.5) promises to lower the energy at which FVM’s for individual cavity drives become essential.

Surplus RF power is required even if the Vector Sum Regulation works perfectly. The surplus power for the main linac is shown in Figure 64 and discussed in sect.12.4.

### 13.5 Weighted Vector Sum Regulation for Proton Linacs

A promising method has recently been suggested<sup>127</sup> for extending the performance and range of applicability of Vector Sum Regulation to proton linacs. This method is not yet included in our baseline simulations, but should result in a substantial improvement in the system performance when implemented. In particular, it should extend the range of applicability of the Vector Sum Regulation method to lower  $\beta$  and thereby reduce the number of FVM’s needed in the Proton Driver linac.

The idea behind Weighted Vector Sum is to *predict* the linac output energy fluctuation in real time using the measured fluctuations in the individual cavity voltages, and to *correct* the linac energy fluctuations using LLRF drive of nearby klystrons. The method depends on an approximate knowledge of the longitudinal focusing lattice of the linac, and works as follows:

Proton linac energy fluctuations can be analyzed in terms of the coefficients which relate a change in each cavity’s resonance voltage to the change in the linac output energy. These “sensitivity coefficients” are plotted in Figure 67 for the  $\beta=1$  section of the linac. The sensitivity coefficients can be positive, negative, or zero depending on the synchrotron phase advance between the fluctuating cavity and the linac output. There is a similar set of coefficients relating linac phase fluctuations to individual cavity voltage fluctuations.

The first-order response of the linac energy or phase is nonzero only for the “in-phase” component of the cavity resonance voltage. The “quadrature” component of the cavity resonance is responsible for focusing the beam but has no first-order effect on the linac output energy or phase.

The energy fluctuation of the entire linac is equal to the sum of the voltage fluctuations of all cavities, weighted by the sensitivity coefficient for each cavity. If the cavities have uncorrelated Gaussian errors, the linac output energy will fluctuate according to the normal formula for propagation of errors. The worst-case energy fluctuations will occur as a result of a worse-case fluctuation in the cavity voltages.

A similar analysis gives the change in the linac output energy resulting from a change in the drive of a single Klystron feeding multiple cavities. Changing a Klystron drive results in a calculable change in the resonance voltages of all cavities that it feeds. This can be translated into a change in the linac output energy, using a knowledge of the sensitivity coefficients for

each cavity. This yields a “sensitivity coefficient” for each Klystron. It can be positive, negative, or zero according to the average sensitivity coefficients of all cavities driven by that Klystron.

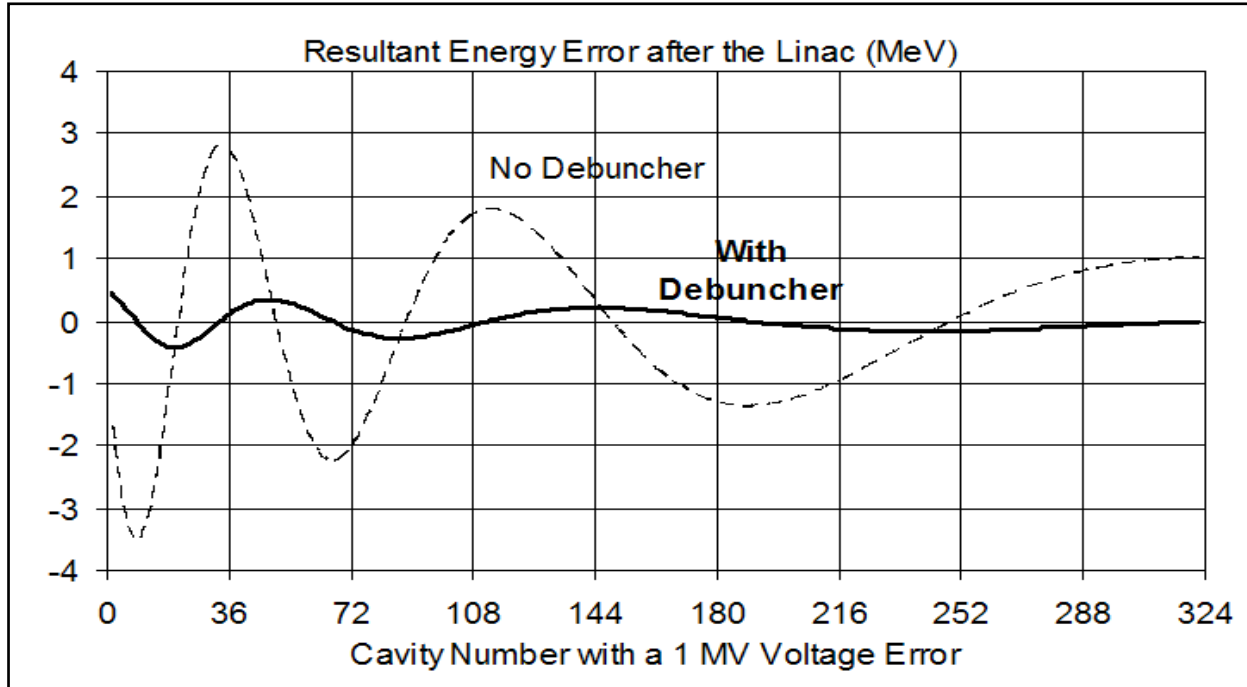


Figure 67 – “Sensitivity Coefficients” which relate the fluctuations in the accelerating component of the voltage of individual cavities to the fluctuations in linac output energy. These are plotted as a function of the cavity number in the  $\beta=1$  main linac. For an electron linac, the sensitivity coefficients are all equal to 1, indicating that a 1 MV error in the voltage of any cavity results in a 1 MeV energy error at the linac output. The passive Debuncher (solid curve) reduces the sensitivity to cavity voltage errors by a factor of  $\sim 5$ .

The Weighted Vector Sum approach uses fast adjustment of the Klystron drives to cancel the effects of the measured cavity resonance errors. In principle, it works perfectly, subject only to Klystron and cavity bandwidth limitations. In practice, the following considerations will apply:

- i) The algorithm requires real time data transmission from the electronics which calculate the weighted vector sums to the nearby klystrons which correct the voltage errors. This should not be a problem using gigabit digital links connecting the FPGAs which perform the calculations and control the LLRF.
- ii) The cavity resonance signals are not digitized perfectly. 12 Bit accuracy for a 40 MV cavity implies  $\sim 10$  kV digitization error per cavity. Assuming uncorrelated digitization errors for 500 cavities and an average “sensitivity coefficient” of 0.2 (see Figure 67) the error in the linac energy from digitization errors is  $\sim 0.05$  MeV.
- iii) Absolute calibrations of the resonance signals are not critical, since the method depends on measurements of *fluctuations* in the cavity resonance signals rather than their absolute magnitude.
- iv) Longitudinal beam dynamics will not be not perfectly known. However, the Klystron sensitivity coefficients can be measured directly by modulating the Klystron drive. This can be combined with a beam-based calibration of the individual cavity resonance signals to obtain adequate sensitivity coefficients for the individual cavities.

### 13.6 Beam-Based Phase and Energy Feedback

Several promising methods exist for using beam feedback within the pulse to further reduce the energy jitter of the linac. These are not included in our baseline simulations, but should result in a substantial improvement in the system performance when implemented.

These methods measure the phase and energy of the beam, compare with a nominal values established by a “reference” pulse, and correct via feedback to nearby klystrons. The advantages of this approach are that it directly regulates the subject of interest (beam phase and amplitude), and that it does not rely on a global model of the linac beam dynamics. Disadvantages are that (like all feedback) it has the potential for oscillations, and that the feedback is not available at the very beginning of the linac pulse before the beam signal arrives and has been processed. The beam feedback signal also disappears during the Main Injector abort gap for  $\sim 0.5$   $\mu\text{sec}$  every 11  $\mu\text{sec}$ .

The most straightforward feedback method is to measure the output energy of the beam via dispersion in the 8 GeV transport line, and correct the beam energy with either the last RF station or with the downstream Debuncher cavities. The simple nature of this feedback loop and the well-defined signal flow and propagation delays leaves relatively little scope for oscillations. This method may be used as a final “clean-up” of the beam energy errors. This is discussed in the Debuncher sections (5.14 and 15).

A second promising method due to Huening and Simrock is to use local measurements of the beam energy and phase to correct the beam energy at each RF station. The beam energy can be measured by time-of-flight (phase differences) between BPM’s along the length of the linac, and a correction is made via the Klystron drive to a nearby RF station. An advantage of this approach is that the beam energy is continuously corrected along the length of the linac, so that worst-case fluctuations are continuously suppressed before they develop. Since this is a local correction, it does not rely on a global model of the beam dynamics but simply a rough idea of the synchrotron phase advance between the measurement points and the cavities used for feedback. This method turns the entire linac into a set of potentially coupled feedback loops, which must be carefully simulated.

The best final solution for linac energy regulation may be to use cavity resonance based feedback (modified vector sum, etc.) during cavity filling time, then to switch over to beam-based feedback shortly after the beam pulse has started.

### 13.7 Linac Energy Stability Simulations

The complex nature of the energy regulation problem requires numerical simulations to set cost-optimized specifications for the RF components. Simulations<sup>128</sup> of linac energy stability in the presence of microphonics are well developed<sup>129,130</sup>, including studies of regulation techniques useful when ganging multiple cavities to a single klystron<sup>131</sup>. Project-specific details include the linac layout and AP design, the response times of the resonance control circuits and RF equipment, and the beam spill structure for transient beam loading. Unique features of the 8 GeV Proton Driver linac include driving many cavities per klystron, the use of Vector Sum Regulation for protons, and the use of Ferrite Vector Modulators which have complex time response characteristics.

A new simulation code<sup>132</sup> was developed and documented<sup>133</sup> for the Proton Driver. The published results<sup>134</sup> which will be described here reflect the baseline for the previous design study<sup>3</sup> rather than the current baseline design. Cavity microphonics of 10 Hz RMS were assumed, i.e.  $\sim 3\times$  larger than those measured on SNS cavities (Figure 66). An RF configuration

similar to the Ultimate RF configuration (12 cavities per Klystron) was assumed. However the economically significant results (i.e. the FVM specification and the energy range where Vector Sum Regulation is useful) are expected to apply to the current baseline design as well. Figure 68 shows a representative result from the simulations. Others are described in<sup>133,134</sup>.

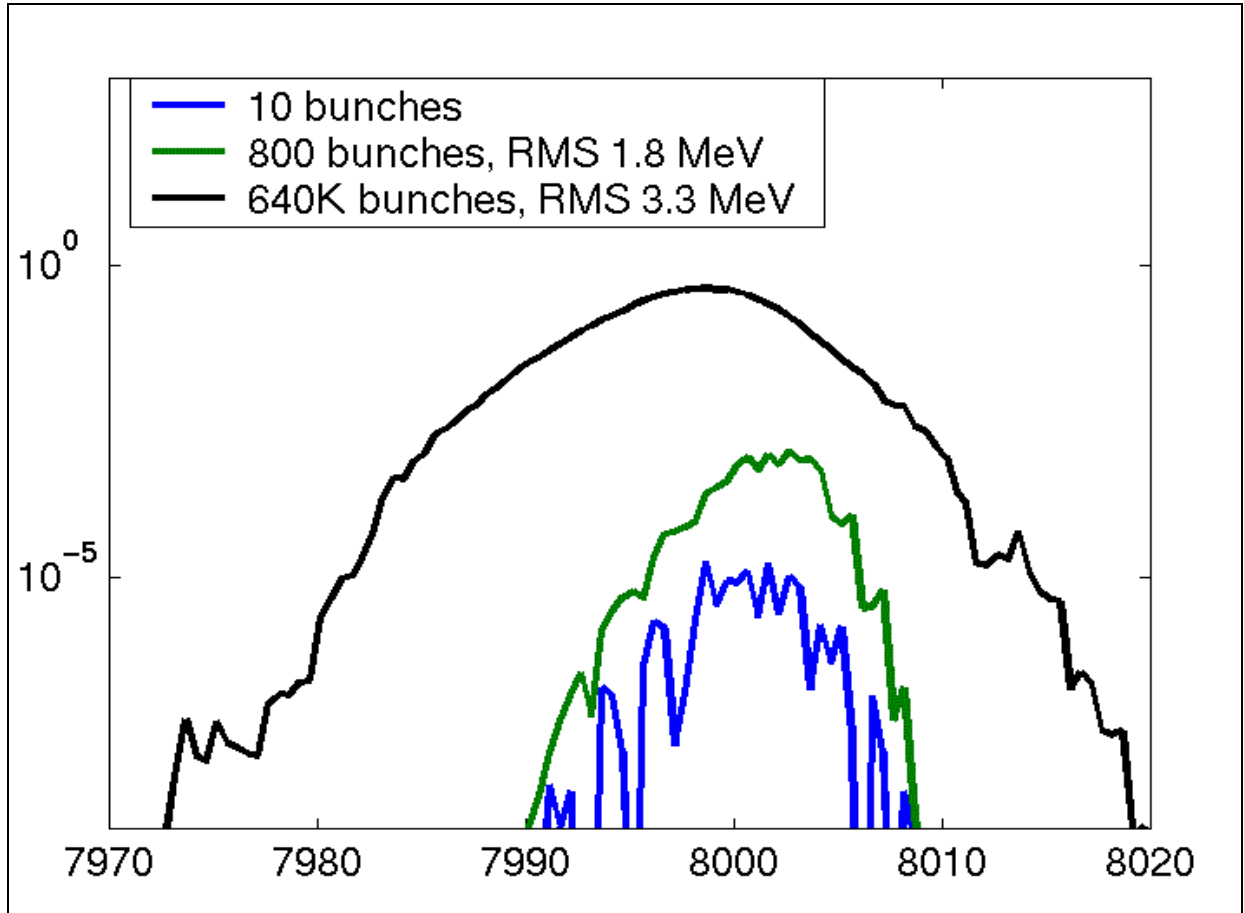


Figure 68 – Simulation of Vector-Sum Regulation with Microphonics in the  $\beta = 1.00$  section of the Proton Driver Linac (configuration from the previous Design Study). Beam was injected into the  $\beta = 1.00$  section at 1.3 GeV with an initial emittance of  $2.2\pi$  eV-s and 0.5 MeV RMS energy jitter. It was then propagated through the linac in the presence of Lorentz detuning and microphonics. Microphonic resonance shifts of  $\sigma = 10$  Hz were assumed, approximately 3x worse than recent measurements of SNS cavities (Figure 66). Bottom trace: energy spread of 10 representative bunches, with a typical emittance of  $2.8\pi$  eV-s (i.e. dominated by the incoming emittance). Middle trace: energy spread of 1 “macro pulse” of 800 bunches. Top trace: energy spread of 800 macropulses, with an energy spread including the pulse-to-pulse fluctuations due to cavity microphonics. The output energy jitter was dominated by microphonics effects as expected, but the output energy spread was limited to  $\sigma(E)/E = 0.04\%$  by vector sum regulation. The final energy spread will be reduced by a further factor of  $\sim 5$  by the passive Debuncher as described in section 5.14. This will bring the energy spread well below the  $\pm 15$  MeV tolerance (section 5.12).

The simulation code is under active development. The code has recently been updated to reflect the current baseline configuration. Numerous improvements are planned including: 1) more detailed models of Lorentz detuning, 2) FVM electromagnetic response times, 3) copper cavity filling times in the front-end linac, and 4) imperfections in the RF distribution components and calibrations. Nonetheless the simulations have already provided valuable

guidance for the design of the linac RF distribution and the R&D targets for the FVM's and their drive electronics.

### 13.8 Specifications for the Ferrite Vector Modulators

The simulations have been crucial in the development of specifications for the Ferrite Vector Modulators (FVM's). Requirements for both the speed of response and the range of phase/amplitude adjustment affect the cost and feasibility of the devices.

Preliminary simulations were used to identify roughly adequate specifications for speed of response and range of adjustment. R&D targets (section 14) were then set ~2x higher to provide adequate headroom in the baseline design. We are maintaining this factor-of-two contingency in the performance specifications of the ferrite tuners until a detailed simulation is complete and full-specification FVMs have been demonstrated. This procedure will converge with full linac simulations based on measured performance of prototype devices, final devices meeting potentially relaxed specifications, and ultimate verification by the beam performance in the front-end linac tests.

The technology and detailed specifications of the ferrite tuners is discussed further in section 14. FVM Phase shifter specifications are summarized in Table 21, and details of the RF distribution losses are in Table 20. A discussion of the general requirements follows.

**Table 21 – Summary of Ferrite Vector Modulator Specifications**

RF Phase and Amplitude Tuners	325 MHz	1300 MHz (Fast)	1300 MHz (Slow) *	* Slow Tuners are option needed for alternating electrons & H-
Included in Baseline	Yes	Yes	NO	
Phase / Amplitude Tuner Type	Coax	Waveguide	Waveguide	
Ferrite	YIG	YIG	YIG	Perpendicular Biased
Phase / Amplitude Tuner Locations	1/cavity	1 / cavity	1 / cavity	
Number of Phase / Amplitude Tuners	73 or 115*	132 or 84*	252	* for 3-spoke or ellip. med-beta
Phase Tuner Adjustment Range (deg)	90 deg	90 deg	360 deg	
Phase Tuner Settling Time (within 1 deg)	100 usec	100 usec	0.1 second	
Phase Tuner Slew Rate	1 deg/usec	1 deg/usec	N/A	
Amplitude Tuner Attenuation Range	6.0 db	6.0 db	none	
Amplitude Tuner settling time (1% F.S)	100 us	100 us	N/A	needs simulation
Tuner Peak Power	0.30 MW	0.60 MW	0.60 MW	worst case for ultimate scenario
Tuner Insertion Loss	0.2 db	0.2 db	0.2 db	Measured on Protos,&AFT Quote
Tuner Avg. RF Power Dissipation	71 W	142 W	142 W	worst case for ultimate scenario
Tuner Coil Average Power Dissipation	25 W	40 W	40 W	target for 1.5% RF Duty Factor
Static RF amplitude error	+/-1%	+/-1%		TBD needs simulation
Static RF phase error	+/-1 deg.	+/-1 deg.		TBD needs simulation
Dynamic RF amplitude error	+/-0.5%	+/-0.5%		TBD needs simulation
Dynamic RF phase error	+/-0.5 deg.	+/-0.5 deg.		TBD needs simulation

### FVM Speed of Response

Energy regulation of the linac takes place both through the fast feedback available via the limited number of Klystron drives, as well as through the one-per-cavity control available from the slower FVMs. This complexity makes the simulations particularly important to setting specs.

The FVM speed requirement comes from their use in both feed-back and feed-forward resonance control. The feedback capability is needed for dealing with microphonics and random fluctuations in beam current. In the feed-forward application, the FVMs must have the phase and amplitude agility to deal with the systematic requirements arising from differing cavity filling, operating gradient, and beam loading transient conditions – all of which differ from cavity to cavity. All of these effects are (at least crudely) included in our simulations<sup>133</sup>.

The response of the system to the beam loading transient needs special consideration. With a programmable bunch-by-bunch chopper in the MEBT (sect. 6.5), the rise time of the beam loading can be as fast as a single bunch. Alternatively, a “soft turn-on” can be programmed by chopping a variable fraction of bunches during the leading edge of the beam pulse. A softer beam loading transient will ease the response time requirement for the FVM’s. This capability of throttling the beam current on a bunch-by-bunch basis can also be used to regulate the beam current against fluctuations from the ion source, which should ease the burden on the LLRF feedback loops. These concepts will be explored in simulations and verified in the front end linac tests in the Meson Lab.

For the part of the feedback that uses the Klystron drives, the loop delay will include the electronic response times needed to down-convert and digitize the cavity resonance signals, execute the feedback algorithms via digital processing in an FPGA, upconvert and transmit the signals to the Klystron drives, and the delay inherent in the  $\sim 1$  MHz klystron bandwidth. Total loop delay for the Klystron part of the feedback will be 1-2  $\mu\text{sec}$  (the same as the XFEL and ILC). A delay time approximating this loop delay is incorporated in our simulation<sup>133</sup>.

The part of the linac energy regulation loop that uses the FVMs has the following contributions to the response time (see sect 14 for FVM device descriptions):

- 1) An electronic processing delay of  $\sim 1$   $\mu\text{sec}$  (similar to the Klystron drive processing delay).
- 2) A FVM bias power supply rise time limitation which is related to both the power supply switching frequency and the time constants of any filters needed to reduce electronic noise from the drive amplifiers. By directly driving the H-bridge on the switching supply directly from the FPGA logic, this should be reduced to one cycle of the  $\sim 300$  kHz switching frequency or  $\sim 3$   $\mu\text{sec}$ . This will be a major component of the “small-signal” response time of the FVM.
- 3) An inductively-limited slew rate on the bias coil, determined by the bias supply voltage and the inductance of the ferrite tuners. This will be the dominant factor in the “large-signal” response time of the FVM. This specification has a big economic impact on the ferrite bias drive supply, which requires a peak power sufficient to deliver the stored energy in the ferrite inductor during the desired rise time of the phase shift.
- 4) An “EM field penetration delay time” caused by the finite skin depth of the metal shell (waveguide or coaxial outer conductor) which prevents rapid field penetration into the ferrite. It is a non-exponential effect with a characteristic time of 10-100  $\mu\text{sec}$ , and depends on metal plating thickness and how the outer metal conductor is sliced. The response time of the ferrite, once the bias field has been applied, is negligible.
- 5) The response time is affected by both the nonlinear response of the ferrite tuners to the control current, and the nonlinear response of the E-H tuners to the phase shift of the individual tuners. Thus the response time of the FVMs will be a strong function of the operating point (phase and amplitude) of the FVM.

Our simulation includes these effects as: i) a fixed 1  $\mu\text{sec}$  electronics processing delay, ii) a single time constant representing an approximation to the settling of the phase shifter magnetic bias field, iii) an analytic approximation to the phase shift vs. bias field characteristic of the tuner, iv) the exact analytic expression for the E-H tuner or hybrid junction. The effect of the E-H tuner on the waveguide match at the cavity coupler has (so far) been neglected; thus the simulation can be thought of as having an “extra” circulator located directly at the cavity. Ion Source current variations are preliminarily included as a 1% Gaussian fluctuations.

The time constant approximating the speed of response of the ferrite tuners was investigated. For a 12:1 cavity fanout, a 200  $\mu$ sec time constant was found to be marginally adequate, and good results were obtained with a 100  $\mu$ sec time constant<sup>132,134</sup>. In the spirit of providing additional headroom during the R&D program, a response time target of 1 degree per  $\mu$ sec (50  $\mu$ sec for a  $\pm 45^\circ$  phase shift) was adopted for both commercial and in-house FVM prototype development (section 14).

For reference, the SNS target specifications for speed of response for their FVM development<sup>135</sup> was a  $\pm 30^\circ$  phase shift with a response time of 100  $\mu$ sec. The SNS targets were based on estimates rather than detailed modeling<sup>136</sup>.

### **FVM Set Point Power Losses**

In simulations to date, it has been found useful to bias the FVM so that a fraction of the waveguide power (typically 5%) is being thrown away at the FVM's under nominal conditions. This considerably speeds up the FVM response to changes in amplitude. These "FVM Set Point Power Losses" are factored into the RF power budget of the linac (see Table 20).

### **FVM Amplitude and Phase Adjustment Range**

The range of adjustment required by the FVM's (Table 21) is set by both the cavity filling strategy and the amplitude compliance needed for feedback. These differ greatly along the length of the linac. Cavities in the front end have large differences in their filling and beam loading characteristics. At the higher energies of the 1300 MHz linac, the spread in cavity filling and beam loading response becomes smaller. The need for FVM control is gradually lessened as beam energy increases and Vector Sum Control becomes more effective at regulating the linac energy.

The range of attenuation required is driven by the range one expects in the operating gradients of the cavities. The RF power split taps off a fixed fraction of the Klystron power to each cavity, irrespective of how much power the cavity is actually going to use. For a low gradient cavity, the surplus RF power must be dumped in the circulator load. This can be done in several ways, including: i) mis-adjusting the RF power coupler to generate high reflected power on flat-top, ii) using a motorized 3-stub tuner to dump the surplus RF power into the circulator, or iii) incorporating enough attenuation range in the FVMs to handle the full range of cavity operating gradients. (This range does not have to include zero, since "dead" cavities can be brought offline by detuning them with the mechanical tuners.)

A uniform specification ( $\pm 45^\circ$  maximum phase shift, -3 dB maximum attenuation) has been adopted as the R&D target for the FVM's. Our present level of understanding is that this is probably overkill for the 1300 MHz linac, and perhaps underspecified for the 325 MHz front end. A discussion follows.

For the part of the 1300 MHz linac that uses FVMs, the baseline design uses 3-stub tuners (in addition to the FVMs) to equalize the cavity filling, gradient, and beam loading behavior among a group of cavities driven by a single klystron. The 3-stub tuners alone have been shown to be adequate for dealing with the range of cavity gradients encountered at TTF. This leaves only the microphonics and uncompensated Lorentz detuning to be handled by the FVM's. For the expected range of these effects (< 10 Hz out of a loaded bandwidth of ~100 Hz) the ( $\pm 45^\circ$ , -3 dB) range of FVM is more than adequate.

The range of adjustment for the 325 MHz linac has not yet been determined. One possible solution is to extend the FVM output range to  $\pm 90^\circ$  maximum phase shift, and infinite maximum attenuation. This may be required when both copper and SCRF cavities are driven by

a single klystron driving the front-end linac. Again, these issues will be addressed in both simulations and the front end linac tests in the Meson Lab.

### **Slow Phase Shifters for Switching from Protons to Electrons**

Although not in the baseline design, the phase shifter requirements for switching the linac between protons and electrons on a pulse-by-pulse basis have been investigated (see the 3<sup>rd</sup> column of Table 21, and Appendix 1). These “slow” ferrite tuners must be located on every cavity of the main linac. They have no amplitude adjustment (i.e. are pure phase shifters) which have the 360° range of adjustment needed to run electrons and protons on alternate pulses in the linac (see Figure 119). The required response time is the 0.1 seconds between linac pulses. They do not need the fast response time required for individual control of cavity voltage in the presence of microphonics, since the main linac will use Vector Sum Regulation for both electrons and protons.

The possible use of the 8 GeV linac to accelerate relativistic muons<sup>137</sup> shortly after filling an accumulator ring with protons will require faster, 360-degree phase shifters on each cavity. In this case the response time must be comparable or faster than the ~0.5 msec filling time of the cavities. This is not in the baseline but nothing prevents a retrofit of these phase shifters.

## 14 FERRITE VECTOR MODULATOR TECHNOLOGY DEVELOPMENT

The Proton Driver linac design uses fast, high power Ferrite Vector Modulators (FVMs) to provide individual RF phase and amplitude control for each cavity up to 1.5 GeV. The FVMs are high-powered versions of devices which are commonly used in microwave work<sup>138</sup>. Specifications for these devices are discussed in section 13.8 and summarized in Table 21. Various technical presentations<sup>139</sup> to the Proton Driver RF working group are available online.

### 14.1 FVM Operating Principles

The basic concept of the FVM is to split incoming RF power into two equal branches, independently phase shift each branch under electronic control, then recombine each branch in a 4-port hybrid junction. Depending on the relative phase shift of the two branches, the hybrid junction will cause a fraction of the recombined power to be sent forward to the cavity, with the remainder of the power being rejected to RF loads. See Figure 61 and Figure 69.

Mathematically, the device sums the two equal-length phase vectors. If each phase can be arbitrarily controlled, any desired output attenuation and phase can be obtained. If only a limited range of phase adjustment is obtainable, then a correlated range of output phase and amplitude is accessible (see Figure 73).

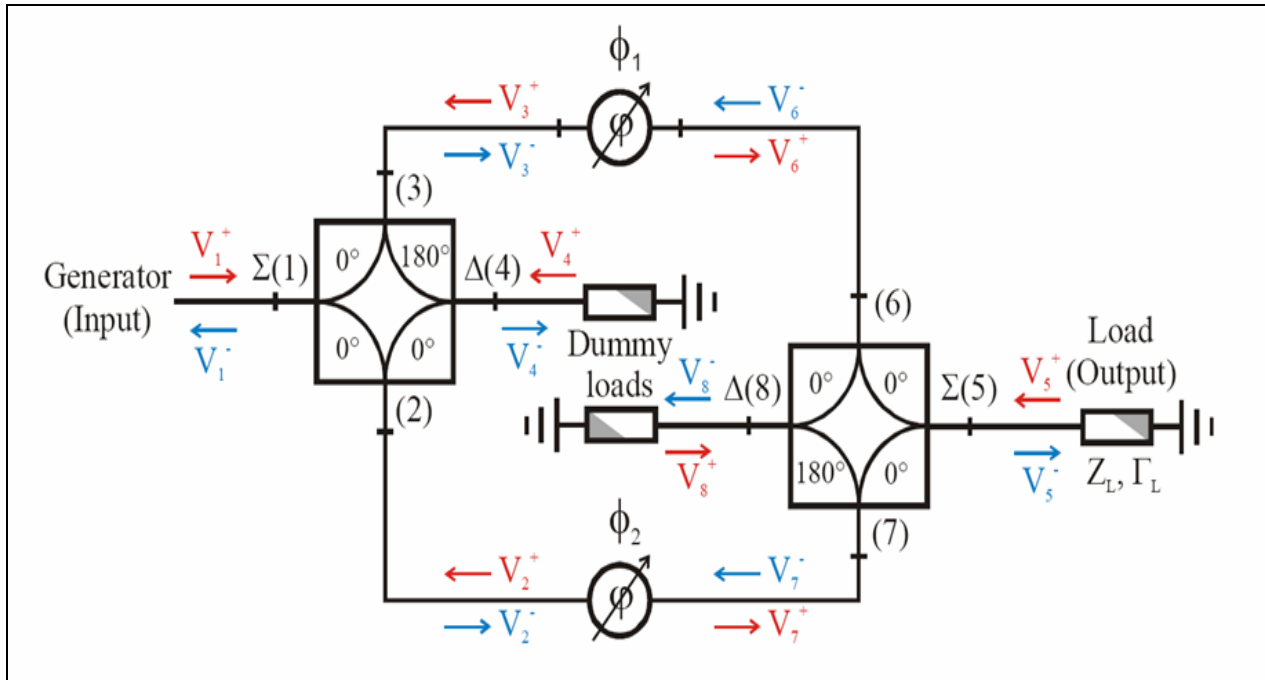


Figure 69 – The simplest FVM design concept uses two hybrid junctions and two ferrite phase shifters to obtain phase and amplitude control on an RF load. From ref. 140. Input power from the “generator” (klystron + circulator) is split into two branches. Each branch is electronically phase shifted via ferrite loaded waveguides or transmission lines, then recombined in a second hybrid. The differential phase shift ( $\phi_1 - \phi_2$ ) controls the amplitude of the RF signal sent to the load, and the average phase shift  $(\phi_1 + \phi_2)/2$  controls the phase of the RF signal at the load. Unused RF power is either dumped in RF dummy loads, or reflected back towards the generator (klystron) where it is absorbed by the klystron’s circulator load. In this topology, no “resonant-line” conditions can exist and all reflected RF power from the cavity is eventually disposed of in matched loads.

It is possible to use a single hybrid junction to both split and recombine the power (see Figure 70). In this case, ferrite loaded shorted stubs (rather than 2-port transmission phase shifters) are used as the phase shifting elements. This is the baseline configuration for the 1300 MHz waveguide-style FVMs (Figure 72).

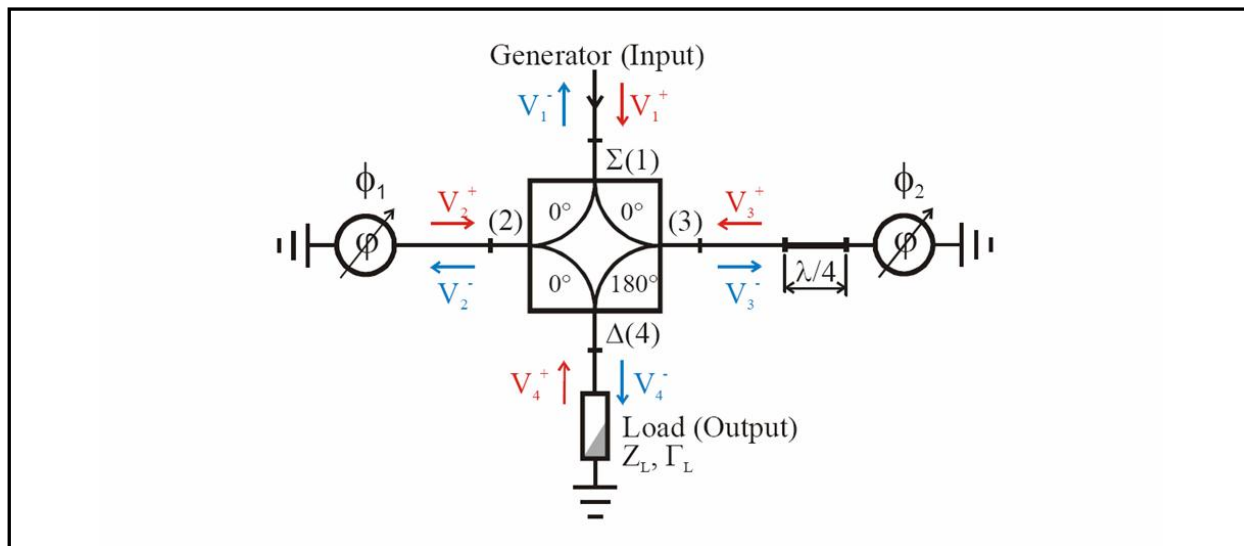


Figure 70 - Single-Hybrid version of the FVM. The phase shifters are ferrite loaded shorted stubs. This is the baseline design for the 1300 MHz waveguide-style FVM's (Figure 72).

In the single-hybrid topology, the Ferrite tuner is also adjusts the loaded Q of the SCRF cavity. This may offer power-saving advantages<sup>2</sup> for both the Proton Driver and the ILC, but complicates the control properties somewhat. For the 325 MHz FVMs for the front-end linac, it is planned to eliminate this “feature” by adding a circulator on the cavity output (see Figure 71).

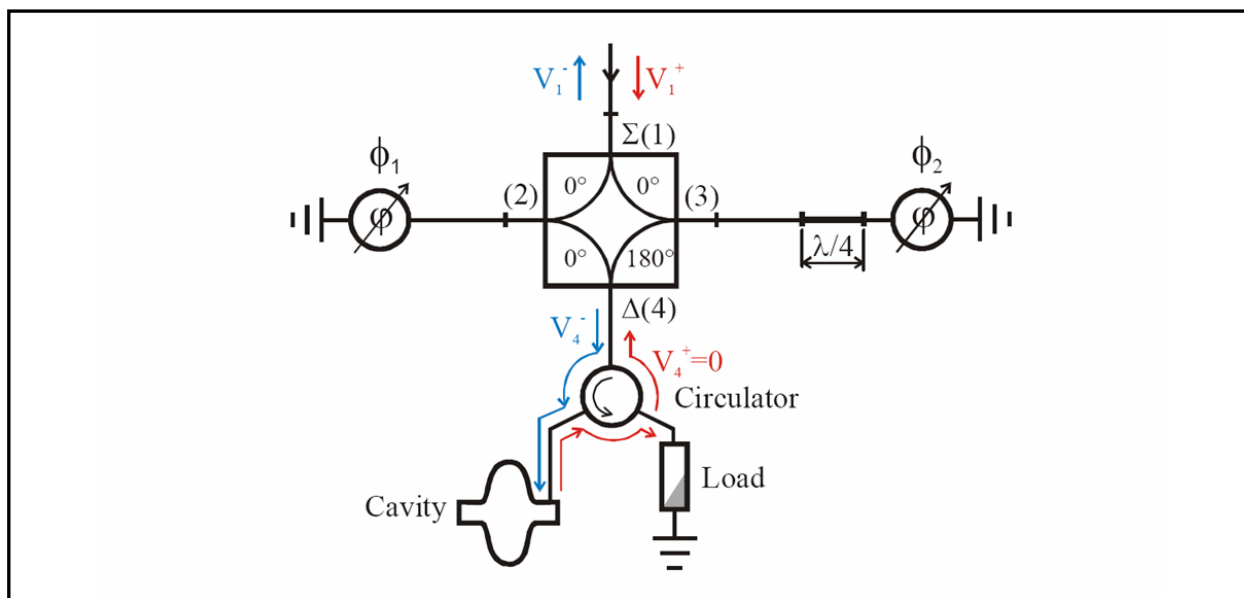


Figure 71 - Single-Hybrid FVM including an output circulator to absorb reflected power from the cavity. This is the baseline design for the 325 MHz coaxial-style FVM's.

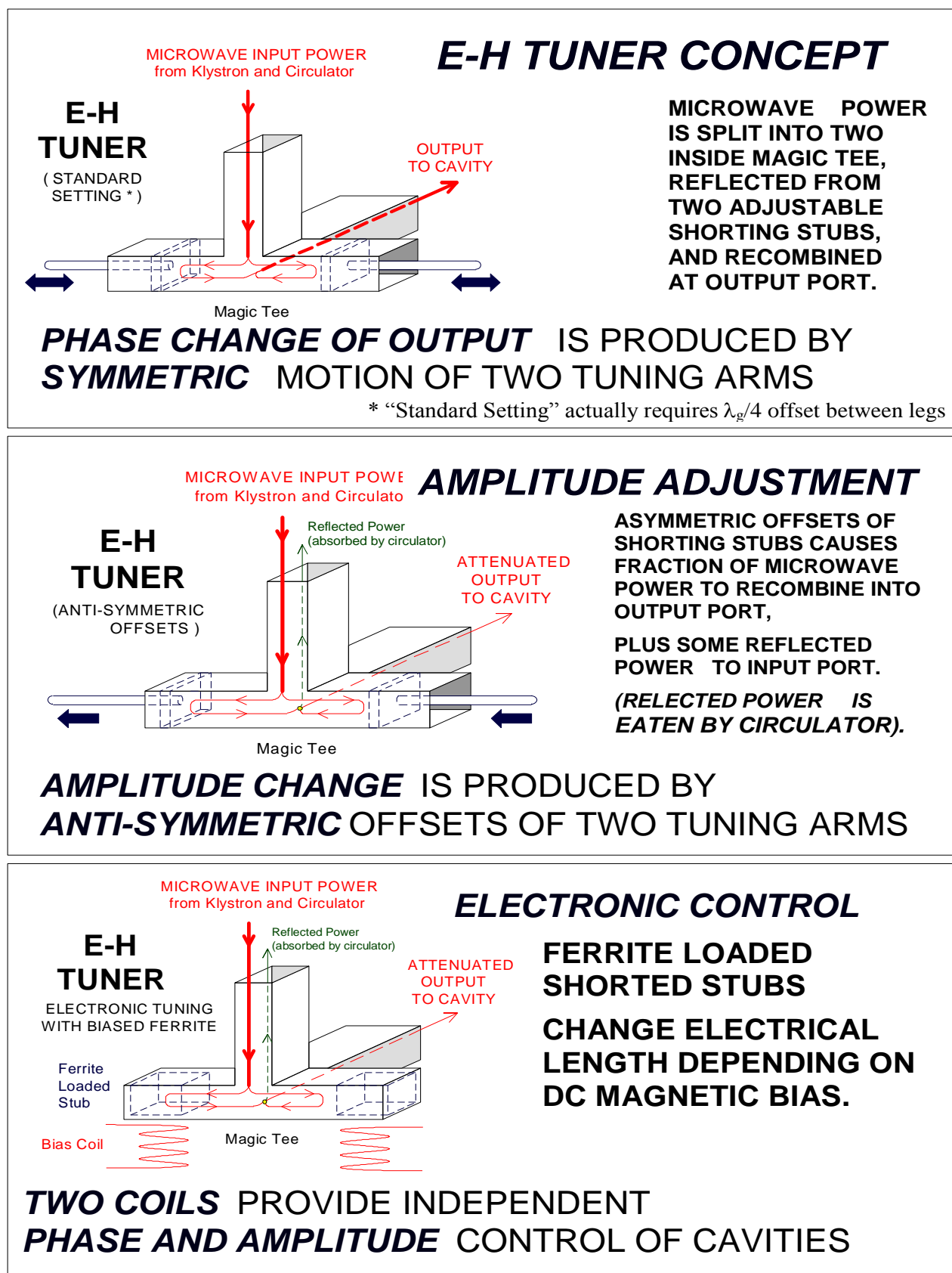


Figure 72 – Waveguide-style single-hybrid FVM (sometimes called an E-H tuner or I-Q modulator).

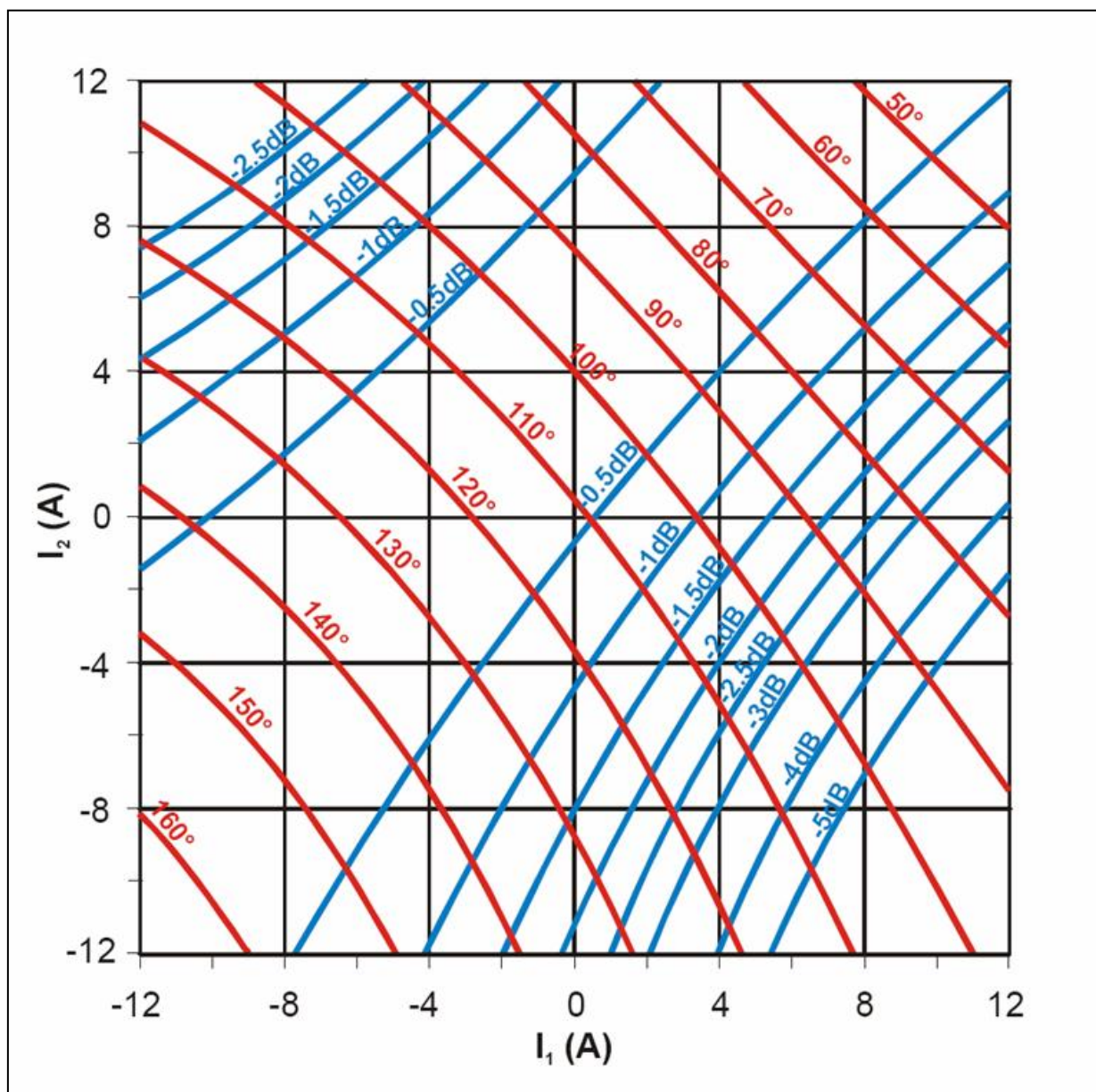


Figure 73 –Transmission Characteristics of a Ferrite Vector Modulator, as a function of the bias currents in the two ferrite phase shifters. The accessible output range depends on the range of the phase shifters. These are measured values<sup>140</sup> for a 352 MHz FVM using ferrite tuners with approximately 120 degrees of phase shift. The bipolar current range is a reflection of the use of permanent magnets in the magnetic circuit to bias the central working point of the YIG.

### Voltage Transients in the Ferrite Tuners

A disadvantage of the single-hybrid topology is that under transient conditions, large standing waves can pile up in the phase shifters. The peak power handling of the ferrite tuners must tolerate this. These have been investigated using a SPICE model of the coaxial version of the FVM<sup>141</sup>.

Under normal operation, the largest transient occurs at the start of cavity filling when 100% of the power is reflected from the cavity. This generates a momentary transient

corresponding to 1.4x the steady-state voltage (2x the steady state power) in the ferrite tuners. An output circulator on the cavity (Figure 71) eliminates this transient.

The theoretical worst case voltage in the stub is generated when the cavity is filled to maximum resonant amplitude, then the Klystron phase is instantaneously jumped by 180° by a (presumably malfunctioning) LLRF system. In this case a single stub experiences the full voltage from the Klystron plus the full voltage being emptied from the cavity – a factor of 2 in voltage (a factor 4 in power) above the nominal power handling for matched beam loading on flat top. This fault condition would normally result in a klystron trip due to excess reflected power, so this is not a fundamental problem. Our prototype ferrite tuners are close to demonstrating the required 4x safety margin on peak power, in which case no protection system would be needed.

## 14.2 Fast Ferrite Phase Shifters

The crucial elements of the Ferrite Vector Modulator are the high power, high speed, ferrite loaded phase shifters. Two of these phase shifters are required for each FVM. The phase shifters rely on the change of RF magnetic properties of ferrite as a function of the DC magnetic bias field. The basic technology of these devices was developed in the 1960's for phased-array radar systems (Figure 74).

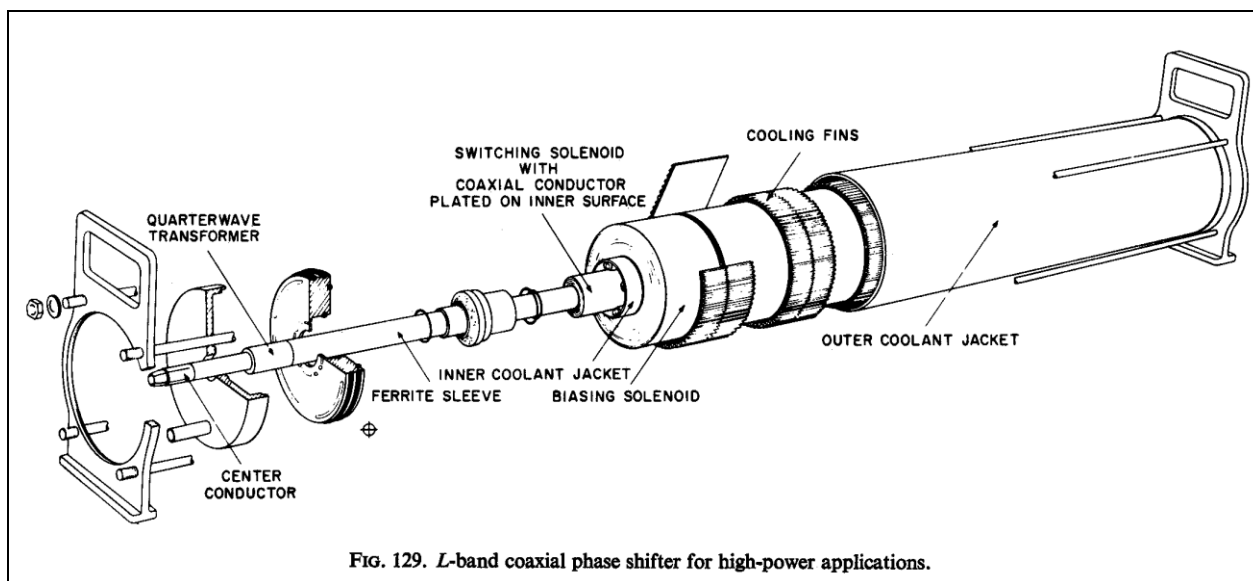


Figure 74 - Coaxial ferrite tuner developed in the 1960's at Bell Labs for phased-array Radar applications<sup>142</sup>. A solenoidal winding biases the ferrite-loaded coaxial transmission line. The unit featured 0.2 dB insertion loss, 360-degree phase adjustment, and 0.5 MW power handling capability at 1.3 GHz.

## Phase Shifter Topologies

Several phase shifter types are possible, including coaxial (sect. 14.3), waveguide (sect. 14.4), and stripline (sect. 14.5) versions. Because of the importance of the FVM to the feasibility of the Proton Driver project, R&D on all three of the designs has been pursued in parallel. Successful in-house designs were built and tested for the waveguide and coaxial geometries, and a commercial procurement is underway for the strip-line version. It presently appears that workable, full-spec devices can be made in all three configurations, and the choice

will be made on the basis of cost and physical size. At 325 MHz the coaxial design is the baseline, and the waveguide is the baseline at 1300 MHz.

Both shorted-stub and transmission type phase shifters are possible in each technology. The baseline designs and our prototypes use the shorted-stub configuration since 1) this requires fewer hybrids, and 2) the cooling of the center conductor is easier for the stub-type phase shifters. A transmission-style 1300 MHz waveguide phase shifter may be desirable for the (beyond-the-baseline) application of switching between electrons and protons (Figure 119).

### **Perpendicular Biased YIG Ferrite**

Phase shifters with the lowest RF losses are obtained by perpendicularly-biased yttrium-iron-garnet (YIG) ferrite<sup>142</sup>. The term “Perpendicular Bias” means that the RF magnetic fields are orthogonal to the applied DC bias magnetic field. These can be generated, for example, by a solenoidal winding wrapped around a ferrite-loaded coaxial transmission line, or a perpendicular dipole field biasing a ferrite loaded strip line, or a perpendicular dipole field biasing a waveguide with ferrite located along the short sidewalls of the waveguide. Under these conditions, the ferrite can be treated as a linear dielectric with a scalar permeability which varies with the DC bias field.

### **Operation Above Resonance**

Another design choice is whether to bias the ferrite above or below the ferromagnetic resonance. Obtaining a useful phase shift requires biasing the ferrite near the ferromagnetic resonance, but not so close to resonance that losses become large. Operating with a DC bias field “below resonance” requires a smaller bias magnet and power supply, but results in a smaller working range and increased losses at high RF power levels<sup>142</sup>.

We have chosen above-resonance operation for all of our prototypes. The minimum distance above resonance is limited by losses (Figure 75). The usable range of phase shift corresponds roughly to the range in which the losses are below ~0.2 dB (~4% RF Power loss) so cooling of the YIG ferrite is not a problem.

### **Magnetic Bias Field from Permanent Magnets and Pulsed Electromagnets**

The “DC” bias field for the ferrite can be obtained either purely by pulsed electromagnets, or with a combination of permanent magnets plus electromagnets. In the latter case, the permanent magnets provide a DC bias field corresponding to the midpoint of the operating range, and the electromagnets provide the control field excursion about the central operating point. The use of permanent magnets to provide the DC bias field is not “free” from the point of view of the electromagnet and drive amplifier, since the addition of the permanent magnets increases the reluctance of the magnetic circuit and decreases the slew rate for a given amplifier voltage. Another consideration is that a tuner biased with permanent magnets requires a 4-quadrant drive amplifier, while a pure-electromagnetic bias coil requires only a 2-quadrant drive amp.

For the coaxial design, permanent magnets are difficult to incorporate into the solenoidal magnet, so pulsed electromagnets will be used. For the strip line geometry, permanent magnets with auxiliary control windings will be used. For the waveguide geometry, both approaches are being tested, and the system which provides the lowest overall system cost will be chosen.

### **Electromagnetic Factors Affecting FVM Speed**

The factors affecting the response time of the entire FVM system are listed in section 13.8. The factors entering into the electromagnetic part of the response time of the FVM are: a) the

magnetic stored energy, which determines the coil inductance and operating voltage and current; and b) the electromagnetic shielding effect of the RF waveguide surrounding the YIG.

The magnetic stored energy is related to the volume of YIG ferrite which must be magnetized, plus the amount of energy “wasted” by magnetizing nearby non-ferrite regions. From this point of view, the magnetic efficiency of the strip line geometry is best, followed by the coaxial and waveguide geometries. Minimizing the YIG volume favors operating a small volume of YIG at high RF field levels, which is clearly a tradeoff with RF reliability. The total volume of YIG is not a major cost driver (a few \$100k for the whole Proton Driver project).

The electromagnetic shielding effects of the RF waveguide are also geometry dependent. The challenge is allowing rapid penetration of the “DC” magnetic bias field into the ferrite, while maintaining low RF losses and good containment of the RF fields inside the waveguide. Waveguide walls must be at least a few skin depths thick to have acceptably low RF losses. Solid waveguides will have eddy current shielding time of a few microseconds depending on wall thickness and geometry. For the coaxial and strip line geometries the problem is easier since the RF currents are axial, so the waveguide walls can be “slit” into axial segments. This breaks up the eddy-current shielding loops while maintaining good axial RF conductivity.

### 14.3 Coaxial Phase Shifter Development

The coaxial phase shifter is the baseline design for the 325 MHz front-end linac. Successful high power tests of prototypes of coaxial phase shifters have been performed both at 352 MHz using the Argonne APS klystron test stand, and at 1300 MHz using the Fermilab A0 photoinjector klystron. Recent high-power testing of 3” OD coax shifters has focused on the 325 MHz application for the baseline design.

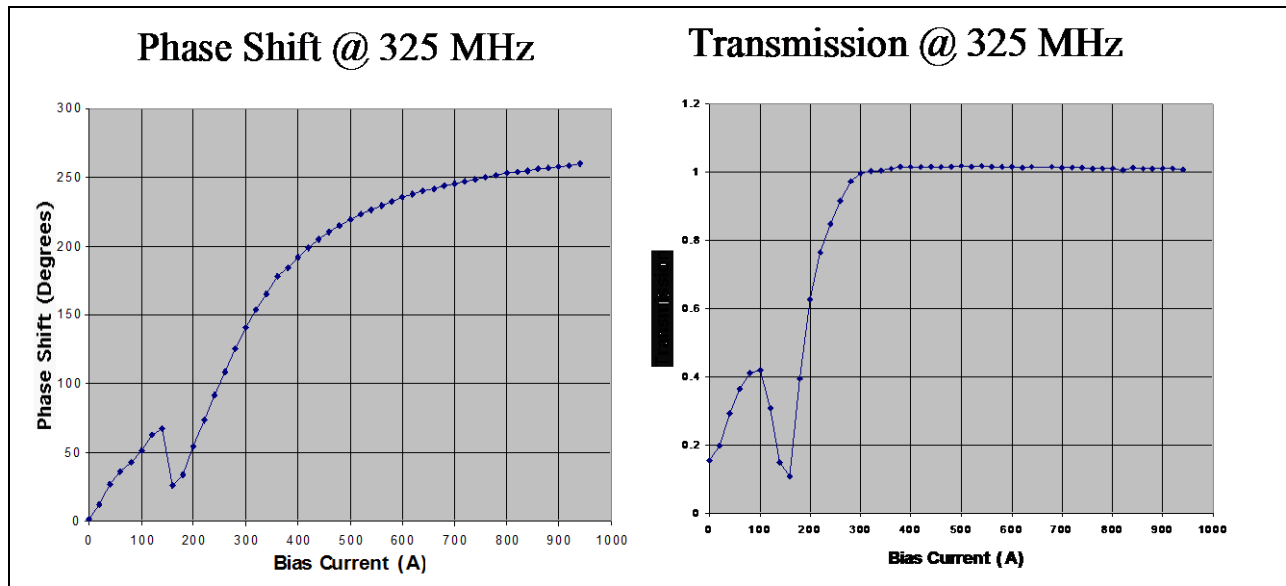


Figure 75 - Measured phase shift and Transmission of a 5” long x 3” diameter Coaxial Phase Shifter at 325 MHz. The usable range of the ferrite stub tuner, corresponding to the region where RF losses are below 0.2 dB, is about 120 degrees.

The measured properties of the coaxial phase shifters agree both with simulations and with a simple model of the YIG as having a scalar RF permeability which depends on bias field. A 6:1 coaxial diameter ratio provides a good match to 50 Ohms over the usable bias range. The

measured phase shift range (Figure 75) is approximately 120 degrees at 325 MHz for a shorted stub loaded with a 5" length of ferrite. The phase shift is proportional to the stub length and roughly proportional to the operating frequency. Both the phase shift and RF losses at high power are consistent with low-power measurements. Peak RF power handling of 440 kW has been demonstrated for long pulses, which is well in excess of the 150 kW per stub required for the baseline design. Average RF power of 1.6 kW (vs. 2 kW in the baseline design) has been tested and results in a few °C temperature rise.



Figure 76 – Coaxial Phase Shifter R&D. Top Left: Coaxial YIG phase shifter in high-speed pulsed coil with soft ferrite flux return yoke. Top Right: Coaxial tuner in high-power test stand with water cooled DC bias coil. Bottom Left: RF power, directional coupler, and water connections to the phase shifter test station. Bottom Right: Argonne APS test stand used for high average power testing. The test stand is driven by a 1 MW CW 352 MHz klystron with the LLRF drive modified to produce 4 msec output pulses.

The early coaxial prototypes were limited by peak power (sparking, especially at 1300 MHz), rather than average power (losses and heating). Weak points for sparking in the design were at the inner conductor at the gaps between ferrite rings which loaded the coaxial line. Sparks occurred at the inner conductor when the anti-node in the standing wave in the stub overlapped a gap between ferrite rings. Filling the ferrite region with SF<sub>6</sub> and oil showed the

expected improvement in performance, and resulted in devices exceeding the required peak power specifications. However, both of these are undesirable from a system point of view.

Recently best results have been obtained *in air* by using a solid 2.5" tube of ferrite (rather than a stack of 0.5" rings), and by shrinking-fitting the ferrite tube over the copper coaxial center conductor. This device has run for extended periods at 440 kW reflected power with a 4 msec pulse width at 1 Hz (the limit of the RF test stand). Because of the 2.5" length, this provided only a 60-degree phase shift rather than the 90-degree baseline specification (Table 21). A longer (5") solid ferrite tube is being prepared, which should provide a 120-degree phase shift and maximum power handling in air.

The response time of the coax tuner, drive coil, and flux return (Figure 76a) should, by design, be faster than 50  $\mu$ sec. At present we have only measured an upper limit of 100  $\mu$ sec for sweeping the full 120-degree phase shift, limited by the available power supply. The high-speed switching supply amplifier modules (section 14.7) will be adequate to test the phase shifter response time down to the 10-30  $\mu$ sec level.

The next steps in the already successful 325 MHz coaxial R&D program are: a) to attempt to reduce the coaxial diameters from the present 3" to 1-5/8" OD, which should result in a faster and cheaper bias drive magnet for the "low-power" channels of the front-end linac, and b) attempts to increase the phase shift range should this prove desirable.

#### **Possible use of the Coaxial Phase Shifter at 1300 MHz.**

Although the baseline design at 1300 MHz is the waveguide-style phase shifter (sect.14.4.), the coaxial design is also usable at 1300 MHz. In our prototypes, the accessible range of phase shift is limited by anomalous losses that appear to be generated by parasitic excitation of higher-order modes. 3-D Electromagnetic simulations indicate that these modes are easily excited at high frequencies due to the 6:1 coaxial diameter ratio of the 50-Ohm prototypes built to date. To ameliorate this, we are investigating smaller coaxial diameter ratios for use at 1300 MHz. A diameter ratio of 2:1 provides a ~20-Ohm impedance which can be matched to 50-Ohms with a quarter-wave transformer. The matching section could ultimately be incorporated into the waveguide-to-coax transition which is required for using the coax design at 1300 MHz.

#### 14.4 Waveguide Phase Shifter Development

The YIG ferrite loaded waveguide-style stub phase shifter is the baseline design for the 1300 MHz FVM's. A total of 168 phase shifters are required in the 84 FVM's used in the baseline linac. Prototype waveguide phase shifters have been built and successfully tested at powers up to 1 MW in air, and 2 MW using SF<sub>6</sub>. This exceeds the 330 kW per stub RF power required in the Ultimate design. The usable phase shift already demonstrated at high power is adequate for baseline requirements. Additional design improvements have been identified which should further increase the power-handling capabilities and expand the usable range of phase shift well past that required for the baseline design.



Figure 77 – Waveguide-style Phase Shifter stub undergoing power testing using a 1300 MHz klystron setup at Fermilab's A0 photoinjector facility.

The FNAL waveguide phase shifter design differs significantly from those previously developed at ANL for SNS R&D (Figure 78). The FNAL design places the YIG bricks along the sidewall of a reduced-height waveguide rather than near the center. This has several advantages. Firstly the electric fields are smaller along the sidewall than at the center of the waveguide, so that peak power handling capability is improved. Secondly, the RF magnetic fields near the sidewalls are mainly axial, so the non-reciprocal behavior from ferrite located at the center of a waveguide is practically absent. This is an advantage in the shorted-stub geometry. Thirdly, the broad face of each brick is in contact with the sidewall of the waveguide, and can be cooled (by water if necessary) without interfering with the magnetic circuit that biases the ferrite.

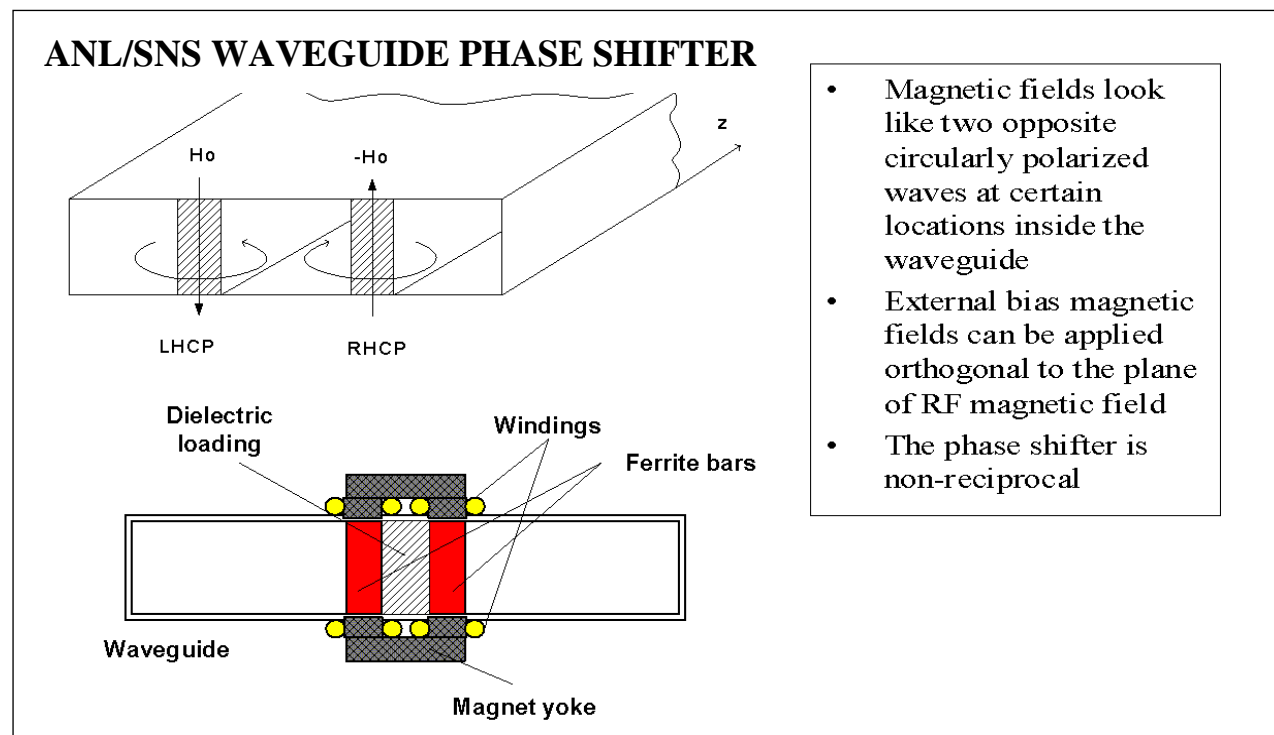
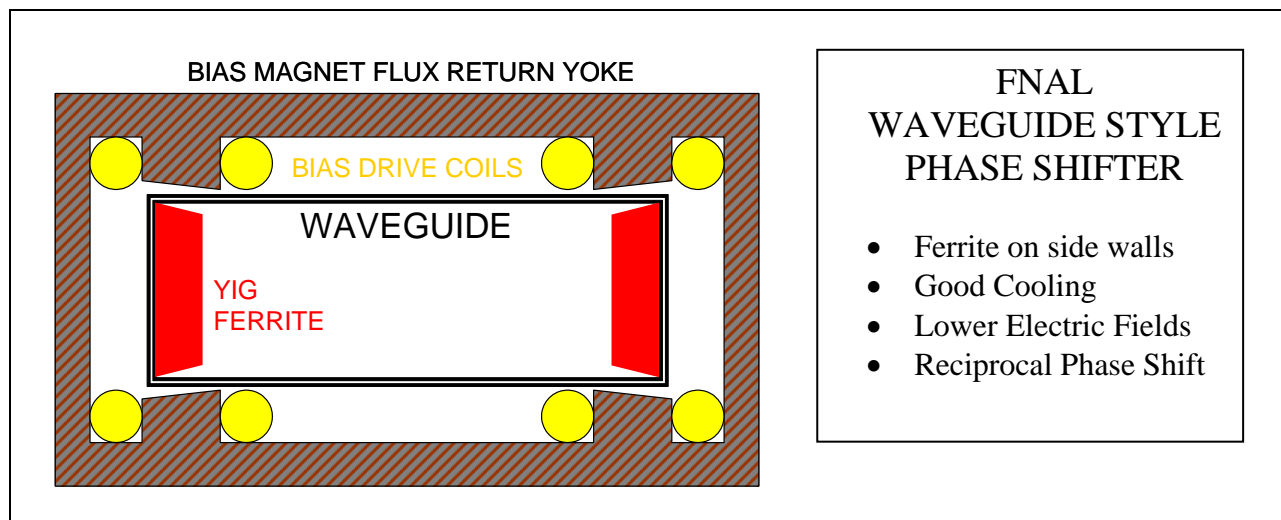


Figure 78 – Comparison of the FNAL and SNS waveguide phase shifter concepts. **Bottom:** design developed by Kang et al.<sup>143</sup> for the SNS. YIG ferrite bricks are placed near the center of the waveguide exhibit an electronically controlled phase shift by varying the current in the windings of the bias magnet. The phase shift is non-reciprocal due to the circular polarization of the RF at the center of the waveguide. This is useful for circulators but is a nuisance in the shorted-stub geometry. The SNS effort progressed through limited prototyping phase but was abandoned due to lack of time available for R&D. **Top:** FNAL design for the waveguide shifter places the YIG bricks along the sidewall, where they can be easily cooled, the electrical fields are lower, and the phase shift is reciprocal (i.e. the same phase shift for RF power flowing in either direction). The YIG blocks in the FNAL design are tapered away from the top wall to reduce the maximum electric field near the ferrite to a value below that which occurs at the center of the reduced-height waveguide.

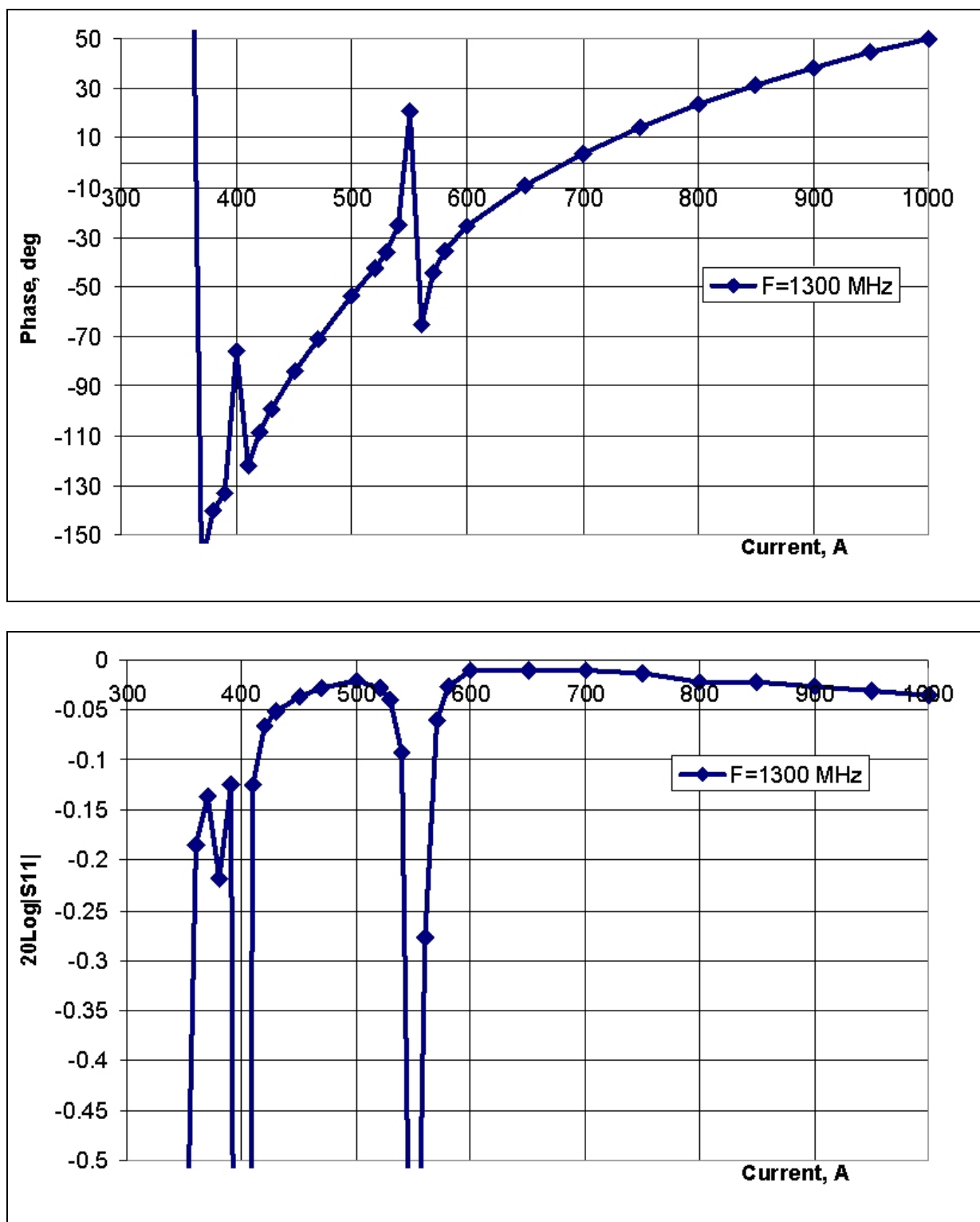


Figure 79 – High power measurements of the phase shift (top) and transmission losses (bottom) of a prototype waveguide phase shifter. The usable phase shift (corresponding to losses < 0.3 dB) is 80 degrees, essentially adequate for the baseline specification. The loss spike at ~570 amps bias current is an HOM resonance. If that resonance can be eliminated as described in the text, the output range will approximately doubled.

### Higher-Order Modes (HOMs) in the Waveguide Phase Shifters

The major challenge that has emerged in the design of the waveguide phase shifter is controlling higher-order modes that create anomalous losses at high RF power, and thereby limit the usable range of phase shift. These were studied both on prototypes and in 3-D simulations, and good understanding and significant design improvements have resulted. The two most significant HOM issues were:

a) The waveguide stub is somewhat sensitive to the vertical placement of the YIG blocks. Early prototypes had vertical centering errors of several mm, which resulted in severe HOM resonances which limited the usable (spark-free) phase shift range. These resonances can be eliminated if the YIG blocks are vertically centered to an accuracy of ~0.5 mm. This should be easily achievable in production.

b) HOM resonances can also be driven by an asymmetry in the bias field of the right and left ferrite blocks. This results in a HOM mode in which the RF power circulates down the length of one YIG block and up the length of the other (i.e. circulates in a loop in the H-plane of the waveguide). This mode can be eliminated by choosing the “anti-parallel” configuration for the magnetic fields, and providing equal magnetic bias to both YIG bricks. At present we equalize the bias with a trim coil on one of the poles. It is hoped that in production, some form of magnetic shim can be used to eliminate this coil. Matching of the two (possibly dissimilar) YIG bricks may also be an issue in production. However even without the trim coil, we were able to obtain phase shift and peak power performance meeting baseline requirements.

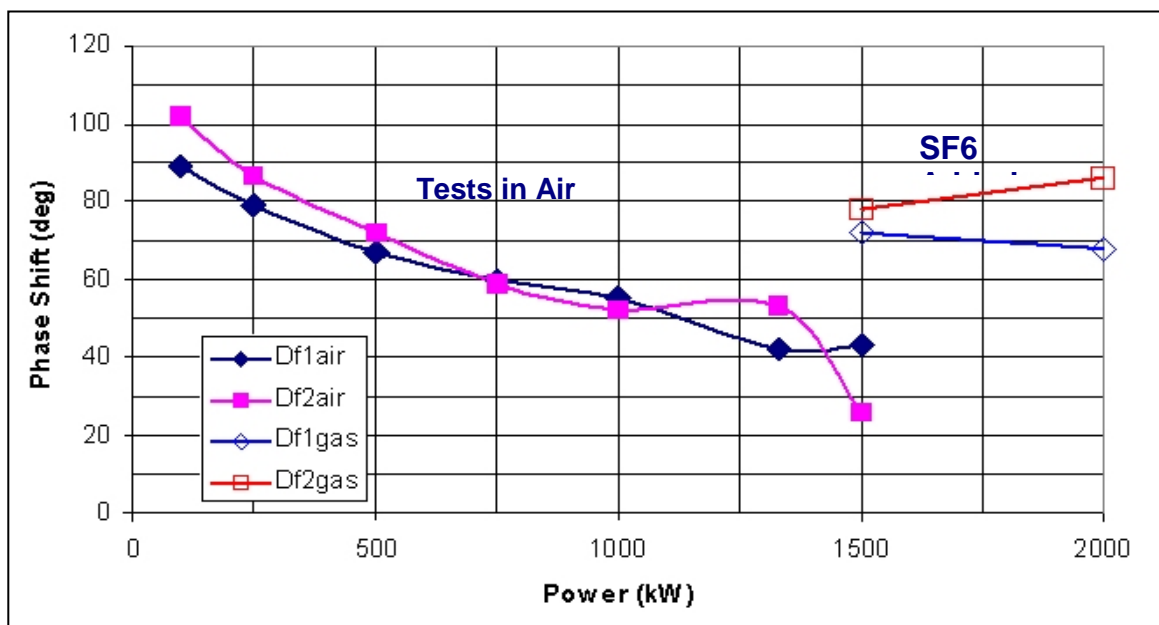


Figure 80 - Measurements of useable phase shift range as a function of incident power for the 1300 MHz waveguide phase shifter. Powers above 1500 kW required sulfur hexafluoride (SF6). The peak power requirement is 220kW for the Baseline design and 660kW for the Ultimate design.

The usable phase shift as a function of incident power is shown in Figure 80. The usable phase shift at the baseline power of 220kW in air was 80° compared to the nominal specification of 90°. The usable range in this test was limited by HOM resonances which caused losses and sparking. The range is more than doubled (at least at low RF power) when the HOMs are eliminated as described in the text. This result will soon be tested at high RF power.

### 14.5 Stripline Phase Shifter Development

In the stripline phase shifter geometry, a high-speed pulsed H-magnet provides a vertical dipole bias field perpendicular to the horizontal RF magnetic fields in a double-sided RF stripline. The main advantages of the stripline geometry are its high magnetic efficiency and the ease of incorporating permanent magnets. The main disadvantage is the need for an impedance match to a very low impedance ( $< 5 \text{ Ohm}$ ) stripline.

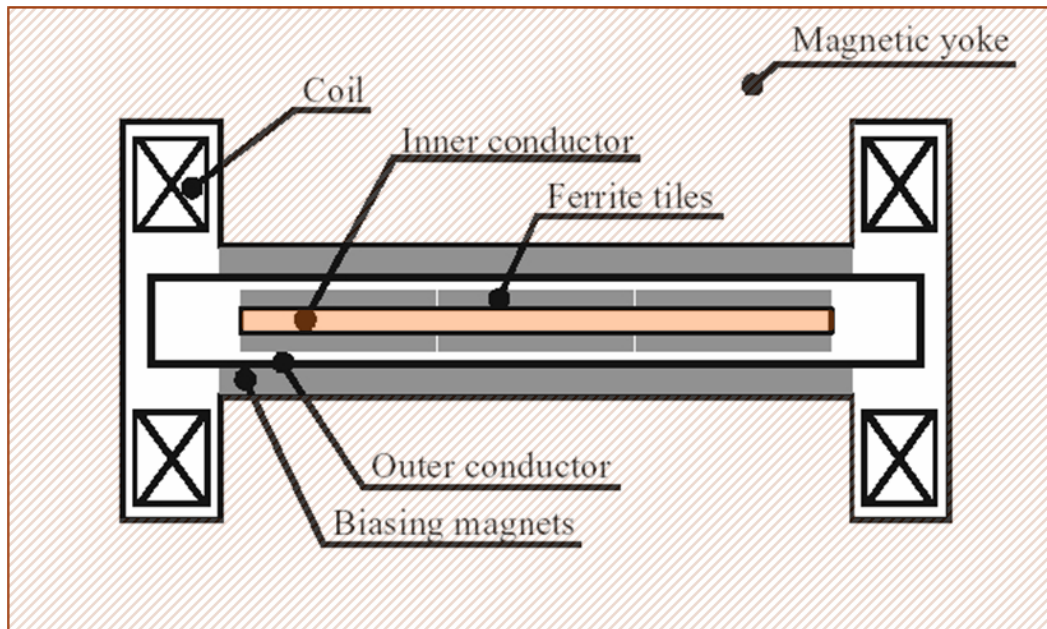


Figure 81 - Stripline style ferrite tuner concept. An H-magnet with pancake coils provides a vertical bias field to low-impedance double-sided RF strip line loaded with YIG ferrite. A layer of permanent magnets is included in the magnetic circuit to provide a DC bias field even with zero current in the windings of the electromagnet.

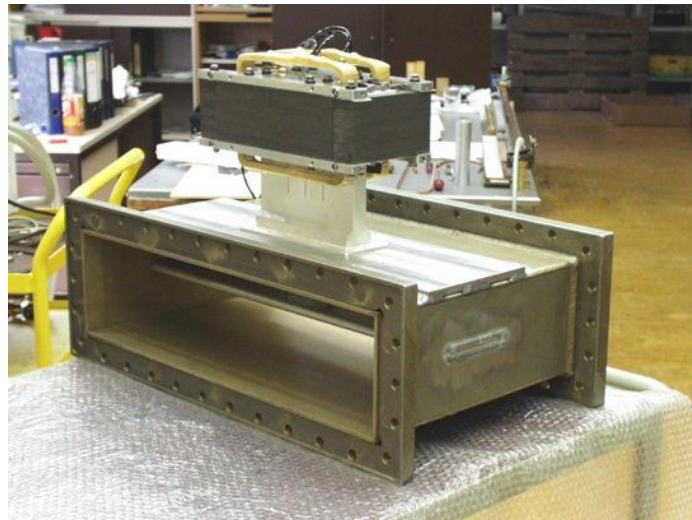
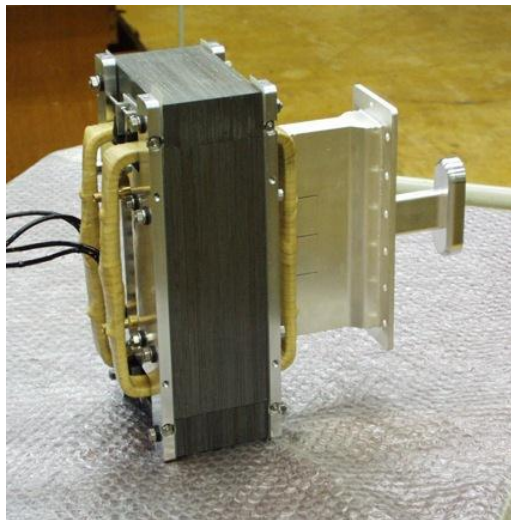


Figure 82 - 352 MHz stripline style ferrite phase shifters built by AFT for the CERN SPL project. A transition from waveguide to a low-impedance shorted stub is required.

### Commercial Procurement of Strip-line Style Ferrite Vector Modulator

The stripline version of the phase shifter has the most recent history of commercial development of 352 MHz versions for at ANL<sup>144</sup> and CERN<sup>140</sup>. We are procuring a complete 1300 MHz FVM from the same company (Advanced Ferrite Technology). The module contains two phase shifters, a 1300 MHz hybrid, and a controller which is directly programmable in phase and amplitude. The present status is that the prototype tuner structure is finished, and testing awaits FNAL's production and delivery of the Bias Coil Drive Amplifiers (section 14.7).

### 14.6 Integrated 325 MHz FVM Module

The front end linac contains more than 100 low-powered 325 MHz FVMs (see Figure 40). If necessary, these could be constructed by purchasing discrete circulators, hybrids, directional couplers, RF loads and ferrite tuners. This approach will probably taken for the small number of high powered (300 kW) FVMs needed to drive the RFQ. However, we anticipate significant system simplification and cost savings by integrating these into a single RF component<sup>145</sup> (Figure 83). The FVM module input will be bolted directly to the distribution waveguide, and the output will drive a Heliax<sup>TM</sup> cable to each cavity load (see Figure 7). Stripline technology is used for the branch line hybrids. The circulator loads are high-power RF resistors. A single water circuit will remove the heat from all components in the module.

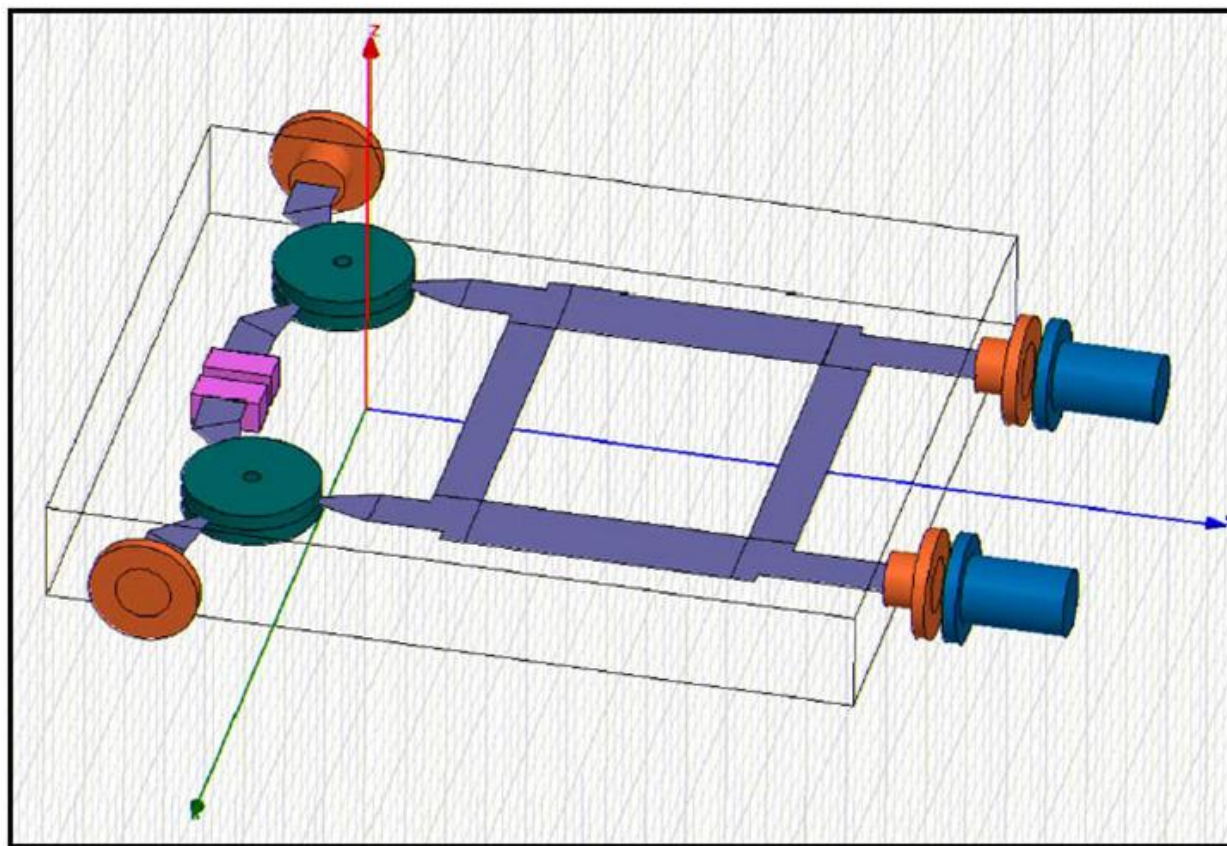


Figure 83 - Integrated FVM Module<sup>145</sup> electromagnetic design and layout. The module contains two circulators, two loads, a branch line hybrid, and connections to two YIG ferrite loaded coaxial phase shifter stubs. Box size: 24" x 20".

A prototype circulator (Figure 84) was built using available ferrite disks is built and measured: achieved low insertion loss (-0.06 dB) and high isolation (-27 dB). The circulator connections are stripline technology that connects directly to stripline hybrid.

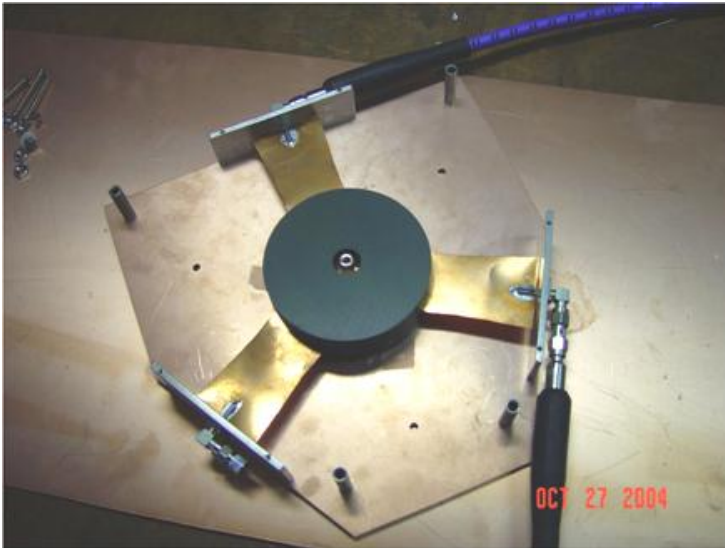


Figure 84 - Prototype 325 MHz circulator for the low-power FVM Module.

A prototype branch-line hybrid was built and performed according to the design equations. The prototype was a circuit-board style hybrid (Figure 85). For the final design we plan to use an air-insulated strip line inside the metal box housing the FVM module (Figure 83) to reach the 50-80kW peak power levels required for most channels of the 325 MHz RF distribution.

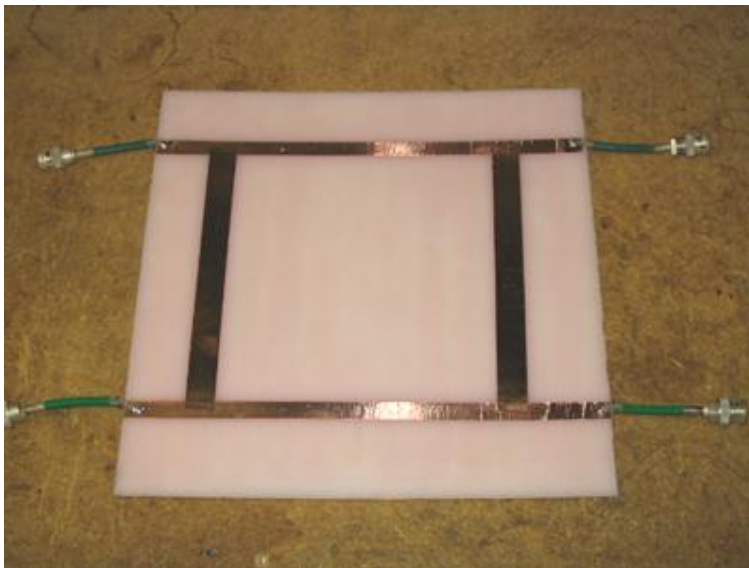


Figure 85 – Prototype branch line hybrid for FVM Module.

The FVM module development plans include having a full-spec integrated FVM module operating at the 50kW level by time the klystron arrives in early 2006. If development is delayed, the linac RF system commissioning can begin using FNAL-built coaxial stubs and commercially produced circulators and hybrids.

## 14.7 Ferrite Bias Drive Amplifier Development

The bias drive amplifiers are a large part of the system cost of the FVM's. The baseline design requires 398 drive amplifiers for the 199 FVMs used on all cavities in the linac up to 1.5 GeV. Our prototypes are high speed (300 KHz) switching amplifiers modeled on the very economical corrector magnet switching supplies and rack assemblies built by the FNAL AD.

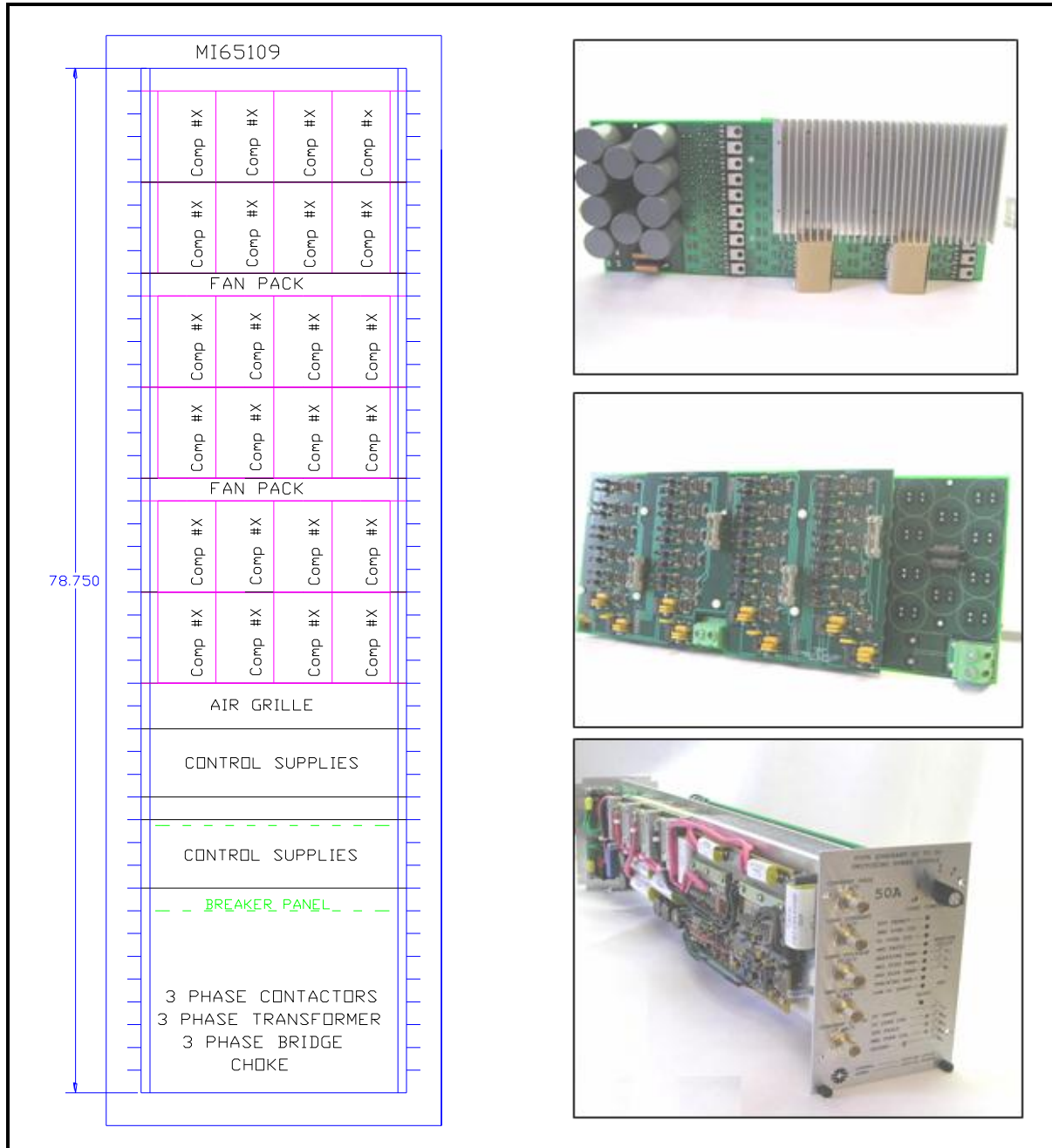


Figure 86 – FVT Drive Amplifier Rack layout (left), prototype switching module circuit card (right top and center) and the switching corrector power supply module on which the design was based (lower right). A bulk supply at the bottom of the rack provides DC power for 24 drive amplifiers for 12 cavities. One such rack is required at each of the first 8 microwave chases in the 1300 MHz linac. The baseline linac design requires 17 total racks.

### **High Speed Switching Drivers for FVT Bias Coils**

The FVM phase shifter bias coils are driven by high speed switching amplifiers. These are IGBT H-bridges driving the coil inductance through a ~100-foot cable. Depending on how the transistors in each quadrant of the H-bridge are programmed, the coil current can be ramped up, ramped down, or recirculated (held constant) on any switching cycle. The prototype drivers (Figure 86) are designed for switching frequencies between 300 kHz and 1 MHz. This switching speed is consistent with the 50-100  $\mu$ sec system response time requirement for the FVTs.

Two control approaches will be tested. The first approach uses a conventional power supply control chip to regulate the coil current to the value specified by an analog command signal from the controller. In the second approach, the H-bridge transistors will be controlled directly and digitally by the FPGA that performs the resonance control for the superconducting cavity. This approach may be more deterministic in that the H-bridge switching is synchronized to the update cycle of the FPGA, so that system latency will be reduced.

### **Switching Amplifiers for FVTs with Permanent Magnets vs. Electromagnet Biasing**

The choice of permanent magnets plus electromagnets, vs. purely electromagnetic coils to bias the YIG ferrite, has implications for the bias coil drive amplifiers.

The working range of the YIG bias is from 40% to 100% of maximum field (see Figure 75). With permanent magnets providing a DC bias field equivalent to 75% of full scale, the bias amplifier has only to drive current equivalent to  $\pm 25\%$  of full scale, rather than 0-100% of full scale with pure electromagnetic bias. However the permanent magnet material increases the reluctance (effective gap length) of the magnetic circuit, so that in reality permanent magnets will require about  $\pm 50\%$  of the full scale current required by pure electromagnets. However since FVMs will be set up so that they spend most of their time near the midrange, savings in RMS current using permanent magnets will be substantial.

The voltage required from the bias amplifier is the same for permanent magnet and pure electromagnet bias. Voltage requirements are determined by slew rate (dB/dt) in the YIG volume, which is the same in both cases.

If pure electromagnets are used, the amplifier only operates with one polarity of output current (two quadrant operation). In this case, two of the four output bridge transistors can be replaced with high-speed switching diodes (SiC or GaAs). The control logic is simplified, and no protection is needed against accidental short-circuiting of the output bridge.

The lower RMS current when using permanent magnets represents a substantial power savings for FVMs operating continuously. However for our pulsed (1.5% duty factor) operation, the power dissipation of the pure electromagnet solution is not a problem and either choice is workable. The decision is coupled to the choice of phase shifter topology, and will be made at the end of the FVM prototype program. Our prototype supplies (Figure 86) provide both the larger current needed for the pure-electromagnet FVMs and the bipolar (4-quadrant) operation needed for permanent-magnet biased FVMs.

## 15 DEBUNCHER

To reduce the momentum spread and jitter of the beam, the Proton Driver includes a Debuncher RF module 640 m downstream of the Linac output. The accelerator physics operation of the Debuncher is described in Section 5.14. The Debuncher is patterned on a similar design<sup>165</sup> for the SNS. It is a “passive” debuncher, that functions by letting the beam drift for a length sufficient for the high momentum particles to move ahead of the slower particles, then putting the beam through a cluster of RF cavities with the phase set to decelerate the early (high energy) particles and to accelerate the late (low energy) particles. This lowers the energy spread and jitter at the expense of increasing the bunch length and phase jitter of the bunches. (The bunch length and phase jitter are irrelevant after MI injection, since the 325 MHz bunch structure is effectively thrown away by the injection process).

Table 22 - Debuncher Parameters

DEBUNCHER	8 GeV Linac	
Status	INCLUDED IN BASELINE DESIGN & COST	
Location (Distance from end of linac)	640 m	
Number of Cavities	16	
Cavity Type	Room-Temperature Copper TESLA cavities	
Frequency	1300 MHz	
Cooling	LCW	Already there for Klystron
Beam Energy (kinetic)	8 GeV	gamma= 9.51
Gamma-T of transport line from linac	38	eta= 0.010363037
Maximum dP/P for correction w/o feedback	0.4%	40 MeV
Phase Err at Debuncher from max dP/P	41 deg	1300 MHz sine is adequately linear
Voltage required for 100% energy correction	61 MV	7.6 MV/cavity
Dispersion at Debuncher cavity	<0.5 m	DPx also small
Feedback	optional	debuncher can run open loop during the pulse
Resonance Control	vector sum of 16 copper cavities	
Energy Spreader Cavity	none	modulate linac LLRF if necessary

### 15.1 Debuncher RF System

The Debuncher RF System is shown in Figure 87. It is located in a downstream enclosure separate from the main Klystron gallery. The system is powered by a standard 1.3 GHz multi-beam Klystron and modulator identical to those in the main linac. The two 5 MW waveguides from each 10 MW Klystron pass through circulators and into microwave chases to the beam tunnel. Inside the tunnel, they undergo a passive 2-stage binary power split using 3dB hybrids to provide power for eight warm-copper “superstructures” with TESLA-like cavity parameters.

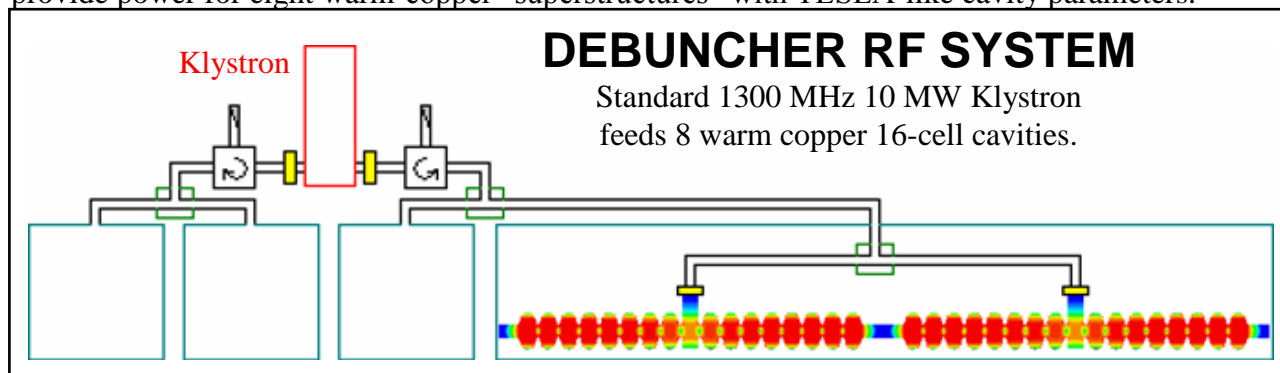


Figure 87 - Debuncher RF System

## 15.2 Warm Copper Debuncher Cavities

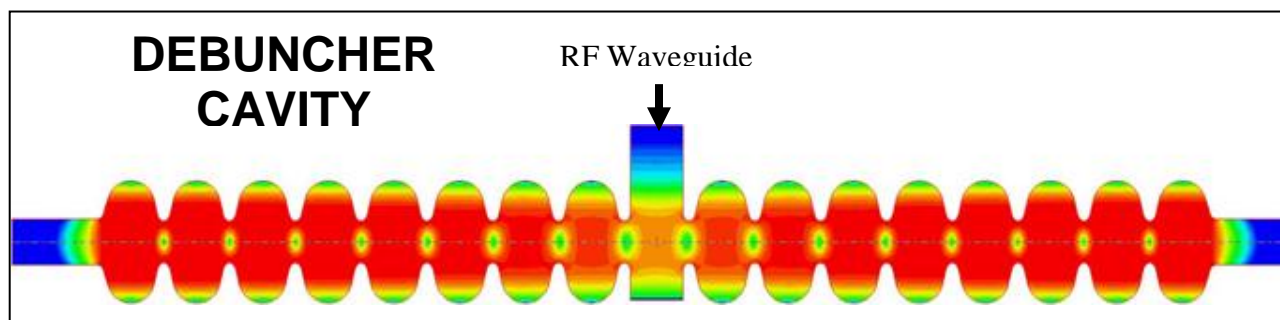


Figure 88 - Debuncher Warm Copper Cavity EM Design. The cavity is a 16-cell "Superstructure" built from warm-copper versions of TESLA cavities. The RF feed is from a waveguide coupler at the center of the cavity. Each superstructure generates 8 MV at 1300 MHz. RF power required is 1 MW peak, 10 kW average per superstructure. The Debuncher requires eight of these two-cavity "superstructures".

Room temperature copper cavities (Figure 88) are chosen, rather than the SCRF debuncher chosen in the previous design study, for the following reasons:

- 1) The cost and heat load of the 640 m Cryogenic Helium Transfer line connecting the Linac to the Debuncher would be large.
- 2) A standard 10 MW RF station provides the 60 MV required, even with copper cavities. The Debuncher RF system is shown in Figure 87. The power savings from a SCRF Debuncher operating from a presumably smaller Klystron would be offset by the maintenance headache of having another type of Klystron in the linac.
- 3) A superconducting debuncher cavity operating at 90-degree synchronous phase means that the beam would be passing the cavity iris at the time of maximum electric field, producing a worst-case situation for H- stripping from cavity fields (see section 5.17). This would produce a "cavity stripping radius" of  $\sim 2$  cm which would be the limiting aperture in the transfer line. For the lower electric fields of a copper debuncher this is not a problem.
- 4) A warm-copper cavity has better phase agility than an SCRF debuncher, which allows the possibility of using of the Debuncher as a beam energy and phase feedback corrector with a response time of a few microseconds<sup>61</sup>.

## 15.3 Debuncher RF Phase Jitter

Jitter and drift between the phase of the Debuncher cavity and the linac output beam phase will be directly reflected in the beam energy at the output of the Debuncher. The 60 MV total RF voltage in the debuncher implies a sensitivity of 1 MeV per degree of phase error. The associated energy fluctuations must be small compared to the  $\pm 13$  MeV window for MI injection, so a reasonable phase tolerance is  $\pm 2$  degrees. Fast measurement of cavity and beam phases with modern electronics is precise<sup>146</sup> to  $\sim 0.1^\circ$  so measurement accuracy is not an issue.

The strategy for holding this tolerance is depends on the time scale of the fluctuation:

- a) Slow drift in the linac output phase and Debuncher phase will be removed by pulse-to-pulse feedback loops implemented in software.
- b) Systematic phase slewing within a pulse due to Lorentz detuning, beam chopping, cavity filling and beam loading systematics will be dealt with via a feed-forward algorithms which gradually tune up the Klystron drive waveforms over a series of pulses.

- c) Random phase slewing of the beam output phase due to microphonics in the main linac, if they are an issue in practice, can be dealt with via measurement of the beam phase at the linac output and passing the signal forward to set the Debuncher cavity phase. This loop, if needed, could be incorporated into the Beam Energy feedback loop (below).
- d) Fast bunch-to-bunch jitter cannot be generated in the SCRF linac due to the high resonant Q of the cavities. However, any phase/energy jitter present in the front-end linac will be passed through to the linac output. Fortunately any incoming phase jitter is attenuated by a factor of  $\sim 4$  by the adiabatic damping (bunch shortening) in the Main Linac (see Figure 26). As can be seen from the figure, bunch shortening in the linac makes the Debuncher very effective at reducing the energy spread from this source to unimportant levels.

#### 15.4 Active Feedback Option for Debuncher

The “passive” debuncher principle (section 5.14) works well for reducing momentum spread from all sources: energy spread within a bunch, bunch-to-bunch momentum jitter, pulse-to-pulse linac energy jitter, and intra-pulse energy variations. The most difficult to quantify are phase and energy errors due to microphonics and dynamic Lorentz detuning. If these are in the expected range, the LLRF system and Ferrite Vector Modulators will reduce these to a level where a “passive” debuncher is sufficient to reduce energy jitter well inside the acceptance window of the Main Injector<sup>62</sup>. Nonetheless, it is useful to identify fallback strategies if these are worse than expected.

Microphonics and dynamic Lorentz detuning are inherently audio-frequency phenomena, with characteristic times of milliseconds to hundreds of microseconds. They produce fluctuations in linac energy which are not high-frequency bunch-to-bunch jitter, but rather slewing of the Linac output energy over hundreds of microseconds. Most of these fluctuations can be tracked and cancelled with the FVM’s and the Klystron drive (section 13.7).

Fast feedback to the Debuncher cavity represents a last line of defense against linac energy fluctuations. Residual energy fluctuations at the linac output can be tracked and cancelled by fast feedback adjustments of the phase of the Debuncher (section 15.4). The warm copper debuncher cavities have filling times of  $\sim 5 \mu\text{sec}$ , so a 10-degree phase jump (corresponding to a 10 MeV energy adjustment) can take place in a few microseconds. Two strategies for calculating this adjustment are:

1. Direct feedback of the beam energy measured in the dispersive arc (see section 5.12). This is the most forgiving and precise feedback system, and should be capable of sub-MeV beam energy regulation. A disadvantage of this system is that no feedback signal exists prior to the start of the beam spill or during the abort gap, so a small portion of the leading edge of the beam pulse may be lost.
2. Digital feed-forward of the calculated energy fluctuation based on digitized cavity resonance signals. This error signal can be generated prior to the start of the beam spill. Modern measurement techniques can digitize cavity phase and amplitudes to of order 0.1% and  $0.1^\circ$ , which is sufficient in principle to predict the linac energy fluctuations at the MeV level prior to the start of the beam spill. Digital calculations of the predicted beam energy fluctuation proceed by summing all cavity voltage fluctuations, weighted by a coefficient that reflects the synchrotron phase advance and bunch length compression from the cavity to the linac output (sect. 13.5).

Ultimately the best solution may be to use the cavity resonance signals for feedback prior to the start of the spill, and then switch to beam-energy feedback once the spill begins.

## 16 CRYOMODULES

The Proton Driver linac uses two classes of cryomodules. The 1300 MHz elliptical cavity cryomodules are patterned on the ILC (TESLA TTF3) design. The 325 MHz front end linac uses spoke resonators and cryomodules similar to the RIA designs.

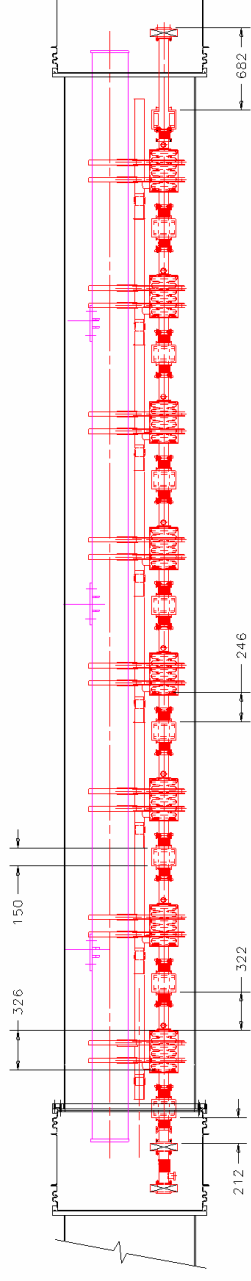
### 16.1 1300 MHz Cryomodules

The baseline design of the Main Linac (Figure 5) uses 36 standard TESLA (TTF3) cryomodules. In addition, the  $\beta = 0.81$  segment of the baseline design uses six more 1300 MHz cryomodules with the same cross section and basic design. The elliptical-cell cavity option for  $0.4 < \beta < 0.7$  (not the baseline) would, if chosen, use an additional six TESLA-style cryomodules of two different types. In all cases, each TESLA-style cryomodule holds 8 cavities. The number of quadrupoles varies from segment to segment. (See Table 23 and Figure 89).

Table 23 – 1300 MHz Cryomodule Parameters for the Proton Driver Linac

Elliptical Cavity Cryomodules		8 GeV Linac (Elliptical Cavity Section)				
Number of Cryomodules	48	(42 if 3-Spoke Option Chosen)				
Cryomodule Style	TESLA (TTF3)	Beta<1 have modified lengths and quads				
Warm-Cold Beam Pipe Transitions	No					
Bayonet Cryo Disconnects & cold box	No					
Quadrupole Type	Cold	runs at 2K				
Cryostat Pipe Diameter (OD)	38 in.	965 mm				
Cryostat Material	Low Carbon Steel	de-Gaussed <i>in situ</i>				
Magnetic field at cryomodules from rebar	< 0.005 Tesla	low-carbon steel cryostat provides shielding				
Magnetic Shield Material around Cavities	cryoperm foil?					
Radiation Hardness	1.0E+08 Rads	TBD				
Cavity alignment tolerance WRT Cryomod	+/-1 mm	TBD				
Cavity tilt tolerance relative to cryomodule	+/-1 mrad	TBD				
Cryomodule transverse alignment tolerance	+/-1 mm	TBD				
Quad Alignment Tolerance WRT Cryomod	+/-0.5 mm	TBD				
Transportation Distance from Factory	2 km	FNAL IB2 to Front-End Bldg.				
ELLIPTICAL CRYOMODULE TYPES		LOW	MEDIUM	HIGH	TESLA (TTF3)	
Cryomodule Geometrical Beta of Cavities	0.47	0.61	0.81	1.00		48
Number Elliptical Cryomodules in Linac	2	4	6	36		
Spare Cryomodules	1	1	2	4		
Length of Cryomodule slot for each Beta	9.396 m	9.615 m	11.682 m	12.175 m		
Number of Cavities Per Cryomodule	8	8	8	8		
Number of Quads Per Cryomodule	9	5	3	1		
Slot Lengths (approx)						
Cavity Slot Length incl. avg. Bellows	0.607 m	0.707 m	1.032 m	1.323 m		
Quad Assy Slot Lengths	0.437 m	0.437 m	0.727 m	0.727 m		
Beam Profile Monitor Slot Length	0.066 m	0.066 m	0.066 m	0.066 m		1/cryomod
Cryostat Interconnect Length*	0.541 m	1.708 m	1.178 m	0.800 m		*tweaked
Cold Mass						
Cold Mass of Quad/BPM Assy	14 kg	14 kg	33 kg	33 kg		see quad sect
Total 2K Cold Mass per Cryomodule	752 kg	769 kg	935 kg	974 kg		rough est.
Total 5K Cold Mass per Cryomodule	47 kg	48 kg	58 kg	61 kg		rough est.
Total 50K Cold Mass per Cryomodule	141 kg	144 kg	175 kg	183 kg		rough est.
Heat Loads (1.5% RF Duty Factor)						Linac Total
2 K static heat load per Cryomodule	4 W	4 W	4 W	4 W		198 W
2 K total heat load per Cryomodule	16 W	16 W	16 W	16 W		789 W
5K Static Heat Load per Cryomod	13 W	13 W	13 W	13 W		637 W
5K Total Heat Load per Cryomod	21 W	21 W	21 W	21 W		1009 W
40K static heat load per Cryomodule	90 W	90 W	90 W	90 W		4410 W
40K total heat load per Cryomodule	234 W	234 W	234 W	234 W		11466 W
RF Coupler Type	TTF	TTF	TTF	TTF		
Coupler LHe consumption / cryomodule	0	0	0	0		cond. cooled

# 8 GeV Linac 1300 MHz Elliptical Cavity Cryomodules



**Beta = 0.47**

**2 Cryomodules  
16 Cavities**

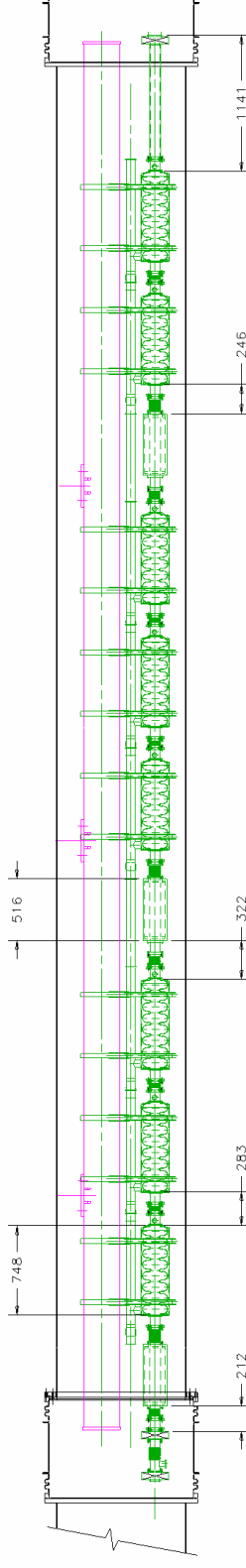
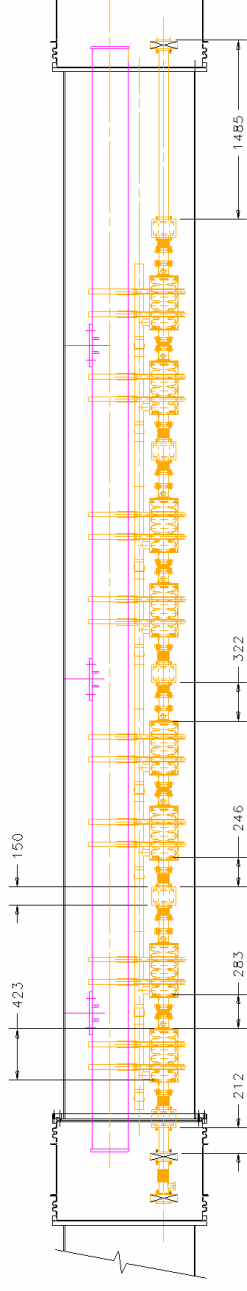
**Elliptical  
Cavity  
Option  
for**

**110 MeV**

**Beta = 0.61**

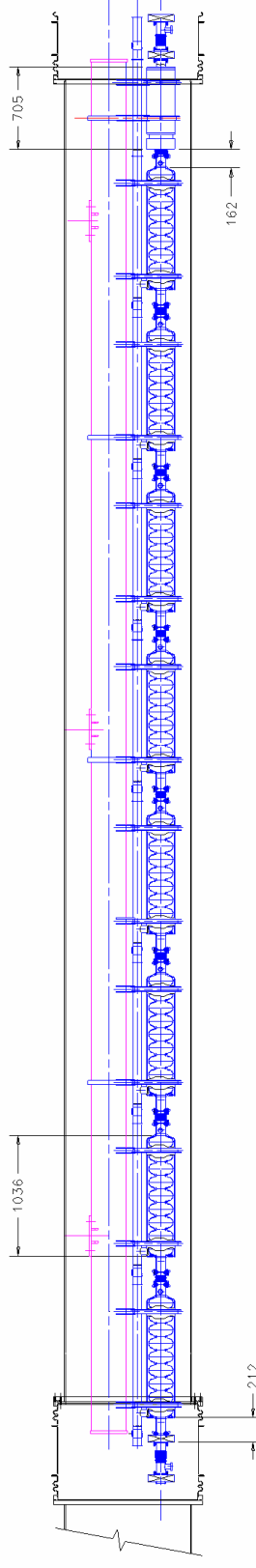
**4 Cryomodules  
32 Cavities**

**to  
400 MeV**



**Beta = 0.81**

**6 Cryomodules  
48 Cavities**



**Beta = 1.00**

**36 Cryomods  
288 Cavities**

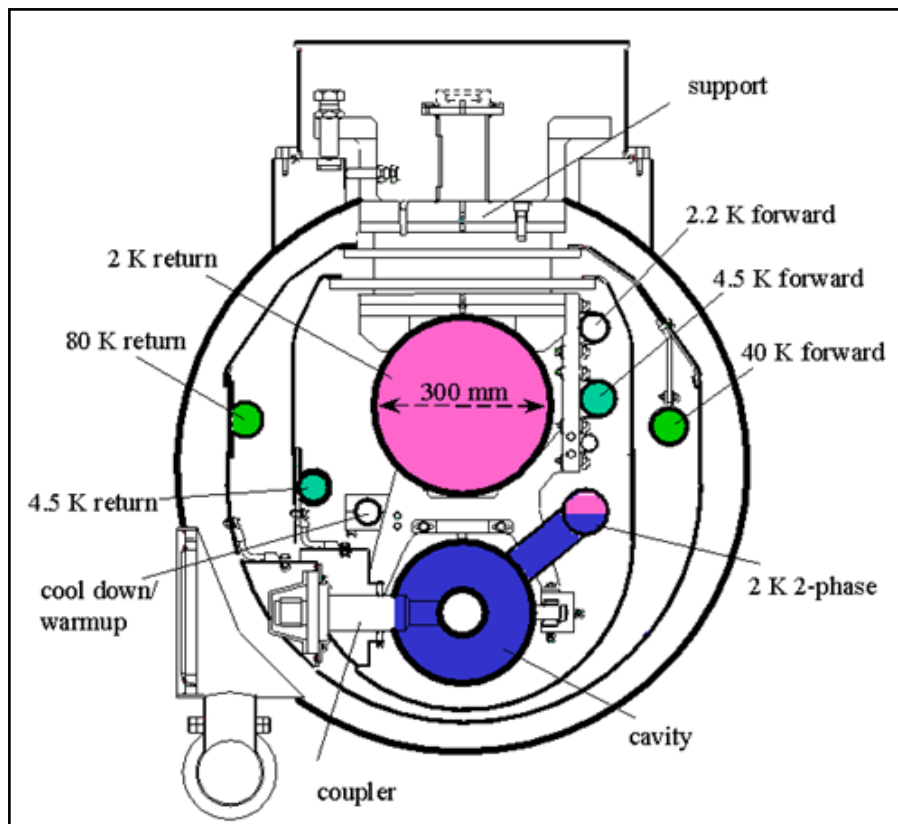


Figure 90 – Section of the TESLA (TTF3) cryomodule used in the baseline design.

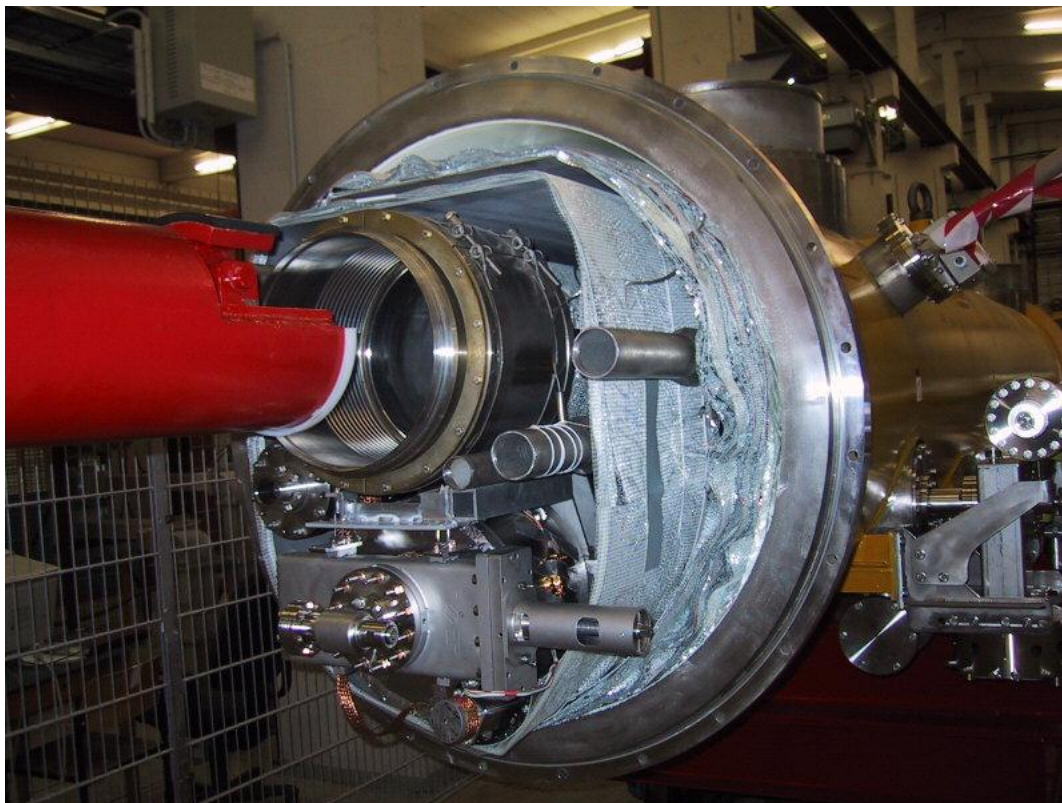


Figure 91 - End view of the TESLA Cryomodule.

## 16.2 325 MHz Cryomodules

The 325 MHz front end linac uses three types of cryomodules for 1, 2, and 3-spoke resonators. The same basic cross section (Figure 92) is used for all three. Nine cryomodules each ~10 m long are required. A focusing magnet (solenoid or quadrupole) is placed between each cavity. Segment details and slot lengths are shown in Table 8 and Figure 23.

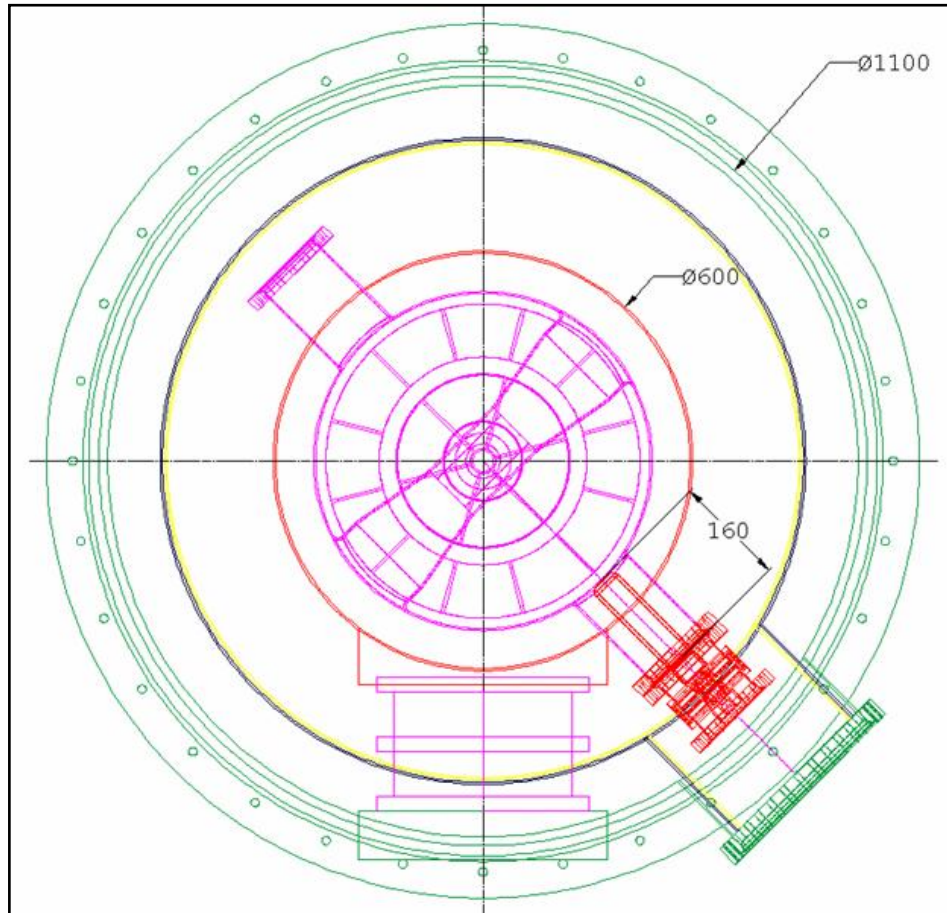


Figure 92 – Cross section of the 325 MHz spoke resonator cryomodule. The coupler enters from 45 degrees below horizontal and the cavity is supported from a post.

The 4.5°K operating temperature and the relatively small number of spoke cryomodules place less of a premium on static heat load reduction than the 2 K cryosystem of the TESLA design. A simpler cryostat design with a single 60-80 K shield is planned.

Like the RIA and SNS cryomodules, the 325 MHz cryomodules have bayonet connections and warm gate valves at each end. This approach has advantages for modular commissioning and servicing of the front end linac.

The power coupler enters from 45° below horizontal to satisfy the constraints that no spoke can be horizontal (to allow bubbles to escape during 2-phase cooling), that the electric coupler must be in a low-loss orientation WRT the nearest spoke, and that the coupler enter from below so that it won't drop dust into the cavity. A two-part TESLA-style coupler with both warm and cold ceramics is planned. This permits clean-room assembly of the cavity string, with final assembly of the coupler, shields, and cryomodule in a semi-clean-room environment.

### 16.3 Cryomodule Design Choices for the Baseline Design

The Proton Driver baseline design uses TESLA-style cryomodules for 1300 MHz elliptical cavities, and modified CEBAF/RIA style cryomodules for 325 MHz spoke resonators. This section discusses the tradeoffs, alternatives, and motivations for the baseline designs.

Three well-developed cryomodule designs are available as a starting point for the Proton Driver Linac design: The TESLA/TTF cryomodule<sup>147</sup>, the CEBAF cryomodule that forms the basis of the SNS design<sup>148</sup>, and the RIA “box”-style cryomodules. The choice between these cryomodules has major implications for the cost, length, and serviceability of the linac.

The Proton Driver linac, like the SNS, can tolerate scattered single-cavity failures<sup>149</sup>. The sensitivity to cavity failures is greatest at the front end of the linac, and decreases in the main linac where multiple cavity failures can be tolerated. Thus the emphasis gradually shifts from rapid and convenient servicing in the front end linac, to economical and efficient design in the  $\beta = 1$  section of the main linac.

**The TESLA (TTF3) Cryomodules** (Figure 93) hold 8 cavities, have internal cold (superconducting) quadrupoles, and no warm-cold transitions at the ends. It is the most economical cryomodule design and results in the shortest linac. There is no external LHe Transfer line to bypass cryogenics around a failed module, so the design requires warming up the entire string when any module develops a serious leak or similar “hard” failure. For the TESLA design, the 2.5 km cryogenic string length results in a 25-day replacement or repair time for a failed cryomodule<sup>150</sup>. For the Proton Driver linac, the shorter string length (~24 cryomodules, ~300 m) results in a ~3 day replacement time<sup>151</sup> for a failed cryomodule in the main linac.

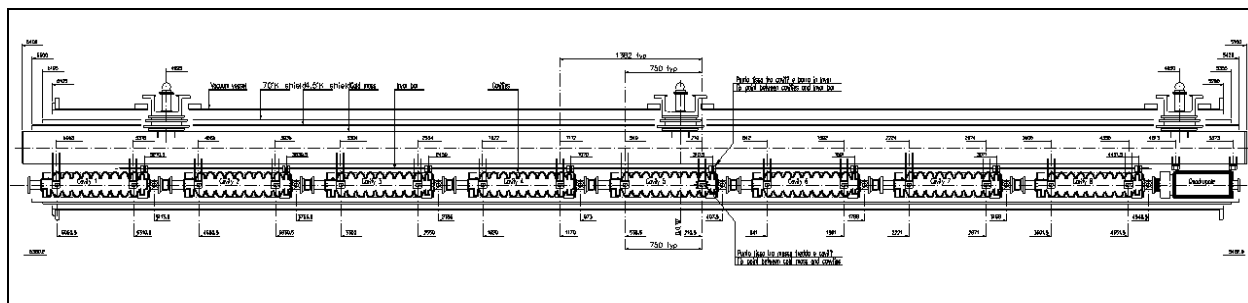


Figure 93 - The TESLA (TTF) cryomodules.

The baseline design for the Proton Driver Main Linac uses the TESLA (TTF3) style cryomodule for both the Main linac, and slightly modified versions for the 1300 MHz  $\beta < 1$  elliptical cell linac segments. The deciding factors are the economy of the TESLA design and the advantages of compatibility with the ILC. The limited number of changes anticipated for the ILC baseline design<sup>31</sup> will not affect the compatibility with the Proton Driver.

**The SNS/CEBAF cryomodules** (Figure 94) hold 3-4 cavities, have warm-cold transitions and gate valves at both ends of the cryomodule, individually removable bayonet connections to an external LHe transfer line. Warm (resistive) quadrupoles are placed in the warm insertions between cryomodules. The SNS cryomodule has an integral cold box with J-T valve and controls to make the 2 K helium locally. The 2 K cold box overlaps the warm insertion for the focusing quadrupoles.

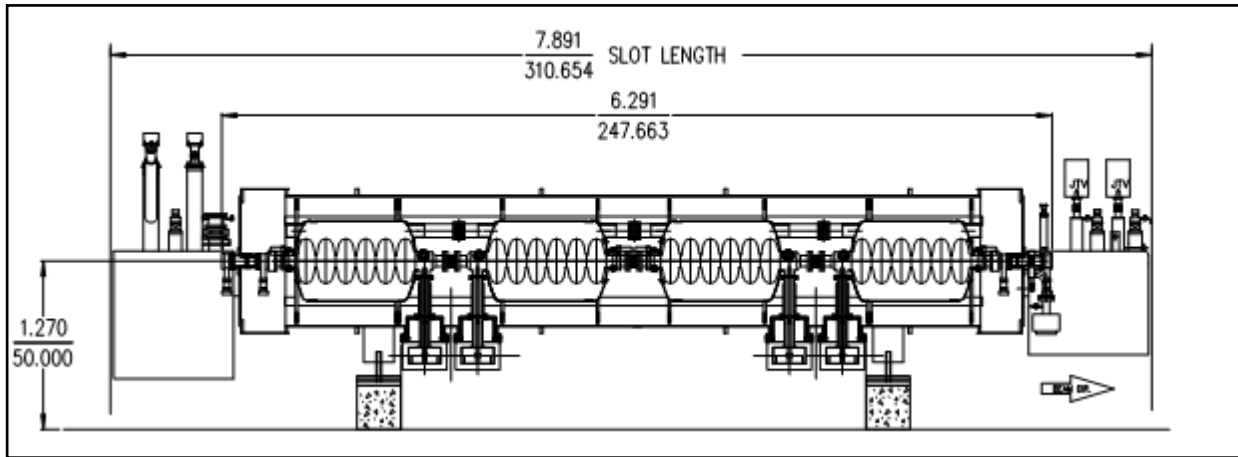


Figure 94 - The CEBAF/SNS Cryomodule.

These features add significantly to the length and cost of the SNS linac. This design has the advantage that each module is cryogenically independent so that a module can be replaced and cooled down in less than a day, without the risks of thermal cycling other components in the linac. It also simplifies testing of individual cryomodules, and minimizes the amount of assembly labor required in the linac tunnel.

*The RIA “box”-style cryomodule*<sup>152</sup> can also be considered. In this design all components are suspended from a top plate which also serves as an alignment strong back. Like the SNS/CEBAF design, there are cold gate valves at the end of each module. Cold (superconducting) focusing magnets are chosen since beam dynamics for both RIA and the front end of the Proton Driver require focusing magnets between each cavity.

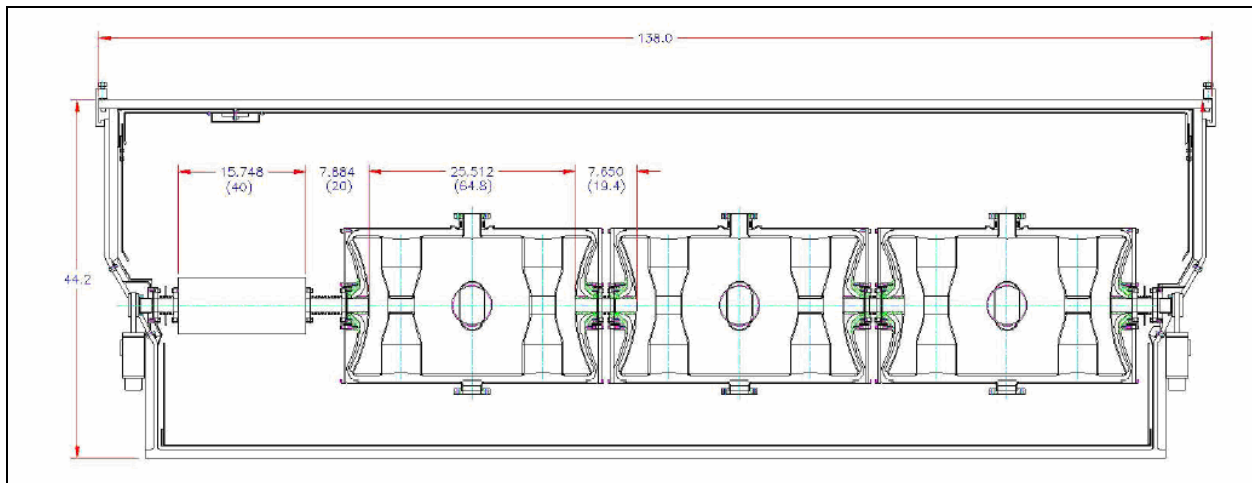


Figure 95 - The RIA “box” style Cryomodule.

The cryomodules for the 325 MHz front end linac (Figure 92) are a hybrid with features of both the RIA and CEBAF/SNS cryomodules. They are self-contained with warm gate valves on each end. Like RIA cryomodules, they have internal superconducting magnets and no 2 K cold box. The cylindrical shape of the CEBAF/SNS cryomodules is chosen. However they are longer and contain more cavities than either SNS or RIA (10 m typical length, see Table 8) to minimize disruption to the regular focusing lattice of the linac.

## 17 SUPERCONDUCTING MAGNETS

Transverse focusing in the Proton Driver is provided by electrostatic lenses below 50 keV, RF focusing in the warm RFQ up to 2.5 MeV, superconducting solenoids up to 110 MeV, and superconducting quadrupoles at higher energies.

The main design issues for the superconducting magnets are maintaining as compact a lattice as possible, and minimizing stray fields which interfere with SCRF cavity operation. The magnets are weaker than is technologically possible to avoid H- stripping in the magnetic fields.

### 17.1 Superconducting Quadrupoles

The Proton Driver Linac uses 126 superconducting quadrupoles of three different types (see Table 24). The  $\beta=1$  main linac quadrupoles are identical to those of the TESLA (TTF3) cryomodules. The  $\beta < 1$  elliptical cell linac uses shortened versions. The quadrupoles for the 325 MHz triple-spoke cryomodules use shorter versions which match the smaller bore of the spoke cavities.

The choice of cold superferroc quadrupoles for the main linac follows the TESLA/TTF3 cryostat design. This approach avoids the warm-to-cold transitions at each quadrupole location, and permits an optimal placement of quadrupoles inside the cryostats (see Sect 16). The aperture radius of 40 mm exceeds the iris aperture of the SCRF cavities (Figure 28). Independent power supplies and HTS current leads are provided for each quadrupole.

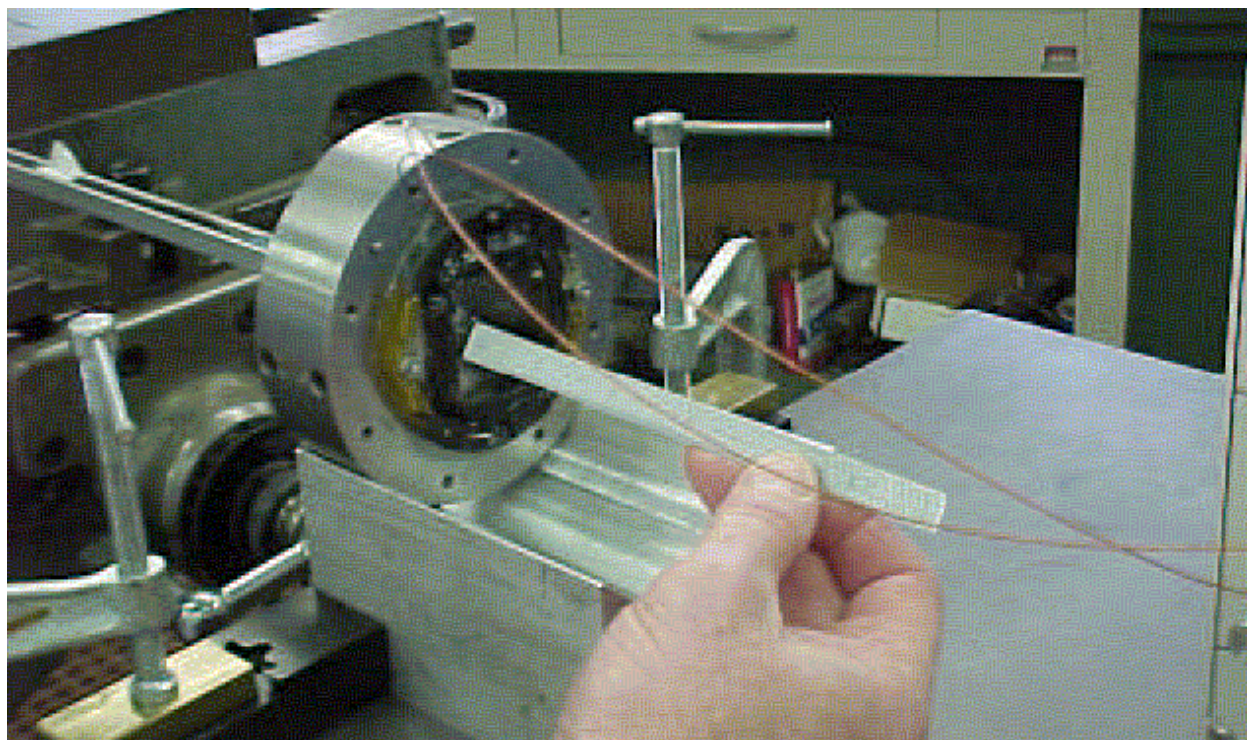


Figure 96 - Superferroc quadrupole developed at Michigan State Univ. for the TRASCO SCRF linac.

Low stray fields are needed for SCRF cavity performance. This has been verified in the case of the TESLA (TTF3) designs. The 325 MHz quads are modeled on the MSU design<sup>153</sup> (Figure 96) for the TRASCO (TRAsmutazione SCOrie) low energy SCRF linac<sup>154</sup>. The design features a stray field of 1  $\mu$ T at a 10 cm distance from the quadrupole.

Table 24 - Superconducting Quadrupole Parameters

SRF LINAC QUADRUPOLES	8 GeV Linac				
Number of Quadrupoles in Cryomodules	92		depends on 3-spoke vs. elliptical medium-beta		
Focusing structure	FODO				
Quadrupole type	Cold Superferric Quads inside cryomodules (MSU/TRASCO & TTF)				
Trim Dipole Windings Inside Quads	both H & V each quad				
Trim Dipole Downstream Orbit Deflection	+/-1 cm		typical, varies along lattice		
Stray Field at Cavites (quads unpowered)	1 uT		during cavity cooldown		
Stray Field at Cavites (quads powered)	10 uT		after cavites are SC		
Cryomodule Type (Beta)	3-Spoke	LOW	MEDIUM	HIGH	TESLA
Number of Quads Per Cryomodule	7	9	5	3	1
Number of Quadrupoles	42	18	20	18	36
Quad + BPM Slot Length	0.423 m	0.423 m	0.423 m	0.864 m	0.864 m
Quad Magnetic Length	0.150 m	0.150 m	0.150 m	0.516 m	0.516 m
Quad Integrated Strength (at max energy)	2.50 T	2.39 T	2.39 T	2.70 T	1.5 T
Quad Gradient at max energy	16.7 T/m	15.9 T/m	15.9 T/m	5.2 T/m	2.9 T/m
Quad Aperture Radius	20 mm	40 mm	40 mm	40 mm	40 mm
Quad Pole Tip Field at max energy	0.33 T	0.64 T	0.64 T	0.21 T	0.12 T
H-minus Stripping Field at max energy	5.62 T	1.35 T	0.58 T	0.27 T	0.06 T
Beam Radius for Stripping (at max energy)	337 mm	85 mm	37 mm	52 mm	21 mm
SRF Quadrupole Design Details					
Amps	10 A	10 A	10 A	10 A	10 A
Amp-Turns per pole	2,653	10,122	10,122	3,326	3,326
Turns/pole	265	1012	1012	333	333
Stored Energy (approx)	8 J	112 J	112 J	41 J	13 J
Inductance (scaled from RHIC corrector)	0.15 H	2.23 H	2.23 H	0.83 H	0.26 H
Charge/discharge time w/ +/-50V supply	DC	DC	DC	DC	0.05 sec
SC Strand Diameter (including Insulation)	0.50 mm	0.50 mm	0.50 mm	0.50 mm	0.50 mm
SC Coil Area (pole winding)	66 mm^2	253 mm^2	253 mm^2	83 mm^2	83 mm^2
SC Coil Azimuthal Thickness	8 mm	16 mm	16 mm	9 mm	9 mm
SC Coil Radial Thickness	8 mm	16 mm	16 mm	9 mm	9 mm
SC Coil Inner Radius	25 mm	45 mm	45 mm	45 mm	45 mm
Lamination Return Leg Thickness	10 mm	13 mm	13 mm	10 mm	10 mm
Lamination Outer Radius	43 mm	74 mm	74 mm	64 mm	64 mm
Approximate Weight	6 kg	14 kg	14 kg	33 kg	33 kg
SRF Quadrupole Current Leads					
Number of Leads per quad	4	4	4	4	4
Number of Leads per Cryomodule	28	36	20	12	4
Number of Leads per Cryomodule Type	168	72	80	72	144
2K Heat Load per cryomodule from Leads	0.08W(4K)	0.10 W	0.06 W	0.03 W	0.01 W
50K Heat Load per cryomodule from Leads	10.11 W	13.00 W	7.22 W	4.33 W	1.44 W
Current Lead Type	HTS (BSCCO) conductively cooled with 50K Intercept				
Heat Leak per Lead to 2K	0.003 W / Lead		Scaled per Amp from TESLA TDR		
Heat Leak per Lead to 50K	0.361 W / Lead		Scaled per Amp from TESLA TDR		

The H<sup>-</sup> stripping field at 8 GeV is ~600 Gauss (sect. 5.17). Therefore the quadrupoles of the  $\beta = 1.00$  section must be long and weak at the high-energy end of the linac to avoid stripping the H<sup>-</sup> ions in the quadrupole magnetic field. With the exception of the very end of the linac, H<sup>-</sup> ions will hit the cavity iris before being stripped in the magnetic field. See Figure 28.

Steering corrector capability is provided by two additional sets of windings on each quadrupole. Each dipole winding has 20% of the amp-turns of the primary quadrupole winding. These windings can move the effective quadrupole center by  $\pm 4$  mm. This is sufficient to produce a downstream beam motion of 3~5 mm, depending on the phase advance in the lattice. This is adequate for beam studies. A single corrector will typically be incapable of knocking the beam into the superconducting cavities.

Quadrupole requirements for the (*non-baseline*) application of running electrons and protons on alternate machine cycles have been investigated. Sharing the focusing quadrupoles of the  $\beta = 1.00$  section between electrons and protons is most straightforward if the quadrupoles are ramped to different currents in the 0.1 seconds between linac pulses. The ramping range may approach 0-100% of the quadrupole strength if low energy ( $\sim 200$  MeV) electrons are injected into the start of the  $\beta = 1.00$  section. Fortunately these weak magnets have low stored energy (13 J) and inductance (0.26 H) so that they can ramp between zero and full current with a modest  $\pm 25\text{V} / 10\text{A}$  power supply (sect 21).

AC losses may be important when ramping the  $\beta = 1.00$  quadrupoles since the magnets run at 2 K. The rate of change of the magnetic field at the pole tip is  $\text{dB}/\text{dt} = 0.8 \text{ T/sec}$ . Both hysteretic losses in the iron and in the superconducting strand may be significant. If losses become important the magnets may be conductively cooled with a copper strap to the 6-8 K cryogen line.

## 17.2 Superconducting Solenoids

A total of 53 superconducting solenoids of two different types are used for beam focusing<sup>155</sup> in the front end linac below 110 MeV. Accelerator physics issues are discussed in section 5.7 and solenoid parameters are given in Table 25.

A **warm bore 5.5 T solenoid**<sup>156</sup> (Figure 97) is used in the Medium-Energy Beam Transport (MEBT) and Room-Temperature Triple-Spoke Resonator (RT-TSR) sections. This is a 4.5 K pool-boiling design with cryogenics fed from an overhead distribution line (Figure 36). Documentation includes an analysis of mechanical stress<sup>157</sup> and prototype design review materials<sup>158</sup>. An active prototype program is in progress.

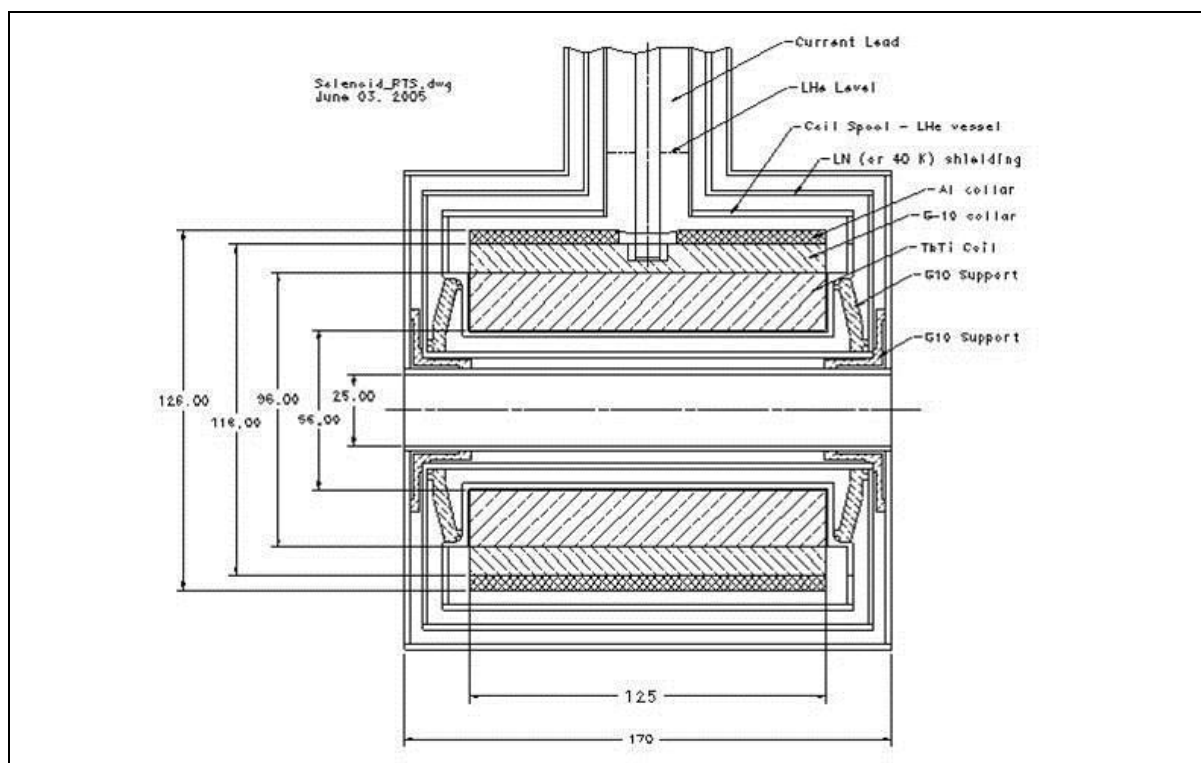


Figure 97 – Warm Bore 5.5T solenoid used in the MEBT and RT-TSR sections of the front end linac.

Table 25 - Superconducting Solenoid Parameters for the Proton Driver linac

SC SOLENOIDS IN LINAC	8 GeV Linac			
Number of Solenoids	53			
Number of Solenoid Types	3			
Focusing structure	FOFO			
Solenoid type	Superconducting			
Operating Temperature	4.5K			
SteeringTrims Inside Solenoids	H & V each magnet (TBD)			
	MEBT	RT TSR	1-Spoke	2-Spoke
Solenoid Bore Type	WARM BORE		COLD BORE (inside cryomod)	
Number of Solenoids Per Module	1	1	16	7
Number of Solenoids per Section of Linac	2	21	16	14
Solenoid Slot Length	0.180 m	0.180 m	0.180 m	0.320 m
Solenoid Magnetic Length	0.180 m	0.180 m	0.180 m	0.180 m
Solenoid Peak Field	5.0 T	5.5 T	6.0 T	5.4 T
Stray Field at Cavities (during cooldown)	no spec	no spec	< 10 uT	< 10 uT
Stray Field at Cavities (after cooldown)	< 1 T	< 1 T	< 10 mT	< 10 mT
Solenoid Clear Bore (radius)	15mm	15mm	15mm	15mm

**Cold Bore 6 T Solenoids**<sup>158</sup> (Figure 98) are used in the Single-Spoke Resonator (SSR) and Double-Spoke Resonator (DSR) cryomodules. Two variants with different lengths and strengths are used. The solenoids operate in close proximity to the superconducting cavities, so both the fringe fields in operation and the remnant fields during cool down are of concern. The fringe fields are reduced by anti-solenoid windings and end coils that are powered in series with the main solenoidal winding. Recent encouraging results<sup>159</sup> for a similar 9 T solenoid operated close to a superconducting spoke resonator indicate that this is a tractable problem, although the situation is not fully resolved and the issue of remnant fields will require continuing attention.

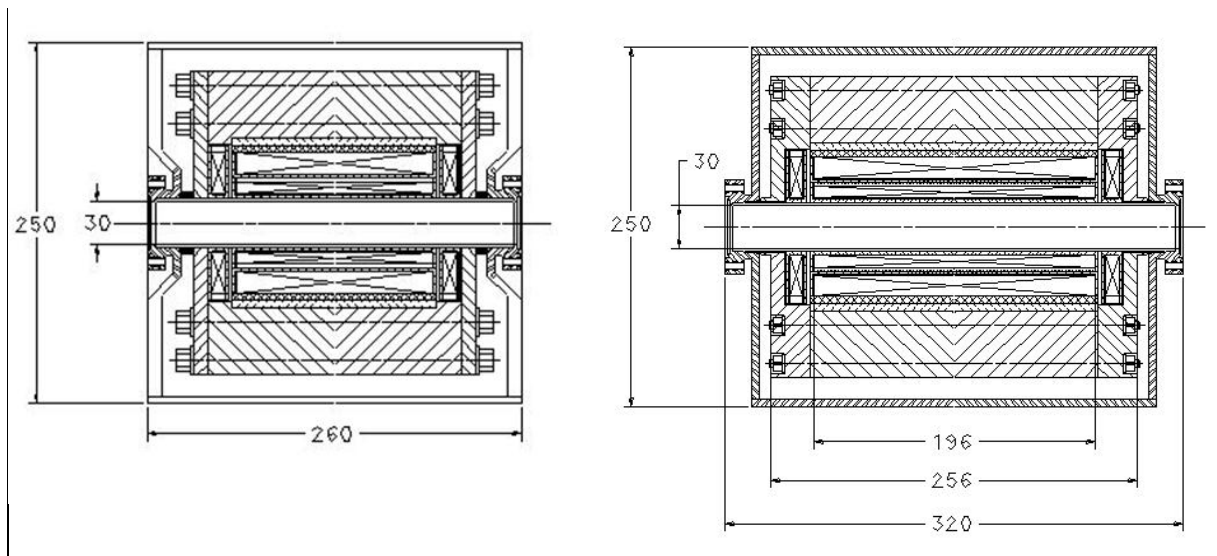


Figure 98 – Cold Bore 5.4 and 6 T solenoids used inside the cryomodules of the SSR and DSR linac.

## 18 CRYOGENIC SYSTEM

The Proton Driver linac has both a 4.5 K cryogenic system<sup>160</sup> for the 325 MHz front end linac and a 2 K cryogenic system for the 1300 MHz main linac. The 4.5 K system serves both the spoke resonator front end linac and its superconducting solenoids. The 2 K cryogenic system serves both the  $\beta = 1$  “TESLA” linac and the  $\beta < 1$  “Squeezed TESLA” sections.

The 2 K cryogenics system design is largely determined by the choice of the TESLA/TTF style cryomodules. The cavities are cooled by 2°K helium produced at the cryoplant. Shield flows at 6-8 K and 50-60 K GHe are distributed inside the string of cryomodules. This represents a simpler, but less modular cryogenic system than the CEBAF/SNS design in which the 2 K Helium is produced locally in each cryomodule.

The 4.5 K cryogenic system supplies LHe for 2-phase cooling for the spoke resonator cavities and solenoids. The 4.5 K distribution system is a conventional transfer-line-and-bayonet distribution system to the 9 independent cryomodules of the front end linac.

Shield flows for the 4.5 K front end linac cryomodules are designed to be operable with either 40-60K GHe, or LN2 for commissioning and Meson area prototype tests. The feasibility of early commissioning using LN2 in the shields of the TESLA-style cryomodules is under investigation. This may prove attractive for the project schedule if the Fermilab CHL can be used for early (albeit cryogenically inefficient) commissioning of the Proton Driver.

The overall size and cost of the cryogenic system (2.05 MW of installed compressor power to service a nominal load of 5.2 kW of 4.5 K equivalent refrigeration) is comparable to the SNS. This is reasonable since although the Proton Driver linac has an 8x higher beam energy than the 1 GeV SNS, it also has a 6x smaller RF duty factor (1.5% instead of 9%). The more efficient TESLA-style cryomodules also reduces the static heat load of the Proton Driver linac.

### 18.1 Cryogenic System Layout

In the baseline design the cryogenic plant is located halfway along the 2 K, 1300 MHz SCRF linac. This results in two 250 m long strings of TESLA-style cryomodules, plus one 110 m long string of nine 4.5 K cryomodules with an independent transfer line and bayonet connections to each cryomodule.

The flow schematic for the 2 K linac (Figure 99 and Figure 100) is similar to the TESLA cryogenic system<sup>161</sup>. Two strings of 21 TTF3 cryomodules (168 cavities each) extend upstream and downstream from the cryoplant. Each string can be warmed or cooled independently of the other.

As in the TESLA design, there is no separate cryogenic service pipe outside the 2 K cryomodules. This means that there is no mechanism for bypassing cryogens around a failed cryomodule, and the entire string must be warmed up or cooled down as a unit. All cryomodules on a string must be thermally cycled to fix a cryogenic fault on any cryomodule. This greatly increases the number of lifetime thermal cycles. The reduction in thermal cycling from halving the string length is a major motivation for bisecting the 2 K linac.

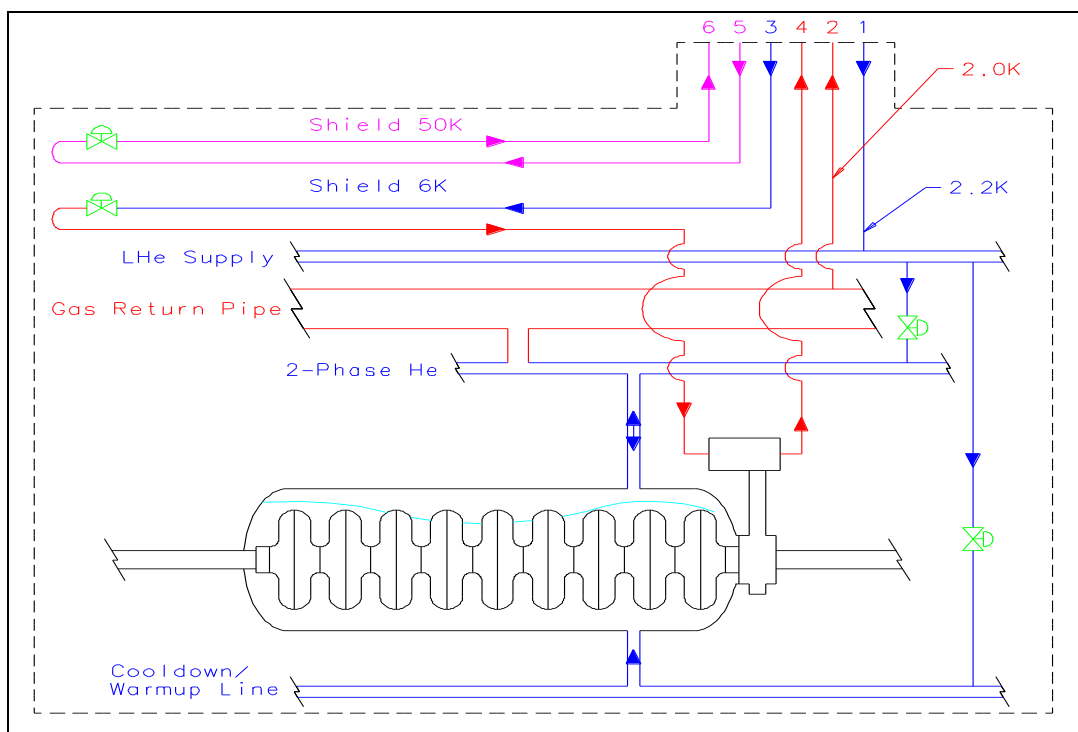


Figure 99 - Simplified flow diagram for one of two 2 K cryogenic strings in the Proton Driver linac. The two strings each contain 21 cryomodules (168 cavities).

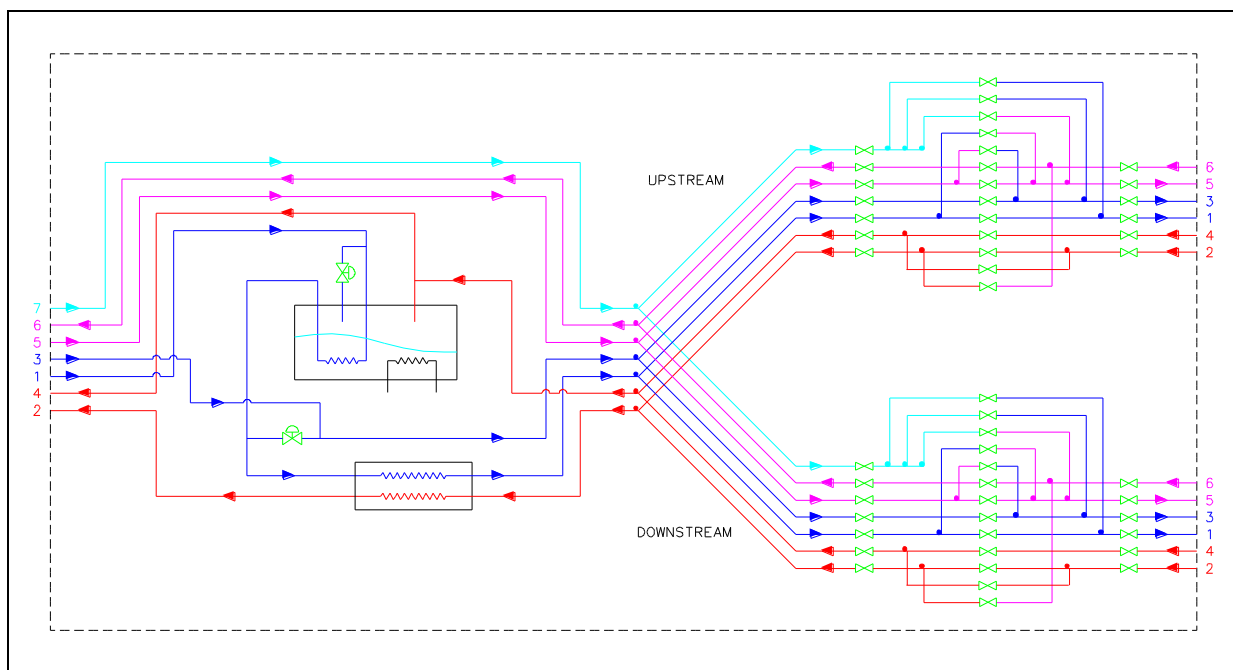


Figure 100 - Transfer Line and Distribution Boxes connections for upstream and downstream 2 K cryomodule strings. The cryogenic plant is located at the center of the 1300 MHz Linac, and the upstream and downstream 2 K strings can be warmed up or cooled down independently. A third independent 4.5 K circuit (not shown) services the front-end linac.

## 18.2 Cool Down and Module Replacement Time

A critical factor in the choice of cryomodules is the time needed to repair or replace a failed cryomodule. In the SNS linac, single-cavity failures can typically be worked around by retuning the linac<sup>149</sup>. It is expected that this will be the case for the Proton Driver linac as well. However serious failures such as cold leaks that bring down multiple cavities will require immediate repair. As in the TESLA cryomodules, flanged joints occur only between the beam vacuum and insulating vacuum. The helium space inside the cryomodules is an all-welded system. This will contribute to cryogenic reliability.

A preliminary analysis of the time taken to replace a failed cryomodule in the Proton Driver linac was performed<sup>151</sup>. One string of 21 cryomodules was to be warmed up for cryomodule repair/replacement with the other string left cold. The conclusion was that a 3-day minimum replacement time for a failed cryomodule was possible. This time was close to the initial design goal of 2 days, which remains the design target. Further brainstorming and a detailed availability analysis is indicated. In any case this represents a big improvement over the 25-day repair time<sup>150</sup> for the TESLA TDR design.

## 18.3 Cryogenic Heat Loads

The static and dynamic heat loads for the Proton Driver linac were compiled<sup>162</sup>. They are dominated by the heat loads of the 42+9 individual cryomodules. Static and dynamic 2 K heat loads are about equal at 10 Hz operation. The basis of estimate for most of the heat loads (Table 26) were the measured heat loads from TESLA Test Facility (TTF).

Table 26 – Cryomodule Static and Dynamic Heat Loads (W)

Proton Driver Baseline	Qty [ # ]	Heat Load			
Item		2K	4K	5K	40K
Solenoid WRF (NbTi)	25	-	250	-	-
Single Spoke Resonator CM	1	-	81	-	-
Solenoid 1spoke	16	-	32	-	-
Double Spoke Resonator CM	2	-	142	-	-
Triple Spoke Resonator CM	6	-	217	-	-
Solenoid 2 spoke	14	-	28	-	-
Beta=0.81 Cryomodules	6	96	-	124	1409
Beta=1 (ILC) Cryomodules	36	579	-	742	8453
Total Estimated, [W]		675	751	865	9,862
Uncertainty Factor		1.3	1.3	1.3	1.3
Capacity Required, [W]		878	976	1,125	12,820

## 18.4 Cryogenic Plant

A preliminary design analysis and cost estimate for the Proton Driver linac cryogenic plant was performed<sup>163</sup>. The refrigeration system is summarized in Table 27 below. The design includes both an overcapacity factor of 1.5 and a heat load uncertainty factor of 1.3, and includes allowances for heat losses in distribution boxes, transfer lines, etc. Although the cryogenic process differs from the SNS cryoplant, the overall scope of the refrigeration plant is similar.

Table 27 – Cryogenic Refrigeration Plant Summary

CRYOGENIC SYSTEM		8 GeV Linac			
Nominal Refrigeration Power	5.21 kW of 4.5K	Equiv. Refrigeration			
Nominal Compressor Wall Power	1.37 MW	at 10 Hz operation			
Installed Compressor Power	2.06 MW	includes overcapacity for cool down, etc.			
Electrical Service Required @Cryoplant	3 MW				
Number of Indep. Cryogenic Segments	1+2	one 4.5K upstream & two 2K Downstream			
Cryomodule Replacement Time	48 hrs	Target, TBD			
Warm-up or Cool Down time	18 hrs	Prelim. Est.			
Distance between Vacuum Breaks	50 m	TBD			
<b>Inventory Control</b>					
Helium Inventory	1800 kg He	100%	rough est.		
Liquid Storage	2500 kg He	139%	one 20,000 gal LHe dewar		
Gas Storage	2000 kg He	111%	eight 30,000 gal gas tanks		
Warm Gas Return Header for Cooldown	600 m	6" IPS SS pipe in tunnel			
<b>Cryogenic Transfer Lines</b>					
Cryoplant to Linac	60 m	TBD	Across the street		
Cryoplant to 4.5K Front End	250 m	Assuming F.E. Runs at 4.5K			
Cryomodule Test Stand	20 m	TBD	Assume Test Stands near cryo building		
<b>CRYO LOADS (SPOKE BASELINE)</b>	<b>2K</b>	<b>4K</b>	<b>6K</b>	<b>50K</b>	
Predicted Static Heat Load [W]	182	1,154	616	5,429	
Predicted Operating Heat Load [W]	687	1,271	935	11,506	
Static to Total Ratio	26%	91%	66%	47%	
Heat Uncertainty Factor	1.3	1.3	1.3	1.3	
Nominal Operating Load [W]	893	1,652	1,216	14,958	
Overcapacity Factor	1.5	1.5	1.5	1.5	
Installed Capacity [W]	1,340	2,478	1,823	22,437	
4.5K Equivalent Heat Load [W @4.5K]	1,982	1,496	771	960	5,209 W @4.5K
COP, [W/W]	588	240	168	17	
Nominal Operating Power [kW]	599	256	231	285	1371 kW total
Installed Operating Power [kW]	899	384	347	428	2057 kW total

## 18.5 Possible use of Fermilab's Central Helium Liquefier for Linac Commissioning

The capacity of Fermilab's Central Helium Liquefier (CHL) is more than adequate for initial commissioning of the 4.5 K front end of the Proton Driver linac, and perhaps commissioning of the entire linac. The ring cryogenic transfer lines near D-zero are within a few hundred meters of the Proton Driver front end (Figure 13). It is also conceivable that a large fraction of the 1300 MHz main linac might be commissioned, at least at 4.5 K, using the capacity of the CHL and satellites. The cryogenic efficiency of the system will be poor and it will pay to eventually procure a purpose-built cryogenic plant.

Early commissioning using CHL is very attractive from a project schedule point of view due to the long lead times for cryogenic plant procurement. Not only is the cryogenic plant a possible critical-path item for project completion, it competes for first-year funding obligations which delays other parts of the project. A project plan which allows completion of the purpose-built cryogenic plant after linac commissioning will be more flexible and easier to manage.

## 19 BEAM TRANSPORT AND COLLIMATION LINE

The 970 m transfer line<sup>164</sup> from the Proton Driver linac to the Main Injector (Figure 101) is patterned after the SNS beam transport line<sup>165</sup>. The function of the line is to transport the H-beam from the end of the superconducting linac to the Main Injector injection point, providing emittance and momentum collimation in the process. The length of the line is set by the drift necessary to for the debuncher cavity, and by the desire to locate the main linac in a flexible and environmentally benign area inside the main ring. Linac siting is discussed further in 3.6.

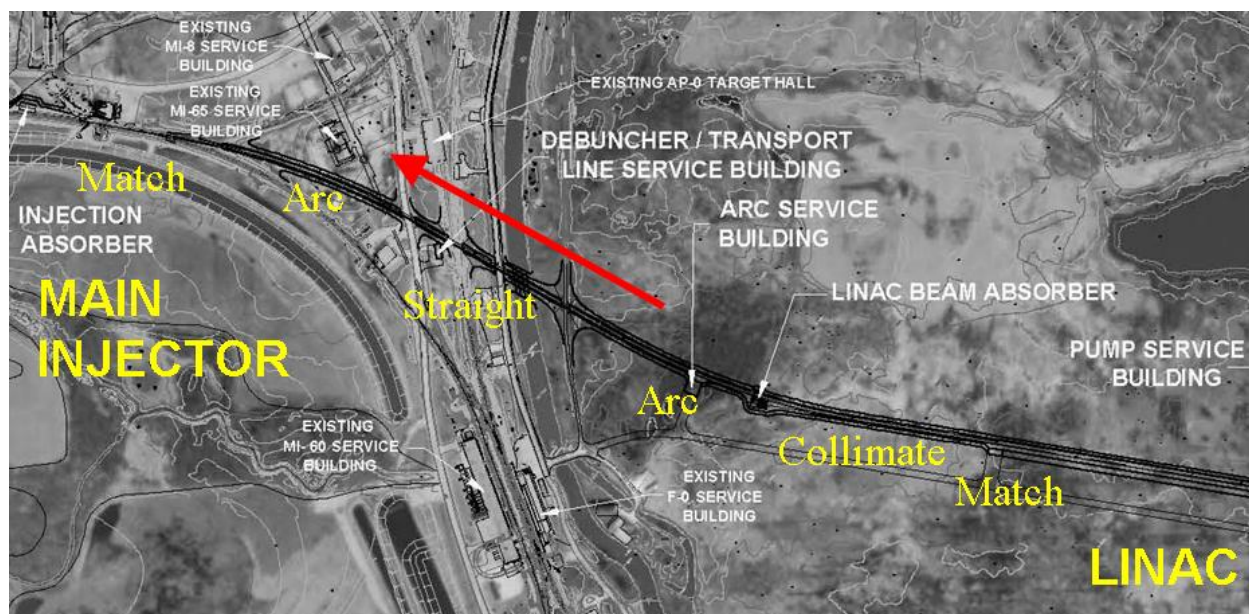


Figure 101 – Beam Transport Line form the Proton Driver Linac to the Fermilab Main Injector.

The linac civil construction includes one additional TESLA RF station to provide an energy upgrade (or performance contingency) of ~1 GeV of beam energy. Immediately downstream of the linac, two stages of betatron collimation clean the transverse halo from the beam. The main linac beam stop is located straight ahead along the linac beam line.

A pair of opposite sign bends develops the ~7 m dispersion used for momentum collimation. Each 17° bend is smaller than the 45° bends of the SNS transfer line due to the higher energy beam optics. The debuncher cavity is located at the downstream end of the straight section between bends. A 20 mrad injection bend occurs immediately before the foil stripping injection into the Main Injector at the MI-10 straight section.

### 19.1 Transport Line Optics and Cell Layout

The optical design of the transport line (Figure 102) is a regular FODO lattice with 60° phase advance per cell and a half-cell length of 21.5 m. The layout of the transport line FODO cell is shown in Figure 103. The half-cell length accommodates three B2 dipole magnets in each bending half-cell cell, plus correctors, BPMs and vacuum pumps. The straight section cells are identical except they are missing the three dipole magnets.

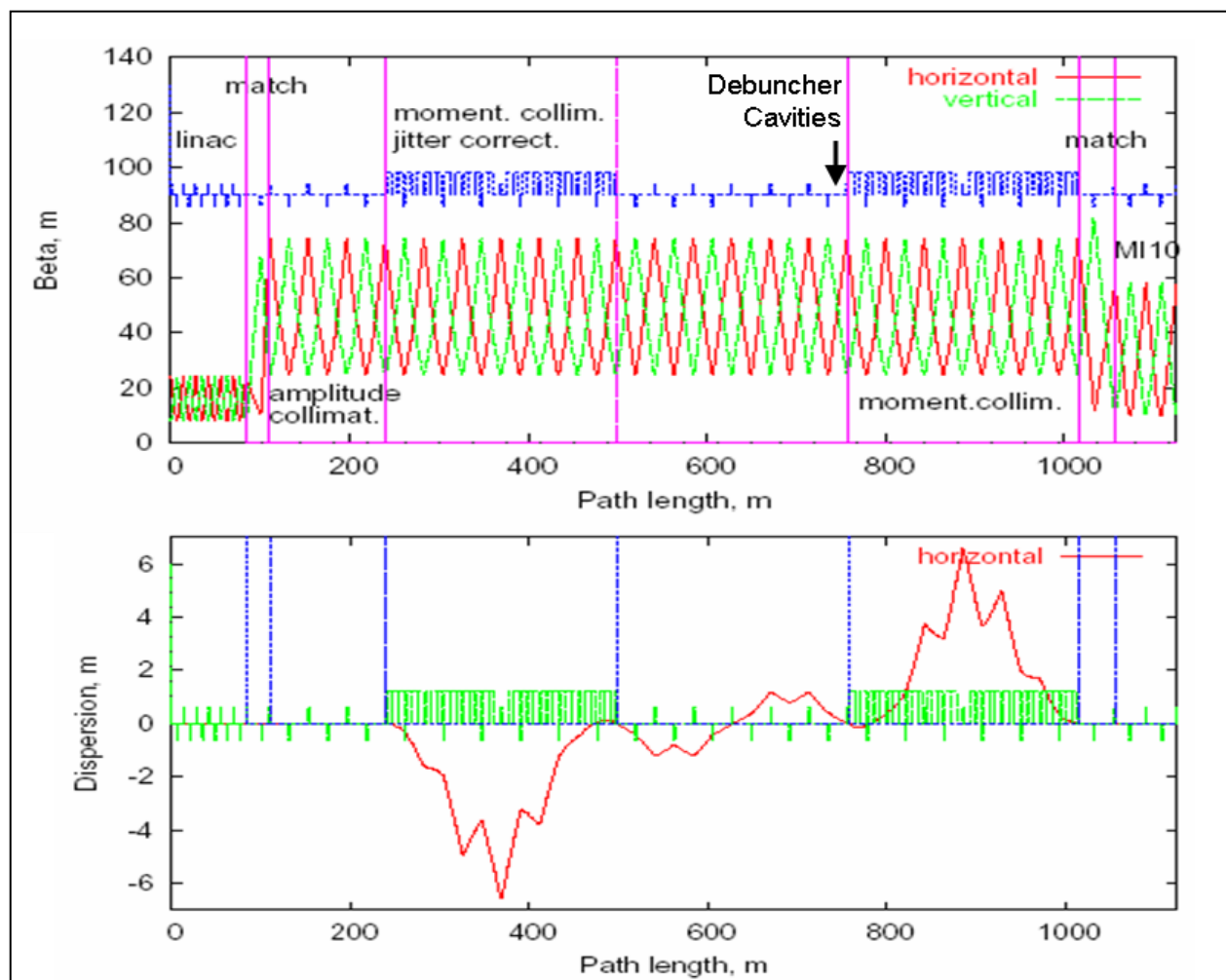


Figure 102 – Beam Optics of Transport and Collimation Line from the PD Linac to the Main Injector.

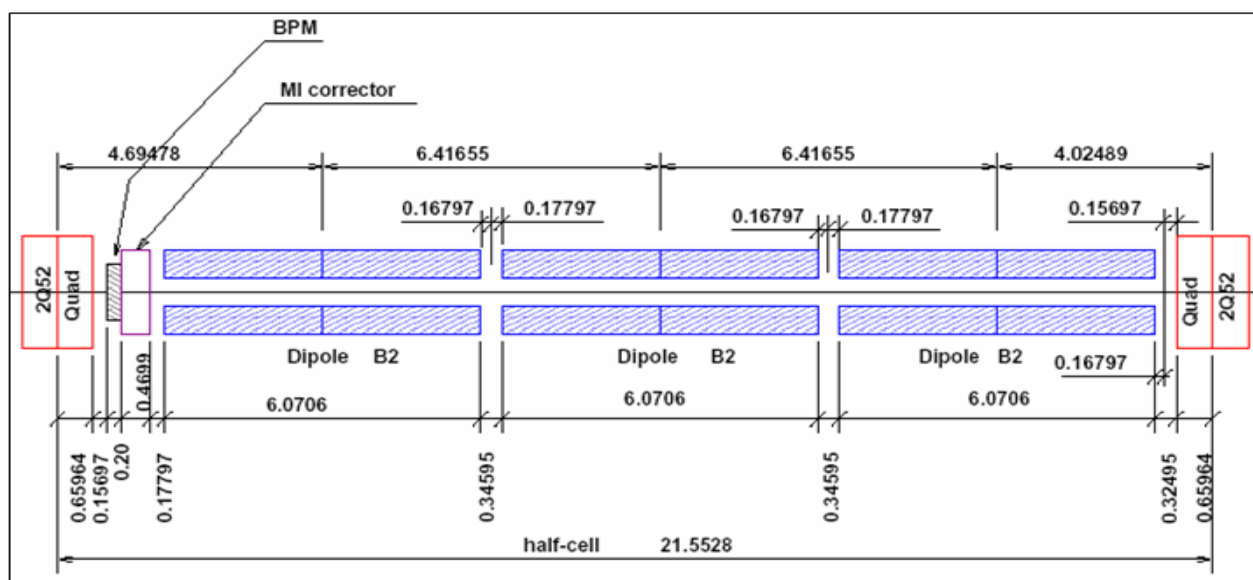


Figure 103 – Bend Cell for Transport and Collimation Line from the PD Linac to the Main Injector.

Table 28 - Beam Transport Line Parameters

TRANSFER LINE TO RING	8 GeV Linac	
Transfer Line Length to Ring	972.456 m	incl. momentum collimation bend
Injection Point to Main Injector	MI-10	baseline design; others possible
Quad Focusing	FODO	
Phase Advance per cell	60 degrees	
Number of half-cells (quads)	47	
half-cells in matching section from linac	2	non-standard cell
half-cells in collimation straight	6	standard cells
half cells in right bend	12	standard cells
half cells in positioning straight	12	standard cells
half cells in left bend	12	standard cells
half cells in match to Main Injector	3	non-standard cell
Half-cell length, standard	21.553 m	3 B2's per half-cell
Half-cell length, linac match	13.28 m	
Half-cell length, MI match	13.56 m	
Beta-Max (H & V)	77 m	
Beta-Min (H & V)	20 m	
Number of Bend half-cells	24	
Transfer Line Total Bend	2 x 20 deg	two achromatic arcs
Dispersion at entrance and exit	0 m	
Dispersion Max (at momentum collimation)	8.85 m	
Vacuum Required	1E-07 torr	TBD for < 1e-4 beam loss from stripping
<b>QUADRUPOLES in transfer line</b>	<b>47</b>	
Quad Length	1.308 m	New Construction
Quad Gradient	1.06 T/m	
<b>DIPOLES in transfer line</b>	<b>68</b>	
C magnets in first half cell	3	New design
B2 dipoles in standard cell	3	
Missing dipoles in arc centers	4	
Total B2 dipoles	65	
Dipole Field	0.05 Tesla	limited from H-minus stripping at 10 GeV
Dipole Length	6.07 m	Main Ring B2 @125A
Horizontal Trims in transfer line	24	at every F-quad
Vertical Trims in transfer line	23	at every D-quad

## 19.2 Dipoles

The dipoles are reused B2 dipoles from the Main Ring. The beam tube aperture is approximately 48.3 mm high by 99.1 mm wide. The magnet steel length is 6.071 m. Running at 125 A the magnet produces 0.05 T field strength. The resistance is about 6.7 mOhm per magnet, so it only dissipates about 100 W, allowing it to run with air cooling alone. A total of 68 magnets are required.

The magnets are currently stored in the Tevatron tunnel where they were left after the decommissioned of the Main Ring. They will be refurbished before installation. This will include performing standard electrical measurements. Flanges will be added to each end of the beam tube, after replacing the bellows if required. Each magnet will have a vacuum pump-out port. New power flags will be added to better match the low current bus.

In the first half-cell the B2 dipoles will be replaced by three new dipoles with the same gap, number of turns, and conductor, producing same integrated field with the same power requirements. These will be C magnets to allow the controlled escape and containment of off-momentum low energy beam due to linac problems. The first quadrupole may need special treatment, or the second half cell may need C magnets, as well, but the power requirements will remain the same.

### 19.3 Quadrupoles

The line contains 47 quadrupole magnets. They are of a new design optimized for the low field required to avoid stripping of the negative ions. The 41 magnets in the arcs and straight sections all run at the same excitation. Three magnets between the end of the linac and beginning of the transport and collimation line match the optics between the two, as do three magnets between the line and the Main Injector. These match quads run from 35% to 130% of the excitation of the standard quads. The higher excitation is acceptable here, as the matches occur in zero dispersion regions where the beam is smaller than it is in the arcs and thus does not see the higher fields.

The pole tip diameter of the new quadrupoles is 79 mm, providing a good match to the dipole aperture. The magnet steel length is 1.308 m. With 8 turns per pole, the standard excitation is 41 A to produce a gradient of 1.06 T/m, or 0.0419 T at the pole tip. The resistance is 230 mOhm per magnet. Dissipating less than 400 W each, the magnets only need air cooling.

The outside dimensions of the magnet are 200 mm x 200 mm. It is a single lamination. The coils are simple racetrack windings, 8 turns in each of two layers. There is ample room to slip the coils in to the aperture and onto the poles.

A C-magnet variant may be needed at the entrance to the first arc to accommodate any off-momentum low energy beam. The yoke is far from saturated, so no trouble is expected if that is required.

### 19.4 Correctors

The line contains 47 quadrupole magnets. A correction dipole is placed at each quad location. The Main Injector trim dipole designs (horizontal and vertical) provide adequate strength to explore the full aperture of the beam line at each quadrupole while keeping the current under 5 A. Resistance of a horizontal (vertical) trim is 2.2 Ohm (2.4 Ohm). At these currents the magnets are quite satisfactory in air-cooled operation

### 19.5 Beam Loss in the 8 GeV H<sup>-</sup> Transport Line

Uncontrolled beam loss in the 8 GeV H<sup>-</sup> transport line arises predominantly from stripping the loosely bound second electron (binding energy 0.7 eV) from the H<sup>-</sup> ion. The resulting H<sup>0</sup> is promptly lost. These were discussed in a workshop on H<sup>-</sup> transport<sup>166</sup> held at Fermilab in 2004.

There are three major loss mechanisms: H<sup>-</sup> stripping from magnetic fields, H<sup>-</sup> stripping from blackbody radiation, and H<sup>-</sup> stripping from residual gas. These are summarized in Table 29. Blackbody stripping dominates by an order of magnitude. The fractional beam loss is  $\sim 10^{-6}$  per meter, or 0.1% for the entire 1 km beam line.

Table 29 – Beam Loss in 8 GeV H<sup>-</sup> Beam Transport Line

H- LOSS MECHANISM	Magnetic Stripping	Blackbody Stripping	Vacuum Stripping	TOTAL
driving parameter for losses	500 Gauss	305 K	1E-7 torr	
fractional loss per meter of transport line	1E-09 /m	8E-07 /m	1E-07 /m	9E-07 /m
fractional loss through entire line (1 km)	1E-06	8E-04	1E-04	9E-04
Beam power loss (baseline: 133 kW into MI)	0.0001 W/m	0.1067 W/m	0.0133 W/m	<b>0.1201 W/m</b>
Beam power loss {Ultimate: 2 MW thru line}	0.0020 W/m	1.6000 W/m	0.2000 W/m	1.8020 W/m

The sum of all beam losses should be small compared to the canonical 1 W/m beam loss allowable for “hands on” maintenance. As can be seen from Table 29, this is the case for the baseline scenario which injects 200 kJ of beam into the Main Injector every 1.5 seconds.

For a possible Ultimate upgrade scenario that puts all 2 MW of beam power as H<sup>-</sup> into the Main Injector, the losses exceed 1 W/m. Two palliatives are under consideration: copper collimation blocks inside each B2 dipole that bury the beam losses in the middle of the magnet, and a 77°K beam screen retrofit inside the magnets which would improve both the vacuum and blackbody stripping. Either of these would gain a factor of >100 improvement in residual radioactivation at the magnets ends.

## 19.6 H<sup>-</sup> Stripping from Magnetic Fields

Magnetic fields are limited to ~500 Gauss in both the dipoles and quadrupoles of the 8 GeV transport line, to avoid stripping of the H<sup>-</sup> ions in the magnetic fields (sect 5.17). At the design point of 500 Gauss, the magnetic stripping losses are < 1 mW/m.

Magnetic stripping represents a hard upper limit to the energy upgradability of the 8 GeV injector linac. If the beam energy is increased by 10%, both the dipole field and the beam momentum are increased by 10%, resulting in a 20% increase in the rest-frame electric field. Since the H<sup>-</sup> stripping lifetime depends exponentially on the rest-frame electric field, the turn-on is very sharp. The beam losses rise from 1 mW/m to approximately 200 mW/m as the beam energy is raised from 8 GeV to 9 GeV.

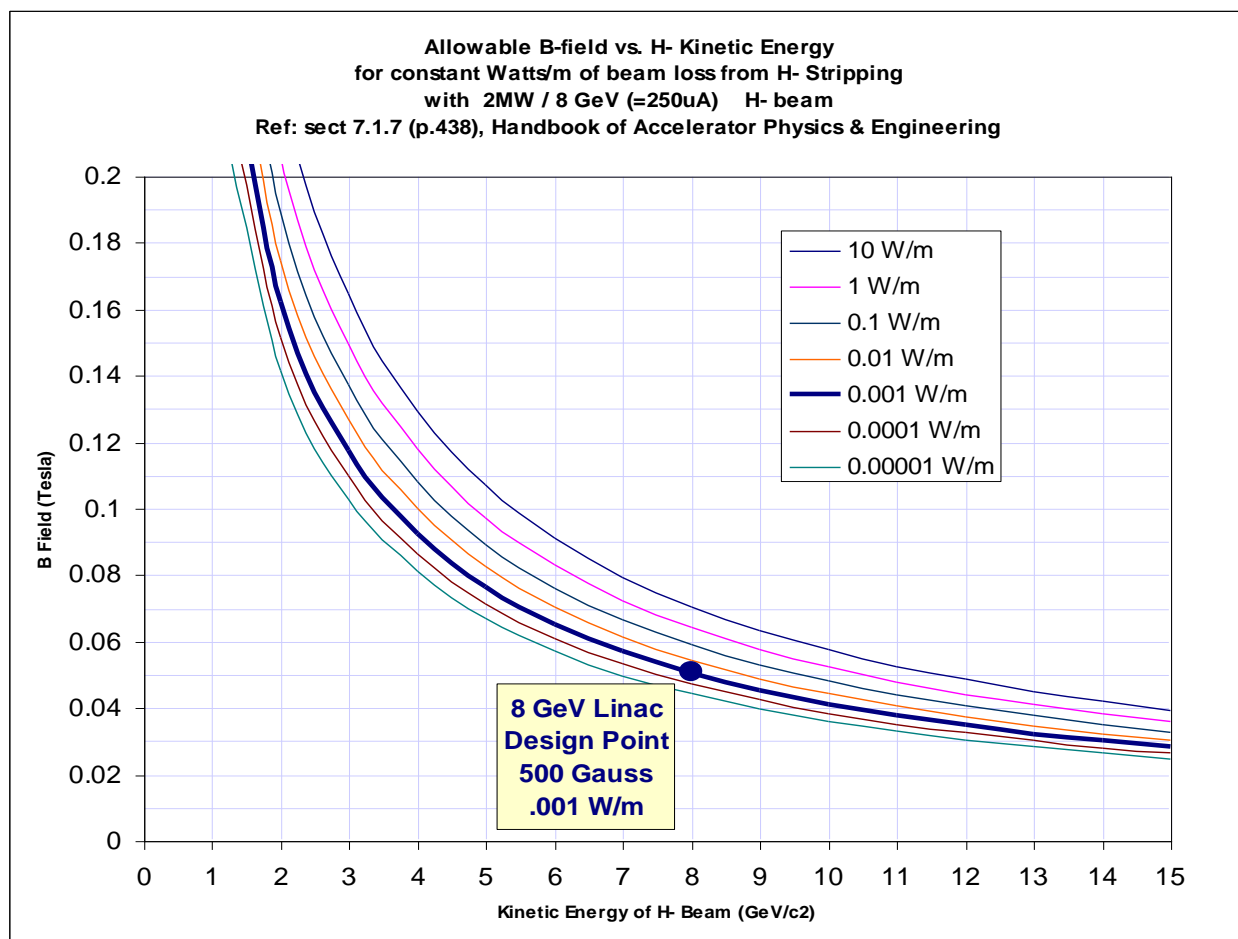


Figure 104 - Allowable bend fields for a given beam loss (in W/m) from H<sup>-</sup> stripping, as a function of the H<sup>-</sup> kinetic energy, for a 25 uA average current H<sup>-</sup> beam. (This current corresponds to 2 MW beam power at 8 GeV). The canonical limit for “hands-on” maintenance of equipment is ~1 W/m.

## 19.7 Vacuum for the Transport Line

The proposed transfer line vacuum system is similar to other beam lines at Fermilab. The total length of this line is 972 m. Of that length, the 65 refurbished Main Ring B2 dipoles (at 6.417 m each) occupy 417 m. The three C magnets occupy 19 m. The quads, correctors, BPM's, and associated beam tube occupy 108 m. The collimation dumps occupy 16 m. The collimation foil systems, miscellaneous instrumentation, the debuncher cavity, and other such stuff will take a minimal space. The remainder is about 412 m of straight pipe.

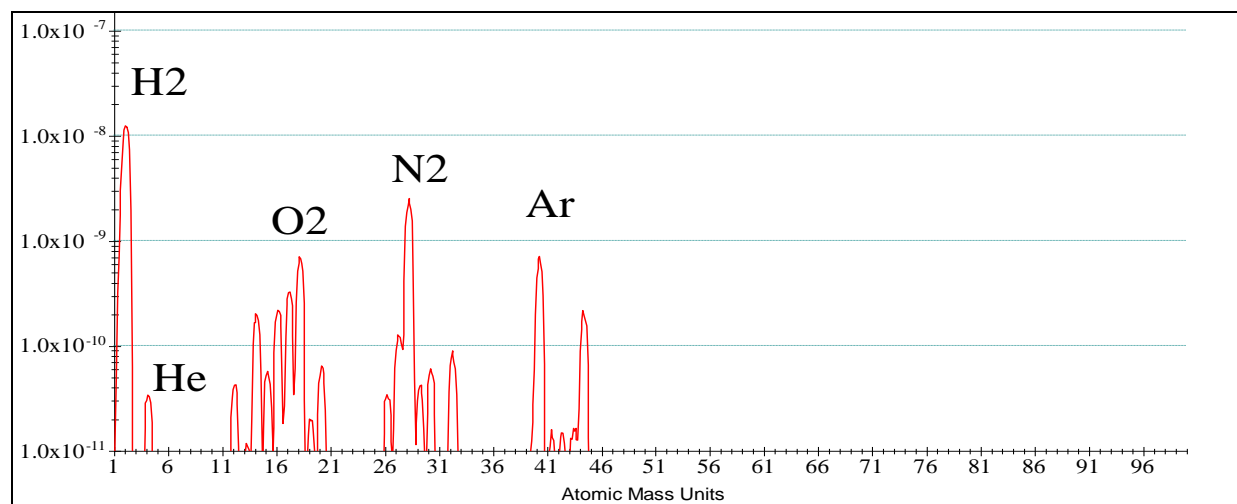


Figure 105 – Residual gas analysis (RGA) of the Fermilab A150 Transfer line, which uses similar vacuum components to those for the PD transport line. This measurement was used to estimate the beam loss from residual gas stripping of the H<sup>+</sup>.

The expected performance of the transport line vacuum system will be similar to other FNAL beam lines which use similar components. Figure 105 shows the Residual Gas Analysis (RGA) of the Fermilab A150 Transfer line. The stripping cross section of H<sup>+</sup>/H<sub>2</sub>, H<sup>+</sup>/N<sub>2</sub> and H<sup>+</sup>/O<sub>2</sub> at 8 GeV can be obtained by scaling from Born approximation. Assuming 50% H<sub>2</sub> and 50% N<sub>2</sub>-O<sub>2</sub>, the lifetime and stripping rate of H<sup>+</sup> can be calculated<sup>167</sup>.

The B2 magnets come with a beam tube potted in place. The C magnet beam tube is new construction. The horizontal aperture will be maintained through the quadrupoles by using an oval beam tube to allow any stripped ions to exit gracefully. The quadrupole beam tube assembly will include a BPM, a bellows, and enough pipe to extend through the quad and the associated corrector. The collimators and their dumps will have dedicated vacuum systems. Vacuum for all these devices is included in the cost of the components.

Pneumatic gate valves are located between the linac and the first emittance collimator, after each subsequent emittance collimator dump, on each side of the first momentum collimator/dump, at the end of the first arc, on either side of the debuncher section, before the start of the second arc, on either side of the second momentum collimator/dump, and at the end of the second arc, for a total of 16 valves. The ability to isolate instrumentation sections may also be valuable, so we take as our nominal count 24 valves.

Compressed air is provided to control the pneumatic gate valves (1000 m). Between quadrupoles in the straight sections where there are no other devices to support the beam tubes, stands will be used every 6 m or so (70 total). Connections between sections will be made with flanges and seals. These are included in the cost of the individual components, such as magnets

and collimators, but we count here those connections involving the roughly 50 plain beam tubes lengths (100). The bellows are treated the same way (50).

Vacuum Pumps are placed at the end of every dipole, for spacings of 6.4 m, 6.4 m, and 10.4 m through the arcs (68 pumps). If needed, an additional pump can be added to split the 10.4 m span into one 6.4 m and one 4.0 m section (12 pumps). In the straight sections, where the quads are spaced at 21.5 m, the larger 5.5" beam tube allows one pump per quad (35 pumps). Additional pumps are provided at the start of the line (3), in the beam dump (5), at each collimator system (8), at the debuncher cavity (2), at isolatable instrumentation locations (8), and in the injection region (5). The pump count totals  $68+12+35+3+5+8+2+8+5=146$ .

The possible upgrade of a cryogenic inner shield mentioned in section 19.5 has been considered. It would be a trace-cooled copper or aluminum liner held at about 80 K by liquid nitrogen. The cryogenic shield would cut both blackbody radiation and vacuum stripping losses by orders of magnitude. The shield would fit inside the existing dipole beam tube through the dipole magnets, the smallest aperture, while still leaving generous clearance for the beam. The liner would be formed of copper sheet to be roughly rectangular. Copper tubes brazed to either side would carry liquid nitrogen and cool the whole tube by conduction. An alternative is to use aluminum extrusions with Invar trace lines press-fit into the extrusion, as was done for the shields on the VLHC transmission line magnet drive conductor<sup>24</sup>. Spacers with low thermal conductivity would hold the liner in position.

## 19.8 Collimation of Betatron Beam Halo

We adopt the very clever foil stripping collimation system that has been developed for the SNS beam transport line<sup>22</sup>. In this scheme, the  $H^-$  beam passes through a thick foil with a hole in it. The hole dimensions correspond to several  $\sigma$  of the beam size. Beam halo outside of several  $\sigma$  strike the foil and are stripped to  $H^+$  (protons). These are then magnetically separated from the collimated  $H^-$  beam by a weak dipole downstream of the foil, and sent to an absorber or dump. The system is analogous to the "foil stripping extraction" employed in cyclotrons<sup>168</sup>. The clean magnetic separation of the stripped halo avoids the problem with classical collimation that there is always a big mess downstream of the jaws.

Two stations of betatron collimation are provided, 90 degrees apart in betatron phase, immediately downstream of the end of the Linac. Rather than using a single foil, a set of foils are used to provide an adjustable aperture. Details and preliminary simulation results are given in ref. 169.

## 19.9 Momentum Collimation

Momentum collimation is provided by a similar pair of foil stripping stations<sup>169</sup> located at the positions of maximum dispersion in each bend of the transfer line. The collimation is meant to deal with not only "momentum halo" i.e. beam outside  $dP/P \sim 4\sigma$ , but also badly off-momentum linac beam pulses. The combination of betatron collimation followed by momentum collimation eliminates the possibility of badly off-momentum beam reaching the Main Injector.

Depending on how often the linac puts out off-momentum beam pulses, it may also be desirable to have stripping collimation stations at the beginning of the arc bends (not just the middle of the arc) to cleanly separate and absorb rogue pulses. These may be as simple as thick foils permanently fixtured in the inner and outer edges of the beam pipe in a "C"-magnet, with a beam crotch and absorber block downstream to deal with the separated stripped beam as it gets ejected from the C-magnet. The mechanism of a stripping foil inside a C-magnet allows both

high and low momentum pulses to end up in an absorber block rather than inside the first dipole of the transfer line.

**Table 30 – Transfer Line Collimation System Parameters**

Collimation in Transfer Line		8 GeV Linac	
BETATRON COLLIMATION IN TRANSFER LINE			
Collimation Type	H-minus halo stripping foils followed by magnets & Dump (like SNS)		
Location	first 3 cells of transferline downstream of Linac		
Number of collimators	12	+/-X, +/-Y at 3 locations each	
Phase advance between stations	60 degrees		
Beta Functions at collimation	76.9 m	scrape at Beta-max in each coord	
Beam Size at Collimators (sigma)	2.0 mm		
Nominal Collimator settings	4.0 sigma	TBD	
	8.0 mm	radial from beam center	
Disposal of Collimated Particles	downstream absorber		
MOMENTUM COLLIMATION IN TRANSFER LINE			
Number of stations	2		
Location	midpoint of each arc (dispersion max)		
Dispersion at Collimation Point	8.85 m		
Collimation Type	H-minus halo stripping foils followed by magnets & collimators		
Number of collimators per station	2	+/-X	
Beta Function (X) at collimators	76.9 m		
Betatron Beam Size at Collimators (sigma)	2.0 mm	same in X and Y	
Nominal Collimator settings (betatron)	5.0 sigma	TBD	
	10.1 mm	from beam center	
Nominal dP/P acceptance of Collimation	+/-0.11 %	for no betatron amplitude	
dP/P acceptance of Main Injector ring	+/-0.75 %	measured, at injection	
dP/P acceptance for MI Transition Crossing	+/-0.20 %	0.7 eV-S per 19ns bucket	

## 19.10 Linac Beam Absorber

The Proton Driver linac beam absorber is patterned after the Main Injector beam absorber<sup>170</sup>. The Main Injector beam dump was originally designed for 300 kW, and had been reevaluated for use at higher intensities in the study of MI upgrades for 2 MW beams<sup>171</sup>. The shielding and civil construction configuration are found to be adequate for a 2 MW 120 GeV proton dump, so that the civil construction costs and sarcophagus dimensions of a 2 MW, 8 GeV dump should be similar.

**Table 31 – Beam Absorber Parameters for the Proton Driver Linac**

<b>LINAC BEAM STOP</b>	<b>8 GeV Linac</b>	
Model for Cost Estimate	Main Injector Beam Dump	
Location	Straight downstream of Linac, outside of transferline bend	
Beam Energy	8 GeV	electrons, H-, or (stripped) Protons
Average Total Beam Power (max)	2 MW	
Core Material	graphite/aluminum	
Shielding Material	steel/cement	
Cooling	RAW, heat exchanged with Tunnel LCW in beam stop enclosure	
RAW Circulation Flow at Full Beam Power	1500 liters/min	396 GPM (Peak Demand)
RAW Delta-T	20 deg C	36 deg F
LCW Flow	549 liters/min	145 GPM
LCW Delta-T	10 deg C	18 deg F

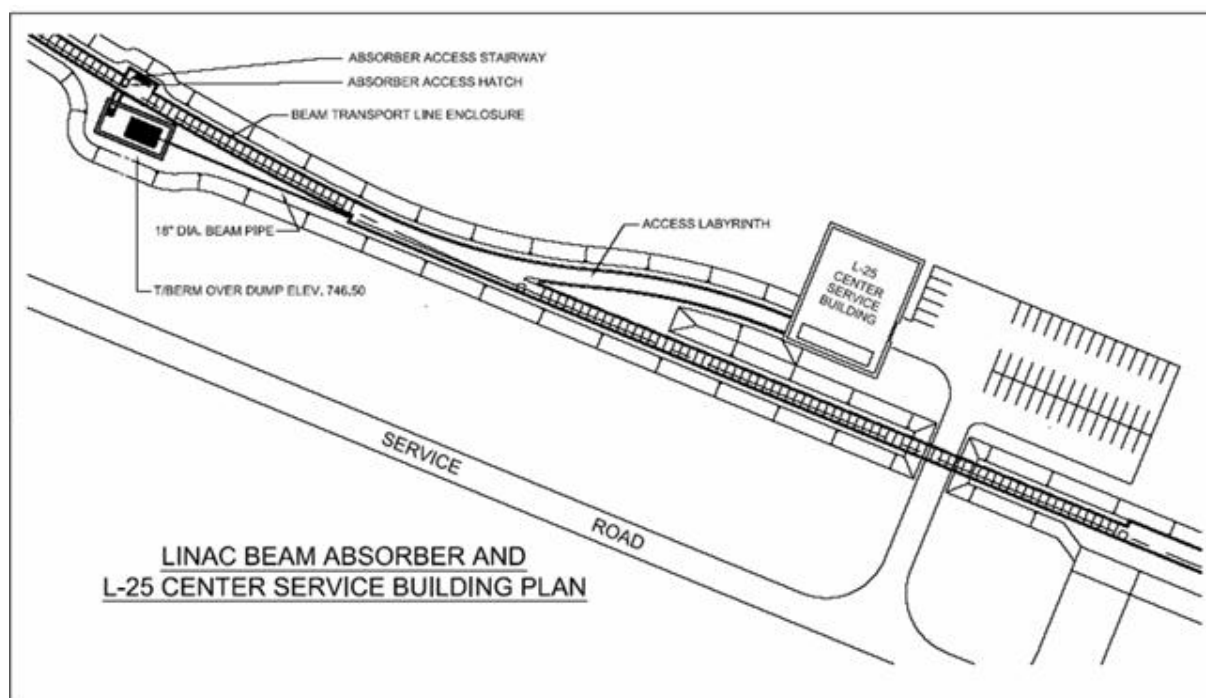


Figure 106 – Beam Absorber location and nearby service buildings in the Proton Driver Linac.

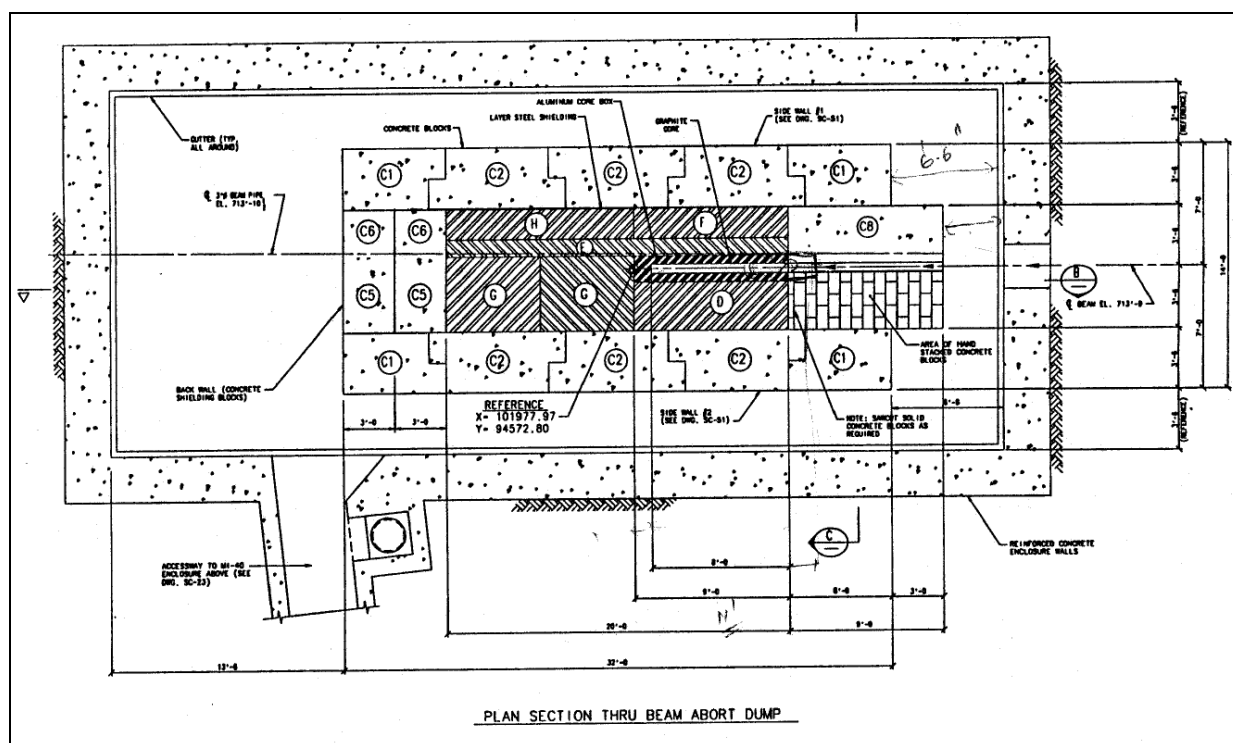


Figure 107 - Main Injector beam dump (plan view). The graphite core is surrounded by a water-cooled aluminum core box (Figure 108), which is placed inside stacked steel and concrete shielding which forms a “sarcophagus”. The Dump is housed in a cast-in-place concrete vault.

For the 2 MW, 120 GeV beam in the MI dump an increase in the length of the graphite core (Figure 108) from 2.4 m to 3 m was desirable to limit the peak temperature<sup>171</sup>. It is unlikely that for Proton Driver linac beam this increase in graphite core length will be necessary. In fact at 8 GeV it might be possible to remove the graphite core entirely and deposit the beam energy directly in the water-cooled aluminum block that extracts the heat<sup>172</sup>. An increase in the Radioactive Water (RAW) cooling flow would be required in either case. This is reflected in the LCW system design (sect. 23).

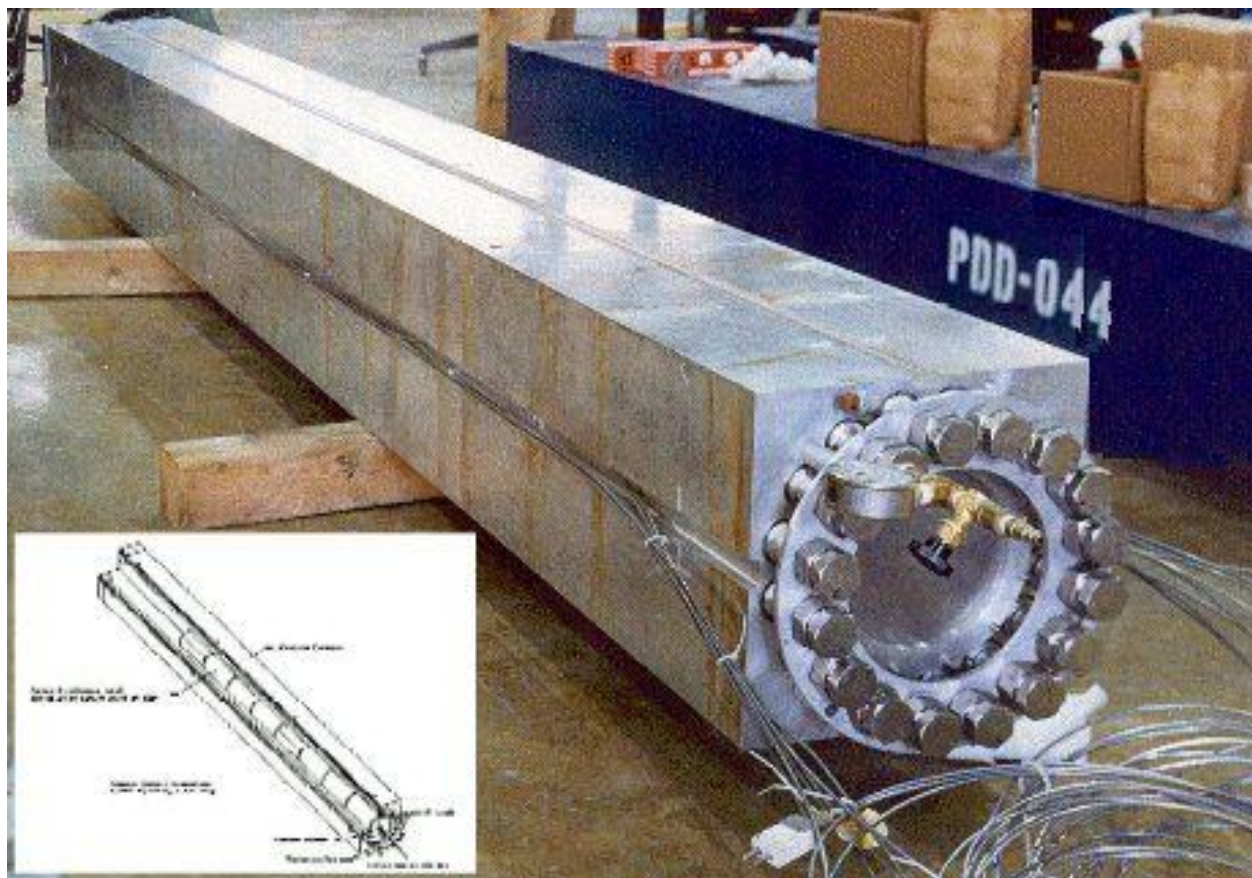


Figure 108 – Absorber Core Box for the Main Injector Beam Dump<sup>173</sup>. This is a graphite core surrounded by water-cooled aluminum. The entire assembly is enclosed in a cement sarcophagus in an underground enclosure.

The transport line to the dump has not been designed, but could be modeled after the SNS linac beam dump optics<sup>174</sup>. A useful feature of the SNS linac dump optics is the use of a rather thick (2 mm) Inconel window to multiple-scatter the beam and ensure a minimum spot size on the dump. Beam window survival should not be an issue since the physical beam size and charge per pulse in the Proton Driver linac is the same as the SNS, while the pulse rate is 6-100 times lower than the 60 Hz pulse rate of the SNS.

Using the same dump for both protons/H- and electrons (*beyond the baseline scope*) should present no radiological or thermal problems. Depending on the emittance of the electron beams in question, it may be necessary to revisit the issues of window survival, beam spot size, and peak temperature in the target. These will require study and simulation.

## 20 H<sup>-</sup> INJECTION

The charge-exchange stripping method of Alvarez<sup>175</sup> and Budker and Dimov<sup>176</sup> is used to inject the H<sup>-</sup> beams of the Proton Driver linac into the Main Injector. The beam layout is similar to those of the JHF 3 GeV synchrotron<sup>177</sup>, the SNS<sup>178</sup>, and the Fermilab Booster<sup>179</sup> and other proton synchrotrons.

The charge-per-pulse for the Proton Driver linac is identical to the SNS, and the injection rate is lower (0.67 Hz compared to 60 Hz for the SNS). Challenging features of the 8 GeV injection layout include the maximum B field of 600 Gauss (bend radius  $\rho = 500$  m) needed to avoid stripping the 8 GeV H<sup>-</sup> ions, and the small spot size on the injection foil ( $\sigma = 1\text{--}2$  mm). One favorable aspect compared to the SNS is the 15 m free space between quadrupoles in the Main Injector straight section, which eases the layout.

The H<sup>-</sup> injection issues were extensively discussed at the H<sup>-</sup> transport and injection workshop<sup>180</sup> at Fermilab in 2004. Although the injection design is not trivial, no fatal problems were uncovered<sup>64</sup>.

### 20.1 Example Injection Layout

A representative injection layout (Figure 109), transverse painting scenario, and loss simulation was developed by A. Drozhdin for this design study<sup>181</sup>.

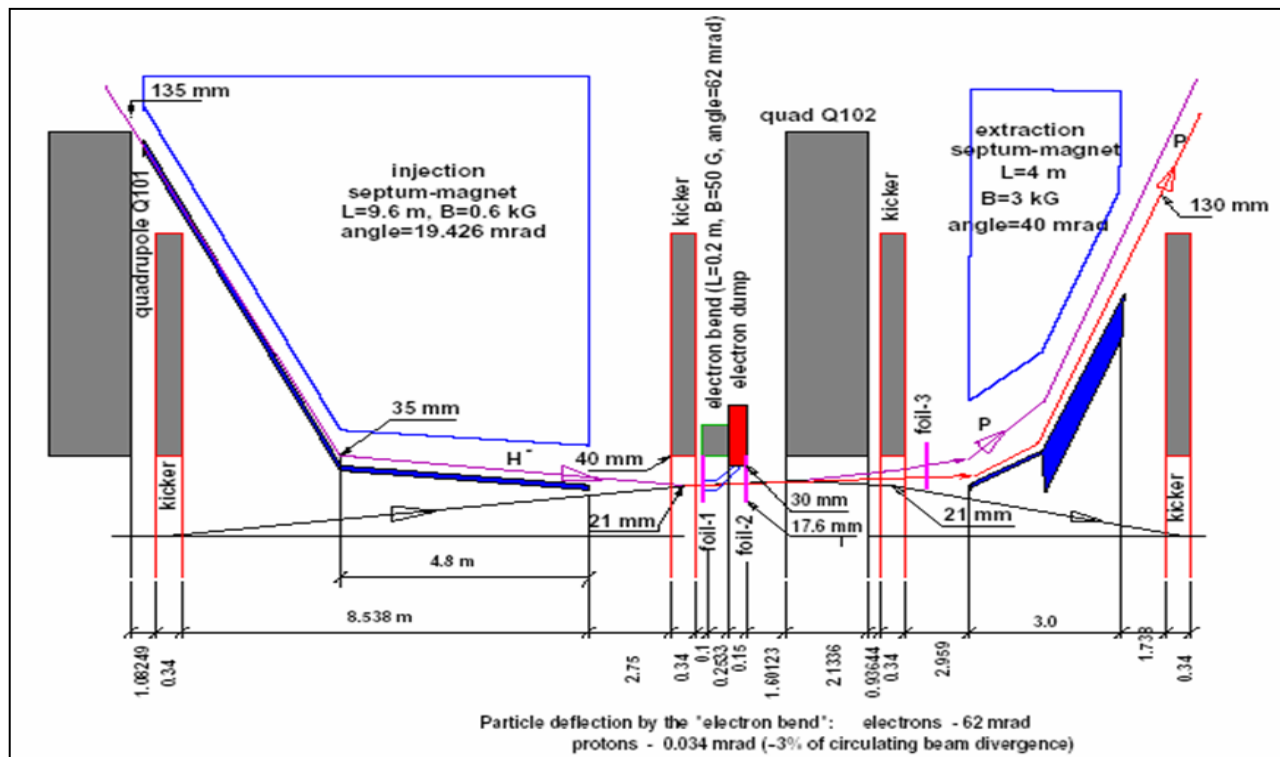


Figure 109 - H<sup>-</sup> Injection layout in the MI-10 straight section. A horizontally bending septum magnet brings the incoming H<sup>-</sup> beam within 23 mm and 2 mr of the circulating beam trajectory as it reaches focusing quadrupole Q102. Simultaneously the proton beam orbit is bumped outwards 23 mm by a set of three pulsed “bump” dipoles. The two beams are merged in a 300 gauss dipole field as they pass through Q102 off center. Downstream of Q102 a pair of 300  $\mu\text{g}/\text{cm}^2$  stripping foils converts 99.6% of the H<sup>-</sup> to protons<sup>182</sup>. The remaining H<sup>0</sup> and H<sup>+</sup> ions are separated from the circulating proton beam by downstream magnets and sent to a beam dump.

## 20.2 Phase Space Painting

The stripping foil geometry is shown in Figure 110. The 12 mm x 14 mm foil is supported on two edges. The injected beam is continuously targeted at the corner of the foil, and the circulating beam is gradually drawn away from the foil as the injection proceeds.

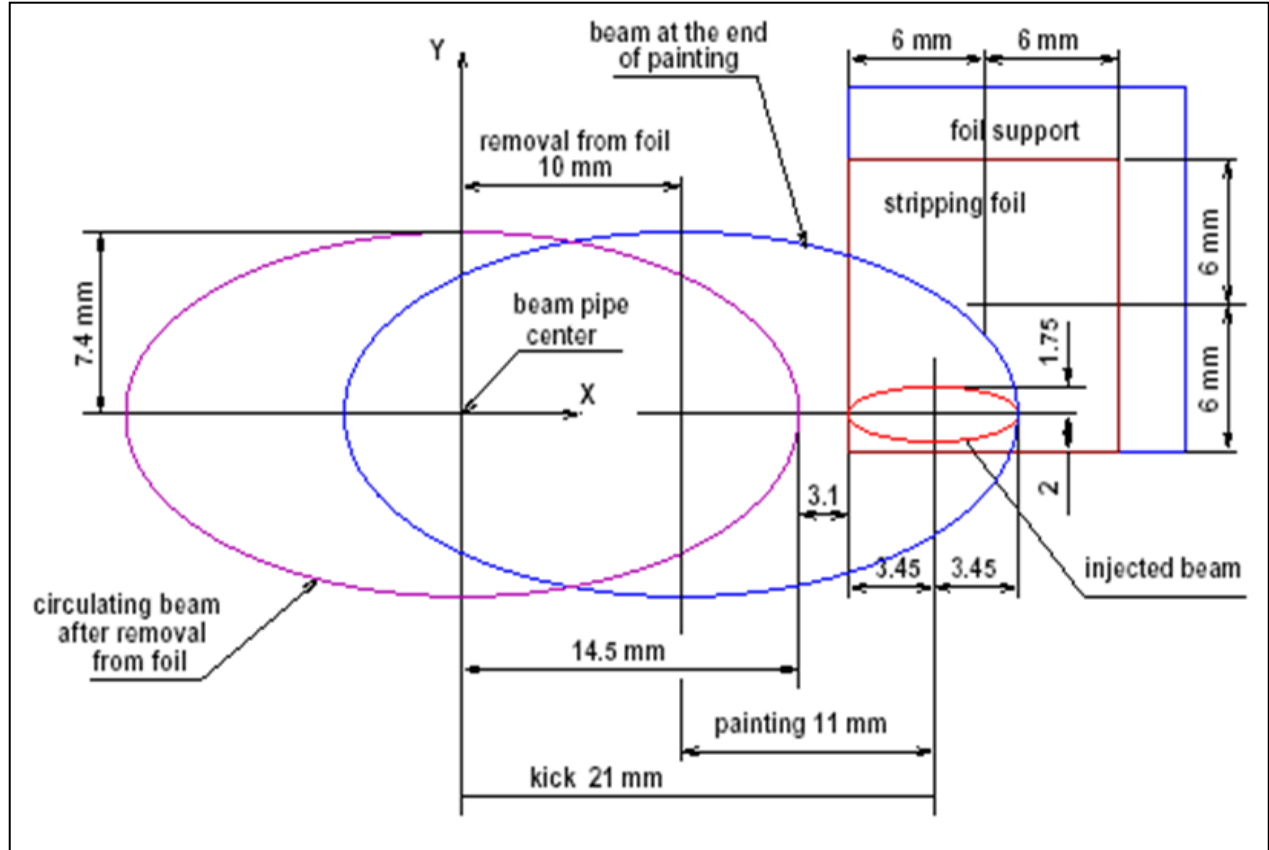


Figure 110: H- stripping foil geometry for the Proton Driver linac.

At the start of injection painting the circulating beam orbit is bumped horizontally outwards by 21 mm. The amplitude is gradually decreased as painting proceeds. The injected H- beam envelope (small orange ellipse) stays fixed on the foil. A separate set of vertical bump magnets in the injection line (not shown) control the vertical angle on the foil. The vertical angle is initially a maximum and is gradually decreased to zero as painting proceeds. The circulating beam envelopes at the end of injection, and after the circulating beam is removed from the foil, are also shown.

Horizontal phase space painting is accomplished by collapsing the bump in the closed orbit as injection proceeds. Vertical phase space painting is accomplished with vertical bump magnets in the H- injection line (not shown in Figure 109) to produce a vertical angle bump at the foil. The vertical angle decreases from an initial maximum value to zero as the bump proceeds, producing an “uncorrelated” painting pattern<sup>177</sup> that avoids injecting particles that have the maximum betatron amplitude in both coordinates.

### 20.3 Optimum Painting Waveforms

The optimal injection painting waveforms<sup>183</sup> to produce an “uncorrelated” beam for 270-turn (3 msec) injection are:

In the horizontal (orbit bump) plane, the bend field B vs. turn number N is given by:

$$B = B_0 \left[ 0.5217 + 0.4783 \left( 1 - \sqrt{\frac{2N}{270} - \left( \frac{N}{270} \right)^2} \right) \right] \quad \text{for } N < 270$$

$$B = B_0 \left[ 0.5217 - \left( \frac{N - 270}{3.83} \right) \right] \quad \text{for } N > 270$$

and in the vertical (injection angle bump) plane, the vertical slope at the foil is:

$$Y' = 0.6789 \text{ mrad} \left( 1 - \sqrt{\frac{2N}{270} - \left( \frac{N}{270} \right)^2} \right)$$

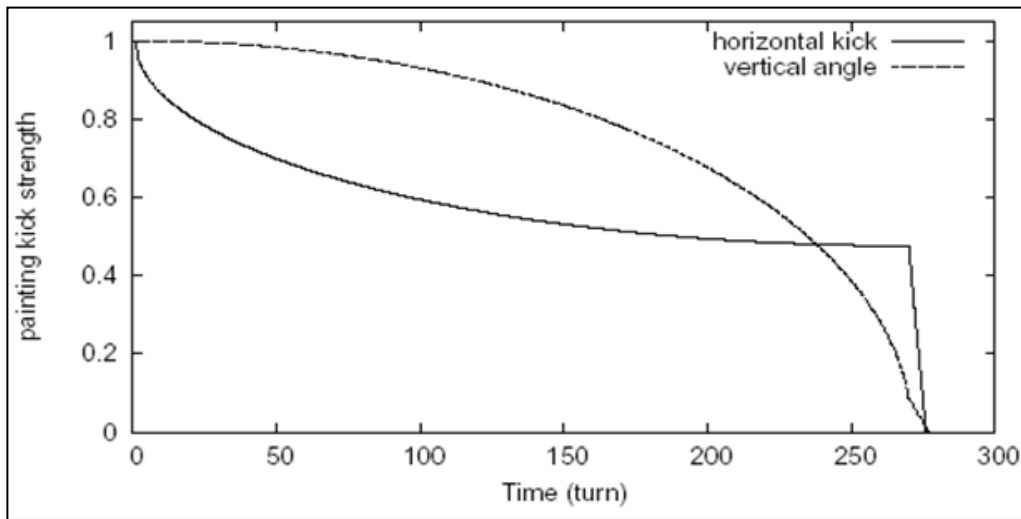


Figure 111 – Normalized painting waveforms on the injection painting magnets for 270-turn baseline injection. The waveforms for 90-turn Ultimate injection scenario are similar.

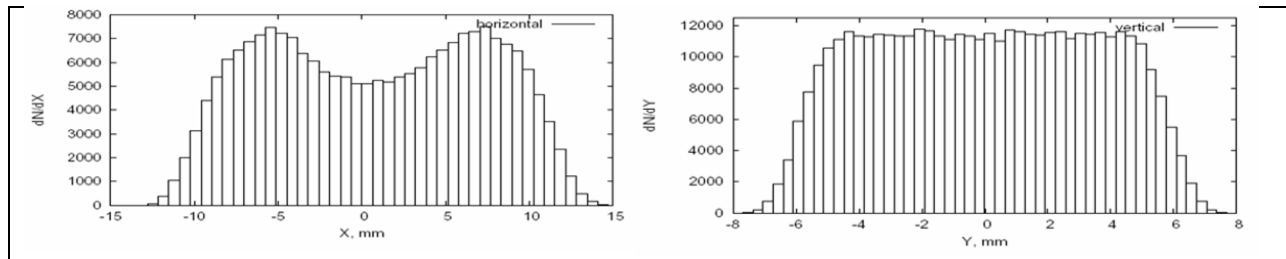


Figure 112 - Horizontal and Vertical Phase Space Distributions at the end of the 270-turn phase space painting injection.

## 20.4 Stripping Foil Heating and Lifetime

Stripping foil performance and survival was considered at the FNAL Workshop on 8 GeV Transport and Injection<sup>166</sup> in Dec. 2005. The situation is comparable to the SNS since the beam charge-per-pulse (which drives the pulsed heating of the foil) is identical to the SNS. The proton driver repetition rate is much lower (0.67 Hz for the baseline design vs. 60 Hz for the SNS). The number of injection turns is smaller (270 {90 Ultimate}) vs. 1060 turns for the SNS. However the beam spot size on the foil is smaller for the Proton Driver and the phase space painting pattern is more constrained due to the smaller beam pipe of the Main Injector. The qualitative conclusion from the workshop was that the Proton Driver Baseline (270-turn) injection was comparable to the SNS and should probably use the diamond stripping foils being produced for the SNS, whereas the Ultimate {90-turn} injection was somewhat easier than the SNS and could be performed with conventional graphite foils.

The baseline design<sup>184</sup> uses two 300  $\mu\text{g}/\text{cm}^2$  thick foils in series to achieve a stripping efficiency of 99.5% and allowing 21 W {7 W Ultimate} of uncontrolled beam loss from nuclear scattering in the foil. The choice of foil thickness is a tradeoff between uncontrolled beam loss from nuclear scattering in the foil (which increases linearly with total foil thickness) and controlled beam loss from unstripped  $\text{H}^0$  beam sent to the injection dump (which is exponentially reduced with increasing foil thickness).

Some uncertainties exist in the stripping foil thickness that will be required<sup>184</sup> for the H-stripping at 8 GeV for the Proton Driver, since these must be extrapolated from lower-energy measurements. Thus it is possible that slightly thicker foils or an additional 3<sup>rd</sup> foil may be required. Each additional 100  $\mu\text{g}$  of foil thickness reduces the un-stripped beam by a factor of  $\sim 2.5$  while adding only 3 W of uncontrolled beam losses downstream of the stripping foil, so an acceptable compromise will be found.

There is a limit to the thickness of a single foil from the pulsed heating at a given charge-per-pulse, since the  $dE/dX$  rises linearly with increasing foil thickness while the radiative heat dissipation is independent of foil thickness. This is why the baseline design uses two medium-thickness foils rather than a single thick foil.

For the baseline (270-turn) injection, each proton passes through the foil once as an  $\text{H}^-$  ion and an average of 16 times as a stripped proton. The  $dE/dx$  for the  $\text{H}^-$  is three times larger than for the circulating protons. An ANSYS simulation<sup>181</sup> indicated an adiabatic temperature rise of 2400°C for a single shot through a single foil. This is probably acceptable if the  $\text{H}^-$  injections are separated by 1.5 seconds. If the MI injections occur at 10 Hz (for example in some sort of 8 GeV stretcher-ring scenario), a peak temperature of 3500°C is reached, which is near the temperature required for prompt failure of carbon foils<sup>185</sup>. This is the motivation for using multiple foils in the baseline design, or eventually switching to SNS-style diamond foils<sup>186</sup>.

It is clear that there is not a lot of margin on the stripping foil survival in the simplest scenarios. An engineered design of the injection region is a high priority, and a good prospect for inter-laboratory collaboration on the Proton Driver.

## 20.5 Main Injector Beam Loss Calculation from Foil Scattering and Interactions.

The simulation of  $\text{H}^-$  injection losses<sup>181</sup> included foil nuclear interactions, multiple scattering, the proposed injection and painting geometry and the focusing lattice and aperture restrictions in the Main Injector. The loss pattern in the Main Injector is shown in Figure 113. The fraction of beam loss from nuclear interactions in the foil was  $2 \times 10^{-5}$  and the overall fractional loss from the combination of painting and multiple scattering in the foil was  $2.5 \times 10^{-4}$ . This simulation does not

include losses from RF capture, space charge, or other loss mechanisms which will probably be dominant.

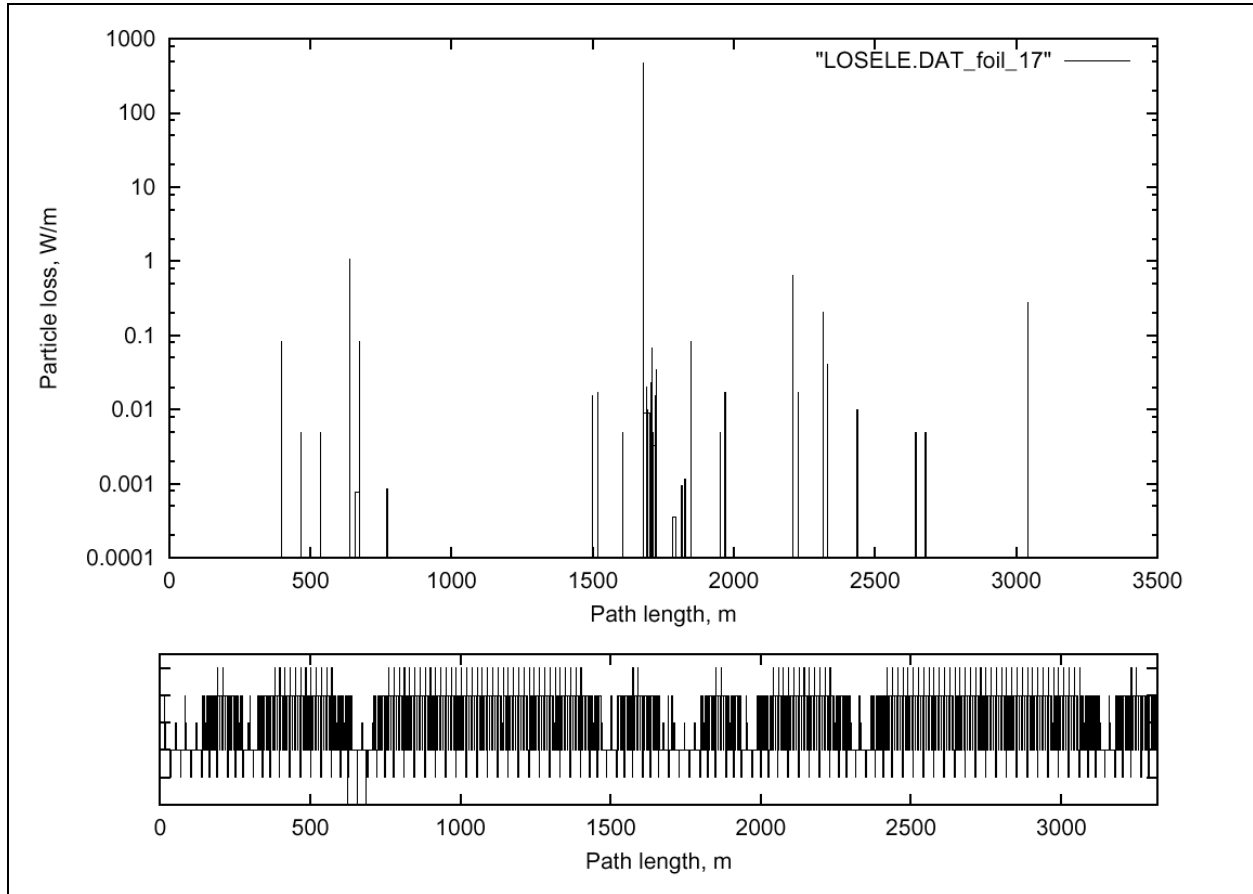


Figure 113 - Injection Beam loss distribution in the Main Injector with graphite foil thickness of 1.5  $\mu\text{m}$  and 90-turn injection of painted beam with nominal emittance. The largest spike (note log scale) corresponds to ~30 Watts of beam loss immediately downstream of the stripping foil and is the result of nuclear interactions in the foil. Distributions for 270-turn injection are similar but approximately 3x higher due to the larger number of passes through the stripping foil.

## 20.6 $\text{H}^0$ Excited States and Delayed Stripping

The excited Rydberg states of neutral hydrogen are significant source of beam losses downstream of the stripping foil<sup>177</sup>. These excited states are quickly stripped in magnetic fields exceeding a critical value, which depends on the principal quantum number  $N$ . Downstream losses result when these are magnetically stripped partway through the bend magnets that complete the proton orbit bump.

In the baseline layout (Figure 109) these losses are suppressed by deliberately stripping a subset of the Rydberg states by placing a dipole magnet of judiciously chosen strength downstream of the foil<sup>187</sup>. At 8 GeV, a value of 410 Gauss will strip states with  $N \geq 5$  while leaving  $N < 5$  largely untouched<sup>187</sup>. The stripped states will fall largely inside the ring acceptance, while the unstripped states will hit the neutral stripping foil and be taken to the injection beam dump.

## 21 MAGNET POWER SUPPLIES

A preliminary list of the 466 magnet power supplies for the Proton Driver linac is given in Table 32. Most of the channels are the independently powered superconducting quadrupoles and trims in the SCRF linac. It is assumed that to switch between protons and electrons, the magnets of the  $\beta = 1.00$  (1207.5 MHz) SCRF section can be ramped from 0% to 100% strength in 0.1 seconds between pulses, and that on the down-ramp the inductive energy is put back into the supply capacitor. These requirements can be met by Fermilab's corrector magnet supplies<sup>188</sup>, which cost about \$1000/channel<sup>189</sup>. The average power per channel is ~60 W and the total power is 27 kW.

Table 32 - Magnet Power Supplies for the PD linac, Transfer Line, and Injection

Magnets & Power Supplies	8 GeV Linac				
	Number	Volts/mag	Current	Power/mag	Total Power
<b>Power Supply Total</b>	<b>449</b>			<b>83W. Avg</b>	<b>37 kW</b>
MEBT matching Quads	4	10 V	10 A	100 W	400 W
SC Solenoids (non-ramped) in 325 Linac	56	2 V	10 A	20 W	1120 W
SC Solenoid steering trims(unramped)	112	+/- 2 V	2 A	4 W	448 W
SC Quadrupoles (unramped in beta<1)	60	+/- 25 V	10 A	20 W avg.	1200 W
SC Quad steering trims(unramped)	120	+/- 25 V	2 A	4 W avg.	480 W
SC Quadrupoles (ramped in beta=1)	36	+/- 25 V	25 A	50 W avg.	1800 W
Transfer Line Dipole Bus	1	0.84 V	125 A	105 W	6805 W
C-magnets on Transfer Line Dipole Bus	1	1.68 V	125 A	209 W	628 W
C-magnets on Transfer Line Dipole Bus	1	0.89 V	150 A	134 W	134 W
Transferline Main Quad Bus (41 quads)	1	9.43 V	41 A	387 W	15852 W
Transferline Matching Quad Supplies	6	11.50 V	50 A	575 W	3450 W
Transferline Vertical Correctors	23	+/- 20 V	5 A	100 W	2300 W
Transferline Horizontal Correctors	24	+/- 20 V	5 A	100 W	2400 W
Orbit Bump Painting supplies (1ms pulsed)	4	275 V	75 A	21 W Avg.	83 W Avg.

The normal conducting magnets in the transfer line operate at very low fields (< 500 Gauss) to prevent H<sup>-</sup> stripping the magnetic fields (section 5.17). The main bend and focusing busses run at currents < 500 A.

The pulsed orbit bump and painting magnets have stored energies in the range of 25-50 joules and a rise and fall times of ~1 msec. They are about 30 times slower than the Booster "ORBUMP" magnets since the linac output pulse is ~30x longer. This reduction in peak power greatly simplifies the power supply design. The numbers for these in Table 32 are approximate numbers based on estimates of stored energy.

## 22 INSTRUMENTATION IN THE SCRF LINAC

### 22.1 Main Linac Instrumentation

A preliminary list of the instrumentation<sup>190</sup> for the Proton Driver main linac is given in Table 33.

Table 33 – Instrumentation List for the SCRF Section of the Proton Driver Linac

SRF INSTRUMENTATION		8 GeV Linac (Preliminary Estimate)	
CHANNELS IN SRF LINAC		16,131	
<b>Channels per Each CAVITY</b>	per cavity	per linac	<b>498 total cavities per Linac</b>
Forward & Reverse Power Monitors	4	1992	2 @ Power Split & Input Coupler
Coupler Spark Detector	2	996	Appears SNS has this many?
Coupler IR detector	1	498	PIN diode
Circulator / Isolator Spark Detector	2	996	on circulator and load
Cavity Resonance Pickup	1	498	
Secondary Emission Pickup	1	498	
HOM Signals	2	996	Used for BPM's & cavity alignment check
Step Motor Tuner Drive	1	498	
Step Motor Tuner Readback	1	498	
Step Motor Tuner Limit Switches	2	996	
Piezo Tuner Drive	2	996	
LCW Flow Meters	1	498	one water ckt. per cavity: circulator, load, tuner
Misc. Temperatures	5	2490	TBD
<b>Total Channels Per CAVITY</b>	<b>25</b>	<b>12450</b>	
<b>Channels per Each QUAD LOCATION</b>	Per Quad	per linac	<b>145 (quad+solenoid) locations</b>
BPM and phase monitors	2	290	
Magnet / Lead Protection	2	290	
Alignment Readouts	2	290	TBD
<b>Total Channels per QUAD LOCATION</b>	<b>6</b>	<b>870</b>	
<b>Channels per Each FERRITE TUNER</b>	per Tuner	per linac	<b>195 total tuners per Linac</b>
Ferrite Tuner Drive Amp	2	390	Assume Tuners for E<2.2 GeV only
Ferrite Tuner Current Monitor	2	390	Inside Power Supply (upstairs)
Ferrite Stub RF Power Monitors	2	390	in addition to power monitors per cavity
Ferrite Tuner Temperature Monitor	2	390	?use B-H saturation point to measure Temp?
<b>Total Channels Per TUNER</b>	<b>8</b>	<b>1560</b>	including debuncher and 2 test stands
<b>Channels per Each CRYOMODULE</b>	per CM	per linac	<b>51 total Cryomodules per Linac</b>
Beam loss monitors	1	51	
Beam Profile scanners	1	51	TBD--maybe laser windows
Number of Cryo Temp Sensors	8	408	
Insulating Vacuum TC gages	1	51	
Coupler Vacuum Ion Pump	1	51	
Coupler Vacuum TC gage	1	51	
Alignment Readouts	4	204	TBD
<b>Total Channels per Cryomodule</b>	<b>17</b>	<b>867</b>	
<b>Channels per Each KLYSTRON (initial)</b>	per Klystron	per linac	<b>12 Klystrons (initial) incl. debuncher</b>
Vacuum	3	36	Readback, Interlock, Ion Gauge
Water Flow	3	36	Body, Collector, Solenoid
Solenoid Power Supply	3	36	PS control, PS Readback, Ground Fault
Filament	3	36	Control, Voltage Readback, Current Readback
Forward & Reverse RF Power Monitors	4	48	in addition to power monitors per cavity
Ion Pump Power Supply	1	12	
Waveguide Pressure	2	24	
Pulse Transformer	4	48	Temperature (2+Interlock), Oil Level
Pulse Transformer Bias Supply	2	24	Control & Readback
RF Leak Detector	3	36	
Gun Voltage and Current	2	24	Voltage divider & Current Transformer
RF Power (Directional Coupler)	2	24	Forward & Reverse power at Klystron
<b>Total Channels per Klystron</b>	<b>32</b>	<b>384</b>	including debuncher and 2 test stands

The instrumentation in the main SCRF linac is very repetitive. It can be classed as recurring once per cavity, once per quad location, once per cryomodule, once per Ferrite Vector Modulator, or once per Klystron. The instrumentation which recurs per cavity dominates, accounting for 12,500 out of the 16,000 estimated channels of electronics. The per-cavity electronics are handled in racks in the Klystron gallery immediately in front of the 34 cable ducts from the tunnel. These will be comparable to the electronics at TTF where 8 cavities (1 cryomodule) are serviced by a single rack of electronics. Assuming a density of 6 cavities per rack for the Proton Driver electronics, two racks of per-cavity readout electronics should suffice at each of the 34 cable duct locations in the linac.

Each Klystron location has two racks of control electronics associated with it, roughly corresponding to one rack for interlocks and one rack for LLRF controls.

The Ferrite Vector Modulators (FVMs) require an additional rack of electronics at each cable duct location. These contain the fast slewing power supplies to drive the ferrite bias coils. The rack and crate mechanics (section 14.7 and Figure 86) are identical to the corrector supplies commonly used at FNAL. A bulk supply at the bottom of each rack provides DC power to the high-frequency switching power supplies which drive the 24 bias coils (12 cavities worth) of FVMs. These are only present in the linac below 2.2 GeV beam energy (a total of 17 racks).

## 22.2 Transfer Line Instrumentation

### Beam Position Monitors (BPMs)

As is customary in a regular lattice, we place one BPM in each of the 47 quadrupoles, alternating horizontal and vertical. At the start and end of the line a few locations may be instrumented with both orientations. Additionally, each of the roughly 100 m straight beam lines to the absorbers, one at the start of the first arc and one after the injection point, will also have a BPM approximately every 20 m and a pair just before the dump. The total count is thus  $(47+6+6+6=65)$ .

With minimal extra effort some, if not all, of the stations will be equipped to read out at a few MHz, allowing monitoring of variation in the beam position and (at high dispersion points) energy during the pulse.

We expect a simple shorted stripline with two pick-ups per plane to be sufficient. The cables running upstairs will need to handle the relatively high 325 MHz frequency of the beam structure.

The general approach to the electronic has not been explored, let alone details. Although the RF will have left the beam in 1207.5 MHz bunches, only every third bucket will be populated.

### Beam Loss Monitors (BLMs)

We will place a beam loss monitor at each quadrupole, at a dozen other potentially tight spots, and extras around the collimation dumps and the high power absorbers (85 total). Each location will require the monitor itself, cable to a service building, amplifier/integrator electronics, and controls readout.

The possibility of beamline-style BLMs using gas-filled Heliax cable will be considered. An advantage of this approach is that in principle it offers ~100% coverage of the beam line (no dead spots). This may make it useful as a redundant beam loss abort device without adding many electronics channels. A difficulty is verifying the calibration and gas integrity along the

entire length of the BLM line. An inorganic, permanently sealed, semi-rigid BLM line might be considered.

### **Beam Current Transformers (BCT)**

There will be one beam current transformer at the start of the line (end of the linac) and one at the end of the line (before the split between Main Injector and 8 GeV primary beam for neutrinos). There will also be BCT's before each high power absorber. The total count is thus four.

### **Beam Profile Monitors**

Ideally, two profile monitors  $\pi/4$  apart at the head of the line would allow checking of the transverse phase space at the end of the linac. The half cell phase advance of  $\pi/6$ , makes that more difficult, so we will place three monitors at the head to paint a complete picture of the beam there, and similarly at the end of the beam right before injection. Careful study of those two matching sections may allow a reduction to two monitors in each section. Additionally, pairs of profile monitors will be located at the end of the transverse collimation section, in the middle of each arc, at each end of the central straight section, and in front of each high power absorber. The total count is 18 profile monitors, each with two-plane capability.

Due to the issue of ion stripping, careful consideration must be given to the choice of profile device type. Standard Fermilab beam line profile monitors rely on intercepting the beam. If that continues to be the choice, appropriate provision must be made for the stripped protons and strict limits on operation must be enforced. From that point of view, ionization profile monitors are attractive, but their increased complexity is problematic. The SNS choice seems to be SEM wire scanners. Laser beam scanners would also be interesting to consider. If possible, a system that is compatible with electron operation would be very attractive.

Whatever the system chosen, it will require mechanical hardware, front end electronics, cabling, controls, and software.

### **Energy Monitor**

In the middle (high dispersion point) of each arc, one horizontal beam position monitor will be equipped with fast electronics to measure the position (and thereby the linac output energy) continuously throughout the pulse. Noise in this measurement due to fluctuations in horizontal steering will be removed by a similar horizontal monitor located at the zero-dispersion entrance to the arc 180 degrees in betatron phase from the beam energy monitor. This can be used in conjunction with the Debuncher cavity and LLRF controllers to implement a fast feedback regulation of the Linac output energy as described in section 15.4.

## 23 COOLING WATER (ICW and LCW SYSTEMS)

The cooling system for the Proton Driver is shown in Figure 15 of Appendix 3. The system is a conventional closed-loop Low-Conductivity Water (LCW) system. Heat is exchanged with Industrial Cooling Water (ICW) piped from the Fermilab Central Utility Building (CUB). A summary of the LCW system parameters are given in Table 34.

The Figure indicates a single Water Pump / Cryogenics building at a common location near the center of the Linac. A decentralized system of 4 smaller LCW/HTX enclosures distributed along the linac is also under consideration. This configuration has advantages for redundancy, and reduces the maximum flow rates in distribution headers.

Cooling of the Linac Beam Dump takes place via heat exchange of the LCW with a Radioactive Water (RAW) loop patterned after the Main Injector Beam Dump RAW system. The system is sized to absorb 100% of the theoretical power that can be sent to the beam dump in the Ultimate beam power configuration.

Excess ICW capacity exists for the 3.6 MW heat load for the baseline configuration. The Ultimate 10.4 MW heat load of the Ultimate configuration can also be supported by planned pipe sizes and existing CUB capacity, providing the simultaneous operation of existing loads (e.g. Linac, Booster and Pbar) is not required. LCW filling and makeup water for the Linac is obtained from the Main Injector LCW loop at the Linac tie-in to the MI tunnel.

The cryogenic plant cooling is provided by conventional air towers. Cryogenic cooling requirements (2 MW dissipation) are identical for the baseline and Ultimate configurations.

### 23.1 LCW Load Variability

The Low-Conductivity cooling Water (LCW) system has to deal with substantial minute-by-minute variations in the power dissipation in the tunnel(s). Worst-case tunnel power dissipation occurs with the Linac cycling continuously with no beam present. In this case, all 3.6 MW {10.2 MW Ultimate} of electrical power delivered to the modulators ends up as waste heat in the gallery and tunnels. This power dissipation can come and go on a minute-by-minute basis during operational changeover or Linac trips.

About 40% of this power dissipation can migrate between the Klystron Gallery and the Linac Tunnel, depending on whether the klystrons are being fully modulated by the RF drive or not. If the beam is present, the 0.5 MW {2 MW Ultimate} of beam power disappears from the tunnel power dissipation but presumably shows up as heat loads in the experimental areas or beam dump. These heat loads will have to be operationally managed with care. To provide flexibility and operating margin, conservatively large LCW pipe sizes, operating at large flow rates and small delta-T's were chosen.

### 23.2 Differences from the TESLA Cooling Design

The Proton Driver linac LCW system differs substantially from the TESLA TDR design. Firstly, there are two separate LCW piping runs, one each in the Klystron Gallery and Beam Line Tunnel. Secondly, the maximum allowable LCW temperature of 80°C (176°F) in the TESLA TDR design has been reduced to more usual Fermilab maximum operating temperatures of 47°C (117°F). Thirdly, the pipe sizes and flow rates have been specified to produce lower pressure drops. There is also an oft-expressed desire by those working in the Linac gallery and tunnel to minimize acoustic noise from the LCW system, which requires larger pipe sizes than strictly required for efficient distribution. All of these changes increase cost.

Table 34 - Individual LCW Heat Loads for the Proton Driver linac (prelim.)

GALLERY LCW LOADS		8 GeV Linac Initial {multiply GPM x3 for ULTIMATE}				
325 MHz RF STATIONS						
	Modulator Chassis	10 kW	9.7 l/m	2.6 GPM	15 degC	
	Pulse Transformer	3 kW	2.9 l/m	0.8 GPM	15 degC	
	Number of Klystrons/modulator	1				{2 Ultimate}
	Klystron Collector	26 kW	113.6 l/m	30.0 GPM	3 degC	Toshiba
	Klystron Body	8 kW	9.1 l/m	2.4 GPM	15 degC	Toshiba
	Klystron Solenoids	10 kW	10.0 l/m	2.6 GPM	15 degC	Toshiba
	325 MHz RF Station Total	57 kW	145.19 l/m	38.4 GPM	15 degC	
	Number of 325 MHz Rf Stations	1				
	Total all 325 MHz RF Stations In Gallery	57 kW	145.2 l/m	38.4 GPM	5.6 degC	
1300 MHz RF STATIONS						
	Modulator Chassis	34 kW	32.3 l/m	8.5 GPM	15 degC	
	Pulse Transformer	3 kW	2.9 l/m	0.8 GPM	15 degC	TESLA TDR
	Klystron Collector	103 kW	250.0 l/m	66.1 GPM	6 degC	Thales
	Klystron Body	8 kW	10.0 l/m	2.6 GPM	11 degC	Thales
	Klystron Solenoid	5 kW	10.0 l/m	2.6 GPM	7 degC	Thales
	1300 MHz RF Station Total	153 kW	305.2 l/m	80.6 GPM	7.2 degC	
	Number of RF Stations	11		Linac+debuncher		{31 Ultimate}
	Total all 1300 MHz RF Stations	1681 kW	3357.0 l/m	887 GPM	7.2 degC	
TUNNEL LCW LOADS		8 GeV Linac Initial {multiply GPM x3 for ULTIMATE}				
RFQ+DTL+SPOKE RF LCW Loads		26 kW	25 l/m	7 GPM	15.0 degC	
1300 MHz Cavity LCW Loads		One Circuit for (Circulator + Ferrite Tuner +Water Load Absorber) in series				
	Number of Cavity RF Stations in Tunnel	392	assume all stations are equal to worst case (pessimistic)			
	Circulator	0.2 kW				
	Ferrite Tuners	0.4 kW	sum of 2 tuners with 0.2dB total losses			
	Water Load	3.6 kW				
	Total per Cavity	4.1 kW	4.0 l/m	1.0 GPM	15 degC	
	Total for all Cavity Stations in Tunnel	1623 kW	1550.5 l/m	409.6 GPM	15.0 degC	
BEAM DUMP RAW System (Initial)		575 kW	549 l/m	145 GPM	15 degC	
	Beam Stop Location	Along Transfer Line to Ring				
	Pump & Heat Exchanger Location	In Beam Dump Enclosure				
	Beam Heat Load (nominal)	0.5 MW	{2 MW Ultimate}			
	Beam Heat Load (design)	2 MW	design for Ultimate			
	Beam Heat Load (typical)	<10 kW	typical during running			
	RAW Pump Heat Load	75 kW	100 HP WAG			
	Heat Exchanger	With Downstream LCW flow in tunnel				
LCW SYSTEM TOTALS		Heat Load (worst-case)		FLOW		Delta-T
Klystron Gallery Header Totals (initial)		1738 kW		3502 l/m	925 GPM	7.1 degC
Linac Tunnel Header Totals (initial)		1649 kW		1576 l/m	416 GPM	15.0 degC
Test Stand LCW Totals (initial)		210 kW		450 l/m	119 GPM	6.7 degC
RAW HTX Header Total (initial)		575 kW		549 l/m	145 GPM	15.0 degC
INITIAL LCW SYSTEM		3597 kW*		6077 l/m	1606 GPM	8.5 degC
ULTIMATE LCW SYSTEM		10372 kW*		16233 l/m	4289 GPM	9.2 degC
LCW Supply Temperature (nominal)		32 degC		90 degF		
LCW Max. Temp (anywhere in system)		47 degC		117 degF		
* note: Worst-Case Heat Load of entire LCW system is less than the sum of the individual worst cases.						

## 24 WALL POWER SUMMARY FOR PROTON DRIVER LINAC

The wall power dissipation of the Proton Driver has been calculated<sup>191</sup> and is summarized in Table 35 below. The AC power is dominated by the RF station and Cryogenics which are based on bottom-up total of the specific technical components. The conventional power in the gallery and tunnel was estimated by taking the average (600 W/m) of comparable enclosures at Fermilab. This estimate is hopefully conservative, especially in the Initial Baseline scenario where the linac gallery is >2/3 empty and the spacing between linac RF stations is 180 ft.

The AC wall power of the baseline Proton Driver linac is 5.5 MW, and the efficiency for converting wall power to beam power is  $(0.5 \text{ MW Beam Power} / 5.5 \text{ MW AC}) = 9\%$ . The efficiency of the ultimate configuration is  $(2 \text{ MW Beam power} / 12.8 \text{ MW wall power}) = 16\%$ . For comparison, the power draw of the existing Booster/linac combination is ~7 MW, and the efficiency is  $(40 \text{ kW typ.} / 7 \text{ MW}) = 0.6\%$ .

Table 35 – Site Power Summary for the Proton Driver linac

Wall Power Summary	8 GeV Linac			
	INITIAL (0.5 MW Beam)		ULTIMATE (2.0 MW Beam)	
	Nominal [MW]	Installed [MVA]	Nominal [MW]	Installed [MVA]
RF Stations	2.700	6.000	10.000	18.000
Cryogenics	1.371	2.057	1.070	1.682
LCW Pump Power	0.300	0.471	0.400	0.471
Beamline Technical	0.082	0.219	0.082	0.219
Conventional Power @600 W/m *	1.044	1.228	1.264	1.448
<b>TOTAL</b>	<b>5.5 MW</b>	<b>10.0 MW</b>	<b>12.8 MW</b>	<b>21.8 MW</b>

\*Note: The 600 watts/meter is a Fermilab average for (Tunnel+gallery) conventional power including instrume

## 25 MAIN INJECTOR RF UPGRADE

The new RF system<sup>192</sup> is the most important feature of the Main Injector upgrade for 2 MW beam power (5x the original design of the MI). Beam power upgrades can be accomplished by increasing the beam current, by increasing the accelerating voltage and ramp rate, or by a combination of both. In either case beam stability issues and cavity impedance play an important role in overall system optimization.

The philosophy of the baseline design is to reach 2 MW by building new cavities which can handle higher beam current (5x Main Injector Design) under conservative assumptions about beam stability and feedback requirements. Upgrades above 2 MW beam power can be accommodated by increasing the accelerating voltage and ramp rate to decrease the cycle time. This additional voltage can be produced either by adding additional cavities, or by possibly by design modifications (raising the Q of the cavity) which generates higher RF voltage per cavity but which increases dependence on electronic feedback for beam stability.

Table 36 - Main Injector RF Upgrade Parameters

MI Intensity	1.5E14	Protons/cycle
MI Beam Current	2.2	Amps
Maximum ramp rate	305	GeV/s
Number of RF stations	18	(same as now)
Cavity peak voltage	300	kV / cavity
Peak Power to Beam	405	kW / cavity
Peak Power Dissipation	450	kW /cavity
Frequency (min)	52.814	MHz
Frequency (max)	53.104	MHz
Frequency (sweep)	290	kHz
Cavity Rs/Q	25	(currently 104)
Cavity Rs	100	kΩ
Cavity Q	4000	(adjustable via Cu plating)
Cavity Tuner Material	YIG	Yttrium Iron Garnet, Al-doped
Cavity Tuner Geometry	Coax	Solenoid for Perpendicular bias
Tube type	Tetrode	
Tube Model(s)		Thales TH525 (1.5 MW) - or - CPI Eimac 8973 (1.0 MW)
Tube Input Drive Pre Amp	Existing PA	

### 25.1 New Cavity Design for Main Injector RF Upgrade

The new Main Injector RF cavity<sup>193</sup> is shown in Figure 18 and Figure 114. It is a low-impedance coaxial structure with large gap capacitance (low R/Q) to reduce the effects of beam loading. A compact, non-folded single gap design driven by a single tube is chosen. Although the cavity is designed as a 1-for-1 replacement for each of the existing 18 RF stations, the design is compact enough that as many as 24 RF stations might be installed in the MI-60 straight section.

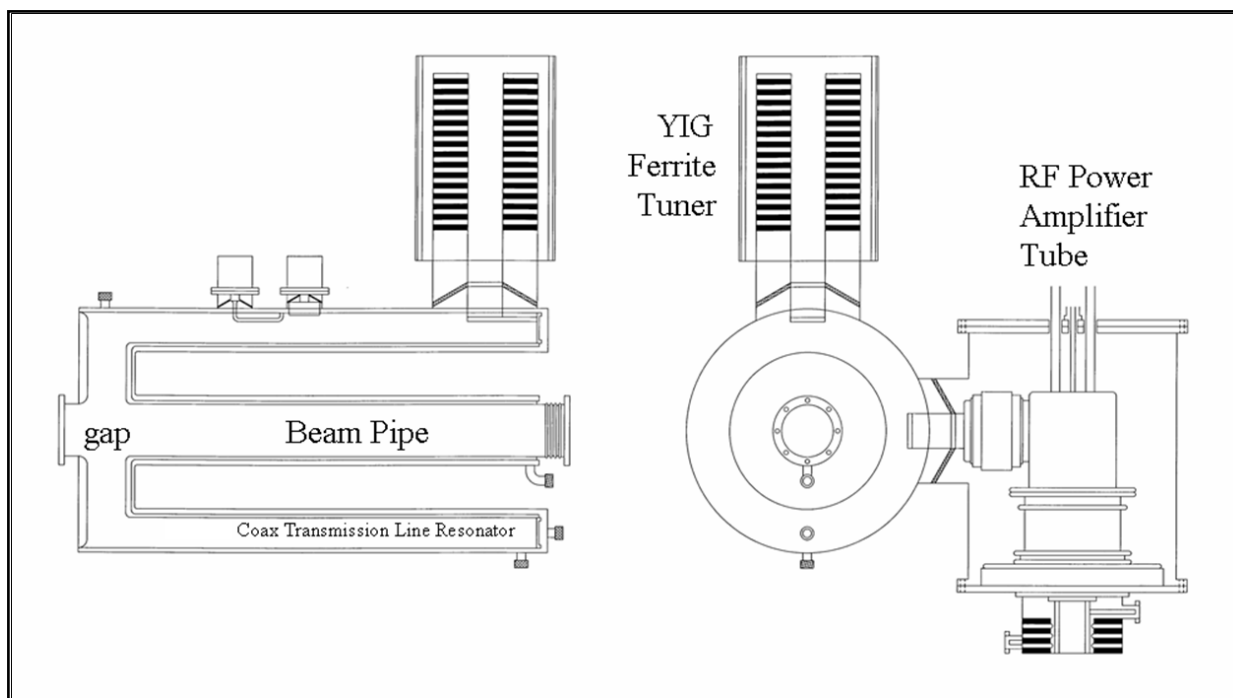


Figure 114 - Main Injector RF Upgrade Cavity.

The cavity is stainless steel with copper plating in the high-current regions near the shorted end of the coaxial resonator. LCW cooling is provided in the annular region between double-shelled inner and outer coaxial conductors of the resonator.

## 25.2 Beam Loading and R/Q

The  $R/Q = 25 \Omega$  of the coaxial cavity resonator for the upgrade has been reduced by a factor of four compared to the existing Main Injector cavities ( $R/Q = 104 \Omega$ ). Since beam loading voltage is proportional to (beam current)  $\times$  ( $R/Q$ ), the beam current can be increased by a factor of four with exactly the same beam loading voltage and influence on beam dynamics as in the current RF system. Thus most of the beam stability requirements for 5x higher beam current in the baseline design will be met automatically by the 4x lower  $R/Q$  design. Only a modest  $(5x/4x) = 1.25x$  increase in normalized beam current will need compensation via improvements in active beam loading compensation and feedback.

Transient beam loading effects will be much smaller and more controlled with direct Linac injection than with synchrotron injection. With linac injection, the beam current is uniform around the ring, and gradually fades in over the 1-3 msec injection period. Only the abort gap transient is present, and is brief enough (800ns or  $\sim 40$  RF cycles) that the cavities can largely coast through it. In contrast, synchrotron injection requires a 100% modulation of the beam loading compensation current over variable fractions of the azimuth, with shocks to the beam loading compensation system as each new batch is injected.

It is possible that operational experience in handling beam currents in excess of the MI design with the existing (high-Q) cavities will provide a basis for increasing the Q of the upgrade cavities. The lower losses would increase the fraction of the RF power available to the beam. The system design would benefit by increased beam current, increased cavity voltage (faster

ramp rate and smaller cycle time), or by reducing the number of RF cavities required. This can be accommodated by varying the amount of copper plating on the cavities.

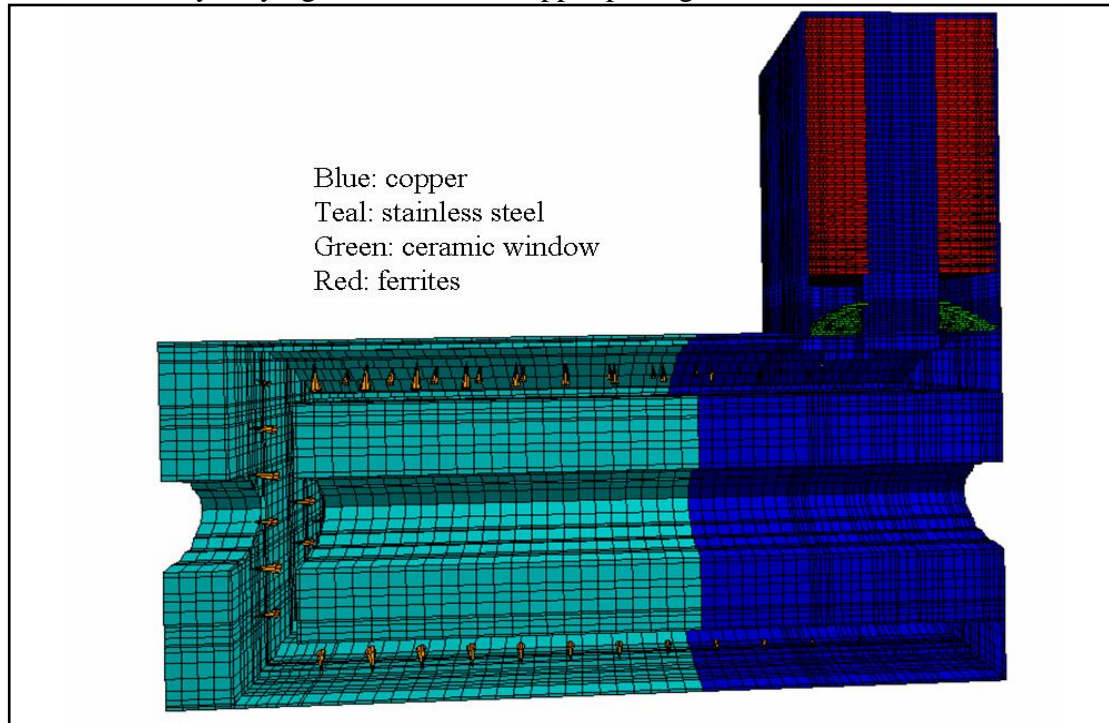


Figure 115 - Electromagnetic Simulations of the Main Injector Upgrade RF Cavity. The Q of the cavity is adjusted by varying the fraction of the cavity that is copper plated. Adjusting the fraction of the cavity which is copper plated allows the Q of the cavity to be adjusted to the design value of 4000, or to higher values (up to ~8000) if desired.

### 25.3 Electromagnetic Design of the RF Cavity

Electromagnetic simulations<sup>193</sup> of the RF upgrade cavity have been carried out using MAFIA and HFSS. Both give consistent results. The RF simulations were used to verify and optimize the cavity operating frequency, tuning range, and RF power coupler designs for the HOM couplers.

### 25.4 YIG Tuner Development

The MI cavity tuners use the same technology (transverse biased YIG loaded coaxial stubs) as the 325 MHz coaxial FVM phase shifters for the Proton Driver Main Linac. See section 14.3. Similar cavity tuners have been used previously for focus-free transition crossing at FNAL<sup>194</sup>.

The required cavity frequency tuning range is 291 kHz which is larger than the natural cavity bandwidth of 13 kHz. Frequency tuning will be provided by a single ferrite stub tuner located at the shorted end. The tuner is a copper coaxial resonator filled with 30 aluminum doped yttrium iron garnets with 0.5 cm garnet separation. It will be perpendicularly biased. The dimensions of the garnets are 32 cm (outer diameter)  $\times$  12 cm (inner diameter)  $\times$  1 cm (thickness). Tuners with dc bias magnetic field transverse to the RF magnetic field have lower ferrite losses and require less ferrite as compared to tuners with parallel bias. The perpendicular bias field will be provided by a single layer of solenoidal coils around the tuner. For transversely biased tuners, the permeability ( $\mu_r$ ) is related to the bias magnetic intensity ( $H_{dc}$ ) by  $\mu_r = 1 +$

$4\pi M_s/H_{dc}$ , where  $4\pi M_s$  is the saturation magnetization of ferrite. During acceleration, the bias field will vary from 300 G to 2250 G to produce a change in  $\mu_r$  of 2.5 to 1.2. For all simulations, a permittivity ( $\epsilon_r$ ) of 13.5 is used for the garnets.

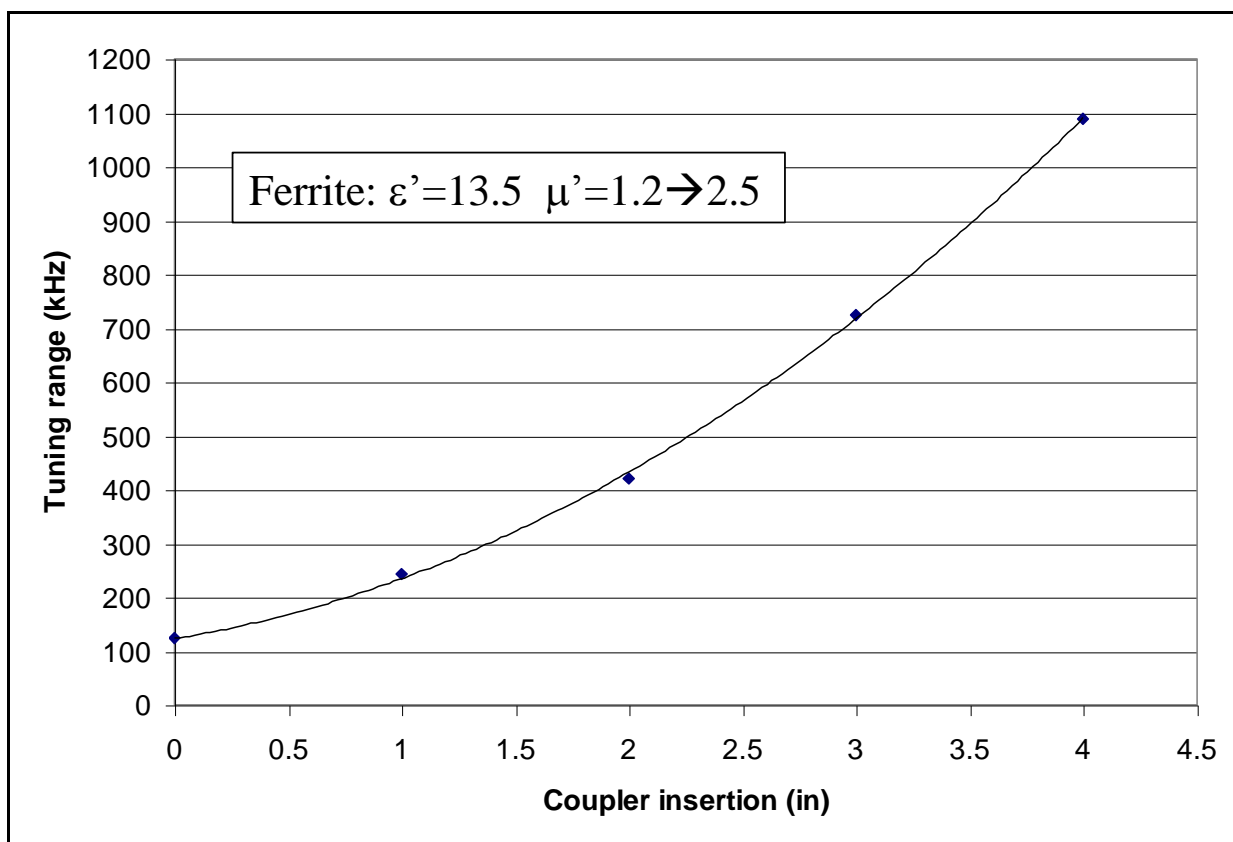


Figure 116 - Tuning Range of Main Injector Upgrade cavity with YIG Ferrite tuner, as a function of the depth of the RF coupler loop insertion distance. The required frequency swing is 291 kHz.

## 25.5 Power Amplifier

The existing power amplifier (PA) will be reused as the driver/preamplifier, adding a final gain stage consisting of a single power tetrode: CPI Eimac 8973 (1 MW) or Thales TH525 (1.5 MW). The prototype is planned using the Thales 1.5 MW tube and socket (on hand). No series modulator tube will be used.

## 25.6 Civil Construction for the RF upgrade

Civil construction for the MI RF upgrade includes:

- 1) An additional 200 GPM of LCW at each of the 18 RF stations in the MI-60 tunnel.
- 2) Additional pulsed AC power of 36 MW peak (~18 MW average) to the MI-60 area.
- 3) A new anode supply building approx. 25' X 300'.

Much of the cooling and AC power capacity could be recovered from surplus made available from the decommissioning of the Linac, Booster, and (possibly) Antiproton facilities. If

necessary, a preliminary plan has been made for an expansion of the MI-60 cooling pond which could provide 100% of the required cooling capacity on an independent basis.

## 26 COST ESTIMATE

A preliminary cost estimate for the *Bare H Injector* was obtained and published<sup>195</sup>. Direct project cost was \$318M (FY04), and the total project cost (TPC, including G&A and Contingency) was \$497M.

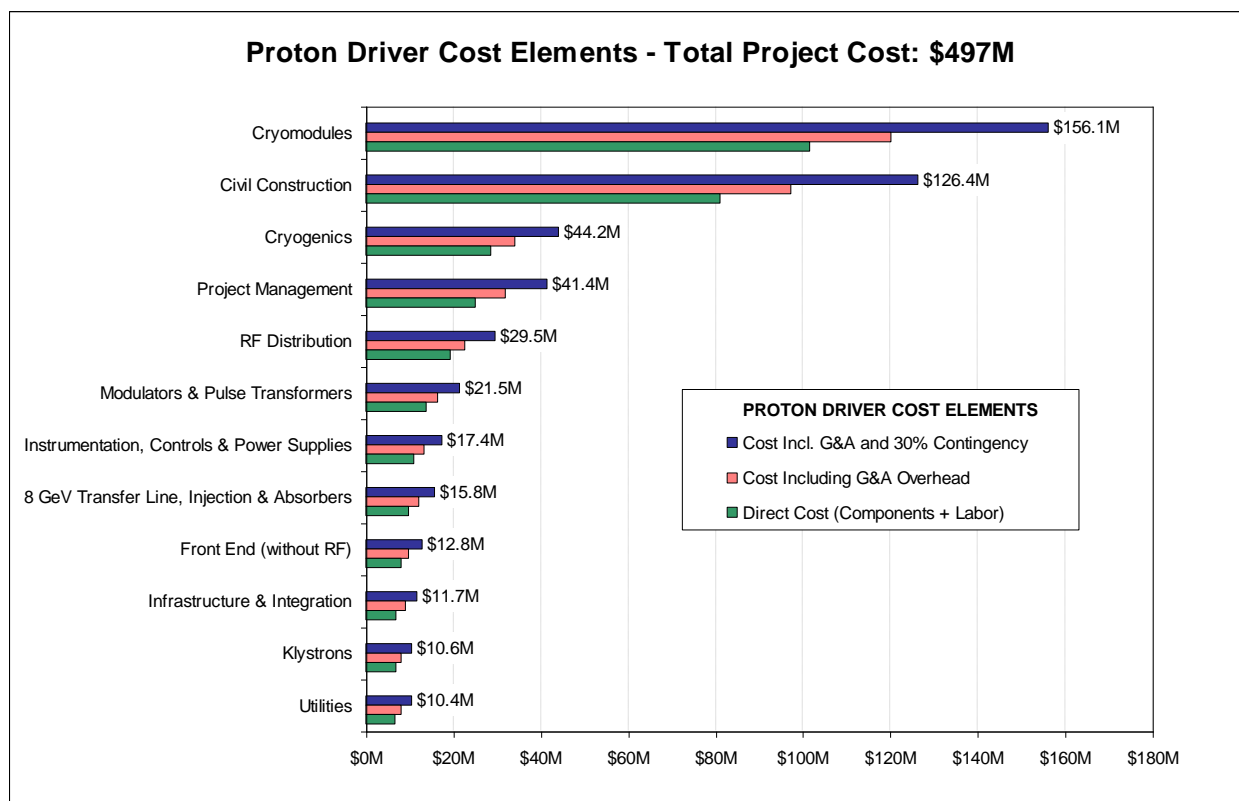


Figure 117 – Distribution of Costs in the Proton Driver Linac

The cost estimate was given brief examination by an external review committee<sup>196</sup> and found to be roughly consistent with recent comparable projects such as the SNS. We note that this is a very different metric than has been applied to past projects at Fermilab: for example, under current accounting rules the SNS spent ~\$300M (more than the Fermilab Main Injector) for a 1 GeV synchrotron ring which does not accelerate the beam<sup>197</sup>. As another example, the Proton Driver TPC includes project management costs of (\$25 M) x (1.3 G&A) x (1.3 contingency) = \$42 M, which is far in excess of what has been budgeted for project management in past FNAL projects. The application of current accounting procedures, however painful for the TPC, is reasonable & prudent if the Proton Driver is to proceed as multi-lab collaboration.

The direct project cost was consistent the previous, less detailed 2002 cost estimate<sup>198</sup> for the Linac Proton Driver. Between 2002 and 2004 a large shift in the Euro/Dollar exchange rate increased the cost for (Euro-denominated) cryomodule and cryoplant components by a factor of ~1.5. It is hoped that the development of U.S. based vendors will recover this cost shift, but at present no credit can be taken for this. Higher G&A rates are also assumed in the present cost estimate. These rates are typically negotiated with lab management as the project is baselined.

## 26.1 Scope of the Cost Estimate

Included in the estimate are:

- all costs associated with civil construction, power & utilities;
- costs for procuring, fabricating and installing all technical components up to and including injection into the Fermilab Main Injector;
- costs to set up tests of production cryomodules at Fermilab
- additional civil construction costs to support the Ultimate linac upgrade
- cost of Project Management (including reviews)

NOT included in the cost estimate are:

- costs of additional beam lines, targets and experiments supported by the Proton Driver
- costs associated with MI Upgrades, including specifically the MI RF Upgrade
- costs for setting up SMTF and the cryomodule factories (assumed to be an ILC collaboration and/or funded under ongoing generic SCRF R&D at Fermilab)
- costs associated with ongoing and near-term R&D efforts
- costs for spares

## 26.2 Methodology

The “baseline” design as defined and documented in the 35-page Parameter Book<sup>10</sup> was used in the cost estimate. This contained detailed component lists, key specifications, etc. for a technically consistent baseline design. Bottom-up cost estimates for major components were obtained from vendor quotes or produced by engineers experienced in the production of recent comparable subsystems. Where possible, the engineers also performed a “reality check” against comparable subsystems at recent projects such as the SNS, FMI, or recent FNAL beam lines.

G&A overheads of 30.4% were applied to labor costs and 16.1% to M&S costs. An across-the-board 30% contingency was applied to all cost elements since a detailed contingency analysis has not been performed. The cost estimate was performed in FY04 dollars, so no escalation to “then-year dollars” has been applied.

The cost estimate is for the baseline (0.5 MW stand-alone linac power) configuration. Costs for the Ultimate upgrade were included only in cases where retrofitting the Ultimate capability would be significantly increased if the up-front investment were not included. Examples of this include RF power couplers and RF distribution capable of supporting the ultimate beam current, LCW and ICW distribution piping sufficient to handle the Ultimate heat load, and AC distribution, ductwork and transformer pads anticipating the Ultimate configuration. The additional cost to the baseline project of supporting the Ultimate upgrade is estimated to be less than \$20 M.

There is substantial *technical* contingency in the baseline design for which no *cost* credit was taken. Examples of this include the fact that the Main Injector can probably cycle ~20% faster than the 1.5 sec cycle time assumed in the baseline; that the modulator and Klystron pulse widths will support a ~15% longer beam pulse than required by the baseline design, and that the installed RF power will in principle support a beam current ~20% above the baseline requirements. This could be relevant since there is some freedom to trade cost against technical performance during project construction; if the project gets into cost trouble, this technical contingency could be “cashed in” by relaxing component specifications without compromising high-level project performance goals.

Finally, no cost credit was taken for the possibility that the Proton Driver Main Linac could serve as an Engineering Test Facility for the International Linear Collider (ILC). Most of the Proton Driver cost is in the  $\beta=1$  main linac, which is technically identical to the ILC.

### 26.3 Major Cost Elements

A spreadsheet was created (available online)<sup>199</sup> with hierarchical expansion to various levels of detail to allow the interested reader to form an opinion about the detail, accuracy, and completeness of the cost estimate. Below is a discussion of the major cost elements, in order of decreasing cost. More details are provided in the review presentations<sup>195,200</sup>.

Two costs are quoted for each element: both the “direct” costs (components + labor), and “burdened” costs (including G&A overhead and contingency). → *Burdened costs are italicized.* The burdened cost is larger than the direct cost by a factor of typically ~1.6, depending on the labor content of the component. See Figure 117.

**Cryomodules (\$102M direct → \$156M *burdened*)** costs were dominated by direct M&S Costs of \$86.7M. Details of the cryomodule cost estimation procedures are given in ref. 200. Approximately 55% of the cryomodule costs were based on quotes obtained specifically for the Proton Driver from experienced SRF vendors. Additional costs were based on TTF and SNS experience, mainly with final assembly and testing costs. Design phase EDIA costs of \$3.3M were assumed on the basis of 500 drawings per cryomodule design x 20 hrs/drawing. This is consistent with LHC and CMS experience at Fermilab. The EDIA estimate assumed that all drawings for all cryomodules would have to be completely reworked at the start of the PD project, which may be pessimistic if we use (as planned) essentially unmodified cryomodule designs from the ILC and Proton Driver R&D efforts.

Assembly Costs were \$10.7 M. This assumes an assembly crew of 18.5 technicians performing a combination of assembly, QC, alignment and testing, spread over 2 facilities for the 1300 MHz and 325 MHz cryomodules. Assembly labor was estimated at 7 weeks/CM for the 325 MHz and 5 weeks/CM for the 1.3 GHz “TESLA” cryomodules, with 4 FTE engineers associated with overseeing the assembly teams. Cryomodule installation costs (\$1.1M) assumed \$10K M&S (rigging/transportation) + 2 techs for 2 weeks + EDIA.

The Spokes-vs.-Elliptical cavity technology choice for the 100 MeV – 400 MeV energy range appears to be cost neutral. Independent cost estimates based on vendor quotes were performed for both the baseline (325 MHz triple spokes) and alternate (1300 MHz elliptical) cavity options. At the present level of accuracy, the costs were the same for both options. This will be revisited after we gain cost and performance experience with both the  $\beta=0.81$  elliptical and spoke cavities being built by Fermilab-led collaborations with MSU/JLAB and ANL.

The final direct cost (\$101M for ~55 cryomodules) indicated that the FY2001 “rule of thumb” that “all cryomodules cost \$1,000,000”<sup>201</sup> needs to be updated to state “all cryomodules cost 1,500,000 Euros” (and also to reflect the recent escalation in the price of steel).

**Civil Construction (\$81M → \$126M)** cost estimates were based on specific facilities descriptions and the drawings of Appendix 2. Bottom-up estimates for each facility were developed based on standard unit costs, including an allowance for vendor overhead and profit.

The costs reflect environmental permitting and wetland mitigation costs. These are estimated to be small for the “inside the ring” footprint that was chosen for the baseline (see sect. 3.6). This footprint is the most flexible footprint option for future site expansion, but is also one of the most costly of the options considered.

The cost estimates were verified against recent experience with comparable civil construction at Fermilab. Civil construction has an inherent ~25% cost uncertainty depending on market conditions. In principle this should be covered by the 30% across-the-board contingency on the project. The major residual cost risk in the civil construction is design uncertainty, particularly if decisions are made to include civil construction to support the broader physics program made possible by the Proton Driver.

**The Cryogenic System (\$28.6M → \$44.2M)** cost estimates were performed by the FNAL Accelerator Division /Cryogenics Department using a cost model from the LHC for refrigeration cost versus capacity. The model also correctly reproduces the actual costs of the SNS cryogenic facility. The cryogenic system costs do not include the civil construction costs for the cryo plant building and support utilities, which are included in the civil construction estimate.

The cost estimate assumes an all-new, purpose built cryogenic plant. The possibility of re-using some of the Tevatron cryogenic infrastructure will be investigated in the next phase of detailed project planning. Removing items such as helium inventory storage, etc. from the project cost will be beneficial. Using CHL for early linac commissioning, with eventual replacement of CHL by a modern and efficient cryoplat, could ease the commissioning schedule and help flatten the obligation profile of the project.

**Project Management (\$25.0M → \$41.4M)** costs were included as a lumped item as per S. Holmes. This is intended to cover management, collaboration, and review costs. Some members of the Director's External Review Committee regarded this allocation as generous. It does not have to cover environmental permitting and construction management costs, which are separately included under civil construction.

**RF Distribution (\$19.2M → \$29.5M)** costs include a large number of standard catalog items (such as waveguide, circulators, directional couplers, RF loads...) plus a single lumped (28%) top-down allocation for the Ferrite Vector Modulators and their drive electronics.

Vendor quotes were obtained for the complete set of "standard" RF components in the baseline design. Pricing from U.S and Western European vendors was used. If a decision is made to use offshore vendors (as was done for parts of the TESLA cost estimate, but not for the SNS project), substantial cost reductions could result for many components.

The Ferrite Vector Modulators represent the largest area of cost uncertainty. Although a commercially built unit is on order, no full-spec prototype exists, and the vendor indicated that the price was a strong function of the final specification for response time and range of adjustment. The FVM drive electronics are expected to be a dominant cost in the system. This will be firmed up after the performance of the prototype electronics (sect. 14.7) is demonstrated.

RF installation costs were estimated at roughly 10% of materials costs. Installation oversight is budgeted separately in the Infrastructure and Integration (I&I) cost element. The EDIA for the RF systems is a top-down estimate which is inconsistent with the SNS EDIA for their RF systems. This remains to be understood, and may be related to the multi-lab collaboration nature of the SNS project.

**Modulators and Pulse Transformers (\$13.9M → \$21.5M)** costs were estimated<sup>202</sup> by D. Wolff on the basis of the actual costs of the most recent two TESLA/TTF modulators his group built. Corrections were made for inflation (1996→2002), technological improvements in capacitors, IGBT switches, and controls; and for the larger quantities of identical components. Two new

modulators being built for SMTF will be used to update the costs. The total of 14 modulators to be built includes two test stands which also serve as spares.

**Instrumentation, Controls, and Power Supplies (\$11.0M → \$17.4M)** costs were included as a lump sum. This item does not have to cover modulator controls, power supplies, or klystron protection circuitry, which are separately included in the modulator cost. It does not have to cover the FVM drive electronics, which are included in the FVM costs. It does not have to cover the Cryogenic, vacuum system, or LCW controls which are covered as part of these subsystems. Safety and interlock systems are separately budgeted under the I&I category.

Major items in the linac electronics are the LLRF cavity resonance control and beam instrumentation systems. In the one-klystron-feeds-many-cavities approach, there are approximately 20 channels of electronics (and their cable pulls) associated with each cavity (~8000 channels total). At \$1500/channel this uses up 2/3 of the electronics budget. A bottom-up cost estimate based on the actual electronics channel counts (sect. 22) and rack and cable layouts will be performed in the next cost iteration.

Power supplies can be estimated either on a per-channel or a per watt basis. At \$5/watt, the 37kW of supplies (Table 32) would be \$185K (probably too low). Since most of the 468 channels are similar or identical to corrector supplies in use at Fermilab, at an estimated installed cost of \$2k/channel this is less than a million dollars.

**8 GeV Transfer Line, H<sup>-</sup> injection, and Beam Absorbers (\$9.9M → \$15.8M)** were estimated by D. Harding on the basis of Main Injector beamline costs and recent beam lines at Fermilab. The detailed breakdown is available online<sup>199</sup> and includes 8 GeV Transfer Line Magnets, Power Supplies, Vacuum System, beamline Instrumentation, Injection Magnets, Injection Power Supplies, Beam Absorbers and Miscellaneous Elements.

This does not have to cover the civil construction costs for these items, or their associated water cooling systems, which are included in the civil construction estimate.

The injection region and collimation hardware represents an area of cost uncertainty, since no detailed technical design exists. The allocation is smaller than the SNS costs for their comparable systems. The estimate reflects a 100% in-house effort at FNAL, and the costs may be affected if a decision is made to pursue the transfer line as a multi-lab collaboration.

**Front End Linac (\$8.1M → \$12.8M)** costs, (not including the RF systems), were estimated at a component-by-component level. These will be updated based on actual costs of the prototype front-end system being built as part of the SMTF/Meson effort. No credit was taken for the possible re-use of the components built at SMTF/Meson (which may ultimately serve as spares), or the probable re-use of successfully demonstrated designs and documentation.

**Infrastructure and Integration (\$6.9M → \$11.7M)** costs include: Interlocks, Installation Coordination, Component Transportation & Installation, Alignment, Misc. Cabling and Electrical Integration, and Support for PD Testing at SMTF. This cost will be iterated following development of a detailed installation plan, and cost experience with the front end tests at SMTF/Meson.

**Klystron (\$6.9M → \$10.6M)** costs were obtained from (FY04) vendor quotes from Thales for the 1300 MHz multi-beam klystron, and the actual cost (FY05) of the 325 MHz klystron purchased for the front end tests at SMTF/Meson. Development costs related to demonstrating

the 4.5 msec pulse widths for the baseline design were assumed to be covered by the ongoing R&D program. As is traditional for recent FNAL construction projects, spare Klystrons (as well as other spare items) were assumed to be covered off-project.

**Utilities (\$6.7M → \$10.4M)** included the LCW and vacuum systems costs. The LCW systems included all piping, pumps, and installation inside the enclosures, and the ICW systems (outside the enclosures) were included as part of the civil construction estimate. The online spreadsheet<sup>199</sup> contains a bottom-up estimate of each of these systems.

## Appendix 1 – MULTIPLE MISSIONS FOR THE PROTON DRIVER LINAC

### Running Electrons and Protons in the same Linac

Although not in the baseline design, the 8 GeV Proton Driver linac design anticipates the possibility of running both protons and relativistic particles (electrons or muons) in the  $\beta = 1.00$  section (the last 6.7 GeV) of the linac. The  $\beta < 1$  sections are not shared.

This section discusses several accelerator physics and technical issues which arise for interleaving protons and electrons in the same linac: 1) the efficiency for accelerating electrons with cavity groups designed for lower  $\beta$  protons, 2) the cavity-to-cavity phase shifts needed when switching between e- and p while driving many cavities from a single klystron, and 3) sharing the transverse focusing lattice (quadrupole strengths) between protons and electrons of different momenta.

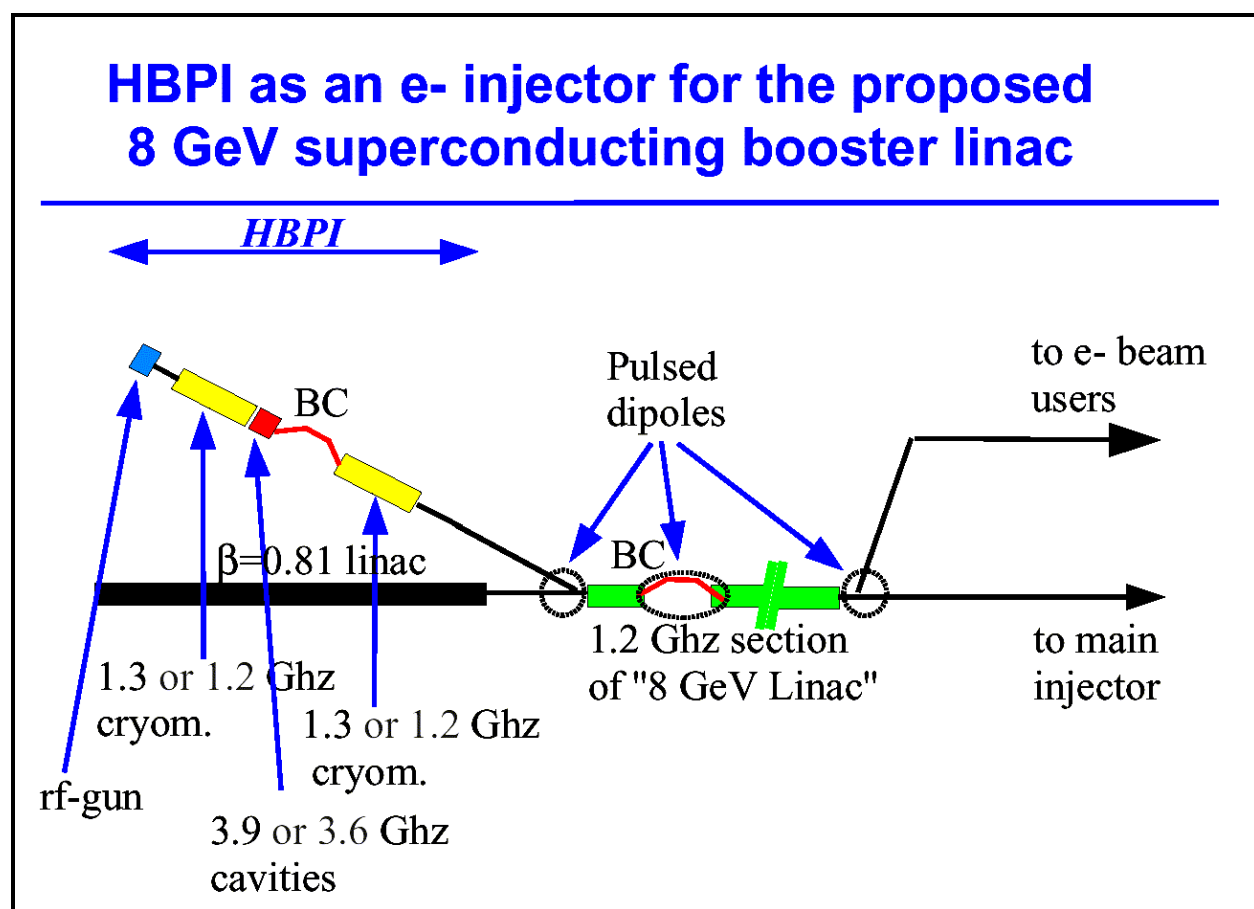


Figure 118 – Concept for sharing the main  $\beta=1$  section of the Proton Driver linac between H-/protons and electrons (from ref. 203). The electron photoinjector could be located in a parallel tunnel stacked on top of the tunnel for the RFQ/DTL front end of the H/proton linac, so that the infrastructure of the klystron gallery and front-end building can be shared. Stacking the tunnels should be possible because of the modest shielding requirements for the front end linac.

The  $\beta = 1.00$  cavities in the last 7 GeV of the Proton Driver linac can obviously accelerate relativistic electrons and muons. The energy gain will actually be larger for electrons

than for protons because: a) the  $\beta$  match is perfect for all energies (see Figure 46), b) electrons are accelerated at nearly zero synchronous phase (i.e. on the crest of the RF) whereas the synchronous phase for protons is in the range of 15-20°, and c) the RF power overhead required for resonance regulation in electron machines (e.g. 6% for the TESLA TDR) is typically smaller than the 10-30% margin assumed in this design study (Figure 64). As a result the  $\beta = 1.00$  section of the proton linac should provide more than 8 GeV of energy gain for electrons and relativistic muons.

The energy stability requirements for electrons will depend on the application. The Proton Driver RF system contains all capabilities of the TESLA/XFEL “Vector Sum Regulation” LLRF system, plus the additional per-cavity capabilities of the Ferrite Vector Modulators. LLRF and clock distribution specifications are typically tighter for ILC/XFEL applications than for proton linacs, but these tighter specifications might be met at small additional cost if modern, common hardware is used for both projects.

### Cavity phase shifts between $e^\pm$ and p with many cavities per klystron.

The phase of the RF drive to each cavity must be adjusted when switching between electrons and protons. If a single large klystron is used to drive many cavities, the klystron drive can be adjusted to provide zero phase error at the center of the group of cavities. However the difference in the time of flight between electrons and protons will create additional phase errors for cavities at the ends of each group. These phase shifts are plotted for the Ultimate scenario (12 cavities per Klystron) in Figure 119. The phase shifts for the baseline (36 cavities/Klystron) are 3x larger. In any case, a full 360-degree phase shift is needed on at least some channels.

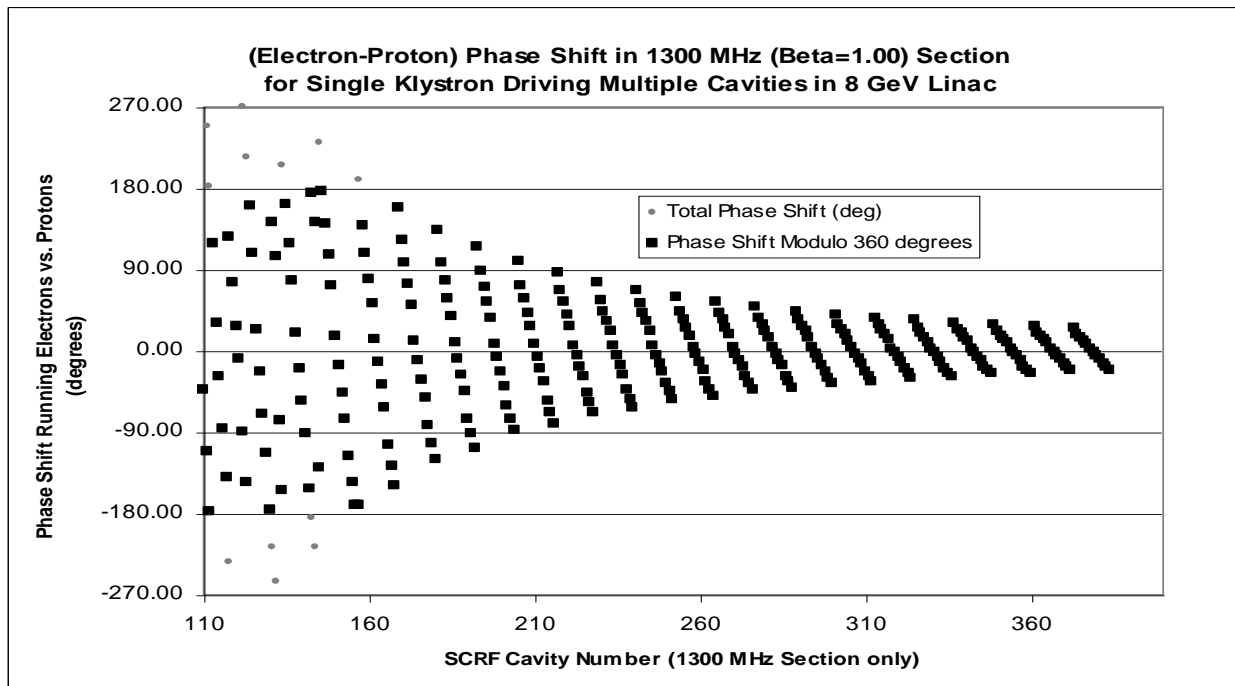


Figure 119 – “Slow” phase shift required in cavity drive when changing between electrons and protons in the Proton Driver linac. A single 1300 MHz klystron drives a group of 12 cavities in the  $\beta = 1$  section. The klystron phases are adjusted for zero phase error in the middle of each group of cavities, but differences in the time-of-flight create phase errors at the end of each group. These phase errors must be corrected by individual phase tuners on each cavity.

### **Sharing Transverse Focusing between Electrons and Protons**

Currents in the quadrupoles of the beta=1.00 section are ramped in the 0.1 seconds between Linac pulses to allow electrons and protons of different momenta to share the quadrupole lattice. (The alternative of keeping linac quadrupoles at DC, while feasible<sup>204</sup> in the high-energy end of the linac, requires an electron injector of ~1 GeV.

A related question is the peaceful coexistence of the bunching chicanes, etc. normally found in electron linac with the frequent longitudinal focusing normally required for nonrelativistic protons. This could be the subject of an interesting design workshop involving both  $e^+$  / FEL and  $H^+$  / ion linac physicists.

## **Appendix 2 - CIVIL CONSTRUCTION DETAILED FACILITIES DESCRIPTIONS**

Construction of the below grade enclosures and above grade service buildings will be similar to previously utilized and proven construction methods at Fermilab. Conventional facilities will be constructed to accommodate both the baseline design and a future upgrade to the Ultimate (2 MW stand-alone linac beam power) configuration.

Sustainability is broadly defined as the design and implementation of projects to simultaneously minimize their adverse environmental impacts, maximize occupants' health and well-being, and improve bottom line economic performance. The concept of sustainability is a desirable approach to development that recognizes that resources are limited, and that there is a responsibility of the present generation to preserve resources for future ones. The project processes and each project element will be evaluated during design to reduce their impact on natural resources without sacrificing program objectives. The project design will incorporate maintainability, aesthetics, environmental justice and program requirements to deliver a well-balanced project.

Provisions for radiation, fire protection and conventional safety will be addressed in detail during facility design. Quality assurance provisions will be part of all project phases including conceptual, preliminary, and final design, construction, and construction management.

The attached drawings show locations and dimensions of all features of the civil construction described below:

### Earthwork and Utilities

Site drainage will be controlled by ditches and culverts while preserving the existing watershed characteristics both during construction and subsequent operation.

Road construction is anticipated for this project. A temporary construction road will be extended from the existing Swenson Farm Road off SR 56. A new road will be constructed from the southeast side to the west side of Main Ring Road to parallel the new Linac and Klystron Gallery. Main Ring Road will be upgraded for anticipated traffic from A-0 Road to the new road at the Linac. The road and the adjacent cooling pond will require steel shielding for adequate radiation shielding protection. Kautz Road near MI-62 will need to be rebuilt as part of the Transport Line construction. Parking lots will be constructed at each building.

Power and communications will tie into existing systems. Machine power at 3.02 MW will come from Master Substation (MSS) via existing duct bank of feeder 41 to the WH footprint area, which then be extended via new duct bank to western end of the Linac. Conventional power of 1.04 MW will be supplied from MSS via existing duct bank of feeder 40, which then will be extended via new duct bank to the Pump Service Building. Redundant power for both these electrical feeds will be from Kautz Road Substation (KRS) via new duct banks. 0.94 MW of power for the cryogenics will be from existing feeder 46B (MSS) already existing in the Main Ring duct bank system. Redundancy for this will be feeder 46A (KRS). Backup for the

cryogenics is via existing overhead power from Frog Farm Substation, and via new duct bank from near MI-20 to the Cryo Service Building.

Industrial cooling water, sanitary sewer, and domestic water will tie into existing utilities at the CDF-D0 Utility Corridor and at MI-60, creating a loop for these systems. Cooling water will be taken from CUB via new piping to the Pump Service Building at the midpoint of the Linac.

Excess spoil from the construction of the underground enclosures will be stockpiled on the Fermilab site in an appropriate manner during construction, and then be used to raise the grade of the service buildings and klystron gallery to improve drainage at the buildings.

### Landscaping

Construction yards will be removed after completion of the construction phase of the project. All disturbed areas will be returned to a natural state or landscaped in a similar manner as found at other Fermilab experimental facilities. Erosion control will be maintained during all phases of construction.

### Linac Enclosure

The linac enclosure is a 2200 ft long, cast-in-place concrete enclosure, 15' wide and 11' high, with 24.5' of equivalent earth radiation shielding at the berm, and 26' of shielding at structures. Construction will be with standard cut and cover excavation methods. Walls and roofs may be pre-cast as U-shaped elements, as in past Fermilab enclosure projects. It will be located at the same floor elevation as the existing Main Injector tunnel. This region will house beam line components to accelerate protons from 0 to 8 GeV.

### Transport Line Enclosure

The transport line enclosure is a 3411 ft long, cast-in-place concrete enclosure, 10' wide and 8' tall with 24.5' of equivalent earth radiation shielding at the berm, and 26' of shielding at structures. It will be located at the same floor elevation as the existing Main Injector tunnel. This region will house beam line components to transport protons from the linac to Q104. Construction methods will be similar to the Linac Enclosure. Where the Transport Line enclosure crosses the Main Ring and Antiproton enclosures, it is anticipated the existing enclosures will be removed and replaced to allow the Transport Line to be built below them. Connection at the Main injector enclosure will require rebuilding of some length of the 8 GeV and Main Injector enclosures.

### Linac Beam Absorber

The beam absorber will be similar to the existing beam absorber at MI-40. This below grade cast-in-place concrete structure will entomb an absorber capable of handling the power emitted by the 8 GeV 2 MW beam. Steel shielding will be 9'x9'x20' long, concrete shielding will be 16'x16'x26' long. The room size will be 18'-4 high x 23' wide x 52' long, with concrete walls minimum 0.5 m thickness, and roof 3' minimum thickness, with a ceiling space of 3.5'. The floor of the absorber will be located at the same elevation as the rest of the new enclosures.

### Injection Beam Absorber

Located downstream of the injection point at Q104, the injection absorber will be comparable to or smaller than the linac beam absorber. Due to the existing surrounding enclosures, some of the existing tunnel in the area will require rebuilding to accommodate the beam pipe to the absorber. The scope of the injection beam absorber depends on the detailed design of the foil stripping injection hardware (particularly the fraction of the beam expected to escape stripping in the foil). This detailed design work has not taken place.

### Upstream Service Building (L-0)

The Upstream Service Building is a 7500 square foot industrial steel-framed building with metal siding. Approximately 5000 square feet will be a high bay area with overhead crane and drop hatch, utilized to access the beamline enclosure. The remaining 2500 square feet will be a low bay used for control, testing and office space. See attached sketches for location and dimensions.

### Klystron Gallery Building (L-1)

The Klystron Gallery will have an interior clear space of 18' wide and 12' high, and of similar construction to the Upstream Service Building. It will parallel the linac enclosure for a total length of 2200 ft, and be integral with the Upstream and Pump Service Buildings. Overall size will be approximately 39,600 square feet. The building will house klystrons, power supplies and relay racks necessary to support the RF cavities housed in the adjacent enclosure. Thirty-six waveguide chases will be constructed between the building and the enclosure to carry RF waveguides and cables.

### Cryo Service Building (L-10)

The Cryo Service Building will be a 12,000 square foot high bay industrial building similar to the SNS cryogenic facility. This facility houses all equipment required to supply cryogenics to the superconducting cavities and to reject heat from the LCW system. The building may also include a test stand facility. The straight penetration to the tunnel will be from the building floor to the sidewall of the cryo alcove below. To allow sufficient space for material deliveries during operation, this building will be located on the far side of the road from the gallery building.

### Pump Service Building (L-11)

The Pump Service Building will house LCW pump equipment and heat exchangers. It will be located across the road from the Cryo Service Building, and provide an access to the beamline enclosure. Construction will be similar to typical Fermilab service buildings with structural steel framing and metal siding.

### Arc Service Building (L-23)

The Arc Service Building will house magnet power supplies and other controls. Its construction will be similar to the Pump Service Building.

Center Service Building (L-25)

The Center Service Building is located north of the enclosures and will provide personnel and equipment access via an enclosure that intersects the Transfer Line Enclosure near its upstream end. The building crane and hatch will be sized to handle cryomodules and magnets.

Debuncher/Transport Line Service Building (L-42)

The Debuncher Service Building will be a 5000 square foot industrial building. Construction will be similar to the Pump Service Building. This building will house all equipment to supply electrical services to the Debuncher. The building will also be utilized for magnet power supplies.

### **Appendix 3 - CIVIL CONSTRUCTION FIGURES**

1. Site Plan
2. Criteria and Utility Plan
3. Plan & Profile Through AP/TeV Enclosures
4. Plan and Profile at MI Connection
5. MI – Proton Driver linac Transport Connection
6. Linac Beam Absorber and L-25 Service Building
- 6A L-25 Center Building and Hatch Section
7. L-0 Upstream Service Building
8. Klystron Gallery Floor Plan
9. SNS Central helium Liquefier
10. Klystron Gallery and Beamline Enclosure
11. Section at Main Ring & AP0 Crossover
12. Transport Line Enclosure
13. Beamline Enclosure Exit Stair Plan
14. Stair Sections
15. Cooling Schematic – Ultimate Configuration
- 16A. Cryoplant Power – Electrical Single Line
- 16B. Conventional Power – Electrical Single Line
- 16C. Machine Power – Electrical Single Line

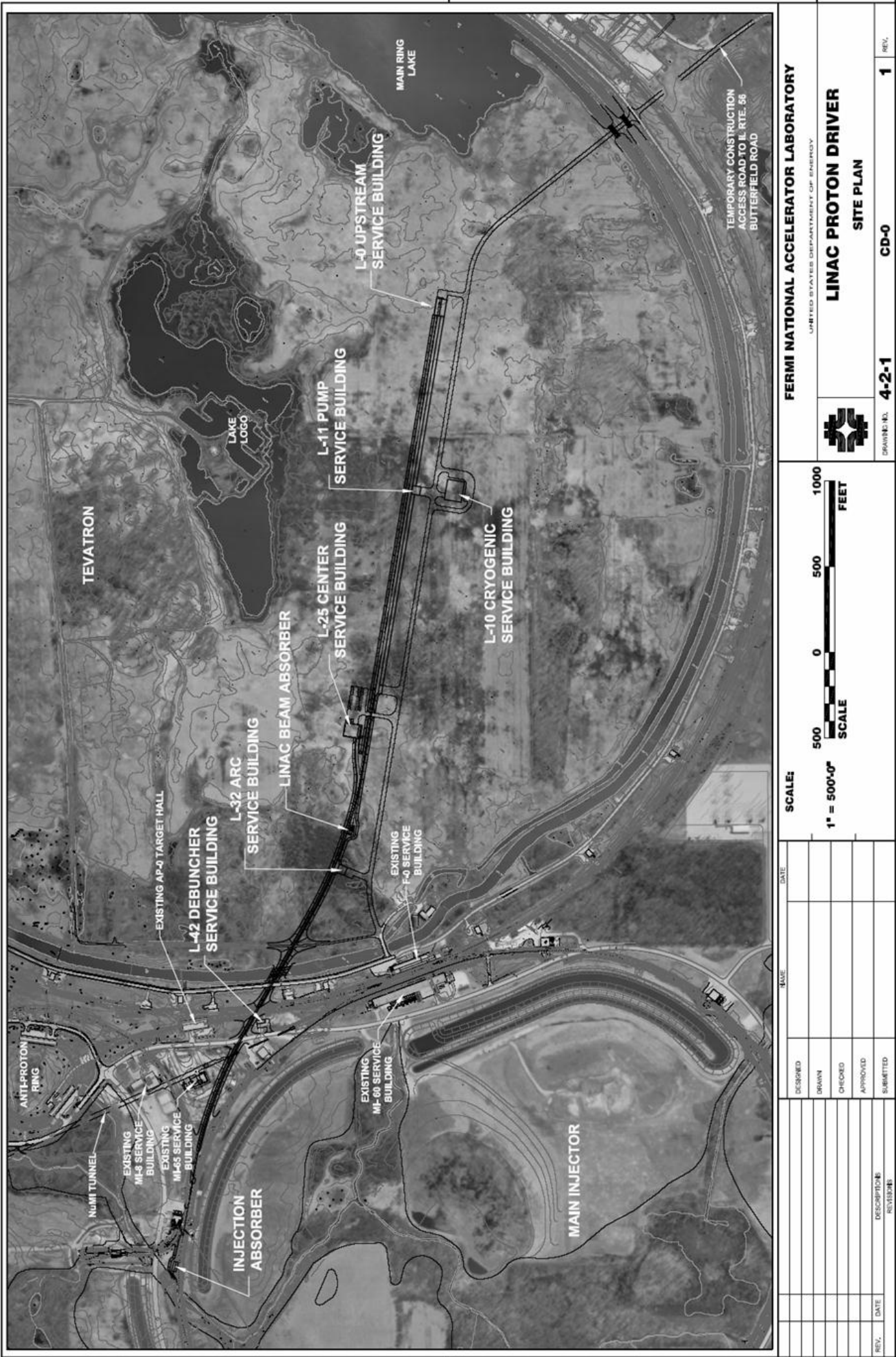
These drawings are available electronically as a .PDF file at:

[http://tdserver1.fnal.gov/8gevinacPapers/FESS\\_Civil\\_Construction\\_Drawings/LINAC%20PROTON%20DRIVER%20CIVIL%20COMPILED%20DWGS%20MAR%202005/LINAC%2520PROTON%2520DRIVER%2520CIVIL%2520COMPILED%2520DWGS%2520MAR%25202005.pdf](http://tdserver1.fnal.gov/8gevinacPapers/FESS_Civil_Construction_Drawings/LINAC%20PROTON%20DRIVER%20CIVIL%20COMPILED%20DWGS%20MAR%202005/LINAC%2520PROTON%2520DRIVER%2520CIVIL%2520COMPILED%2520DWGS%2520MAR%25202005.pdf)

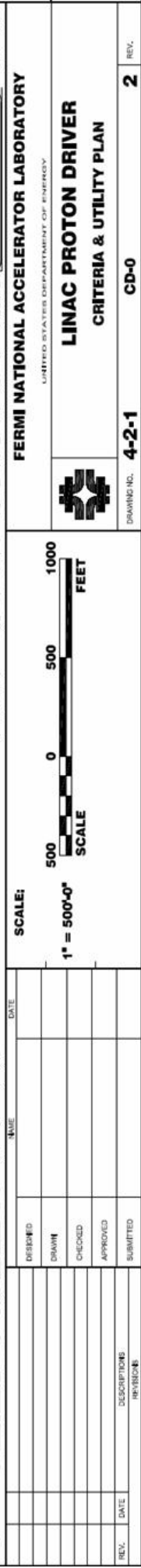
and as a PowerPoint file at:

[http://tdserver1.fnal.gov/8gevinacPapers/FESS\\_Civil\\_Construction\\_Drawings/CivilDrawingsMarch05.ppt](http://tdserver1.fnal.gov/8gevinacPapers/FESS_Civil_Construction_Drawings/CivilDrawingsMarch05.ppt)

1. Site Plan



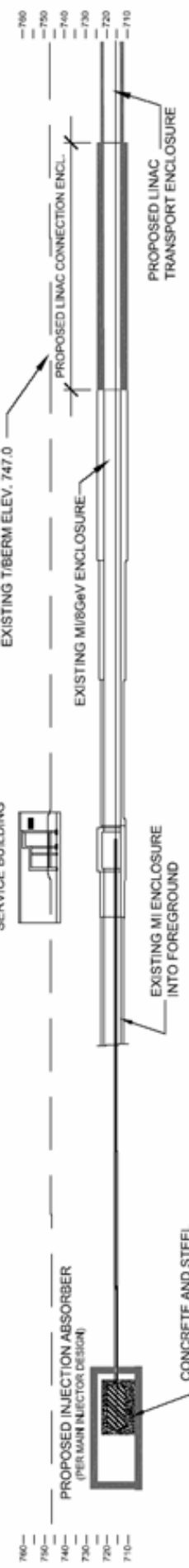
--	--	--	--	--	--	--	--	--	--	--	--	--	--	--	--	--	--	--	--	--	--	--	--	--	--	--	--	--	--	--	--	--	--	--	--	--	--	--	--	--	--	--	--	--	--	--	--	--	--	--	--	--	--	--	--	--	--	--	--	--	--	--	--	--	--	--	--	--	--	--	--	--	--	--	--	--	--	--	--	--	--	--	--	--	--	--	--	--	--	--	--	--	--	--	--	--	--	--	--	--	--	--	--	--	--	--	--	--	--	--	--	--	--	--	--	--	--	--	--	--	--	--	--	--	--	--	--	--	--	--	--	--	--	--	--	--	--	--	--	--	--	--	--	--	--	--	--	--	--	--	--	--	--	--	--	--	--	--	--	--	--	--	--	--	--	--	--	--	--	--	--	--	--	--	--	--	--	--	--	--	--	--	--	--	--	--	--	--	--	--	--	--	--	--	--	--	--	--	--	--	--	--	--	--	--	--	--	--	--	--	--	--	--	--	--	--	--	--	--	--	--	--	--	--	--	--	--	--	--	--	--	--	--	--	--	--	--	--	--	--	--	--	--	--	--	--	--	--	--	--	--	--	--	--	--	--	--	--	--	--	--	--	--	--	--	--	--	--	--	--	--	--	--	--	--	--	--	--	--	--	--	--	--	--	--	--	--	--	--	--	--	--	--	--	--	--	--	--	--	--	--	--	--	--	--	--	--	--	--	--	--	--	--	--	--	--	--	--	--	--	--	--	--	--	--	--	--	--	--	--	--	--	--	--	--	--	--	--	--	--	--	--	--	--	--	--	--	--	--	--	--	--	--	--	--	--	--	--	--	--	--	--	--	--	--	--	--	--	--	--	--	--	--	--	--	--	--	--	--	--	--	--	--	--	--	--	--	--	--	--	--	--	--	--	--	--	--	--	--	--	--	--	--	--	--	--	--	--	--	--	--	--	--	--	--	--	--	--	--	--	--	--	--	--	--	--	--	--	--	--	--	--	--	--	--	--	--	--	--	--	--	--	--	--	--	--	--	--	--	--	--	--	--	--	--	--	--	--	--	--	--	--	--	--	--	--	--	--	--	--	--	--	--	--	--	--	--	--	--	--	--	--	--	--	--	--	--	--	--	--	--	--	--	--	--	--	--	--	--	--	--	--	--	--	--	--	--	--	--	--	--	--	--	--	--	--	--	--	--	--	--	--	--	--	--	--	--	--	--	--	--	--	--	--	--	--	--	--	--	--	--	--	--	--	--	--	--	--	--	--	--	--	--	--	--	--	--	--	--	--	--	--	--	--	--	--	--	--	--	--	--	--	--	--	--	--	--	--	--	--	--	--	--	--	--	--	--	--	--	--	--	--	--	--	--	--	--	--	--	--	--	--	--	--	--	--	--	--	--	--	--	--	--	--	--	--	--	--	--	--	--	--	--	--	--	--	--	--	--	--	--	--	--	--	--	--	--	--	--	--	--	--	--	--	--	--	--	--	--	--	--	--	--	--	--	--	--	--	--	--	--	--	--	--	--	--	--	--	--	--	--	--	--	--	--	--	--	--	--	--	--	--	--	--	--	--	--	--	--	--	--	--	--	--	--	--	--	--	--	--	--	--	--	--	--	--	--	--	--	--	--	--	--	--	--	--	--	--	--	--	--	--	--	--	--	--	--	--	--	--	--	--	--	--	--	--	--	--	--	--	--	--	--	--	--	--	--	--	--	--	--	--	--	--	--	--	--	--	--	--	--	--	--	--	--	--	--	--	--	--	--	--	--	--	--	--	--	--	--	--	--	--	--	--	--	--	--	--	--	--	--	--	--	--	--	--	--	--	--	--	--	--	--	--	--	--	--	--	--	--	--	--	--	--	--	--	--	--	--	--	--	--	--	--	--	--	--	--	--	--	--	--	--	--	--	--	--	--	--	--	--	--	--	--	--	--	--	--	--	--	--	--	--	--	--	--	--	--	--	--	--	--	--	--	--	--	--	--	--	--	--	--	--	--	--	--	--	--	--	--	--	--	--	--	--	--	--	--	--	--	--	--	--	--	--	--	--	--	--	--	--	--	--	--	--	--	--	--	--	--	--	--	--	--	--	--	--	--	--	--	--	--	--	--	--	--	--	--	--	--	--	--	--	--	--	--	--	--	--	--	--	--	--	--	--	--	--	--	--	--	--	--	--	--	--	--	--	--	--	--	--	--	--	--	--	--	--	--	--	--	--	--	--	--	--	--	--	--	--	--	--	--	--	--	--	--	--	--	--	--	--	--	--	--	--	--	--	--	--	--	--	--	--	--	--	--	--	--	--	--	--	--	--	--	--	--	--	--	--	--	--	--	--	--	--	--	--	--	--	--	--	--	--	--	--	--	--	--	--	--	--	--	--	--	--	--	--	--	--	--	--	--	--	--	--	--	--	--	--	--	--	--	--	--	--	--	--	--	--	--	--	--	--	--	--	--	--	--	--	--	--	--	--	--	--	--	--	--	--	--	--	--	--	--	--	--	--	--	--	--	--	--	--	--	--	--	--	--	--	--	--	--	--	--	--	--	--	--	--	--	--	--	--	--	--	--	--	--	--	--	--	--	--	--	--	--	--	--	--	--	--	--	--	--	--	--	--	--	--	--	--	--	--	--	--	--	--	--	--	--	--	--	--	--	--	--	--	--	--

$$\begin{array}{c} SC \\ PM \end{array}$$


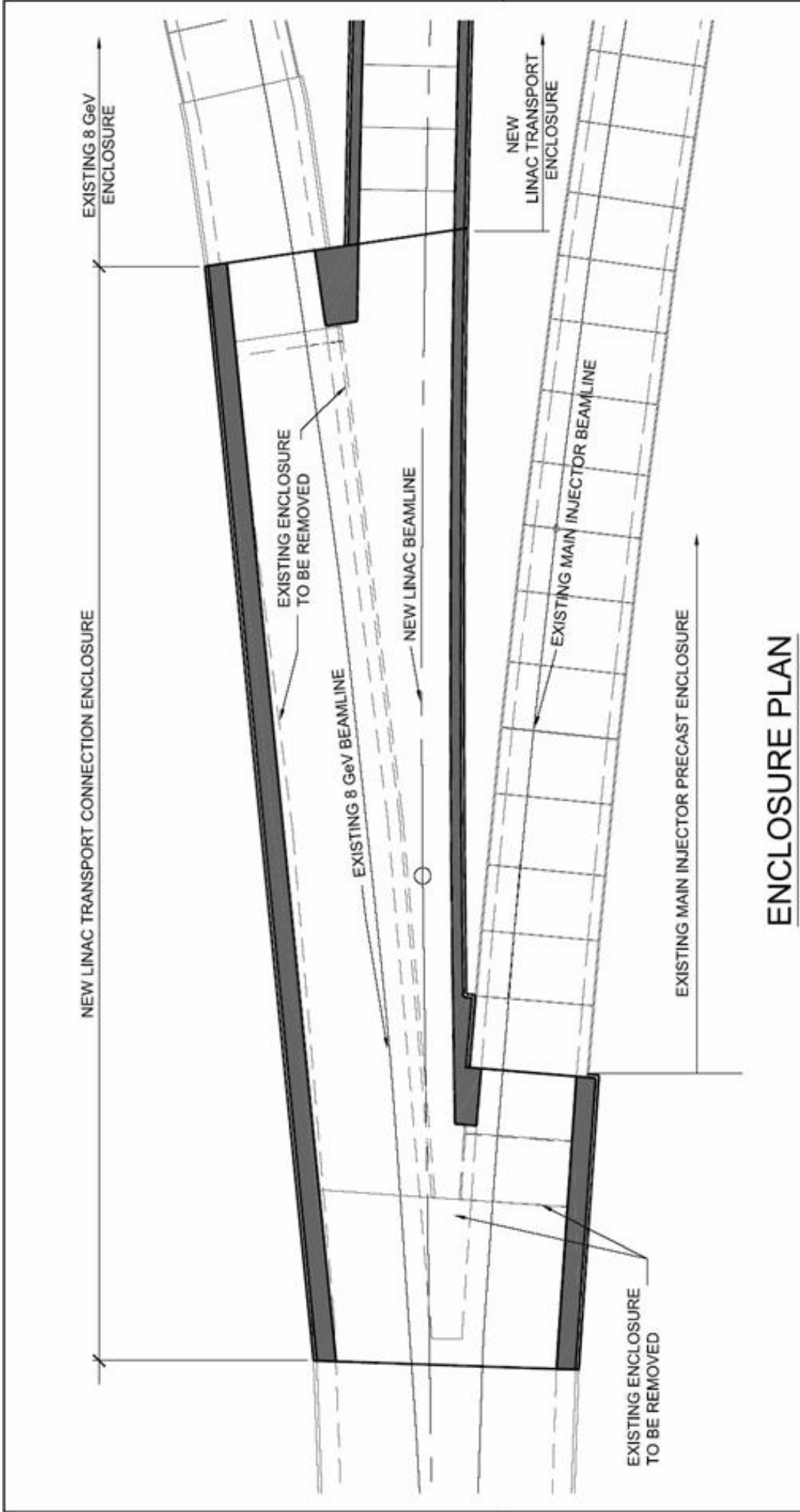
[illegible]

[illegible]

# SITE PLAN

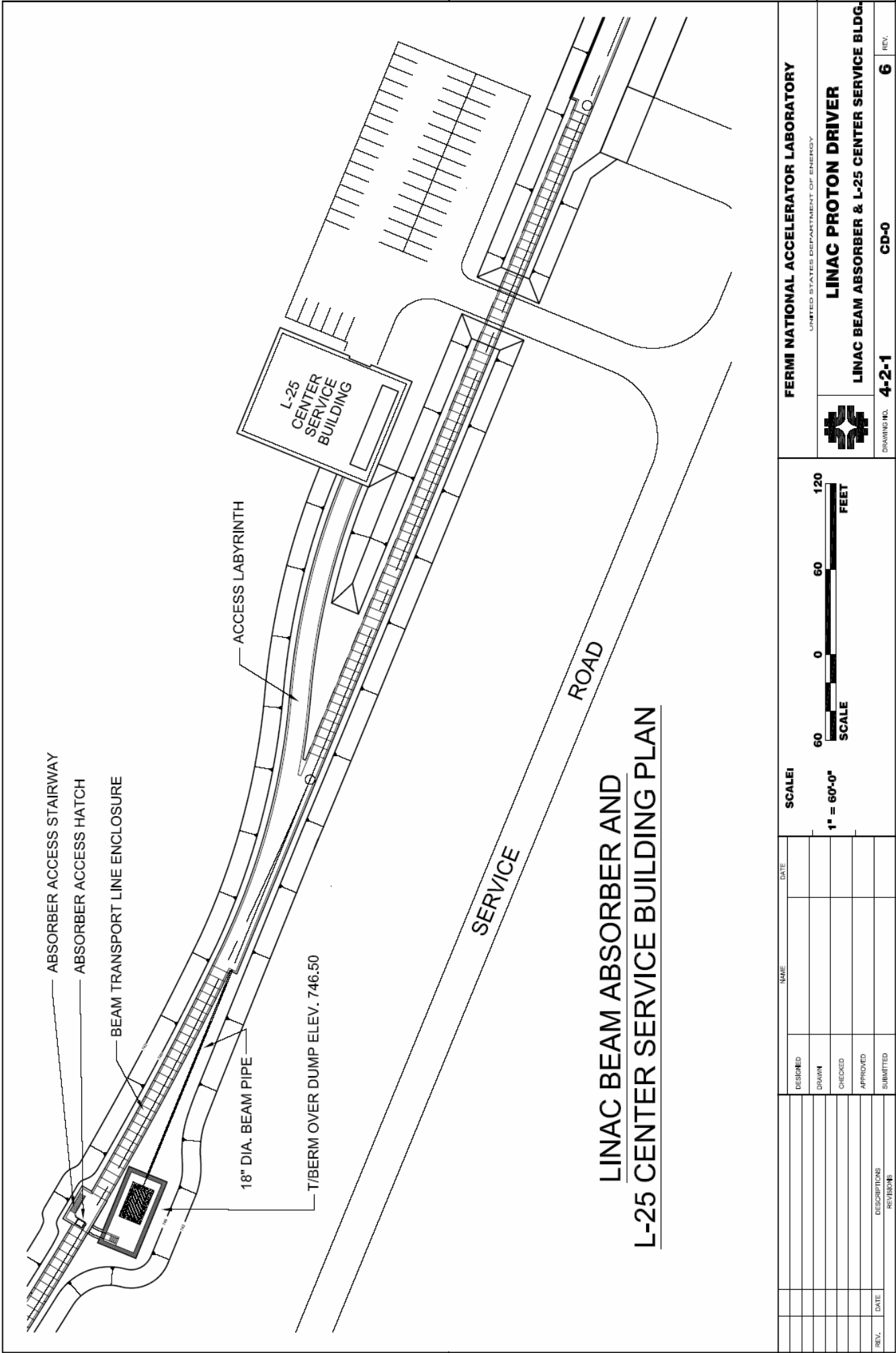
[illegible]

# 5. MI - 8 GeV Linac Transport Connection



FERMI NATIONAL ACCELERATOR LABORATORY				CD-0		5
LIMITED STATUS EXPERIMENT OF ENERGY				REV.		
LINAC PROTON DRIVER				MI - 8GeV / LINAC TRANSPORT CONNECTION		
DRAWING NO. 4-2-1				REV.		
SCALE: 1" = 10'-0"				FEET		
DATE				DATE		
DESIGNED				DATE		
DRAWN				DATE		
CHECKED				DATE		
APPROVED				DATE		
SUBMITTED				DATE		
DESCRIPTION: MI-8GeV				DATE		

# 6. Linac Beam Absorber and L-25 Service Building



80'-0" CRANE SPAN

MIN. 3" CLEAR TO OBSTRUCTION

3 1/2" CRANE RAIL

ROOF BEAM

2'-10" TROLLEY

20 TON TOP RIDING BRIDGE CRANE.

EL. 742'-6"

EL. 713'-6"

62'-6"

18'-1" (CLEAR) 3'-2" CRANE GIRDER

28'-6 1/2" FROM FLOOR TO T/STEEL

ACCESS LABYRINTH

12'-0" WIDE

8'-0"

SCALE: 3/32" = 1'-0"

0 4 8 12 16 20 24 28 FEET

LONGITUDINAL SECTION THROUGH PIT & BUILDING

L-25 CENTER SERVICE BUILDING

REV.	DATE	DESCRIPTION	BY	DATE	SCALE	DATE
DESIGNED						
DRAWN						
CHECKED						
APPROVED						
SUBMITTED						

FERMI NATIONAL ACCELERATOR LABORATORY  
UNITED STATES DEPARTMENT OF ENERGY

6A

CD-0

4-2-1

REVISIONS

DATE

DESCRIPTION

BY

DATE

APPROVED

CHECKED

DRAWN

DESIGNED

SCALE

DATE

0 4 8 12 16 20 24 28 FEET

3/32" = 1'-0"

ACCESS LABYRINTH

12'-0" WIDE

8'-0"

EL. 742'-6"

EL. 713'-6"

62'-6"

20 TON TOP RIDING BRIDGE CRANE.

20 TON TOP RIDING BRIDGE CRANE.

2'-10" TROLLEY

3 1/2" CRANE RAIL

ROOF BEAM

MIN. 3" CLEAR TO OBSTRUCTION

80'-0" CRANE SPAN

18'-1" (CLEAR) 3'-2" CRANE GIRDER

28'-6 1/2" FROM FLOOR TO T/STEEL

LONGITUDINAL SECTION THROUGH PIT & BUILDING

L-25 CENTER SERVICE BUILDING

FERMI NATIONAL ACCELERATOR LABORATORY  
UNITED STATES DEPARTMENT OF ENERGY

6A

CD-0

4-2-1

REVISIONS

DATE

DESCRIPTION

BY

DATE

APPROVED

CHECKED

DRAWN

DESIGNED

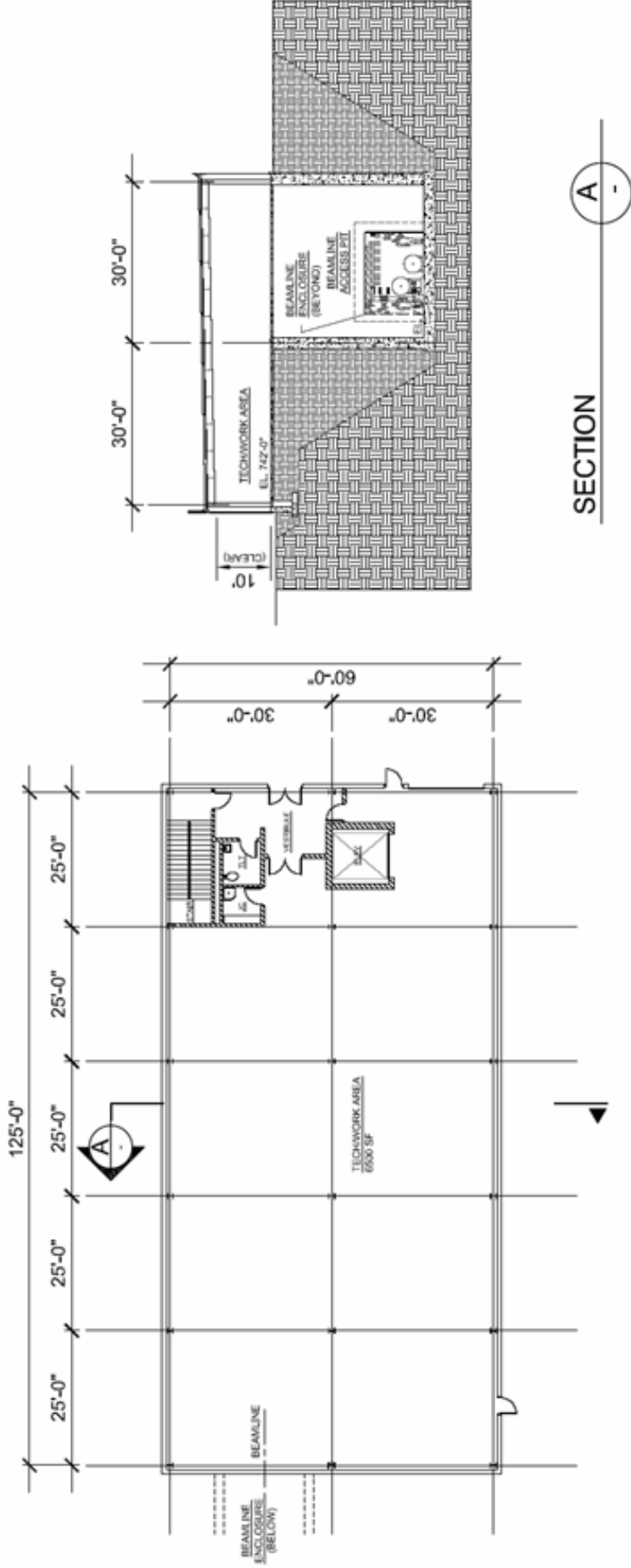
SCALE

DATE


0 4 8 12 16 20 24 28 FEET

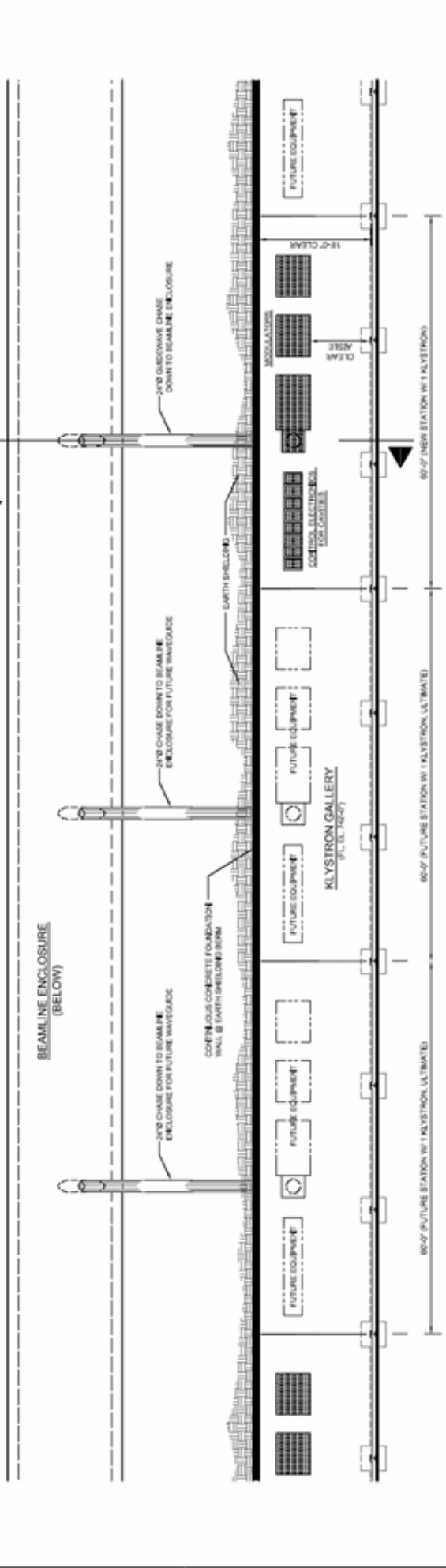
3/32" = 1'-0"

# 7. L-0 Upstream Service Building



FLOOR PLAN  
AREA 7500 SF

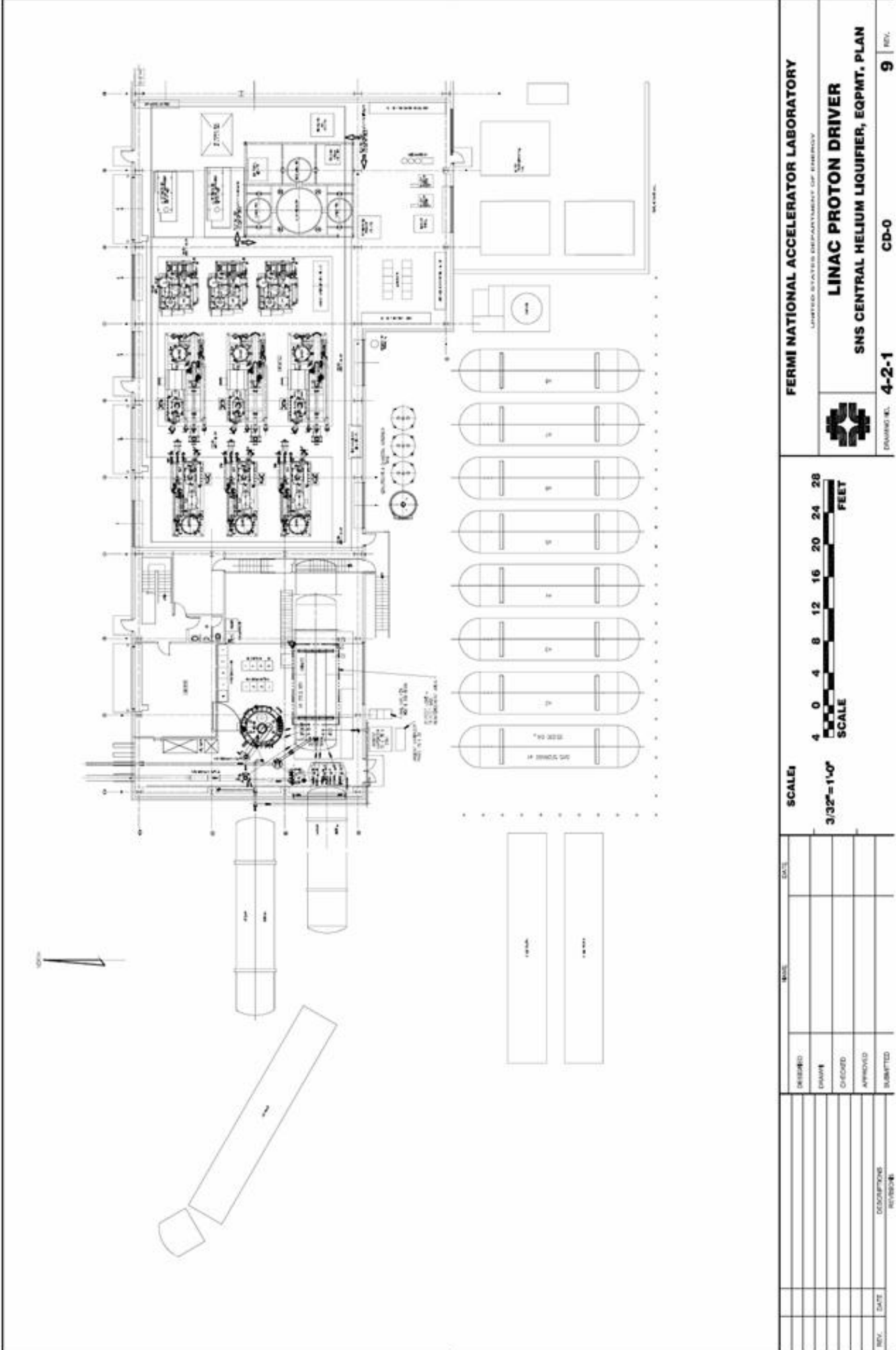
FERMI NATIONAL ACCELERATOR LABORATORY <small>UNITED STATES DEPARTMENT OF ENERGY</small>				LINAC PROTON DRIVER L-0 UPSTREAM SERVICE BUILDING				CD-0	7	REV.
				4-2-1						
				<div> <div>20</div> <div>0</div> <div>20</div> <div>40</div> </div> <div>SCALE</div> <div>FEET</div>						
				<div> <div>1" = 20'-0"</div> </div>						
DESIGNED	DATE	DATE	DATE	DATE	DATE	DATE	DATE	DATE	DATE	DATE
DRAWN										
CHECKED										
APPROVED										
SUBMITTED										
REV.				DATE	DESCRIPTION	REVISIONS				

[illegible]

SCALE: 1/16" = 1'-0"

[illegible]


# 9. SNS Central Helium Liquefier



**SECTION 8**

**TYPICAL CROSS-SECTION THROUGH KLYSTRON GALLERY/BEAMLINE ENCLOSURE**  
(SHOWING 805 MHz KLYSTRON AND CAVITY)

Labels in drawing include: EL. 752'-0", EL. 751'-8", EL. 742'-0", KLYSTRON GALLERY, 12' CLEAR, 18' CLEAR, 21', SLOPE (0.85%), 24'-6", MATCH EXIST. GRADE, SECTION THROUGH WAVEGUIDE CHASE, BEAMLINE ENCLOSURE, Z-573 WAVEGUIDE CHASE (24' TOTAL), SITE TUBE AS REQUIRED, 3/4, 1.



### TYPICAL CROSS-SECTION THROUGH KLYSTRON GALLERY/BEAMLINE ENCLOSURE

(SHOWING 805 MHz KLYSTRON AND CAVITY)

		Date		Status	
				ENTERED	
				ISSUED	
				CHECKED	
				APPROVED	
				SUBMITTED	
PCVA	DATE	DECLARATION OF NON-INTEREST			

• = 5'40"



**Abstract**

## LINAC PROTON DRIVER

**KLYSTRON GALLERY/BEAMLINE ENCL. CROSS-SECTION**

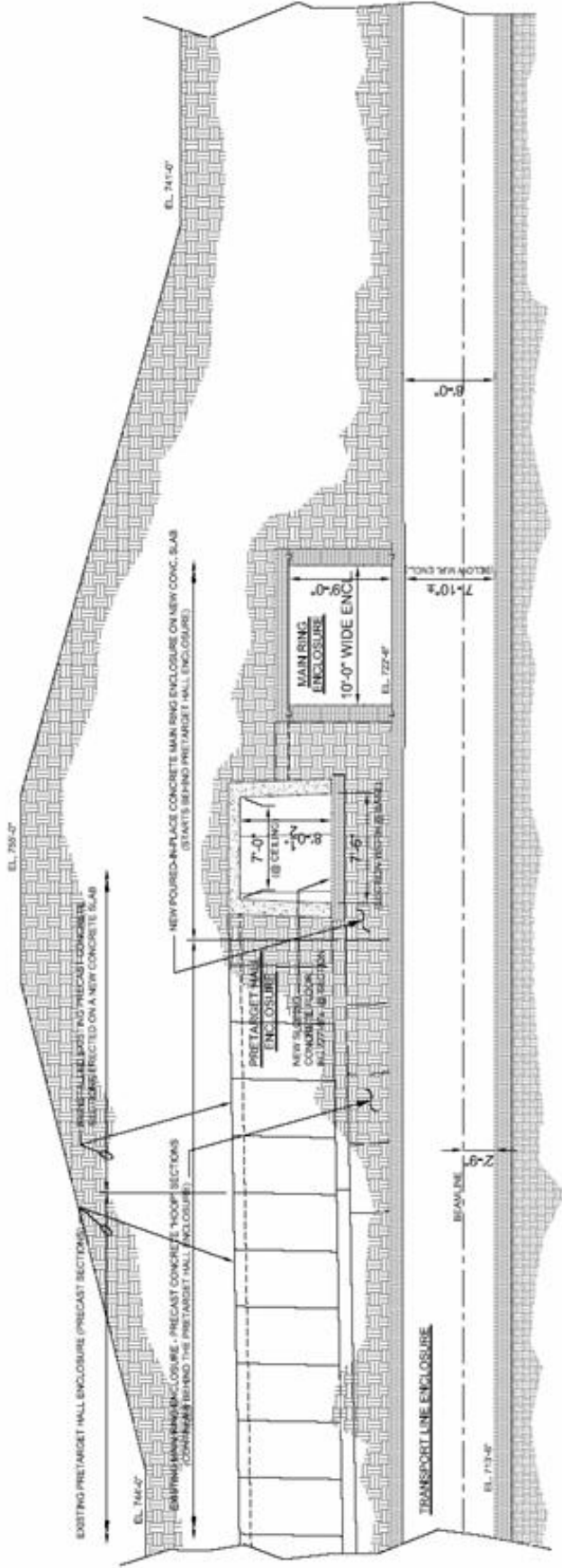
REV.	DATE	DESCRIPTION

CD-0


**4-2-1**

10 RGV,

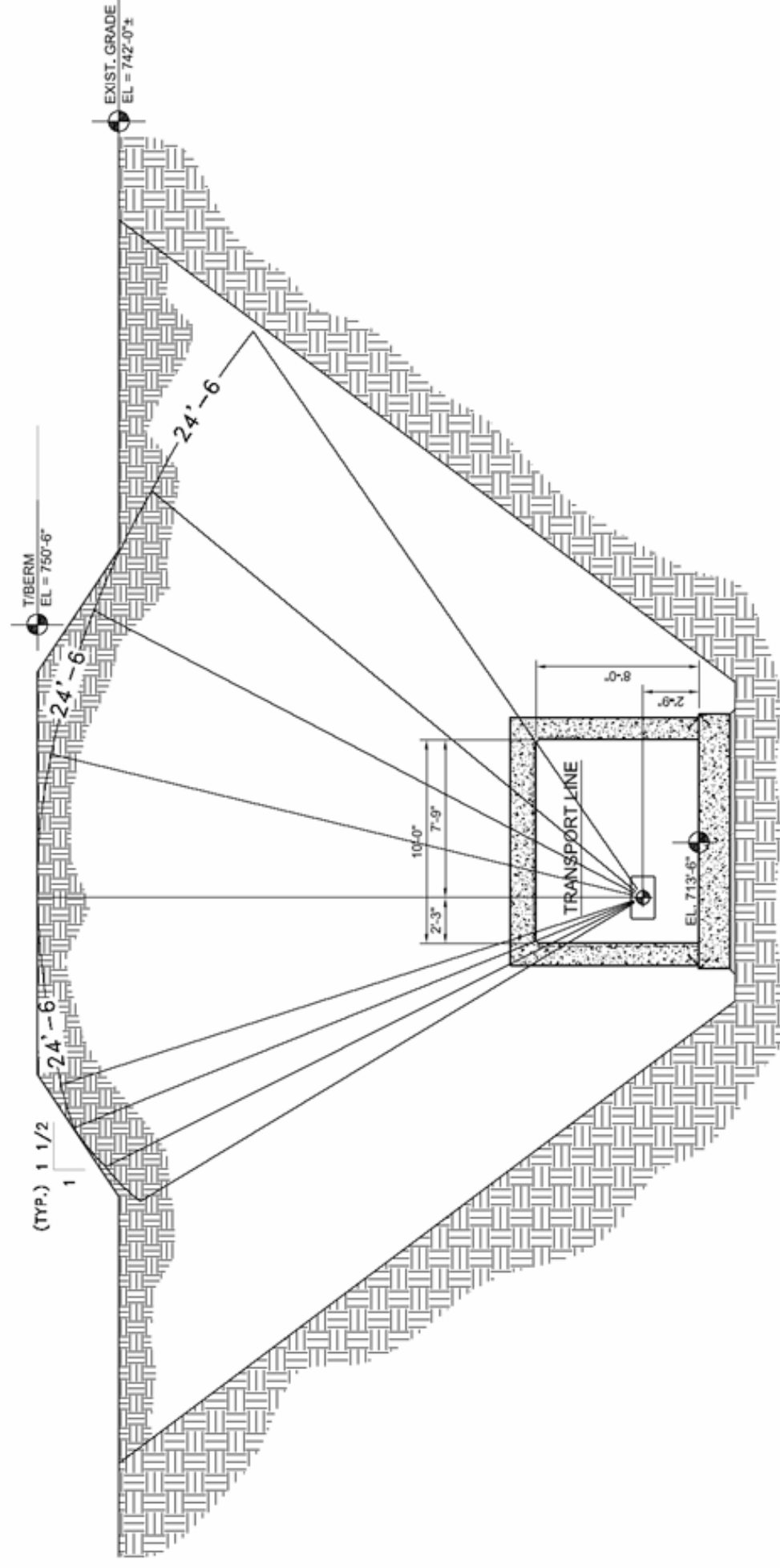
# 11. Section at Main Ring & AP0 Crossover



**SECTION OF TRANSPORT LINE ENCLOSURE BELOW THE MAIN RING (STATION 181+00) AND ANTI-PROTON ENCLOSURES**

FERMI NATIONAL ACCELERATOR LABORATORY <small>UNITED STATES DEPARTMENT OF ENERGY</small>			LINAC PROTON DRIVER SECTION @ MAIN RING/ANTI-PROTON ENCLOSURES		
			QUANTITY NO.	4-2-1	CD-0
SCALE: 1" = 10'-0"			11		
10 0 10 20 SCALE FEET			REV.		
DESIGNED	DATE	BY			
DRAWN					
CHECKED					
APPROVED					
REVISION	DATE	DESCRIPTION			

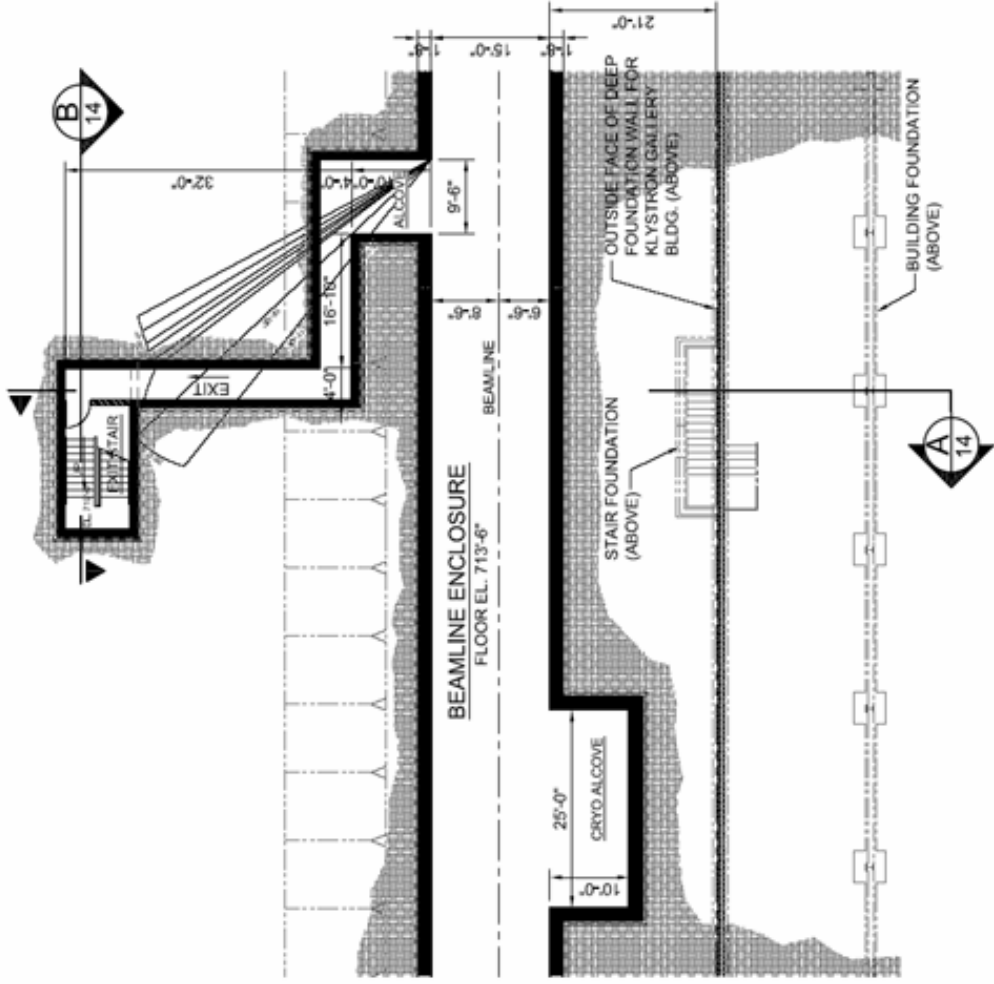
## 12. Transport Line Enclosure



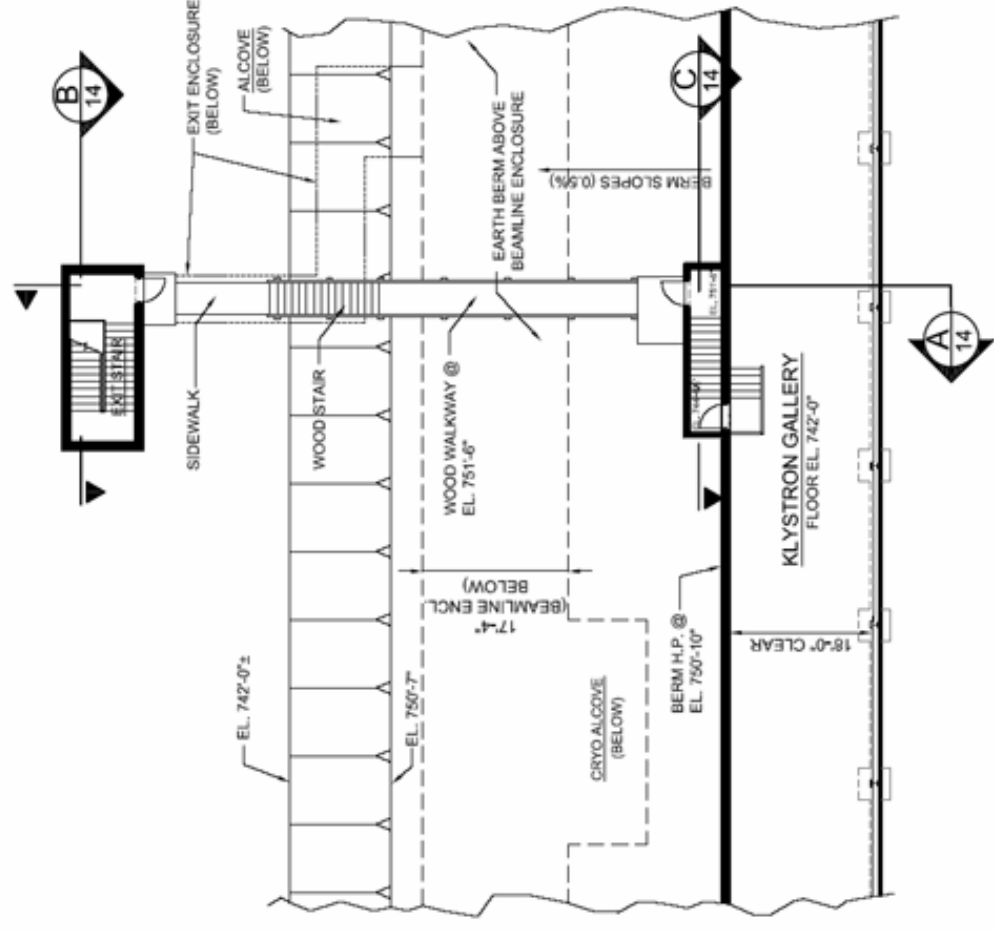
**SECTION THROUGH TRANSPORT LINE ENCLOSURE**

[illegible]

## 13. Beamline Enclosure Exit Stair Plan



**PLAN AT EL. 713'-6"**

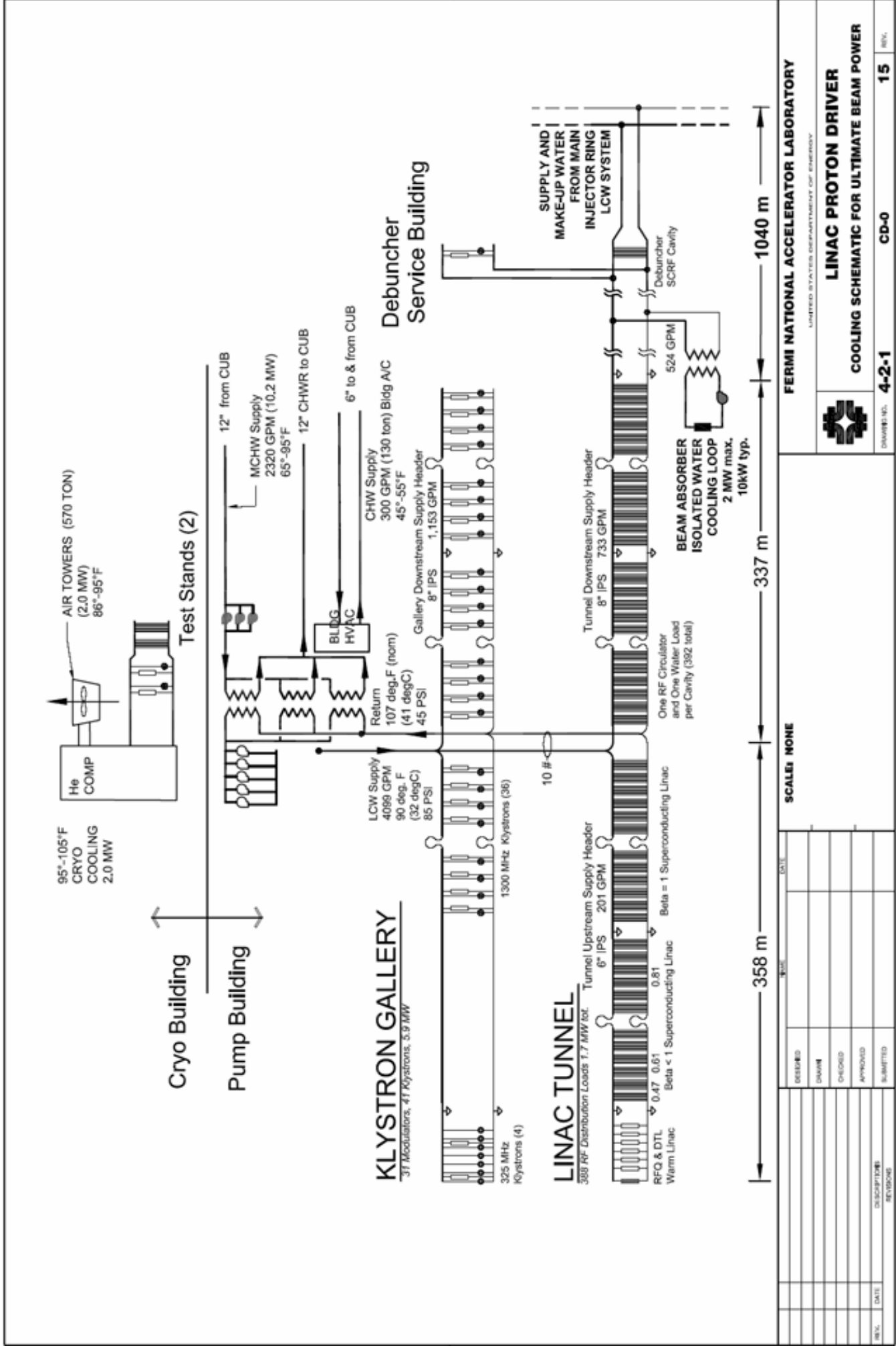


## **PLAN AT GRADE LEVEL**

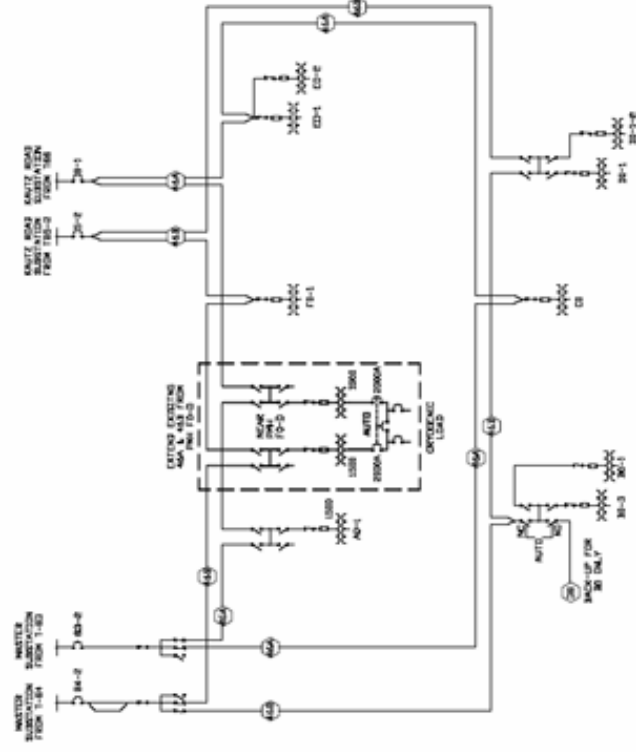
[illegible]

[illegible][illegible]

# 15. Cooling Schematic – Ultimate Configuration



## 16A. Cryoplant Power – Electrical Single Line

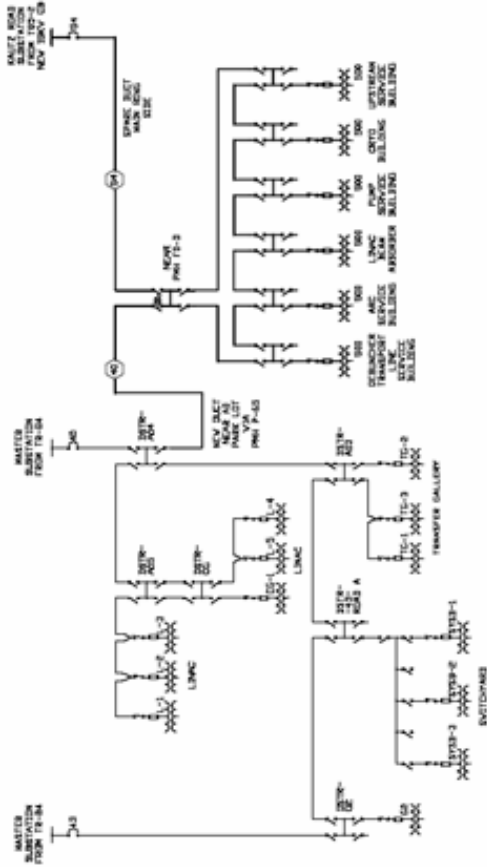


CRYO POWER

	DEMAND CALCULATED	CONNECTED (CALCULATED)	CONNECTED (ACTUAL)
INITIAL	2132 MW	2435 MVA	3000 MVA
ULTIMATE	2132 MW	2435 MVA	3000 MVA

		SCALE	
		SCALE	DATE
	DESIGNED		
	CHECKED		
	APPROVED		
	SUBMITTED		
REV.	DATE	DESCRIPTION	REVISION

# 16B. Conventional Power – Electrical Single Line



CONVENTIONAL POWER

TOTAL POWER REQUIREMENTS (CALCULATED)		LOCATION		INITIAL		ULTIMATE	
DEMAND	CONNECTED	DEMAND	CONNECTED	DEMAND CALCULATED	CONNECTED (ACTUAL)	DEMAND CALCULATED	CONNECTED (ACTUAL)
INITIAL	1,075 MW	1,228 MVA	UPSTREAM SERVICE BUILDING	25%	0.268 MW	0.268 MW	0.367 MVA
ULTIMATE	1,075 MW	1,228 MVA	CYRO BUILDING	25%	0.268 MW	0.268 MW	0.367 MVA
			PUMP SERVICE BUILDING	15%	0.162 MW	0.162 MW	0.184 MVA
			LINAC DOWNSTREAM END	15%	0.162 MW	0.162 MW	0.184 MVA
			ARC SERVICE BUILDING	10%	0.108 MW	0.108 MW	0.123 MVA
			JESUNCHER/TRANSPORT LINE SERVICE BUILDING	10%	0.108 MW	0.108 MW	0.123 MVA
			TOTAL		1.076 MW	1.076 MW	1.228 MVA
							3.000 MVA

FERMI NATIONAL ACCELERATOR LABORATORY  
UNITED STATES DEPARTMENT OF ENERGY



LINAC PROTON DRIVER  
ELECTRICAL SINGLE LINE FOR INITIAL CONV POWER

4-2-1CD-016BREV.

DESIGNED	NAME	DATE
DRAWN		
CHECKED		
APPROVED		
SUBMITTED		
REF.	DATE	DESCRIPTION
		REV 000000

**MACHINE POWER**

**KLYSTRON**

(0.5 MW)

TOTAL POWER REQUIREMENTS CALCULATED		LOCATION		INITIAL		ULTIMATE	
DEMAND	CONNECTED	DEMAND	CONNECTED	DEMAND CALCULATED	CONNECTED ACTUAL	DEMAND CALCULATED	CONNECTED ACTUAL
INITIAL	3,247 KW	6,691 MVA	UPSTREAM SERVICE BUILDING	25X	0.812 MW	1,673 MVA	1,500 MVA
ULTIMATE	11,590 KW	18,693 MVA	PUMP SERVICE BUILDING	30X	0.974 MW	2,007 MVA	3,000 MVA
			LINAC DOWNSTREAM END	25X	0.812 MW	1,673 MVA	1,500 MVA
			ARC SERVICE BUILDING	10X	0.325 MW	0.669 MVA	1,500 MVA
			DEBUNCHER/TRANSPORT LINE SERVICE BUILDING	10X	0.325 MW	0.669 MVA	1,500 MVA
TOTAL	3,247 KW	6,691 MVA	TOTAL		3,247 MW	11,820 MW	18,693 MVA

## **Appendix 4 - FAQ's ON STAGING AND ULTIMATE PERFORMANCE**

This section gives preliminary answers to frequently asked questions regarding possible scope reductions and staging scenarios that may result in a lower initial project cost or higher ultimate performance for the injector linac. The cost numbers are “unburdened” by the factor of 1.6 discussed in section 26.

### **How can the Linac provide protons for beam power above 2 MW?**

The simplest way is to double-pulse the linac. This requires no new hardware. Two successive injections separated by 0.1 seconds (Ultimate scenario) would provide twice the number of protons to the Main Injector while increasing the cycle time from 1.5 to 1.6 seconds. Assuming the Main Injector and experimental targets could handle the additional protons, the beam power would be ~3.7 MW.

A second method is to double the pulse width of all modulators in the Ultimate scenario from 1.5 msec to 3 msec (see Figure 58). The average power of the linac would not be increased since this is driven by average power capabilities of the Klystrons, charging supplies, RF power couplers, etc., but the charge-per-pulse into the Main Injector would be doubled.

A third route to higher beam power is reduction of the Main Injector cycle time. Doubling the beam power to 4 MW could take place by cutting the MI cycle time in half (to 0.75 seconds). This would require more RF voltage and power in the Main Injector, more magnet power supply voltage, but not more resistive current in the magnets. No linac hardware changes are required.

### **How does the cost of the SCRF Proton Driver compare to an 8 GeV ILC test facility?**

The baseline design of the Proton Driver contains nine 1300 MHz RF stations, the same number that would be required for an 8 GeV ILC test facility. This represents 1.6% of the ILC main linac. The average beam current, site power, and cryogenic requirements would be identical.

The proton-specific parts of the Linac that could be stripped away for an ILC test facility are: the H- source and front-end linac, the 325 MHz RF systems, Klystrons, and cryomodules; the beam transfer line and injection technical components, and the civil construction costs associated with the front end linac and beam transfer line. The total is approximately \$100M.

The electron-specific costs which would be added include the high-brightness injector, bunch compressor, and any downstream beam analysis needed. Some of this already exists at the A0 photoinjector. The LLRF and clock distribution systems for an ILC test facility might be different and more expensive. Civil construction costs might be increased if a decision was made to exactly mock up a two-underground-tunnels configuration for the ILC.

The largest cost increment in both cases is the cost to sustain a generation of HEP physicists during the decade needed to organize and build the ILC. In the case of the proton driver, these are the facilities of a world-leading neutrino program; in the case of the ILC, no plan to preserve the health of the U.S. HEP program has been proposed, so the costs are unknown.

### **What if you lower the linac energy below 8 GeV?**

The Main Injector could function down to 4-5 GeV and possibly below that. The magnetic field quality remains good down to at least 4 GeV. However, space charge at MI injection would limit the intensity to less than the Design Study goal of  $1.5 \times 10^{14}$ /pulse (5x the original MI design). The MI RF cavity tuners (and probably the cavity drive) would need upgrading. It is

probably unwise for either the civil construction or the cryogenic plant to limit the energy below 8 GeV, so little or no cost savings would be expected there. Assuming that the cost is linear in the beam energy of the ( $\beta = 1.00$ ) linac segment, the (cryomodule + Klystron + modulator + RF distribution + electronics) savings from dropping from 8 GeV to 5 GeV would be ~\$50M (unburdened).

**What is the cost delta to go immediately to the Ultimate (2 MW) configuration?**

Approximately \$50M (unburdened). This amount is within the project contingency, so a mid-project decision to go directly to the Ultimate configuration is not inconceivable.

**What is the additional cost for accelerating electrons?**

The main cost to the Main Linac is adding the “slow” Ferrite phase shifters (not full vector modulators) on the 1300 MHz ( $\beta = 1$ ) linac, approximately \$12 M. There is a small (<\$500K) additional cost to incorporate fast-slewing (i.e. high voltage) quadrupole power supplies in the  $\beta = 1$  quadrupoles.

The major cost impact comes from adding the electron photoinjector front end, electron experimental areas, and the civil construction associated with them. None of this is included in the baseline cost estimate for the bare H<sup>+</sup> injector. It would be useful to develop a plan and cost estimate for the FNPL facility to evolve into the 8 GeV electron injector.

**What would the TESLA-800 gradients buy you?**

The concept would be to baseline a 5 GeV linac assuming TESLA-500 gradients, and deliver an 8 GeV linac by delivering TESLA-800 gradients. This would save approximately a factor of 5/8 in cryomodules and RF power distribution components, ~\$7M in tunnel and gallery civil construction costs, and a ~\$3M in control electronics. No savings in klystrons or modulators since the RF power is unchanged. Cryogenic plant capacity would have to be increased by ~30%, but this increase could be compensated for by reducing the linac repetition rate or the cryoplant overcapacity margin. Total savings of ~\$35M. This also assumes the RF distribution and RF power couplers could handle 8/5 as much power without increasing in cost (not a sure bet).

**Can the Proton Driver Front End Linac serve as an emergency replacement for the existing front end linac?**

Possibly. The entire linac (up to 400 MeV) would have to be replaced as a unit, due to frequency compatibility issues. The length of the Proton Driver Test Linac up to 400 MeV is 110 m. This fits into the existing linac enclosure. For obvious reasons, the Proton Driver Prototype Test at Meson is being designed from the start for portability. If triple-spoke resonators are used, the linac up to 400 MeV uses a 4.5 K cryosystem. Only two modulators and 4-5 Klystrons are required to support the Ultimate (26 mA) beam current. At this current, the number of Booster Turns for injection would be higher, and this would have to be investigated.

## Appendix 5 - CHOICE OF LINAC OPERATING FREQUENCIES

This appendix summarizes the considerations in the choice of “ILC-compatible” (1300 MHz and 325 MHz) frequencies for the Proton Driver linac. The initial concept for the “Two-Frequency ILC-compatible Linac” was presented in ref. 46. More detailed discussions and presentations regarding the frequency choice are found in the presentations and deliberations of the Proton Driver RF<sup>205</sup> and Cryo/Module<sup>206</sup> working groups.

### Constraints on the Choice of Frequency

The Linac RF frequency can be chosen independently of the 53 MHz RF frequency of the Main Injector. It is unnecessary (and probably undesirable) for the linac to be harmonically related to the revolution frequency of the Main Injector. If this were the case, the H- stripping injection of many short linac bunches on top of each other would generate extremely intense short bunches with problematic beam dynamics<sup>62</sup>. If this happened by accident, small adjustments of the bend field in the Main Injector will destroy any harmonic or near-harmonic relationship between the linac so as to guarantee that the injected charge will be smoothly spread out during the hundreds of turns of injection.

The most cost-effective frequency of an asymptotically large  $\beta=1$  SCRF linac (including cavity, cryogenic, RF and capitalized operating costs) is in the range of 1300 MHz, as has been initially calculated<sup>207</sup> and confirmed by over a decade of development of the TESLA design for the ILC. The cost-optimization of the frequency of the Main Linac of the Proton Driver is identical. Any frequency between 1000 MHz and 1500 MHz could provide a reasonably cost-effective design for either machine.

The front-end proton linac generally favors a lower frequency, in the range of 200-500 MHz. There is incentive to keep injector frequency as low as possible to maximize the capture bucket area in the RFQ; but at frequencies below ~300 MHz the drive klystrons become extremely large. Studies for the APT project indicated that a frequency of ~400 MHz was optimal for obtaining maximum brightness from a RFQ front end operating at CW. If one desires to chop the beam on a bunch-by-bunch basis on the output of the RFQ, then a lower frequency is desired.

The frequencies of the SCRF main linac should be a low multiple of the bunch frequency established by the RFQ & Front End linac. So for example if a main linac frequency of 1300 MHz is chosen, the front end could operate at  $1300/3 = 433$  MHz, or  $1300/4 = 325$  MHz. In these cases only every 3<sup>rd</sup>, or every 4<sup>th</sup> bucket will be occupied in the Main Linac. If more complicated harmonic relationships are attempted (e.g. 3/5, 2/7, etc.) then the fraction of buckets which can be occupied is small, and the charge-per-bunch must be larger to maintain the desired average linac current. This large charge-per-bunch makes the accelerator physics difficult. A complicated harmonic relationship will also require a method for selectively depopulating bunches in the front-end linac.

There is a desire to minimize the size of RF frequency jumps from the accelerator physics point of view. Jumps with large frequency ratios require large bunch rotations coming into and out of the frequency transition in order to match the bunch to bucket. These bunch rotations stir up the longitudinal beam dynamics. In high current linacs, large frequency jumps will require retuning when the linac current changes, and will suffer a longitudinal mismatch when a range of bunch currents is passed during a macropulse. A large frequency jump is easier if it takes place at higher beam energies where space charge effects are smaller, so there is an interplay between the frequency choice and the technological transition (e.g. spokes vs. elliptical cavities) for the linac. Jumps of 4:1 have been successfully used at FNAL and other places.

Klystron availability is crucial to linac development. There is an enormous advantage to designing a linac around an existing, commercially available Klystron. Even in cases where Klystron specifications are well within the state of the art, development of a new Klystron takes years<sup>99</sup> and many millions of dollars. Multiple vendors are desirable from a project point of view, to encourage a competitive procurement and ensure long-term vendor support. Multiple customers for each Klystron type are desirable, both to encourage vendors and to provide an emergency source of spare parts during a vendor availability crisis.

In contrast, SRF cavity development at a new frequency does not appear to be a major hurdle. The SNS experience in developing a new SRF cavity and power coupler, based on frequency-scaled versions of proven designs, is very positive. Tooling costs are modest and the design does not have to be iterated before a production design is obtained. Therefore when the faced with a choice between development of a new Klystron and a new family of SRF cavities, cavity development is preferable.

### Standard Frequencies

In light of these constraints, several families of frequencies were considered:

1. **“SNS Compatible” frequencies** (202.125, 402.5, 805, and 1207.5 or 1610 MHz). The first three frequencies are used by LANL, BNL, FNAL, and the SNS. These frequencies were adopted for the first design study: 402.5 MHz for the RFQ and DTL, and 805 MHz for the  $\beta = 0.47$ , 0.61, and 0.81 SCRF linacs, and 1207.5 MHz for the main linac. The klystrons and  $\beta < 1$  SRF cavities, and portions of the front end linac designs can be used directly from the SNS. A front-end linac built at these frequencies could potentially serve as an emergency replacement for Fermilab’s front end linac. However for the  $\beta = 1$  main linac (1-8 GeV), this required the development of a new “almost ILC compatible” 1207.5 MHz (or 1600 MHz) cavity and klystron design, and a loss of hardware compatibility with the ILC effort.
2. **“CERN Compatible” frequencies** (352 MHz, 704 MHz, 1408 MHz...). Some prototype cavity and front end linac development has taken place along these lines, driven primarily be the availability of surplus LEP klystrons from CERN and the prospect of re-using the 352 MHz LEP SRF equipment. However the LEP klystrons operate CW and do not appear to be available or appropriate for a large new pulsed linac project. The LEP SRF cavities have had their performance eclipsed by modern SRF technology to the point that it is not clear that they are cost-effective to resuscitate. High-power pulsed Klystrons have not recently been built at these frequencies, and there are no installed customers. Again, a not-quite-ILC compatible Multi-Beam Klystron would have to be developed for the main linac. Therefore recent projects (RAL FETS, BSNS, etc) have moved away from these frequencies.
3. **“JPARC Compatible” frequencies** (324 MHz, 748 MHz ...). The JPARC front end linac is the most recently built large linac. Some prototype SCRF cavity and Klystron development work has been done towards and eventual SRF upgrade to the JPARC linac, but at present there is no approved timeline for this upgrade and it is our understanding that the SRF development is on hiatus. Again, this route would require development of an “almost ILC compatible” 1296 MHz Multi-beam Klystron and SRF cavities.

4. **ILC Compatible Frequencies (1300 MHz / 325 MHz) [chosen].** Standardize on the 1300 MHz TESLA/XFEL frequency for the Main ( $\beta = 1$ ) Linac and build downwards in frequency towards the front end. The advantage of this is hardware commonality with the ILC and Euro/FEL for the main linac where most of the costs of the Proton Driver are. Cavities, Klystrons, cryomodule designs, and assembly tooling for the main linac are identical to the ILC & Euro/FEL. Optimized designs developed for those projects can be taken over immediately and used for the Proton Driver. Multiple vendors developed for those projects should generate a competitive procurement environment.

The down side of this choice is that new  $\beta < 1$  cavities must be developed for the 1300 MHz elliptical linac. As mentioned before, development of a new SRF cavity design seems less problematic than klystron development. This approach also allows the application of new cavity design techniques (sect. 8.2), rather than simply cloning the existing SNS cavities.

Spoke resonators have been developed in a bewildering array of frequencies. This is related to the fact that they have been developed for CW applications where the frequency is not tied to the availability of specific klystrons. There is a limited amount of spoke resonator development at 352 MHz and essentially no development at the other standard frequencies. Thus, the development of a all new spoke resonator designs is necessary at whatever frequency is chosen. A collaborative development of a complete suite of optimized “ILC-compatible” spoke resonators and elliptical cavities has the potential to generate a worldwide standard for future SRF linac development.

An “ILC-compatible” front end linac could run at either at  $1300/3 = 433$  MHz, or  $1300/4 = 325$  MHz. The lower 325 MHz frequency was chosen, largely because of the availability of the JPARC klystron (sect 10.1), and the bulk of spoke resonators developed in the 300-350 MHz frequency range.

## References

- <sup>1</sup> Cold Linac Commissioning Major Step For ORNL's Spallation Neutron Source, ORNL press release, Aug '05  
[http://www.ornl.gov/info/press\\_releases/get\\_press\\_release.cfm?ReleaseNumber=mr20050819-00](http://www.ornl.gov/info/press_releases/get_press_release.cfm?ReleaseNumber=mr20050819-00)
- <sup>2</sup> "Comments on the ILC RF System", Sami Tantawi (SLAC), presentation to 1<sup>st</sup> ILC workshop, KEK, Nov. 2004,  
<http://lcdev.kek.jp/ILCWS/Talks/14wg2-4-Sami%20comments%20on%20the%20RF%20system%20of%20the%20ILC1.pdf>
- <sup>3</sup> Proton Driver Design Study II, FNAL-TM-2369  
<http://www-bd.fnal.gov/pdriver/8GEV/>
- <sup>4</sup> Foster and MacLachlan, "A Multi-Mission 8 GeV Injector Linac as a Fermilab Booster Replacement", Linac 2002,  
<http://accelconf.web.cern.ch/AccelConf/I02/PAPERS/FR202.PDF>
- <sup>5</sup> Proton Driver Design Study II, FNAL-TM-2369  
<http://www-bd.fnal.gov/pdriver/8GEV/>
- <sup>6</sup> Proton Driver I Design Study, FNAL-TM-2136  
<http://www-bd.fnal.gov/pdriver/>
- <sup>7</sup> The Proton Driver Physics Study (companion to this document) is available online at:  
<http://home.fnal.gov/~sbrice/PD/Document/Drafts.html>
- <sup>8</sup> The Directors Charge Letter on the Next Steps on the Proton Driver is available online at:  
<http://www-td.fnal.gov/projects/PD/Charge.pdf>
- <sup>9</sup> Director's Preliminary Technical Review of the Proton Driver, March 15-17, 2005  
[http://www.fnal.gov/directorate/DirReviews/Dir'sRev\\_TechnicalReviewoftheProtonDriver\\_0315.html](http://www.fnal.gov/directorate/DirReviews/Dir'sRev_TechnicalReviewoftheProtonDriver_0315.html)
- <sup>10</sup> Proton Driver 8 GeV Linac Parameter Book (CD-0 Baseline)  
[http://tdserver1.fnal.gov/8gevinacPapers/ParameterList2005/CD0\\_Parameter\\_List\\_Current\\_Version.pdf](http://tdserver1.fnal.gov/8gevinacPapers/ParameterList2005/CD0_Parameter_List_Current_Version.pdf)
- <sup>11</sup> Cost Estimate Spreadsheet for 8 GeV Linac  
[http://protondriver.fnal.gov/Proton\\_Driver\\_Cost\\_Dirs\\_Rev\\_03\\_15\\_05.xls](http://protondriver.fnal.gov/Proton_Driver_Cost_Dirs_Rev_03_15_05.xls)
- <sup>12</sup> "Linac Proton Driver Cost Estimate", R. Stanek, Director's review of the Fermilab Proton Driver, March 2005  
[http://www.fnal.gov/directorate/DirReviews/DirRvw\\_Proton%20Driver%20Presentations/PD\\_DIR\\_REV\\_StaneK\\_linac\\_method%5b1%5d.ppt](http://www.fnal.gov/directorate/DirReviews/DirRvw_Proton%20Driver%20Presentations/PD_DIR_REV_StaneK_linac_method%5b1%5d.ppt)
- <sup>13</sup> TRACE3d file (MacLachlan), 8 GeV transfer line MAD file (Foster), Struct input file for H- injection (Drozhdin)
- <sup>14</sup> FESS drawing package (J. Sims, FESS) and AutoCAD files waveguide layout (GW Foster)
- <sup>15</sup> PowerPoint and .PDF files <http://tdserver1.fnal.gov/project/8gevinac/>
- <sup>16</sup> Available at: <http://tdserver1.fnal.gov/project/8gevinac/>
- <sup>17</sup> "A 8 GeV Proton Linac as an Injector for the Fermilab Main Injector", Vinod Bharadwaj, Robert Noble, FNAL, abstract submitted to EPAC1994 (no paper); also V. Bharadwaj, Presentation to John People's Future Working Group, ca. 1994 (unpublished).
- <sup>18</sup> [www.VLHC.org](http://www.VLHC.org)
- <sup>19</sup> TESLA Technical Design Report  
[http://tesla.desy.de/new\\_pages/TDR\\_CD/start.html](http://tesla.desy.de/new_pages/TDR_CD/start.html)
- <sup>20</sup> Physics with Proton Driver presentation, FNAL Long Range Planning Committee  
[http://www.fnal.gov/directorate/Longrange/ProtonDriver\\_Open\\_Meeting.html](http://www.fnal.gov/directorate/Longrange/ProtonDriver_Open_Meeting.html)
- <sup>21</sup> Beam spill requirements for muon experiments at the Proton Driver are discussed at:  
<http://home.fnal.gov/~rray/agenda.html>
- <sup>22</sup> "The Collimation System of the SNS Transfer Lines", N. Catalan-Lasheras, D. Raparia, PAC2001  
<http://accelconf.web.cern.ch/AccelConf/p01/PAPERS/RPPH019.PDF>
- <sup>23</sup> Examples include "An Energy Upgrade from TESLA to a High-Energy mu+mu- Collider", D. Neuffer, H. Edwards, and D. Finley, Snowmass '96.  
<http://www.slac.stanford.edu/pubs/snowmass96/PDF/ACC066.PDF>  
and "2 GeV Superconducting Muon Linac", M. Popovic, Linac 2000  
<http://www.slac.stanford.edu/econf/C000821/THC06.shtml>
- <sup>24</sup> VLHC Design Report, FNAL-TM-2149,  
<http://tdserver1.fnal.gov/tddoc/DesignStudyReport/upload/PDF/>
- <sup>25</sup> *ibid*, ch. 7
- <sup>26</sup> "RF Superconductivity for Accelerators", Hasan Padamsee et al., Wiley. Also see:  
[http://srf2003.desy.de/talks/Padamsee/introSRF2003\\_v3.pdf](http://srf2003.desy.de/talks/Padamsee/introSRF2003_v3.pdf)
- <sup>27</sup> Spallation Neutron Source Project Web site: [www.sns.gov](http://www.sns.gov)  
technical project info is linked from: <http://www.sns.gov/projectinfo/projectinfo.htm>
- <sup>28</sup> "Preliminary Design Report, Superconducting Radio Frequency Linac for the Spallation Neutron Source", Y. Cho ed., SNS-SRF-99-101, December 20, 1999. [http://www.sns.gov/APGroup/Papers/SC\\_LinacCDR.pdf](http://www.sns.gov/APGroup/Papers/SC_LinacCDR.pdf)
- <sup>29</sup> SNS SCRF Beam physics studies, *ibid*.

- 
- <sup>30</sup> Meson Area working group weekly meetings are being run by Bob Webber (PD Integration) and P. Czarapata and Peter Limon (Meson Area Installation). Contact them to volunteer!
- <sup>31</sup> ILC Snowmass 2005 Baseline Configuration Discussion Summaries involving SCRF gradient are available at:  
[http://alcp2005.colorado.edu:8080/alcp2005/program/bcd\\_review\\_Walker.ppt](http://alcp2005.colorado.edu:8080/alcp2005/program/bcd_review_Walker.ppt)  
<http://www.linearcollider.org/cms/?pid=1000019>
- <sup>32</sup> PD Civil Design & Siting Considerations, D. Bogert, Directors's Review of Proton Driver, March 2005,  
[http://www.fnal.gov/directorate/DirReviews/DirRvw\\_Proton%20Driver%20Presentations/PD\\_DIR\\_REV\\_BOGERT%5b2%5d.ppt](http://www.fnal.gov/directorate/DirReviews/DirRvw_Proton%20Driver%20Presentations/PD_DIR_REV_BOGERT%5b2%5d.ppt)
- <sup>33</sup> The design for the "Upper 8 GeV Line" connecting the 8 GeV line from the Booster directly to the Recycler was designed by Gerry Jackson and John Johnstone (lattice files are available from JJ). This line was to support proton beam stacking and early commissioning of the Recycler. Since it was not strictly necessary for use of the Recycler as an antiproton storage ring and was removed from the scope of the Recycler project, although most hooks for its installation remain intact in the design.
- <sup>34</sup> TESLA TDR pages II-234 (Tunnel Layout discussion)  
[http://tesla.desy.de/new\\_pages/TDR\\_CD/PartII/chapter08/chapter08.pdf](http://tesla.desy.de/new_pages/TDR_CD/PartII/chapter08/chapter08.pdf)
- <sup>35</sup> A. Drozhdin, D. Johnson, K. Vaziri, "Radiation, Shielding and Collimation", Chapter 7 of the Main Injector Upgrade section of the Proton Driver Design Study II, FNAL-TM-2369  
<http://www-bd.fnal.gov/pdriver/8GEV/>
- <sup>36</sup> "Design of a New Main Injector Cavity for the Fermilab Proton Driver Era", Vincent Wu, Alex Zuxing Chen, Zubao Qian, David Wildman, proc. PAC 2005  
<http://snsapp1.sns.ornl.gov/pac05/TPPT028/TPPT028.PDF>
- <sup>37</sup> "Un-suppressing MI30 dispersion function for momentum scraping", M.-J. Yang & D.E. Johnson,  
[http://beamdocs.fnal.gov/DocDB/0019/001930/001/scraper\\_location.pdf](http://beamdocs.fnal.gov/DocDB/0019/001930/001/scraper_location.pdf)
- <sup>38</sup> G.P. Jackson, Main Injector Electronic Logbook entries, 2002
- <sup>39</sup> Bruce C. Brown, pvt. comm.
- <sup>40</sup> Fermilab Main Injector Technical Design Handbook, ch.1, p.7  
[http://www-fmi.fnal.gov/fmiinternal/MI\\_Technical\\_Design/index.html](http://www-fmi.fnal.gov/fmiinternal/MI_Technical_Design/index.html)
- <sup>41</sup> "Repetition Rate Upgrade" Ch 20 of Main Injector section of Proton Driver Study II, Fermilab TM-2169, May 2002, <http://www-bd.fnal.gov/pdriver/8GEV/pd2pdf/ch20.pdf>
- <sup>42</sup> Norbert Holtkamp, pvt. comm.
- <sup>43</sup> THE SNS LASER PROFILE MONITOR DESIGN AND IMPLEMENTATION, S.Assadi et al., PAC'03  
<http://accelconf.web.cern.ch/accelconf/p03/PAPERS/WPPG054.PDF>
- <sup>44</sup> SNS AP notes, currently separately archived at: SNS, BNL, and LANL  
<http://www.sns.gov/APGroup/Papers/Papers.html>  
<http://server.ags.bnl.gov/bnlags/bnlsns/sns.lst.htm>  
<http://server.ags.bnl.gov/bnlags/bnlsns/sns.html>  
<http://160.91.225.192/> (Los Alamos SNS note site, seems to have fallen prey to Homeland Security)
- <sup>45</sup> P. Ostroumov et al., contribution to 34<sup>th</sup> ICFA Advanced Beam Dynamics Workshop on High Power Superconducting Proton, Ion, and Multi-Species Linacs.  
[http://www.niu.edu/clasep/Conferences/Academic/HPSL\\_conf/2005/program.html#program](http://www.niu.edu/clasep/Conferences/Academic/HPSL_conf/2005/program.html#program)
- <sup>46</sup> BEAM DYNAMICS IN PROTON AND HEAVY-ION LINACS BASED ON SUPERCONDUCTING TECHNOLOGY, P. Ostroumov, FNAL Accelerator Seminar, January 29 2004,  
[http://tdserver1.fnal.gov/8gevinacPapers/Accelerator\\_Physics/Ostroumov\\_8GeV\\_SCRF\\_talk.pdf](http://tdserver1.fnal.gov/8gevinacPapers/Accelerator_Physics/Ostroumov_8GeV_SCRF_talk.pdf)
- <sup>47</sup> Trace3D and derivatives. Many versions are out there. Some are available at:  
<http://laacg1.lanl.gov/laacg/services.html>
- <sup>48</sup> "TRACK: The New Beam Dynamics Code", Brahim Mustapha, Vladislav N. Aseev, Eliane Schnirman Lessner, Peter Ostroumov (ANL, Argonne, Illinois), proc. PAC2005
- <sup>49</sup> "Proton Driver Accelerator Physics", P. Ostroumov, presentation to Director's Review of P.D., March 2005  
[http://www.fnal.gov/directorate/DirReviews/DirRvw\\_Proton%20Driver%20Presentations/PD\\_DIR\\_REV\\_Ostroumov-1%5b1%5d.ppt](http://www.fnal.gov/directorate/DirReviews/DirRvw_Proton%20Driver%20Presentations/PD_DIR_REV_Ostroumov-1%5b1%5d.ppt)
- <sup>50</sup> "Beam loss in the SNS linac", E. Tanke, J. Galambos, J. Wei, R. Shafer, J. Stovall, T. Wangler, J. Staples, N. Catalan-Lasheras, <http://www.sns.gov/APGroup/Papers/TechMemos/2001/LinacBeamLoss.pdf>, and references therein. Also see: <http://www.c-ad.bnl.gov/Halo03/program.html>
- <sup>51</sup> "ACCELERATOR PHYSICS MODEL OF EXPECTED BEAM LOSS ALONG THE SNS ACCELERATOR FACILITY DURING NORMAL OPERATION", N. Catalan-Lasheras et al., EPAC03  
<http://accelconf.web.cern.ch/AccelConf/e02/PAPERS/THPLE011.pdf>
- <sup>52</sup> "JHF Accelerator Design Study Report", KEK Report 97-16, JHF-97-10, March 1998,  
<http://hadron.kek.jp/member/onishi/tdr2003/>

- <sup>53</sup> R. Kustom, private communication.
- <sup>54</sup> PROGRESS WITH SNS FAST BEAM CHOPPER, S.S. Kurennoy et al., LANL, proc PAC 2001  
<http://accelconf.web.cern.ch/AccelConf/p01/PAPERS/TPAH098.PDF>
- <sup>55</sup> REVIEW OF FAST BEAM CHOPPING, F. Caspers, proc. Linac'04,  
<http://accelconf.web.cern.ch/AccelConf/104/PAPERS/TH202.PDF>  
[http://accelconf.web.cern.ch/AccelConf/104/TALKS/TH202\\_TALK.PDF](http://accelconf.web.cern.ch/AccelConf/104/TALKS/TH202_TALK.PDF)
- <sup>56</sup> "Formation and mitigation of halo particles in the Spallation Neutron Source linac", D. Jeon et al, PR-STAB  
<http://link.aps.org/abstract/PRSTAB/v5/e094201>  
<http://prst-ab.aps.org/pdf/PRSTAB/v5/i9/e094201?cid=798ad1e55c9c1ca5&qseq=1&show=10>
- <sup>57</sup> HIGH CURRENT INJECTION CHANNEL FOR THE LINEAR ACCELERATOR OF THE MESON FACTORY OF THE INSTITUTE OF NUCLEAR RESEARCH, ACADEMY OF SCIENCES OF THE USSR. By A.N. Mirzorian, P.N. Ostroumov, G.V. Romanov, A.P. Fateev (Moscow, INR). 1981.  
 Published in J. of Tech. Phys., 26:1429-1430, Moscow, 1981
- <sup>58</sup> INCREASE OF INJECTION EFFICIENCY IN A HIGH CURRENT LINEAR PROTON ACCELERATOR.  
 By P.N. Ostroumov, G.V. Romanov, A.P. Fateev (Moscow, INR). 1980.  
 Published in J. of Tech. Phys., 25:710-713, Moscow, 1980
- <sup>59</sup> P.N. Ostroumov, "DESIGN FEATURES OF HIGH-INTENSITY MEDIUM-ENERGY SUPERCONDUCTING HEAVY-ION LINAC", <http://www.phy.anl.gov/ria/publications/MO412.pdf>
- <sup>60</sup> "Energy Jitter Correction", G. Jackson (Hbar Technologies), proc Fermilab H- Workshop, Dec 2004.  
<http://www-bd.fnal.gov/pdriver/H-workshop/jackson.pdf>
- <sup>61</sup> J. MacLachlan, pvt. comm.
- <sup>62</sup> G. Jackson Presentation to HPSL05, Naperville, IL 2005.
- <sup>63</sup> H- Transport and Injection Mini-Workshop, December 9-10, 2004, Fermilab,  
<http://www-bd.fnal.gov/pdriver/H-workshop/hminus.html>
- <sup>64</sup> "Conclusions from H- Transport and Injection Mini-Workshop", December 9-10, 2004, Fermilab, W. Chou,  
[http://www-bd.fnal.gov/pdriver/H-workshop/chou\\_4\\_conclusions.pdf](http://www-bd.fnal.gov/pdriver/H-workshop/chou_4_conclusions.pdf)
- <sup>65</sup> "Handbook of Accelerator Physics and Engineering", M. Tigner and A. Chao, ed. , sect 7.1.7 (p.438)
- <sup>66</sup> "H- Field Stripping Measurements", Andrew Jason, presentation to H-Transport and Injection Mini-Workshop, Fermilab, December 9, 2004 <http://www-bd.fnal.gov/pdriver/H-workshop/jason.pdf>
- <sup>67</sup> "LANSCE 800 MeV H-Transport and Injection", T. Spickermann (LANL), H-Injection Mini-Workshop, FERMILAB, December 9-10, 2004 <http://www-bd.fnal.gov/pdriver/H-workshop/spickermann.pdf>
- <sup>68</sup> The relevance of the boosted SCRF cavity fields to H- stripping was pointed out by Gerry Jackson (Hbar Tech).
- <sup>69</sup> "Blackbody Radiation Stripping", H. Bryant et al, Presentation to the Fermilab Mini-Workshop on H- Transport and Injection, Dec. 2004, <http://www-bd.fnal.gov/pdriver/H-workshop/bryant.pdf>
- <sup>70</sup> Photonic, Electronic, and Atomic Collisions XXII International Conference Santa Fe, NM July 18-24, 2001, Eds: Joachim Burgdorfer, et al, Rinton Press, pages 517-524.
- <sup>71</sup> "Linac Front End Design", G. Romanov, presentation to the Director's Review of the Proton Driver.  
[http://www.fnal.gov/directorate/DirReviews/DirRvw\\_Proton%20Driver%20Presentations/PD\\_DIR\\_REV\\_Romanov.ppt](http://www.fnal.gov/directorate/DirReviews/DirRvw_Proton%20Driver%20Presentations/PD_DIR_REV_Romanov.ppt)
- <sup>72</sup> John Carson, FNAL (ret.), pvt. communication.
- <sup>73</sup> A demonstration electrical pulser system for the proton driver fast chopper is being produced by Kentech, a small company closely associated with Rutherford Applications Lab. For the kicker structure, either the design of the CERN meander-line chopper in Figure 38 will be modified for the 2.5 MeV injection energy of the RFQ, or a modification of the RAL metal-and-ceramic chopper structure will be used. The informal collaboration is being organized by Robyn Madrak of FNAL (email: madrak@fnal.gov)
- <sup>74</sup> The GSI, SPL, HIPPI projects.
- <sup>75</sup> Proton Driver Design Study II, FNAL-TM-2369, part 2 (Linac), Ch. 7  
<http://www-bd.fnal.gov/pdriver/8GEV/>
- <sup>76</sup> "Structures for RIA and FNAL Proton Driver", M. Kelly (ANL), SRF2005.  
[http://www.lns.cornell.edu/public/SRF2005/talks/monday/MoP01\\_talk\\_srf2005.pdf](http://www.lns.cornell.edu/public/SRF2005/talks/monday/MoP01_talk_srf2005.pdf)
- <sup>77</sup> "Status of FNAL Single Spokes Design", G. Lanfranco, presentation to Proton Driver cryo working group,  
[http://tdserver1.fnal.gov/8gevlinacPapers/Meeting\\_Minutes/Cryomodules/Cold%20PD%20Working%20Group%20-%20Tuesday/Tuesday.%20Aug.%2030th%202005/Giobatta%20Single%20Spokes%2030th%20Aug%202005.ppt](http://tdserver1.fnal.gov/8gevlinacPapers/Meeting_Minutes/Cryomodules/Cold%20PD%20Working%20Group%20-%20Tuesday/Tuesday.%20Aug.%2030th%202005/Giobatta%20Single%20Spokes%2030th%20Aug%202005.ppt)
- <sup>78</sup> Shepard, Kelly, and Fuerst, proc. PAC 2003
- <sup>79</sup> "Spokes vs. elliptical cavities for the Proton Driver Linac", G. W. Foster (FNAL), SRF2005  
[http://www.lns.cornell.edu/public/SRF2005/talk/wednesday/We\\_HT3\\_talk3.pdf](http://www.lns.cornell.edu/public/SRF2005/talk/wednesday/We_HT3_talk3.pdf)

- “Triple-spoke compared with elliptical-cell cavities”, K. Shepard (ANL), SRF2005  
[http://www.lns.cornell.edu/public/SRF2005/talk/wednesday/We\\_HT3\\_talk1.pdf](http://www.lns.cornell.edu/public/SRF2005/talk/wednesday/We_HT3_talk1.pdf)
- “Elliptical cavities: Proven SRF option”, T. Grimm (MSU), SRF2005  
[http://www.lns.cornell.edu/public/SRF2005/talk/wednesday/We\\_HT3\\_talk2.pdf](http://www.lns.cornell.edu/public/SRF2005/talk/wednesday/We_HT3_talk2.pdf)
- <sup>80</sup> “STATUS REPORT ON MULTI-CELL SUPERCONDUCTING CAVITY DEVELOPMENT FOR MEDIUM-VELOCITY BEAMS”, W. Hartung et al., PAC03  
<http://accelconf.web.cern.ch/accelconf/p03/PAPERS/TPAB070.PDF>
- <sup>81</sup> “Jefferson Lab FY03 R&D Activities in Support of RIA”, J. Delaysen et al, Presentation to the DOE Nuclear Physics Division “Rare Isotope Accelerator (RIA) Research & Development Workshop”, Bethesda, Maryland, August 26 – 28, 2003  
<http://www.c-ad.bnl.gov/RIA/papers/pdf/p-2-2-5.pdf>
- <sup>82</sup> Compton et al., “Niobium Cavity Development for the High Energy Linac of RIA”, PAC01.  
<http://accelconf.web.cern.ch/AccelConf/p01/PAPERS/MPPH116.PDF>
- <sup>83</sup> Solyak et al., internal Proton Driver memo.
- <sup>84</sup> “Proposal for the Development of 1.3 GHz  $\beta=0.81$  Elliptical Cavities for the Superconducting Proton Driver Linac”, R.C. York, T.L. Grimm and W. Hartung, Michigan State University, March 30, 2005
- <sup>85</sup> Carlo Pagani, cavity design summary slides from SEA workshop:  
<http://www.dapnia cea.fr/Sea/Workshop-HPPA/transparentes/pagani.pdf>
- <sup>86</sup> “Superconducting Prototype Cavities for the Spallation Neutron Source (SNS) Project”, Ciovati, Kneisel et al.,  
<http://accelconf.web.cern.ch/AccelConf/e02/PAPERS/THPDO015.pdf>
- <sup>87</sup> TESLA TDR, Part II Ch 2, table 2.1.1  
[http://tesla.desy.de/new\\_pages/TDR\\_CD/PartII/chapter02/chapter02.pdf](http://tesla.desy.de/new_pages/TDR_CD/PartII/chapter02/chapter02.pdf)
- <sup>88</sup> TESLA/Saclay Mechanical Tuner is discussed in the TESLA TDR, Part II, ch3,  
[http://tesla.desy.de/new\\_pages/TDR\\_CD/PartII/chapter03/chapter03.pdf](http://tesla.desy.de/new_pages/TDR_CD/PartII/chapter03/chapter03.pdf) see also:  
“Dynamik Lorentz Force Compensation with a Fast Piezoelectric Tuner”, TESLA 2001-03, M. Liepe et al  
[http://tesla.desy.de/new\\_pages/TESLA\\_Reports/2001/pdf\\_files/tesla2001-03.pdf](http://tesla.desy.de/new_pages/TESLA_Reports/2001/pdf_files/tesla2001-03.pdf)
- <sup>89</sup> J. Hogan et al., “Design of the SNS Cavity Support Structure”,  
[http://www.jlab.org/div\\_dept/admin/publications/papers/01/ACE01-02.pdf](http://www.jlab.org/div_dept/admin/publications/papers/01/ACE01-02.pdf)
- <sup>90</sup> Piezo Tuner Microphonics compensation discussed in:  
[http://srf2003.desy.de/talks/Simrock/simrock\\_srf\\_2003.pdf](http://srf2003.desy.de/talks/Simrock/simrock_srf_2003.pdf)
- <sup>91</sup> “Spoke Cavity Development”, K. Shepard, presentation to Director’s Review of P.D., March 2005  
[http://www.fnal.gov/directorate/DirReviews/DirRvw\\_Proton%20Driver%20Presentations/PD\\_DIR\\_REV\\_Shepard.ppt](http://www.fnal.gov/directorate/DirReviews/DirRvw_Proton%20Driver%20Presentations/PD_DIR_REV_Shepard.ppt)
- <sup>92</sup> “Plans for Beta = 1 Cryomodules & Status at TESLA TTF”, H. Edwards, presentation to Director’s Review of Proton Driver, March 2005,  
[http://www.fnal.gov/directorate/DirReviews/DirRvw\\_Proton%20Driver%20Presentations/PD\\_DIR\\_REV\\_Hedwards-1.2.ppt](http://www.fnal.gov/directorate/DirReviews/DirRvw_Proton%20Driver%20Presentations/PD_DIR_REV_Hedwards-1.2.ppt)
- <sup>93</sup> An SBIR Phase I proposal with AMAC, inc. was approved in FY2005 for development of cost-effective RF couplers for the Proton Driver and similar machines.
- <sup>94</sup> 325 MHz Power coupler development can be tracked in the minutes of the PD Cryo/module working group  
[http://tdserver1.fnal.gov/8gevinacPapers/Meeting\\_Minutes/Cryomodules/](http://tdserver1.fnal.gov/8gevinacPapers/Meeting_Minutes/Cryomodules/)  
and specifically:  
[http://tdserver1.fnal.gov/8gevinacPapers/Meeting\\_Minutes/Cryomodules/Nicol\\_meeting\\_viewgraphs\\_june\\_9\\_2005.ppt](http://tdserver1.fnal.gov/8gevinacPapers/Meeting_Minutes/Cryomodules/Nicol_meeting_viewgraphs_june_9_2005.ppt)  
[http://tdserver1.fnal.gov/8gevinacPapers/Meeting\\_Minutes/Cryomodules/Khabibouline\\_042805\\_Couplers.ppt](http://tdserver1.fnal.gov/8gevinacPapers/Meeting_Minutes/Cryomodules/Khabibouline_042805_Couplers.ppt)
- <sup>95</sup> TESLA/TTF HOM coupler design is described in the TESLA TDR Part II, ch2, fig. 2.1.20  
[http://tesla.desy.de/new\\_pages/TDR\\_CD/PartII/chapter02/chapter02.pdf](http://tesla.desy.de/new_pages/TDR_CD/PartII/chapter02/chapter02.pdf)
- <sup>96</sup> “SNS HOM Damping Requirements via Bunch Tracking”, Sundelin et al., PAC01  
<http://accelconf.web.cern.ch/AccelConf/p01/PAPERS/TPPH135.PDF>
- <sup>97</sup> “Wake Field Effects in the APT Linac”, S. Kurennoy, proc. Linac98  
<http://accelconf.web.cern.ch/AccelConf/198/PAPERS/MO4032.PDF>
- <sup>98</sup> “Klystrons and RF Feed”, Al Moretti, presentation to Director’s review of Proton Driver, March 2005  
[http://www.fnal.gov/directorate/DirReviews/DirRvw\\_Proton%20Driver%20Presentations/PD\\_DIR\\_REV\\_A-Moretti-1%5b1%5d.ppt](http://www.fnal.gov/directorate/DirReviews/DirRvw_Proton%20Driver%20Presentations/PD_DIR_REV_A-Moretti-1%5b1%5d.ppt)
- <sup>99</sup> “The SNS LINAC RF SYSTEM, SYSTEM STATUS AND VENDOR RESULTS”, Lynch et al., LINAC 2002  
<http://accelconf.web.cern.ch/AccelConf/102/PAPERS/MO465.PDF>
- <sup>100</sup> Al Moretti, FNAL, pvt. comm.
- <sup>101</sup> A. Beunas, G. Faillon, S. Choroba, A. Gamp, “A High Efficiency Long Pulse Multi Beam Klystron for the TESLA Linear Collider”, TESLA Report 2001-01.  
[http://tesla.desy.de/new\\_pages/TESLA\\_Reports/2001/pdf\\_files/tesla2001-01.pdf](http://tesla.desy.de/new_pages/TESLA_Reports/2001/pdf_files/tesla2001-01.pdf)

- <sup>102</sup> S. Choroba, presentation to the first ILC meeting, KEK, Japan 2004; and at Snowmass 2005.  
<http://lcdev.kek.jp/ILCWS>
- <sup>103</sup> “Modulators for the Proton Driver”, D. Wolff, Director’s review of Proton Driver, Mach 2005  
[http://www.fnal.gov/directorate/DirReviews/DirRvw\\_Proton%20Driver%20Presentations/PD\\_DIR\\_REV\\_wolff%5b1%5d.ppt](http://www.fnal.gov/directorate/DirReviews/DirRvw_Proton%20Driver%20Presentations/PD_DIR_REV_wolff%5b1%5d.ppt)
- <sup>104</sup> Images of the TESLA RF distribution components are at:  
[http://tesla.desy.de/new\\_pages/wr\\_poster/181001/ModulatorPoster.pdf](http://tesla.desy.de/new_pages/wr_poster/181001/ModulatorPoster.pdf)
- <sup>105</sup> “FIM TECHNOLOGY”, Claude Vincent, TPC, Proc.5th Modulator-Klystron Workshop,MDK-2001,CERN  
<http://mdk2001.web.cern.ch/mdk2001/Proceedings/SessionPoster/vincent.pdf>
- <sup>106</sup> “DESIGN, STATUS, AND FIRST OPERATIONS OF THE SPALLATION NEUTRON SOURCE POLYPHASE RESONANT CONVERTER MODULATOR SYSTEM”, W. A. Reass, PAC’03,  
<http://accelconf.web.cern.ch/accelconf/p03/PAPERS/ROAC007.PDF>
- <sup>107</sup> “Further Improvements in the Reliability of IGBT Modules”, Thomas Schütze, Hermann Berg, Martin Hierholzer Eupec GmbH & Co., proc. IAS1998. (paper provided & interpreted by Dan Wolff, FNAL)  
[http://tdserver1.fnal.gov/8gevlinacPapers/Modulators/Semiconductor\\_Lifetime\\_vs\\_Temperature\\_Swing\\_ias1998.pdf](http://tdserver1.fnal.gov/8gevlinacPapers/Modulators/Semiconductor_Lifetime_vs_Temperature_Swing_ias1998.pdf)
- <sup>108</sup> “A Long Pulse Modulator for Reduced Size and Cost”, H. Pfeffer et al, Presented at 21st International Power Modulator Symposium, Costa Mesa, CA, June 27 - 30,1994,  
<http://library.fnal.gov/archive/1994/conf/Conf-94-182.pdf>  
“A Second Long Pulse Modulator For TESLA Using IGBTs”, H. Pfeffer et al, EPAC96  
<http://accelconf.web.cern.ch/AccelConf/e96/PAPERS/MOPG/MOP048G.PDF>  
“CONSTRUCTION PROJECT REPORT: TESLA MODULATOR DEVELOPMENT: Tesla Modulators Number 2 and 3”, Dan Wolff FNAL Beams Div EE internal memo.
- <sup>109</sup> D. Wolff, presentation to 8 GeV linac group on modulator costs.  
[http://tdserver1.fnal.gov/8gevlinacPapers/Cost\\_Estimate\\_Info/Wolff\\_TESLA\\_Style\\_modulator\\_costs\\_2.ppt](http://tdserver1.fnal.gov/8gevlinacPapers/Cost_Estimate_Info/Wolff_TESLA_Style_modulator_costs_2.ppt)
- <sup>110</sup> DESIGN AND STATUS OF THE POLYPHASE RESONANT CONVERTER MODULATOR SYSTEM FOR THE SPALLATION NEUTRON SOURCE LINEAR ACCELERATOR”, W. A. Reass et al.,Linac02 ,  
<http://epaper.kek.jp/l02/PAPERS/WE202.PDF>
- <sup>111</sup> “THE CONVENTIONAL FACILITIES REQUIREMENTS FOR THE SNS LINAC”, Tallerico et al., PAC01  
<http://accelconf.web.cern.ch/AccelConf/p01/PAPERS/RPPH066.PDF>
- <sup>112</sup> “POWER SUPPLIES FOR TESLA MODULATORS”, Hans-Joerg Eckoldt, Niels Heidbrook, MDK-2001,  
<http://mdk2001.web.cern.ch/mdk2001/Proceedings/Session14/eck.pdf>
- <sup>113</sup> W. Bothe, “Pulse Generation for TESLA, a Comparison of Different Methods”, TESLA 94-21 (July 1994)  
[http://tesla.desy.de/new\\_pages/TESLA\\_Reports/1994/pdf\\_files/tesla1994-21.pdf](http://tesla.desy.de/new_pages/TESLA_Reports/1994/pdf_files/tesla1994-21.pdf)
- <sup>114</sup> TESLA RF Distribution Poster: [http://tesla.desy.de/new\\_pages/wr\\_poster/181001/RF\\_waveguide.pdf](http://tesla.desy.de/new_pages/wr_poster/181001/RF_waveguide.pdf)  
see also “THE TESLA RF SYSTEM”, S. Choroba, MDK-2001  
<http://mdk2001.web.cern.ch/mdk2001/Proceedings/Session11/Choroba.pdf>
- <sup>115</sup> “A HIGH POWER LONG PULSE HIGH EFFICIENCY MULTI BEAM KLYSTRON”, Beunas, Faillon (Thales), Choroba(DESY), proc 2001 Modulator-Klystron Conf (CERN)  
<http://mdk2001.web.cern.ch/mdk2001/Proceedings/Session12/beunas.pdf>
- <sup>116</sup> Markus Huening PhD thesis, DESY 2002
- <sup>117</sup> “Excess RF Power Required for RF Control of the Spallation Neutron Source Linac”, Lynch et al, PAC01  
<http://accelconf.web.cern.ch/AccelConf/p01/PAPERS/ROAA010.PDF>
- <sup>118</sup> Closeout report from the Fermilab Director’s Review of the Proton Driver R&D Program, March 15-17, 2005.  
[http://www.fnal.gov/directorate/DirReviews/Dir'sRev\\_TechnicalReviewoftheProtonDriver\\_0315.html](http://www.fnal.gov/directorate/DirReviews/Dir'sRev_TechnicalReviewoftheProtonDriver_0315.html)
- <sup>119</sup> SNS Parameter List, available online at:  
<http://www.sns.gov/APGroup/Params/Parameters.htm>
- <sup>120</sup> M. Huening, EPAC04, P. Bauer EPAC04, Gerry Jackson HPSL05, SCREAM program documentation, P. Bauer, ed.
- <sup>121</sup> “Lorentz Force Compensation of Pulsed SRF Cavities”, S. N. Simrock, LINAC’02  
<http://accelconf.web.cern.ch/AccelConf/l02/PAPERS/WE204.PDF>
- <sup>122</sup> “SNS Cryomodule Performance”, J. Preble et al., PAC03  
<http://accelconf.web.cern.ch/accelconf/p03/PAPERS/ROAA001.PDF>
- <sup>123</sup> K. Shepard et al PAC05, Z. Conway et al, proc. SRF2005
- <sup>124</sup> Closeout comments from the FNAL Director’s External Review, March 2005
- <sup>125</sup> PROTOTYPE SUPERCONDUCTING TRIPLE-SPOKE CAVITY FOR BETA = 0.63, K.W. Shepard, M.P. Kelly, J.D. Fuerst, M. Kedzie, and Z.A. Conway, ANL, Proc. PAC2005  
<http://snsapp1.sns.ornl.gov/pac05/TPPT099/TPPT099.PDF>

- 
- SUPERCONDUCTING TRIPLE-SPOKE CAVITY FOR  $\beta=0.5$  IONS, K.W. Shepard, M.P. Kelly, J.D. Fuerst, M. Kedzie, and Z.A. Conway, ANL, Proc. PAC2005  
<http://snsapp1.sns.ornl.gov/pac05/TPPT100/TPPT100.PDF>
- <sup>126</sup> EXPERIENCE WITH THE CONTROL OF THE VECTOR SUM AT THE TESLA TEST FACILITY  
 A. Gamp, et al., EPAC98 <http://accelconf.web.cern.ch/AccelConf/e98/PAPERS/WEP38G.PDF>
- <sup>127</sup> “Energy Jitter Correction”, Gerald P Jackson, Hbar Technologies, H- Transport and Injection Mini-Workshop  
 December 9-10, 2004 Fermilab, <http://www-bd.fnal.gov/pdriver/H-workshop/jackson.pdf>
- <sup>128</sup> Some papers on Simulation of cavity resonance control in SC linacs: (there are many)  
 S.N. Simrock et al., “AN ANALYSIS TOOL FOR RF CONTROL FOR SUPERCONDUCTING  
 CAVITIES”, EPAC02, <http://accelconf.web.cern.ch/AccelConf/e02/PAPERS/WEPR1048.pdf>  
 A. Mosnier, “Energy Stability in High Intensity Pulsed SC Proton Linac”, Linac00,  
<http://accelconf.web.cern.ch/AccelConf/100/papers/THB10.pdf>
- <sup>129</sup> See for example: “MINIMIZING RF POWER REQUIREMENT AND IMPROVING AMPLITUDE/PHASE  
 CONTROL FOR HIGH GRADIENT SUPERCONDUCTING CAVITIES, M. Luong, et al., EPAC 2002,  
<http://accelconf.web.cern.ch/AccelConf/e02/PAPERS/THPDO011.pdf>
- <sup>130</sup> “RF Control Modeling Issues for Future Superconducting Accelerators”, Hofler et al, proc. LINAC04,  
<http://accelconf.web.cern.ch/AccelConf/104/PAPERS/MOP69.PDF>
- <sup>131</sup> “Requirements for the RF Control of the Vector Sum for Superconducting Proton Linacs”, M. Huening et al.,  
 L98 <http://accelconf.web.cern.ch/AccelConf/198/PAPERS/TU4064.PDF>
- <sup>132</sup> “SIMULATION OF RF CONTROL OF A SUPERCONDUCTING LINAC FOR RELATIVISTIC  
 PARTICLES”, P.C. Bauer, M. Huening, G. W Foster, proc. EPAC04,  
<http://accelconf.web.cern.ch/AccelConf/e04/PAPERS/THPLT133.PDF>
- <sup>133</sup> Superconducting Relativistic Particle Accelerator Simulation (SCREAM) – Program Documentation, P. Bauer,  
 M. Huening, G.W. Foster, FNAL Tech Division Note TD-04-031, 2004  
<http://tdserver1.fnal.gov/tclib/TD-Notes/2004%20Tech%20Notes/TD-04-031.pdf>
- <sup>134</sup> “VECTOR SUM CONTROL OF AN 8 GeV SUPERCONDUCTING PROTON LINAC”, M. Huening, G.W.  
 Foster, proc. EPAC 2004, <http://accelconf.web.cern.ch/AccelConf/e04/PAPERS/TUPLT150.PDF>
- <sup>135</sup> “FAST FERRITE PHASE SHIFTER FOR THE SNS LINAC”, Yoon Kang SNS presentation, June 2000.  
[http://tdserver1.fnal.gov/project/8gevinlac/useful\\_papers/ferrite\\_tuners/Kang\\_phaseshifter\\_June\\_2000.ppt](http://tdserver1.fnal.gov/project/8gevinlac/useful_papers/ferrite_tuners/Kang_phaseshifter_June_2000.ppt)
- <sup>136</sup> R. Kustom (ANL, ret.) and Yoon Kang (SNS), pvt. comm.
- <sup>137</sup> “Muon Acceleration in a Superconducting Proton Linac”, Milorad Popovic, proc. NUFAC05  
<http://beamdocs.fnal.gov/DocDB/0019/001976/001/LinacFrascati.pdf>
- <sup>138</sup> Low-powered Ferrite Vector Modulators are available from a number of vendors. Try a Google search for the  
 term: “Ferrite Vector Modulator” or “Ferrite IQ Modulator”
- <sup>139</sup> Ferrite Vector Modulator R&D results are summarized in:  
[http://tdserver1.fnal.gov/8gevinlacPapers/Meeting\\_Minutes/WeeklyMeeting/05\\_05\\_05%20Wildman%20-%20RF%20Power%20R&D.ppt](http://tdserver1.fnal.gov/8gevinlacPapers/Meeting_Minutes/WeeklyMeeting/05_05_05%20Wildman%20-%20RF%20Power%20R&D.ppt)  
[http://www.fnal.gov/directorate/DirReviews/DirRvw\\_Proton%20Driver%20Presentations/PD\\_DIR\\_REV\\_terechkin%5b1%5d.ppt](http://www.fnal.gov/directorate/DirReviews/DirRvw_Proton%20Driver%20Presentations/PD_DIR_REV_terechkin%5b1%5d.ppt)  
[http://tdserver1.fnal.gov/8gevinlacPapers/Meeting\\_Minutes/RF/Index.html](http://tdserver1.fnal.gov/8gevinlacPapers/Meeting_Minutes/RF/Index.html)
- <sup>140</sup> HIGH CW POWER, PHASE AND AMPLITUDE MODULATOR REALIZED WITH FAST FERRITE  
 PHASE-SHIFTERS, Dissertation Thesis, Daniel Valuch, Slovak University of Technology, Bratislava,  
 2004  
[http://tdserver1.fnal.gov/8gevinlacPapers/Ferrite\\_Tuners/Valuch\\_Thesis\\_Phase\\_Shifters.pdf](http://tdserver1.fnal.gov/8gevinlacPapers/Ferrite_Tuners/Valuch_Thesis_Phase_Shifters.pdf)
- <sup>141</sup> “Final Hybrid Report”, Shreyas Bhat, Sept 2004.  
[http://tdserver1.fnal.gov/8gevinlacPapers/Ferrite\\_Tuners/Final%20hybrid%20report.doc](http://tdserver1.fnal.gov/8gevinlacPapers/Ferrite_Tuners/Final%20hybrid%20report.doc)
- <sup>142</sup> Von Airlock and Fay, “Linear Ferrites for Microwave Applications”, Academic Press, 1968, p.174-83  
[http://Tdserv1/project/8GeVLinac/Useful\\_Papers/Ferrite\\_Tuners/Phaseshifter\\_for\\_8\\_GeV\\_Linac.doc](http://Tdserv1/project/8GeVLinac/Useful_Papers/Ferrite_Tuners/Phaseshifter_for_8_GeV_Linac.doc)
- <sup>143</sup> Y. Kang, “FAST RF FERRITE PHASE SHIFTER FOR HIGH-POWER APPLICATIONS”, Linac00  
<http://accelconf.web.cern.ch/AccelConf/100/papers/TH19.pdf>
- <sup>144</sup> FAST-FERRITE TUNER OPERATION ON A 352-MHZ SINGLE-CELL RF CAVITY AT THE ADVANCED  
 PHOTON SOURCE, D. Horan, E. Cherubic, proc. PAC 2003.  
<http://accelconf.web.cern.ch/AccelConf/p03/PAPERS/TPAB001.PDF>
- <sup>145</sup> “325 MHZ IQ Modulator”, D. Sun, presentation to the Director’s Review of the Proton Driver. March 2005,  
[http://www.fnal.gov/directorate/DirReviews/DirRvw\\_Proton%20Driver%20Presentations/PD\\_DIR\\_REV\\_Ding%5b1%5d.ppt](http://www.fnal.gov/directorate/DirReviews/DirRvw_Proton%20Driver%20Presentations/PD_DIR_REV_Ding%5b1%5d.ppt)
- <sup>146</sup> Brian Chase, FNAL, pvt. comm. Similar tolerances on phase and amplitude are believed to be required for the  
 Euro-FEL and similar projects.
- <sup>147</sup> THE TESLA CRYOGENIC ACCELERATOR MODULES, TESLA Report 2001-36, C. Pagani et al.,

- [http://tesla.desy.de/new\\_pages/TESLA\\_Reports/2001/pdf\\_files/tesla2001-36.pdf](http://tesla.desy.de/new_pages/TESLA_Reports/2001/pdf_files/tesla2001-36.pdf)
- <sup>148</sup> DESIGN OF THE SNS CRYOMODULE, W.J. Schneider et al., ACE01  
[http://www.jlab.org/div\\_dept/admin/publications/papers/01/ACE01-05.pdf](http://www.jlab.org/div_dept/admin/publications/papers/01/ACE01-05.pdf)
- <sup>149</sup> “CAVITY FAILURE FAULT TOLERANCE”, section 2.4 of ref. 28
- <sup>150</sup> Wolff et al., “THE TESLA CRYOGENIC DISTRIBUTION SYSTEM”, TESLA REPORT 2001-37,  
[http://tesla.desy.de/new\\_pages/TESLA\\_Reports/2001/pdf\\_files/tesla2001-37.pdf](http://tesla.desy.de/new_pages/TESLA_Reports/2001/pdf_files/tesla2001-37.pdf)
- <sup>151</sup> Geynisman’s write-up on 8 GeV Cryomodule swap time:  
[http://tdserver1.fnal.gov/project/8gevlinac/useful\\_papers/cryogenics/8Gev\\_cooldown\\_Geynisman.doc](http://tdserver1.fnal.gov/project/8gevlinac/useful_papers/cryogenics/8Gev_cooldown_Geynisman.doc)
- <sup>152</sup> “Medium Beta Cavity and Cryomodule Prototyping for RIA” J.D. Fuerst, Presentation to the DOE Nuclear Physics Division “Rare Isotope Accelerator (RIA) Research & Development Workshop”, Bethesda, Maryland, August 26 – 28, 2003 [www.orau.org/ria/r&dworkshop/fuerst.pdf](http://www.orau.org/ria/r&dworkshop/fuerst.pdf)
- <sup>153</sup> A. Zeller et al., “A Superferric Quadrupole for use in a SRF Cryomodule”, MT-17, Geneva, Sept. 2001  
[http://www.inl.infn.it/~annrep/readAN/2001/contrib\\_2001/254.pdf](http://www.inl.infn.it/~annrep/readAN/2001/contrib_2001/254.pdf)
- <sup>154</sup> STATUS OF THE HIGH ENERGY SC LINAC FOR THE TRASCO PROGRAM, C. Pagani et al., PAC2001  
<http://accelconf.web.cern.ch/AccelConf/p01/PAPERS/RPPH304.PDF>
- <sup>155</sup> Short Solenoid Lens Focusing Channel for PD Front End, I. Terechkine, FNAL Tech. Div. Note # TD-05-035,  
<http://tdserver1.fnal.gov/tlibrary/TD-Notes/2005%20Tech%20Notes/TD-05-035.pdf>
- <sup>156</sup> “Proton Driver Front End Warm Section Focusing Solenoid”, I. Terechkine, FNAL Tech. Div. Note # TD-05-037, <http://tdserver1.fnal.gov/tlibrary/TD-Notes/2005%20Tech%20Notes/TD-05-037.doc>
- <sup>157</sup> “Analysis of Stress in PD Front End Solenoids”, I. Terechkine, FNAL Tech. Div. Note # TD-05-039,  
<http://tdserver1.fnal.gov/tlibrary/TD-Notes/2005%20Tech%20Notes/TD-05-039.doc>
- <sup>158</sup> Proton Driver Magnet Meeting minutes and review materials can be found at:  
<http://tdserver1/project/8GeVLinac/PD%20Magnets/PD%20Magnet%20Meetings.html>
- <sup>159</sup> Recent Progress in the Superconducting RF. Recent Progress in the Superconducting RF Program at TRIUMF/ISAC, RE Laxdal, proc. SRF2005  
[http://www.lns.cornell.edu/public/SRF2005/talks/monday/MoP06\\_talk\\_srf2005.pdf](http://www.lns.cornell.edu/public/SRF2005/talks/monday/MoP06_talk_srf2005.pdf)  
“Magnetic Field Studies in the ISAC II Cryomodule”, R.E. Laxdal et al., ibid.  
[www.lns.cornell.edu/public/SRF2005/posters/thursday/ThP40\\_poster\\_srf2005.pdf](http://www.lns.cornell.edu/public/SRF2005/posters/thursday/ThP40_poster_srf2005.pdf)
- <sup>160</sup> Cryogenic System Design, J. Theilacker, presentation to the Director’s Review of the Proton Driver, March 2005  
[http://www.fnal.gov/directorate/DirReviews/DirRvw\\_Proton%20Driver%20Presentations/PD\\_DIR\\_REV\\_Theilacker%5b1%5d.ppt](http://www.fnal.gov/directorate/DirReviews/DirRvw_Proton%20Driver%20Presentations/PD_DIR_REV_Theilacker%5b1%5d.ppt)
- <sup>161</sup> TESLA Cryosystem, TESLA TDR Part II, ch.8, sect 8.7  
[http://tesla.desy.de/new\\_pages/TDR\\_CD/PartII/chapter08/chapter08.pdf](http://tesla.desy.de/new_pages/TDR_CD/PartII/chapter08/chapter08.pdf)
- <sup>162</sup> T. Peterson (FNAL/TD) Spreadsheet on Cryo Loads in 8 GeV linac (May ’02). No known write up.
- <sup>163</sup> A. Klebaner spreadsheets for ‘fridge cost and process. No known write up.
- <sup>164</sup> Transfer Line Components”, D. Harding, presentation to the Director’s Review of the Proton Driver.  
[http://www.fnal.gov/directorate/DirReviews/DirRvw\\_Proton%20Driver%20Presentations/PD\\_DIR\\_REV\\_Harding%5b1%5d.ppt](http://www.fnal.gov/directorate/DirReviews/DirRvw_Proton%20Driver%20Presentations/PD_DIR_REV_Harding%5b1%5d.ppt)  
“H- Transport and Stripping”, W. Chou, presentation to the Director’s Review of the Proton Driver.  
[http://www.fnal.gov/directorate/DirReviews/DirRvw\\_Proton%20Driver%20Presentations/PD\\_DIR\\_REV\\_chou\\_h%5b1%5d.ppt](http://www.fnal.gov/directorate/DirReviews/DirRvw_Proton%20Driver%20Presentations/PD_DIR_REV_chou_h%5b1%5d.ppt)
- <sup>165</sup> SNS notes on Transport line:  
<http://accelconf.web.cern.ch/AccelConf/p01/PAPERS/RPPH046.PDF>  
<http://server.c-ad.bnl.gov/esfd/bnlsns/052.pdf>  
<http://server.c-ad.bnl.gov/esfd/bnlsns/sns065.pdf>  
<http://server.ags.bnl.gov/bnlags/bnlsns/097.pdf>
- <sup>166</sup> H- Transport and Injection Mini-Workshop, Fermilab, December 9-10, 2004  
<http://www-bd.fnal.gov/pdriver/H-workshop/hminus.html>
- <sup>167</sup> “8 GeV H- Transport”, Fermilab-TM-2285, W. Chou, ed. See also:  
[http://www.fnal.gov/directorate/DirReviews/DirRvw\\_Proton%20Driver%20Presentations/PD\\_DIR\\_REV\\_chou\\_h%5b1%5d.ppt](http://www.fnal.gov/directorate/DirReviews/DirRvw_Proton%20Driver%20Presentations/PD_DIR_REV_chou_h%5b1%5d.ppt)
- <sup>168</sup> The TRIUMF cyclotron is one example:  
<http://www.triumf.ca>
- <sup>169</sup> “Beam collimation in the transfer line from 8 GeV linac to the Main Injector”, A. Drozhdin, presentation to the mini-workshop on H- Transport and injection, Fermilab, Dec 2004.  
[http://www-bd.fnal.gov/pdriver/H-workshop/drozhdin\\_2\\_collimation.pdf](http://www-bd.fnal.gov/pdriver/H-workshop/drozhdin_2_collimation.pdf)
- <sup>170</sup> The Main Injector Dump is described in the Main Injector TDR  
[http://www-fmi.fnal.gov/fmiinternal/MI\\_Technical\\_Design/index.html](http://www-fmi.fnal.gov/fmiinternal/MI_Technical_Design/index.html)
- <sup>171</sup> The MI Dump upgrade for 2 MW beams is discussed in Fermilab TM-2169, Sect 20.5 (N. Mokhov)

- 
- (in Part I of this document)
- <sup>172</sup> N. Mokhov pvt. comm. This would probably rely on the effectiveness of an upstream window as a spoiler.
- <sup>173</sup> “A High Intensity Beam Absorber Corebox for the Fermilab Main Injector Abort System”, M. Reichanadter, C.M. Bhat, C. Crawford, P.S. Martin, PAC’97  
<http://accelconf.web.cern.ch/accelconf/pac97/papers/pdf/8P014.PDF>
- <sup>174</sup> “Linac Dump Optics with Window Near Quadrupoles”, BNL/SNS NOTE NO. 106, Deepak Raparia  
<http://server.ags.bnl.gov/bnlags/bnlsns/106.pdf>
- <sup>175</sup> L.W. Alvarez, Rev. Sci. Instrum. 22,705(1951)
- <sup>176</sup> G. I. Budker and G. I. Dimov, "On the Charge Exchange Injection of Protons into Ring Accelerators", The International Accelerator Conference, Dubna 1963, CONF-114, USAEC TID-4504, pp. 1372-1377
- <sup>177</sup> H - PAINTING INJECTION FOR THE JHF 3-GEV SYNCHROTRON, Y. Irie et al., EPAC98  
<http://accelconf.web.cern.ch/AccelConf/e98/PAPERS/MOP23C.PDF>
- <sup>178</sup> SNS/BNL Note#3, “H- Charge Exchange Injection into the 1 GeV SNS Accumulator”, Blumberg, Y.Y. Lee  
<http://server.c-ad.bnl.gov/esfd/bnlsns/03.pdf>
- <sup>179</sup> “THE MULTITURN CHARGE EXCHANGE INJECTION SYSTEM FOR THE FERMILAB BOOSTER ACCELERATOR, C. Hojvat et al., FNAL-TM-872 (1979)  
<http://library.fnal.gov/archive/test-tm/0000/fermilab-tm-0872.pdf>
- <sup>180</sup> H- Transport and Injection Mini-Workshop, Fermilab, December 9-10, 2004  
<http://www-bd.fnal.gov/pdriver/H-workshop/hminus.html>
- <sup>181</sup> “MI-10 Injection”, A. Drozhdin, presentation to the Director’s review of the Fermilab Proton Driver, March 2005  
[http://www.fnal.gov/directorate/DirReviews/DirRvw\\_Proton%20Driver%20Presentations/PD\\_DIR\\_REV\\_Drozhdin%5b1%5d.ppt](http://www.fnal.gov/directorate/DirReviews/DirRvw_Proton%20Driver%20Presentations/PD_DIR_REV_Drozhdin%5b1%5d.ppt)  
 A. I. Drozhdin and G. W. Foster, “Painting Injection into the Fermilab Main Injector”, Oct 21, 2003.  
<http://www-ap.fnal.gov/~drozhdin/prdriver/pap.pdf>
- <sup>182</sup> H- Stripping efficiency vs. foil thickness was estimated by neglecting any energy dependence.
- <sup>183</sup> “JHF Accelerator Design Study Report”, KEK Report 97-16, JHF-97-10, March 1998, p3-67ff  
 the most recent version of the JHF TDR is online at:  
<http://hadron.kek.jp/member/onishi/tdr2003/>
- <sup>184</sup> “8 GeV Transport and Stripping”, W. Chou, Director’s review of the Fermilab Proton Driver, March 2005  
[http://www.fnal.gov/directorate/DirReviews/DirRvw\\_Proton%20Driver%20Presentations/PD\\_DIR\\_REV\\_chou\\_h%5b1%5d.ppt](http://www.fnal.gov/directorate/DirReviews/DirRvw_Proton%20Driver%20Presentations/PD_DIR_REV_chou_h%5b1%5d.ppt)
- <sup>185</sup> Lifetime of Carbon Stripping Foils for the Spallation Neutron Source”, C.J. Liaw et al., PAC2001  
<http://accelconf.web.cern.ch/AccelConf/p01/PAPERS/TPAH138.PDF>
- <sup>186</sup> THIN DIAMOND FILMS FOR SNS H- INJECTION STRIPPING, R. W. Shaw et al, PAC03  
<http://accelconf.web.cern.ch/accelconf/p03/PAPERS/ROPB004.PDF>
- <sup>187</sup> Grahame Rees, pvt. comm.
- <sup>188</sup> FOUR QUADRANT DC TO DC SWITCHING SUPPLY FOR THE FERMILAB MAIN INJECTOR  
 L. Bartelson, et al. PAC97 <http://accelconf.web.cern.ch/accelconf/pac97/papers/pdf/5P007.PDF>
- <sup>189</sup> Steve Hays, FNAL AD EE Support, pvt. comm.
- <sup>190</sup> “LLRF & SCRF Instrumentation”, Brian Chase, Director’s Review of the FNAL Proton Driver, March’05  
[http://www.fnal.gov/directorate/DirReviews/DirRvw\\_Proton%20Driver%20Presentations/PD\\_DIR\\_REV\\_Chase%5b2%5d.ppt](http://www.fnal.gov/directorate/DirReviews/DirRvw_Proton%20Driver%20Presentations/PD_DIR_REV_Chase%5b2%5d.ppt)
- <sup>191</sup> C. Jach, “Synchrotron-Linac Wall Power Comparison\_v2a.xls”, prepared for Proton Driver Cost/schedule working group, Feb 2005.
- <sup>192</sup> MI RF upgrade – New Cavity, D. Wildman, Director’s Review of the Proton Driver, March 2005  
[http://www.fnal.gov/directorate/DirReviews/DirRvw\\_Proton%20Driver%20Presentations/PD\\_DIR\\_REV\\_wildman-1%5b1%5d.ppt](http://www.fnal.gov/directorate/DirReviews/DirRvw_Proton%20Driver%20Presentations/PD_DIR_REV_wildman-1%5b1%5d.ppt)
- <sup>193</sup> “Design of a New Main Injector Cavity for the Fermilab Main Injector in the Proton Driver Era”, V. Wu, A. Chen, Z. Qian, D. W. Wildman, FNAL, proc. PAC 2005
- <sup>194</sup> “The High Level RF System for Transition Crossing without RF Focusing in the Main Ring at Fermilab”, J. Dey et al., PAC 1993, [http://accelconf.web.cern.ch/AccelConf/p93/PDF/PAC1993\\_1223.PDF](http://accelconf.web.cern.ch/AccelConf/p93/PDF/PAC1993_1223.PDF)
- <sup>195</sup> “Linac Proton Driver Cost Estimate”, R. Stanek, Director’s review of the Fermilab Proton Driver, March 2005  
[http://www.fnal.gov/directorate/DirReviews/DirRvw\\_Proton%20Driver%20Presentations/PD\\_DIR\\_REV\\_Stane%5b1%5d.ppt](http://www.fnal.gov/directorate/DirReviews/DirRvw_Proton%20Driver%20Presentations/PD_DIR_REV_Stane%5b1%5d.ppt)  
 The cost backup detail spreadsheet is at:  
[http://protondriver.fnal.gov/Proton\\_Driver\\_Cost\\_Dirs\\_Rev\\_03\\_15\\_05.xls](http://protondriver.fnal.gov/Proton_Driver_Cost_Dirs_Rev_03_15_05.xls)
- <sup>196</sup> Section 10 of the Final Closeout report of the Director’s Review of the Proton Driver, March 2005  
[http://www.fnal.gov/directorate/DirReviews/DirRvw\\_Proton%20Driver%20Presentations/Closeout%20Report\\_DR\\_Proton\\_Driver\\_March-2005.doc](http://www.fnal.gov/directorate/DirReviews/DirRvw_Proton%20Driver%20Presentations/Closeout%20Report_DR_Proton_Driver_March-2005.doc)
- <sup>197</sup> C. Rode, pvt. comm. The \$300M number includes a fraction of the project civil construction cost associated with the very high-intensity SNS ring.
- <sup>198</sup> In order to provide the best possible information for strategic planning to the HEP community, the Proton Driver project makes its cost estimates public. The previous cost estimate is available online at

- <sup>199</sup> [http://tdserver1.fnal.gov/project/8gevlinac/8GeV\\_Cost\\_v6.xls](http://tdserver1.fnal.gov/project/8gevlinac/8GeV_Cost_v6.xls)  
The present cost spreadsheet is online at:
- <sup>200</sup> [http://protondriver.fnal.gov/Proton\\_Driver\\_Cost\\_Dirs\\_Rev\\_03\\_15\\_05.xls](http://protondriver.fnal.gov/Proton_Driver_Cost_Dirs_Rev_03_15_05.xls)  
“ $\beta < 1$  Cryomodules & Cost Estimates”, G. Apollinari, Director’s Review of the FNAL Proton Driver, March’05  
[http://www.fnal.gov/directorate/DirReviews/DirRvw\\_Proton%20Driver%20Presentations/PD\\_DIR\\_REV\\_Apollinari-v2%5b2%5d.ppt](http://www.fnal.gov/directorate/DirReviews/DirRvw_Proton%20Driver%20Presentations/PD_DIR_REV_Apollinari-v2%5b2%5d.ppt)
- <sup>201</sup> This rule of thumb came from Ed Daly of JLAB as reported through Tom Nicol.
- <sup>202</sup> Modulator costs spreadsheet (D. Wolff), available from the author.
- <sup>203</sup> “High Brightness Electron Beams at Fermilab and Applications”, Philippe Piot, presentation to the Accelerator R&D subcommittee of the Fermilab Long-Range Planning Committee, Sept 3, 2003.  
[http://www.fnal.gov/directorate/Longrange/FLPRC\\_Wrkplans/accelerator\\_rd\\_files/Piot-3-Sep.pdf](http://www.fnal.gov/directorate/Longrange/FLPRC_Wrkplans/accelerator_rd_files/Piot-3-Sep.pdf)
- <sup>204</sup> “LATTICE MATCHING WITH A QUADRUPOLE MISSING”, Rainer Wanzenberg, Linac00  
<http://accelconf.web.cern.ch/AccelConf/100/papers/MOE07.pdf>
- <sup>205</sup> The Proton Driver RF working group minutes (through early 2005) are at:  
[http://tdserver1.fnal.gov/8gevlinacPapers/Meeting\\_Minutes/RF/Index.html](http://tdserver1.fnal.gov/8gevlinacPapers/Meeting_Minutes/RF/Index.html)  
Discussions of the Frequency Choice for the 8 GeV Linac are at:  
[http://tdserver1/8gevlinacpapers/Meeting\\_Minutes/RF/Frequency\\_Choice\\_for\\_the\\_SCRF\\_Proton\\_Driver\\_Apr\\_13.doc](http://tdserver1/8gevlinacpapers/Meeting_Minutes/RF/Frequency_Choice_for_the_SCRF_Proton_Driver_Apr_13.doc)  
[http://tdserver1/8gevlinacpapers/Meeting\\_Minutes/RF/Kustom\\_Comments\\_On\\_Choice\\_of\\_frequency\\_1300\\_vs\\_1207.doc](http://tdserver1/8gevlinacpapers/Meeting_Minutes/RF/Kustom_Comments_On_Choice_of_frequency_1300_vs_1207.doc)
- <sup>206</sup> The Proton Driver Cryo/Module working group minutes are at:  
[http://tdserver1.fnal.gov/8gevlinacPapers/Meeting\\_Minutes/Cryomodules/](http://tdserver1.fnal.gov/8gevlinacPapers/Meeting_Minutes/Cryomodules/)  
Discussion of the Frequency Choice for the 8 GeV Linac is at:  
[http://tdserver1.fnal.gov/8gevlinacPapers/Meeting\\_Minutes/Cryomodules/Frequency\\_Choice\\_for\\_the\\_SCRF\\_Proton\\_Driver\\_Apr\\_13.doc](http://tdserver1.fnal.gov/8gevlinacPapers/Meeting_Minutes/Cryomodules/Frequency_Choice_for_the_SCRF_Proton_Driver_Apr_13.doc)
- <sup>207</sup> “Review of the Superconducting Approach to Linear Colliders”, H. Padamsee et al, PAC1992, and references.  
[http://accelconf.web.cern.ch/AccelConf/e92/PDF/EPAC1992\\_0378.PDF](http://accelconf.web.cern.ch/AccelConf/e92/PDF/EPAC1992_0378.PDF)